

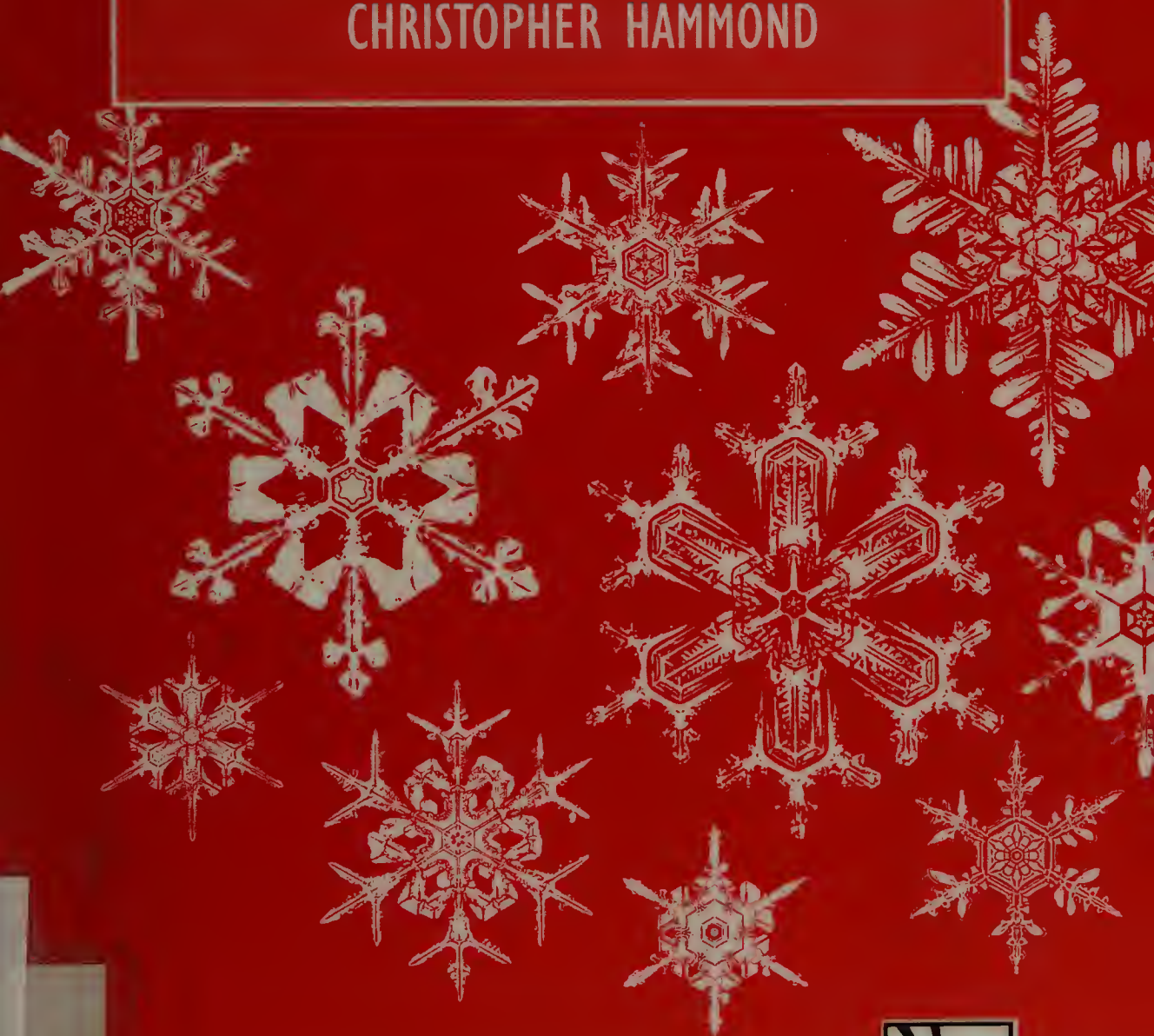


6065559698

TEXTS ON CRYSTALLOGRAPHY · 3

# The Basics of Crystallography and Diffraction

CHRISTOPHER HAMMOND



INTERNATIONAL UNION OF CRYSTALLOGRAPHY  
OXFORD SCIENCE PUBLICATIONS



D 119

DARCODE —

QD  
905  
.2  
HAN  
1997

INTERNATIONAL UNION OF CRYSTALLOGRAPHY TEXTS  
ON CRYSTALLOGRAPHY

IUCr BOOK SERIES COMMITTEE

P Coppens, *Buffalo*  
A M Glazer, *Oxford*  
J P Glusker, *Philadelphia*

" LIBRARY, SOUTH "

Telephone (0"

be r

OXFORD

to latest date

WITHDRAWN FROM RADCLIFFE SCIENCE LIBRARY	
LEGAL DEPOSIT COPY	NO
LAST EDITION COPY	NO
RECENT USAGE	NO

This volume forms part of a series of books sponsored by the International Union of Crystallography (IUCr) and published by Oxford University Press. There are three IUCr series: IUCr Monographs on Crystallography, which are in-depth expositions of specialized topics in crystallography; IUCr Texts on Crystallography, which are more general works intended to make crystallographic insights available to a wider audience than the community of crystallographers themselves; and IUCr Crystallographic Symposia, which are essentially the edited proceedings of workshops or similar meetings supported by the IUCr.

### **IUCr Monographs on Crystallography**

- 1 *Accurate molecular structures: Their determination and importance*  
A. Domenicano and I. Hargittai, editors
- 2 *P. P. Ewald and his dynamical theory of X-ray diffraction*  
D. W. J. Cruickshank, H. J. Juretschke, and N. Kato, editors
- 3 *Electron diffraction techniques, Volume 1*  
J. M. Cowley, editor
- 4 *Electron diffraction techniques, Volume 2*  
J. M. Cowley, editor
- 5 *The Rietveld method*  
R. A. Young, editor
- 6 *Introduction to crystallographic statistics*  
U. Shmueli and G. H. Weiss

### **IUCr Texts on Crystallography**

- 1 *The solid state: From superconductors to superalloys*  
A. Guinier and R. Jullien, translated by W. J. Duffin
- 2 *Fundamentals of crystallography*  
C. Giacovazzo, editor
- 3 *The basics of crystallography and diffraction*  
C. Hammond
- 4 *X-ray charge densities and chemical bonding*  
P. Coppens

### **IUCr Crystallographic Symposia**

- 1 *Patterson and Pattersons: Fifty years of the Patterson function*  
J. P. Glusker, B. K. Patterson, and M. Rossi, editors
- 2 *Molecular structure: Chemical reactivity and biological activity*  
J. J. Stezowski, J. Huang, and M. Shao, editors
- 3 *Crystallographic computing 4: Techniques and new technologies*  
N. W. Isaacs and M. R. Taylor, editors
- 4 *Organic crystal chemistry*  
J. Garbarczyk and D. W. Jones, editors
- 5 *Crystallographic computing 5: From chemistry to biology*  
D. Moras, A. D. Podjarny, and J. C. Thierry, editors
- 6 *Crystallographic computing 6: A window on modern crystallography*  
H. D. Flack, L. Parkanyi, and K. Simon, editors
- 7 *Correlations, transformations, and interactions in organic crystal chemistry*  
D. W. Jones and A. Katrusiak, editors





3028189671

# The Basics of Crystallography and Diffraction

---

Christopher Hammond

*School of Materials, University of Leeds*

INTERNATIONAL UNION OF CRYSTALLOGRAPHY  
OXFORD UNIVERSITY PRESS

Oxford University Press, Great Clarendon Street, Oxford OX2 6DP  
Oxford New York  
Athens Auckland Bangkok Bombay Buenos Aires  
Calcutta Cape Town Dar es Salaam Delhi Florence Hong Kong  
Istanbul Karachi Kuala Lumpur Madras Madrid Melbourne  
Mexico City Nairobi Paris Singapore Taipei Tokyo Toronto Warsaw  
and associated companies in  
Berlin Ibadan

Oxford is a trade mark of Oxford University Press

Published in the United States  
by Oxford University Press Inc., New York

© Christopher Hammond, 1997  
First published 1997  
Reprinted 1998

All rights reserved. No part of this publication may be reproduced, stored in a retrieval system, or transmitted, in any form or by any means, without the prior permission in writing of Oxford University Press. Within the UK, exceptions are allowed in respect of any fair dealing for the purpose of research or private study, or criticism or review, as permitted under the Copyright, Designs and Patents Act, 1988, or in the case of reprographic reproduction in accordance with the terms of licences issued by the Copyright Licensing Agency. Enquiries concerning reproduction outside those terms and in other countries should be sent to the Rights Department, Oxford University Press, at the address above.

This book is sold subject to the condition that it shall not, by way of trade or otherwise, be lent, re-sold, hired out, or otherwise circulated without the publisher's prior consent in any form of binding or cover other than that in which it is published and without a similar condition including this condition being imposed on the subsequent purchaser.

A catalogue record for this book is available from the British Library

Library of Congress Cataloging in Publication Data

Hammond, C. (Christopher), 1942–

The basics of crystallography and diffraction / Christopher Hammond.  
(International Union of Crystallography texts on crystallography; 3)

Includes bibliographical references and index.

1. Crystallography. 2. X-ray crystallography. I. Title. II. Series.  
QD905.2.H355 1997 548--dc20 96-27451

ISBN 0-19-855966-6 (Hbk)

ISBN 0-19-855945-3 (Pbk)

Printed in Great Britain by Bookcraft (Bath) Ltd., Midsomer Norton, Avon

# Preface

This book has grown out of my earlier *Introduction to Crystallography* published in the Royal Microscopical Society's Microscopy Handbook Series (Oxford University Press 1990, revised edition 1992). My object then was to show that crystallography is not, as many students suppose, an abstruse and 'difficult' subject, but a subject that is essentially clear and simple and which does not require the assimilation and memorization of a large number of facts. Moreover, a knowledge of crystallography opens the door to a better and clearer understanding of so many other topics in physics and chemistry, earth, materials and textile sciences, and microscopy.

In doing so I tried to show that the ideas of symmetry, structures, lattices and the architecture of crystals should be approached by reference to everyday examples of the things we see around us, and that these ideas were not confined to the pages of textbooks or the models displayed in laboratories.

The subject of diffraction flows naturally from that of crystallography because by its means—and in most cases only by its means—are the structures of materials revealed. And this applies not only to the interpretation of diffraction patterns but also to the interpretation of images in microscopy. Indeed, diffraction patterns of objects ought to be thought of as being as 'real', and as simply understood, as the objects themselves. One is, to use the mathematical expression, simply the transform of the other. Hence, in discussing diffraction, I have tried to emphasize the common aspects of the phenomena with respect to light, X-rays and electrons.

In Chapter 1 (Crystals and crystal structures) I have concentrated on the simplest examples, emphasizing how they are related in terms of the occupancy of atomic sites and how the structures may be changed by faulting. Chapter 2 (Two-dimensional patterns, lattices and symmetry) has been considerably expanded, partly to provide a firm basis for understanding symmetry and lattices in three dimensions (Chapters 3 and 4) but also to address the interests of students involved in two-dimensional design. Similarly in Chapter 4, in discussing point group symmetry, I have emphasized its practical relevance in terms of the physical and optical properties of crystals.

The reciprocal lattice (Chapter 6) provides the key to our understanding of diffraction, but as a *concept* it stands alone. I have therefore introduced it separately from diffraction and hope that in doing so these topics will be more readily understood. In Chapter 7 (The diffraction of light) I have emphasized the geometrical analogy with electron diffraction and have avoided any quantitative analysis of the amplitudes and intensities of diffracted beams. In my experience the (sometimes lengthy) equations which are required cloud students' perceptions of the basic geometrical conditions for constructive and destructive interference—and which are also of far more practical importance with respect, say, to the resolving power of optical instruments.

Chapter 8 describes the historical development of the geometrical interpretation of X-ray diffraction patterns through the work of Laue, the Braggs and Ewald. The diffraction of X-rays and electrons from single crystals is covered in Chapter 9, but only in the case of X-ray diffraction are the intensities of the diffracted beams discussed. This is largely because structure factors are important but also because the derivation of the interference conditions between the atoms in the motif can be represented as nothing more than an extension of Bragg's law. Finally, the important X-ray and electron diffraction techniques from polycrystalline materials are covered in Chapter 10.

The Appendices cover material that, for ease of reference, is not covered in the text. Appendix 1 gives a list of items which are useful in making up crystal models and provides the names and addresses of suppliers. A rapidly increasing number of crystallography programs are becoming available for use in personal computers and in Appendix 2 I have listed those which involve, to a greater or lesser degree, some 'self learning' element. If it is the case that the computer program will replace the book, then one might expect that books on crystallography would be the first to go! That day, however, has yet to arrive. Appendix 3 gives brief biographical details of crystallographers and scientists whose names are asterisked in the text. Appendix 4 lists some useful geometrical relationships.

Throughout the book the mathematical level has been maintained at a very simple level and with few minor exceptions all the equations have been derived from first principles. In my view, students learn nothing from, and are invariably dismayed and perplexed by, phrases such as 'it can be shown that'—without any indication or guidance of *how* it can be shown. Appendix 5 sets out all the mathematics which are needed.

Finally, it is my belief that students appreciate a subject far more if it is presented to them not simply as a given body of knowledge but as one which has been gained by the exertions and insight of men and women perhaps not much older than themselves. This therefore shows that scientific discovery is an activity in which they, now or in the future, can participate. Hence the justification for the historical references, which, to return to my first point, also help to show that science progresses, not by being made more complicated, but by individuals piecing together facts and ideas, and seeing relationships where vagueness and uncertainty existed before.

## Acknowledgements

In the preparation of this book I should like to thank Dr Kate Crennell, of the British Crystallographic Association, for providing me with information on

computer programs and software for the teaching of crystallography, Dr Michael Hann, of the University of Leeds, for his advice on two-dimensional patterns and symmetry, Dr Pam Champness and Professor Gordon Lorimer, of the University of Manchester/UMIST, for their constructive criticisms throughout, and Dr John Robertson, Chairman of the Book Series Committee of the International Union of Crystallography, for his advice and encouragement.

I should like to thank Miss Susan Toon for typing the manuscript, my colleagues in the School of Materials, in particular Mr David Horner for the photographic work and Mr David Wright for providing the X-ray diffraction data, and generations of students for their criticisms, constructive and otherwise, of my teaching methods.

A number of copyright holders have permitted me to reproduce a number of figures, acknowledgement to which is made in the figure captions. Finally, I ask my readers to bring to my attention any points which may be unclear, ambiguous, or erroneous.

*School of Materials*  
*University of Leeds*  
November 1996

C.H.



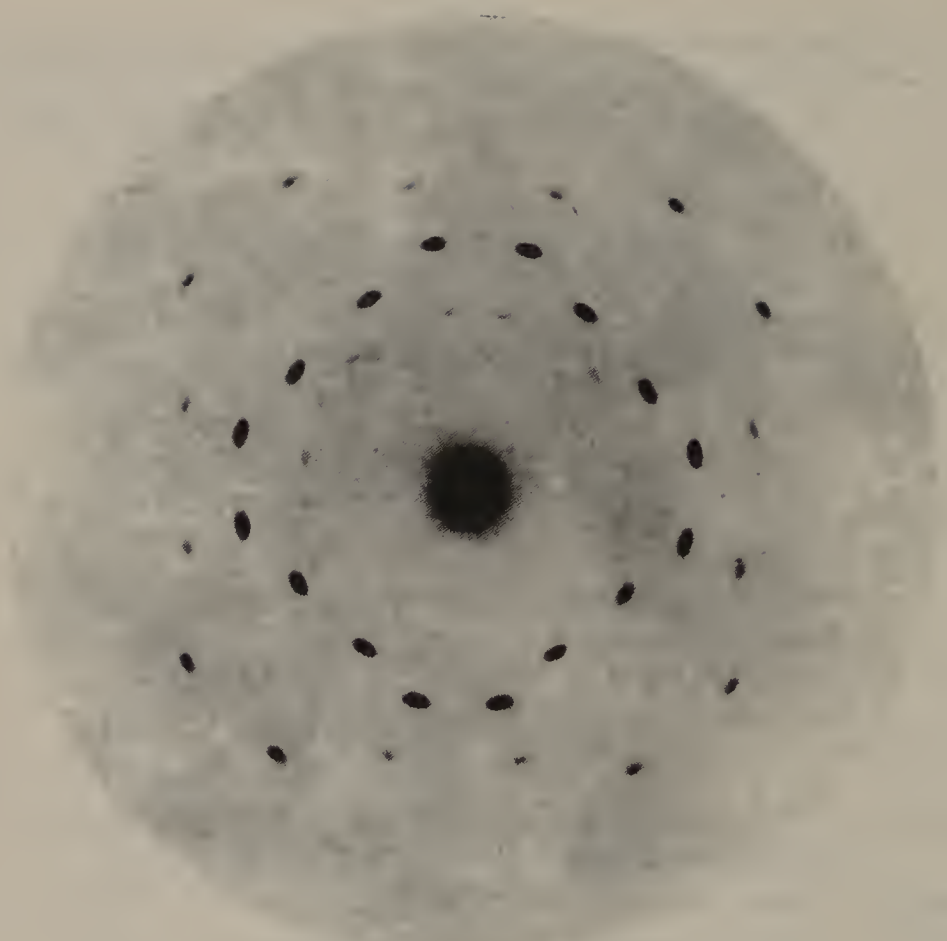


# Contents

①	Crystals and crystal structures	1
1.1	The nature of the crystalline state	1
1.2	Constructing crystals from close-packed hexagonal layers of atoms	5
1.3	Unit cells of the hcp and ccp structures	6
1.4	Constructing crystals from square layers of atoms	9
1.5	Constructing body-centred cubic crystals	10
1.6	Interstitial structures	11
1.7	Some simple ionic and covalent structures	16
1.8	Representing crystals in projection: crystal plans	17
1.9	Stacking faults and twins	19
1.10	Some more complex crystal structures	24
	Exercises	27
②	Two-dimensional patterns, lattices and symmetry	32
2.1	Approaches to the study of crystal structures	32
2.2	Two-dimensional patterns and lattices	33
2.3	Two-dimensional symmetry elements	35
2.4	The five plane lattices	36
2.5	The seventeen plane groups	41
2.6	One-dimensional symmetry: border or frieze patterns	42
2.7	Symmetry, patterns and cultures	44
	Exercises	47
③	Bravais lattices and crystal systems	51
3.1	Introduction	51
3.2	The fourteen space (Bravais) lattices	51
3.3	The symmetry of the fourteen Bravais lattices: crystal systems	55
	Exercises	58
④	Crystal symmetry, point groups and crystal structures: the external symmetry of crystals	59
4.1	Symmetry and crystal habit	59
4.2	The thirty-two crystal classes	60
4.3	Centres and inversion axes of symmetry	61
4.4	Crystal symmetry and properties	65
4.5	Translational symmetry elements	68
4.6	Space groups	72
4.7	Bravais lattices, motifs and crystal structures	74
	Exercises	75

5	Describing lattice planes and directions in crystals: Miller indices and zone axis symbols	76
5.1	Introduction	76
5.2	Indexing lattice directions—zone axis symbols	77
5.3	Indexing lattice planes—Miller indices	78
5.4	Miller indices and zone axis symbols in cubic crystals	81
5.5	Lattice plane spacings, Miller indices and Laue indices	82
5.6	Zones, zone axes and the zone law, the addition rule	84
5.7	Indexing in the trigonal and hexagonal systems: Weber symbols and Miller–Bravais indices	85
5.8	Transforming Miller indices and zone axis symbols	87
5.9	Transformation matrices for trigonal crystals with rhombohedral lattices	90
	Exercises	91
6	The reciprocal lattice	92
6.1	Introduction	92
6.2	Reciprocal lattice vectors	92
6.3	Reciprocal lattice unit cells	94
6.4	Reciprocal lattice cells for cubic crystals	96
6.5	Proofs of some geometrical relationships using reciprocal lattice vectors	97
	Exercises	100
7	The diffraction of light	101
7.1	Introduction	101
7.2	Simple observations on the diffraction of light	103
7.3	The nature of light: coherence, scattering and interference	108
7.4	Analysis of the geometry of diffraction patterns from gratings and nets	111
7.5	The resolving power of optical instruments	118
	Exercises	123
8	X-ray diffraction: the contributions of Max von Laue, W. H. and W. L. Bragg and P. P. Ewald	125
8.1	Introduction	125
8.2	Laue's analysis of X-ray diffraction: the three Laue equations	126
8.3	Bragg's analysis of X-ray diffraction: Bragg's law	128
8.4	Ewald's synthesis: the reflecting sphere construction	130
	Exercises	134
9	The diffraction of X-rays and electrons	135
9.1	Introduction	135

9.2	The intensities of X-ray diffracted beams: the structure factor equation and its applications	138
9.3	The broadening of diffracted beams: reciprocal lattice points and nodes	145
9.4	Fixed $\theta$ , varying $\lambda$ X-ray techniques: the Laue method	148
9.5	Fixed $\lambda$ , varying $\theta$ X-ray techniques: oscillation, rotation and precession methods	149
9.6	X-ray diffraction from single crystal thin films and multilayers	155
9.7	Electron diffraction in the transmission electron microscope	160
	Exercises	167
10	X-ray and electron diffraction of polycrystalline materials	171
10.1	Introduction	171
10.2	The geometrical basis of polycrystalline (powder) X-ray diffraction techniques	172
10.3	Some applications of X-ray and electron diffraction techniques in polycrystalline materials	181
	Exercises	188
Appendix 1:	Useful components for a crystallography model-building kit and suppliers	191
Appendix 2:	Computer programs in crystallography	193
Appendix 3:	Biographical notes on crystallographers and scientists mentioned in the text	199
Appendix 4:	Some useful crystallographic relationships	214
Appendix 5:	A simple introduction to vectors and complex numbers and their use in crystallography	217
Appendix 6:	Systematic absences (extinctions) in X-ray diffraction and double diffraction in electron diffraction patterns	224
	Answers to exercises	232
	Further reading	239
	Index	243



*X-ray photograph of zinc blende*

One of the eleven 'Laue Diagrams' in the paper submitted by Walter Friedrich, Paul Knipping and Max von Laue to the Bavarian Academy of Sciences and presented at its Meeting held on June 8th 1912—the paper which demonstrated the existence of internal atomic regularity in crystals and its relationship to the external symmetry.

The X-ray beam is incident along one of the cubic crystal axes of the (face centred cubic) ZnS structure and consequently the diffraction spots show the four-fold symmetry of the atomic arrangement about the axis. But notice also that the spots are not circular in shape—they are elliptical; the short axes of the ellipses all lying in radial directions. William Lawrence Bragg realized the great importance of this seemingly small observation: he had noticed that beams of light (of circular cross-section) reflected from mirrors also gave reflected spots of just these elliptical shapes. Hence he went on to formulate the Law of Reflection of X-Ray Beams which unlocked the door to the structural analysis of crystals.



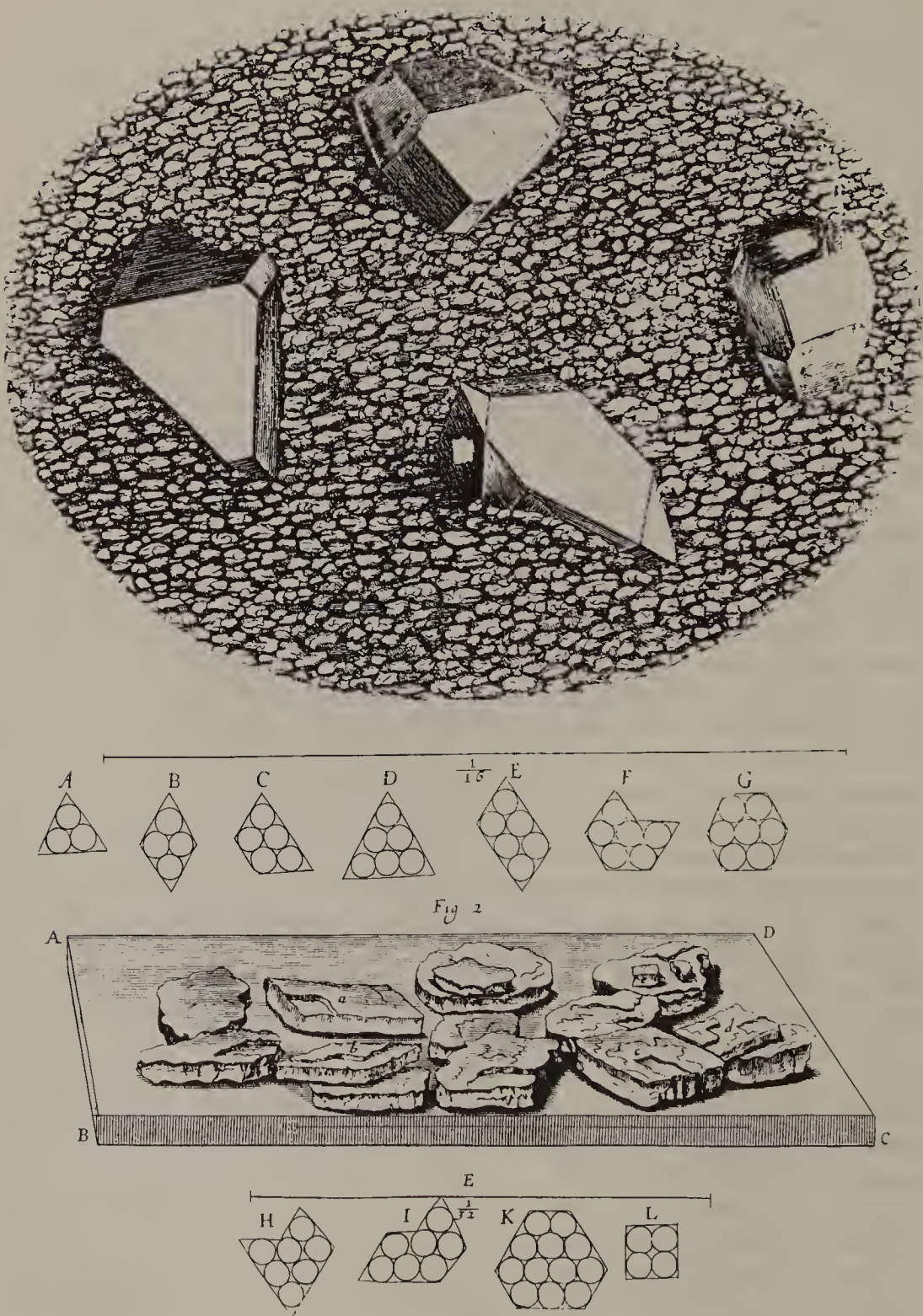
# Crystals and crystal structures

## 1.1 The nature of the crystalline state

The beautiful hexagonal patterns of snowflakes, the plane faces and hard faceted shapes of minerals and the bright cleavage fracture surfaces of brittle iron have long been recognized as external evidence of an internal order—evidence, that is, of the patterns or arrangements of the underlying building blocks. However, the nature of this internal order, or the form and scale of the building blocks, was unknown.

The first attempt to relate the external form or shape of a crystal to its underlying structure was made by Johannes Kepler\* who, in 1611, wrote perhaps the first treatise on geometrical crystallography, with the delightful title, ‘A New Year’s Gift or the Six-Cornered Snowflake’ (*Strena Seu de Nive Sexangula*). In this he speculates on the question as to why snowflakes always have six corners, never five or seven. He suggests that snowflakes are composed of tiny spheres of ice and shows, in consequence, how the close-packing of these spheres gives rise to a six-sided figure. It is indeed a simple experiment that children now do with pennies at school. Kepler was not able to solve the problem as to why the six corners extend and branch to give many patterns (a problem not fully resolved to this day), nor did he extend his ideas to other crystals. The first to do so, and to consider the structure of crystals as a general problem, was Robert Hooke\* who, with remarkable insight, suggested that the different shapes of crystals which occur—rhombs, trapezia, hexagons, etc.—could arise from the packing together of spheres or globules. Figure 1.1 is ‘Scheme VII’ from his book *Micrographia*, first published in 1665. The upper part (Fig. 1) is his drawing, from the microscope, of ‘Crystalline or Adamantine bodies’ occurring on the surface of a cavity in a piece of broken flint and the lower part (Fig. 2) is of ‘sand or gravel’ crystallized out of urine, which consist of ‘Slats or such-like plated Stones...their sides shaped into **Rhombs**, **Rhomboeids** and sometimes into **Rectangles** and **Squares**’. He goes on to show how these various shapes can arise from the packing together of ‘a company of bullets’ as shown in the inset sketches A–L, which represent pictures of crystal structures which have been repeated in innumerable books, with very little variation, ever since. The notion that the packing of the underlying building blocks determines both the shapes of crystals and the angular relationships between the faces was extended by René Just Haüy\*. In 1784 Haüy showed how the different forms (or habits) of

\* Denotes biographical notes available in Appendix 3.



**Fig. 1.1.** ‘Scheme VII’ (from Hooke’s *Micrographia*, 1665), showing crystals in a piece of broken flint (Upper—Fig. 1), crystals from urine (Lower—Fig. 2) and hypothetical sketches of crystal structures A–L arising from the packing together of ‘bullets’.



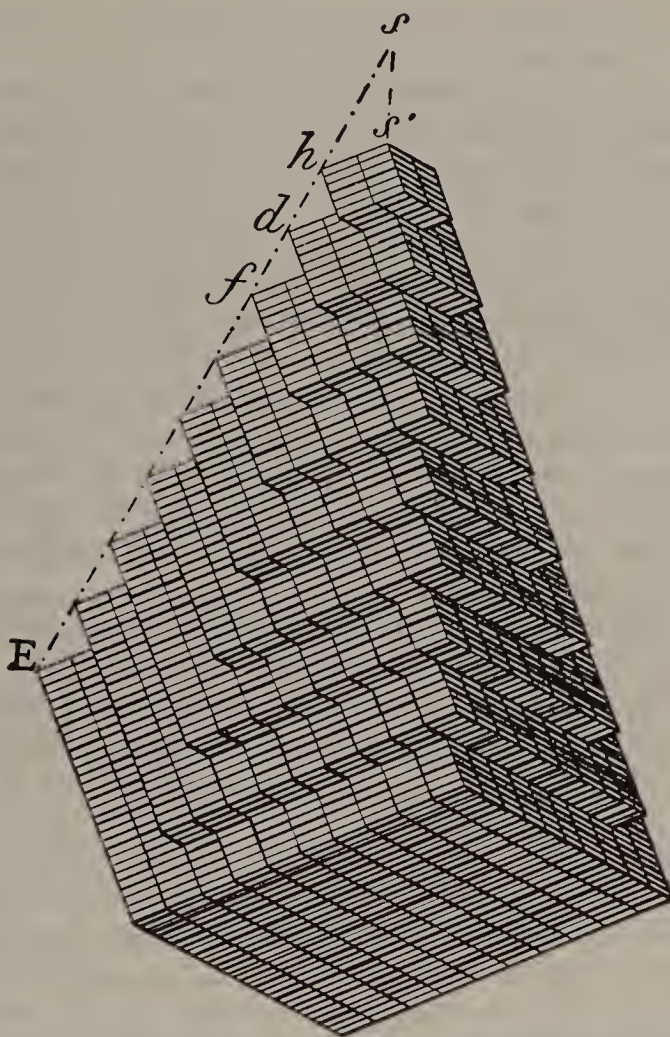


Fig. 1.2. Haüy's representation of dog-tooth spar built up from rhombohedral 'molécules integrantes' (from *Essai d'une théorie sur la structure des cristaux*, 1784).

dog-tooth spar (calcite) could be precisely described by the packing together of little rhombs which he called 'molécules intégrantes' (Fig. 1.2). Thus the connection between an internal order and an external symmetry was established. What was not realized at the time was that an internal order could exist even though there may appear to be no external evidence for it.

It is only relatively recently, as a result primarily of X-ray and electron diffraction techniques, that it has been realized that most materials, including many biological materials, are crystalline or partly so. But the notion that a lack of external crystalline form implies a lack of internal regularity still persists. For example, when iron and steel become embrittled there is a marked change in the fracture surface from a rough, irregular 'grey' appearance to a bright faceted 'brittle' appearance. The change in properties from tough to brittle is sometimes vaguely thought to arise because the structure of the iron or steel has changed from some undefined amorphous or non-crystalline 'grey' state to a 'crystallized'

state. In both situations, of course, the crystalline structure of iron is unchanged; it is simply the fracture processes that are different.

Given our more detailed knowledge of matter we can now interpret Hooke's spheres or 'bullets' as atoms or ions, and Fig. 1.1 indicates the ways in which some of the simplest crystal structures can be built up. This representation of atoms as spheres does not, and is not intended, to show anything about their physical or chemical nature. The diameters of the spheres merely express their nearest distances of approach. It is true that these will depend upon the ways in which the atoms are packed together, and whether or not the atoms are ionized, but these considerations do not invalidate the 'hard sphere' model, which is justified, not as a representation of the *structure* of atoms, but as a representation of the structures arising from the *packing together* of atoms.

Consider again Hooke's sketches A–L (Fig. 1.1). In all of these, except the last, L, the atoms are packed together *in the same way*; the differences in shape arise from the different crystal boundaries. The atoms are packed in a *close-packed hexagonal* or honeycomb arrangement—the most compact way which is possible. By contrast, in the *square* arrangement of L there are larger voids or gaps (properly called **interstices**) between the atoms. This difference is shown more clearly in Fig. 1.3, where the boundaries of the (two-dimensional) crystals have been left deliberately irregular to emphasize the point that it is the internal regularity, hexagonal, or square, not the boundaries (or external faces) which defines the structure of a crystal.

Now we shall extend these ideas to three dimensions by considering not one, but many, layers of atoms, stacked one on top of the other. To understand better the figures which follow, it is very helpful to make models of these layers (Fig. 1.3) to construct the three-dimensional crystal models (see Appendix 1).

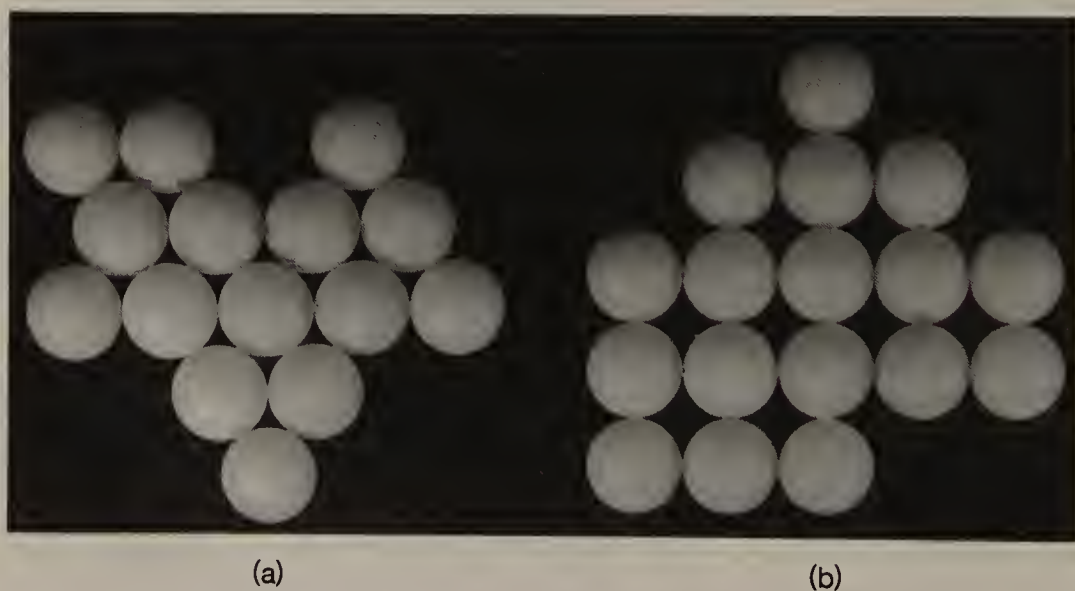


Fig. 1.3. Layers of 'atoms' stacked (a) in hexagonal and (b) in square arrays.

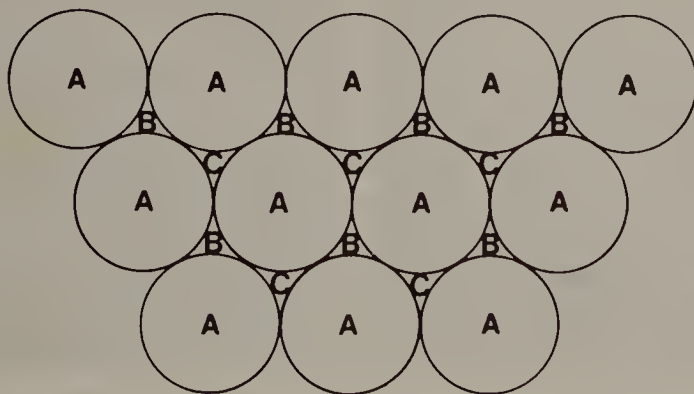
## 1.2 Constructing crystals from close-packed hexagonal layers of atoms

The simplest way of stacking the layers is to place the atom centres directly above one another. The resultant crystal structure is called the **simple hexagonal structure**. There are, in fact, no examples of elements with this structure because, as the model building shows, the atoms in the second layer tend to slip into the 'hollows' or interstices between the atoms in the layer below. This also accords with energy considerations: unless electron orbital considerations predominate, layers of atoms stacked in this 'close-packed' way generally have the lowest (free) energy and are therefore most stable.

When a third layer is placed upon the second we see that there are two possibilities: when the atoms in the third layer slip into the interstices of the second layer they may either end up directly above the atom centres in the first layer or directly above the unoccupied interstices between the atoms in the first layer.

The geometry may be understood from Fig. 1.4, which shows a plan view of atom layers. A is the first layer (with the circular outlines of the atoms drawn in) and B is the second layer (outlines of the atoms not shown for clarity). In the first case the third layer goes directly above the A layer, the fourth layer over the B layer, and so on; the stacking sequence then becomes ABABAB... and is called the **hexagonal close-packed (hcp) structure**. The packing of idealized hard spheres predicts a ratio of interlayer atomic spacing to in-layer atomic spacing of  $\sqrt{2/3}$  and although interatomic forces cause deviations from this ratio, metals such as zinc, magnesium and the low-temperature form of titanium have the hcp structure.

In the second case, the third layer of atoms goes above the interstices marked C and the sequence only repeats at the fourth layer, which goes directly above the first layer. The stacking sequence is now ABCABC... and is called the **cubic close-packed (ccp) structure**. Metals such as copper, aluminium, silver,



**Fig. 1.4.** Stacking sequences of close-packed layers of atoms. A—first layer (with outlines of atoms shown); B—second layer; C—third layer.



gold and the high-temperature form of iron have this structure. You may ask the question: 'why is a structure which is made up of a three-layer stacking sequence of hexagonal layers called *cubic* close packed?' The answer lies in the shape and symmetry of the unit cell, which we shall meet below.

These labels for the layers A, B, C are, of course, arbitrary; they could be called OUP or RMS or any combination of three letters or figures. The important point is not the labelling of the layers but their **stacking sequence**; a two-layer repeat for hcp and a three-layer repeat for ccp. Another way of 'seeing the difference' is to notice that in the hcp structure there are open channels perpendicular to the layers running through the connecting interstices (labelled C in Fig. 1.4). In the ccp structure there are no such open channels—they are 'blocked' or obstructed because of the ABCABC... stacking sequence.

Although the hcp and the ccp are the two most common stacking sequences of close-packed layers, some elements have crystal structures which are 'mixtures' of the two. For example, the actinide element americium has the stacking sequence ABACABAC... a four-layer repeat which is essentially a combination of an hcp and a ccp stacking sequence. Furthermore, in some elements with nominally ccp or hcp stacking sequences nature sometimes 'makes mistakes' in model building and faults occur during crystal growth or under conditions of stress or deformation. For example, in a (predominantly) ccp crystal (such as cobalt at room temperature), the ABCABC... (ccp) type of stacking may be interrupted by layers with an ABABAB... (hcp) type of stacking. The extent of occurrence of these **stacking faults** and the particular combinations of ABCABC... and ABABAB... sequences which may arise depend again on energy considerations, with which we are not concerned. What is of crystallographic importance is the fact that stacking faults show how one structure (ccp) may be transformed into another (hcp) and vice versa. They can also be used in the representation of more complicated crystal structures (i.e. of more than one kind of atom), as explained in Sections 1.6 and 1.9 below.

### 1.3 Unit cells of the hcp and ccp structures

A simple and economical method is now needed to represent the hcp and ccp (and of course other) crystal structures. Diagrams showing the stacked layers of atoms with irregular boundaries would obviously look very confused and complicated—the greater the number of atoms which have to be drawn, the more complicated the picture. The models need to be 'stripped down' to the fewest numbers of atoms which show the essential structure and symmetry. Such 'stripped-down' models are called the **unit cells** of the structures.

The unit cells of the simple hexagonal and hcp structures are shown in Fig. 1.5. The similarities and differences are clear: both structures consist of hexagonal close-packed layers; in the simple hexagonal structure these are stacked directly on top of each other, giving an AAA... type of sequence, and in the hcp structure there is an interleaving layer nestling in the interstices of the layers below and above, giving an ABAB... type of sequence.



Fig. 1.5. Unit cells (a) of the simple hexagonal and (b) hcp structures.

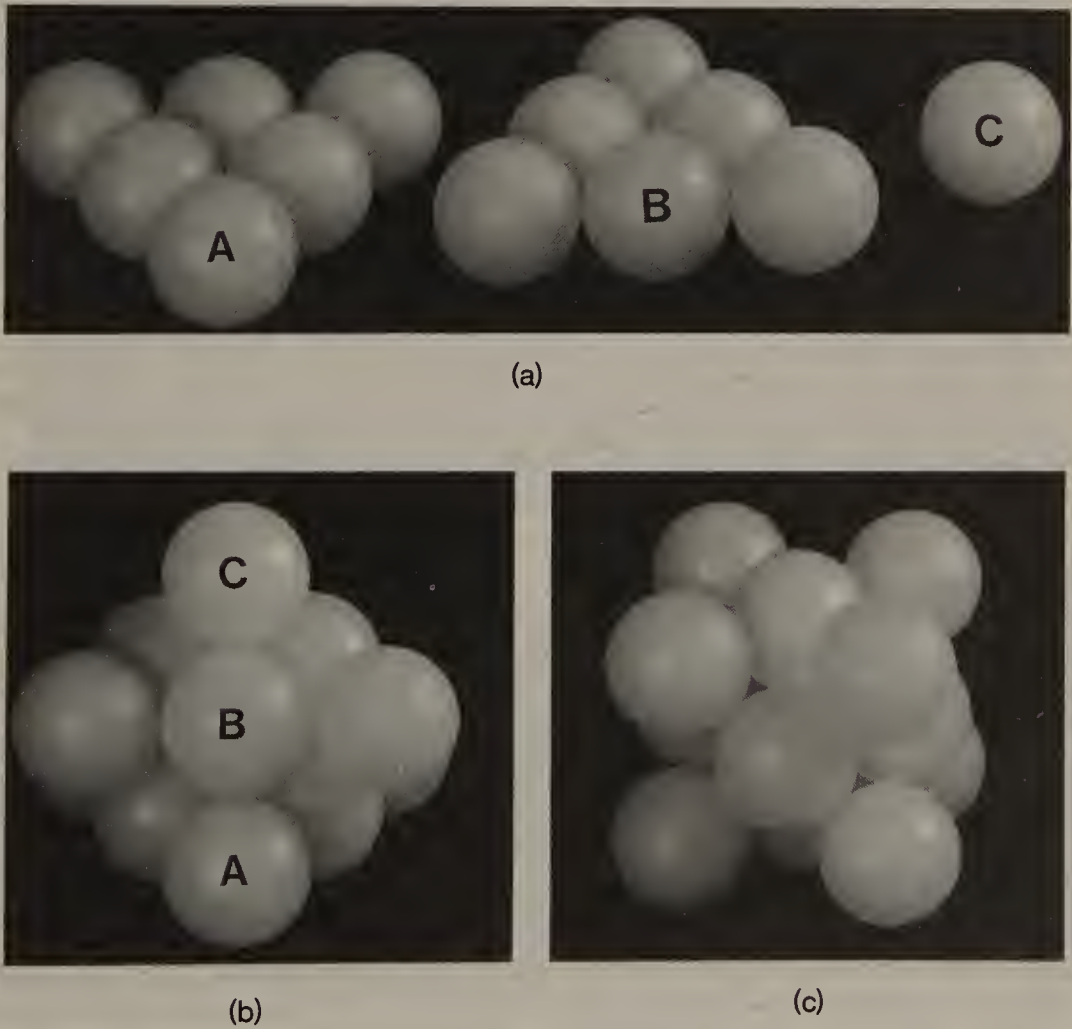
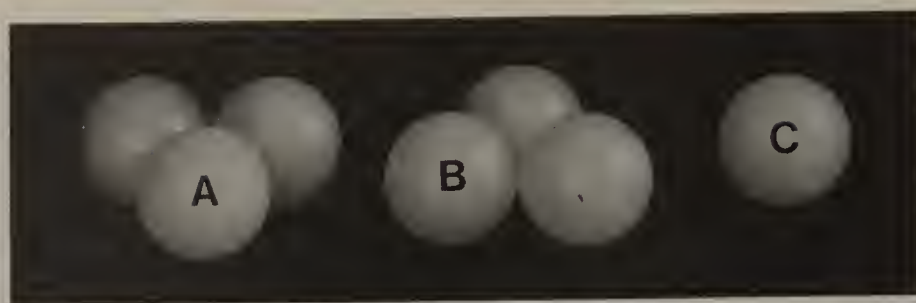
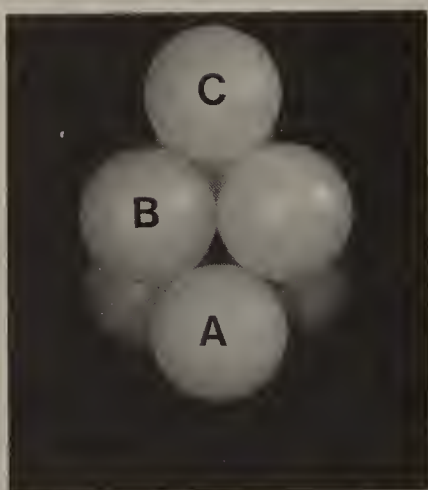


Fig. 1.6. Construction of the cubic unit cell of the ccp structure: (a) shows three close-packed layers A, B and C which are stacked in (b) in the 'ABC...' sequence from which emerges the cubic unit cell which is shown in (c) in the conventional orientation.



(a)



(b)



(c)

**Fig. 1.7.** Construction of the rhombohedral unit cell of the ccp structure: the close-packed layers (a) are again stacked (b) in the 'ABC...' sequence but the resulting rhombohedral cell (c) does not reveal the cubic symmetry.

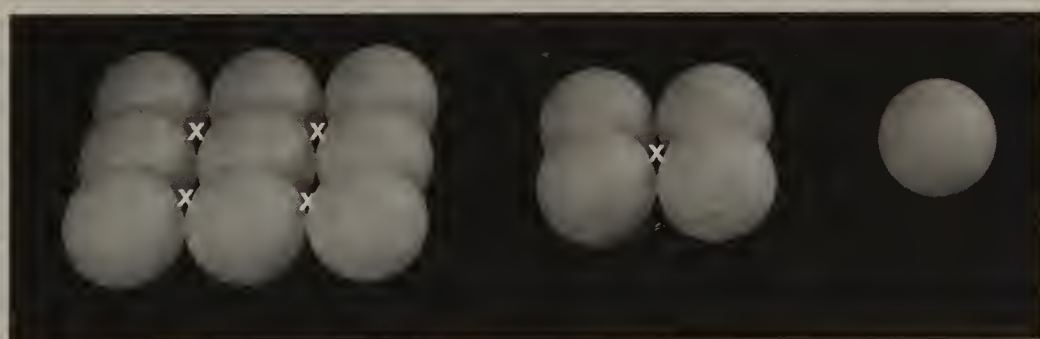
The unit cell of the ccp structure is not so easy to see. There are, in fact, two possible unit cells which may be identified, a cubic cell described below (Fig. 1.6), which is almost invariably used, and a smaller rhombohedral cell (Fig. 1.7). Figure 1.6(a) shows three close-packed layers separately—two triangular layers of six atoms (identical to one of Hooke's sketches in Fig. 1.1)—and a third layer stripped down to just one atom. If we stack these layers in an ABC sequence, the result is as shown in Fig. 1.6(b): it is a cube with the bottom corner atom missing. This can now be added and the unit cell of the ccp structure, with atoms at the corners and centres of the faces, emerges. The unit cell is usually drawn in the 'upright' position of Fig. 1.6(c), and this helps to illustrate a very important point which may have already been spotted whilst model building with the close-packed layers. The close-packed layers lie perpendicular to the body diagonal of the cube, but as there are four different body diagonal directions in a cube, there are therefore four different sets of close-packed layers—not just the one set with which we started. Thus three further close-packed layers have been automatically generated by the ABCABC... stacking sequence. This does not occur in the hcp structure—try it and see! The cubic unit cell, therefore,



shows the **symmetry** of the ccp structure, a topic which will be covered in Chapter 4. The alternative rhombohedral unit cell of the ccp structure may be obtained by 'stripping away' atoms from the cubic cell such that there are only eight atoms left—one at each of the eight corners—or it may be built up by stacking triangular layers of only three atoms instead of six (Fig. 1.7). Unlike the larger cell, this does not obviously reveal the cubic symmetry of the structure and so is much less useful.

## 1.4 Constructing crystals from square layers of atoms

It will be noticed that the atoms in the cube faces of the ccp structure lie in a square array like that in Fig. 1.3(b) and the ccp structure may be constructed by stacking these layers such that alternate layers lie in the square interstices marked X in Fig. 1.8(a). The models show how the four close-packed layers arise like the faces of a pyramid (Fig. 1.8(b)). If, on the other hand, the layers are all stacked directly on top of each other, a **simple cubic structure** is obtained (Fig. 1.8(c)). This is an uncommon structure for the same reason as the simple hexagonal one is uncommon. An example of an element with a simple cubic structure is  $\alpha$ -polonium.



(a)

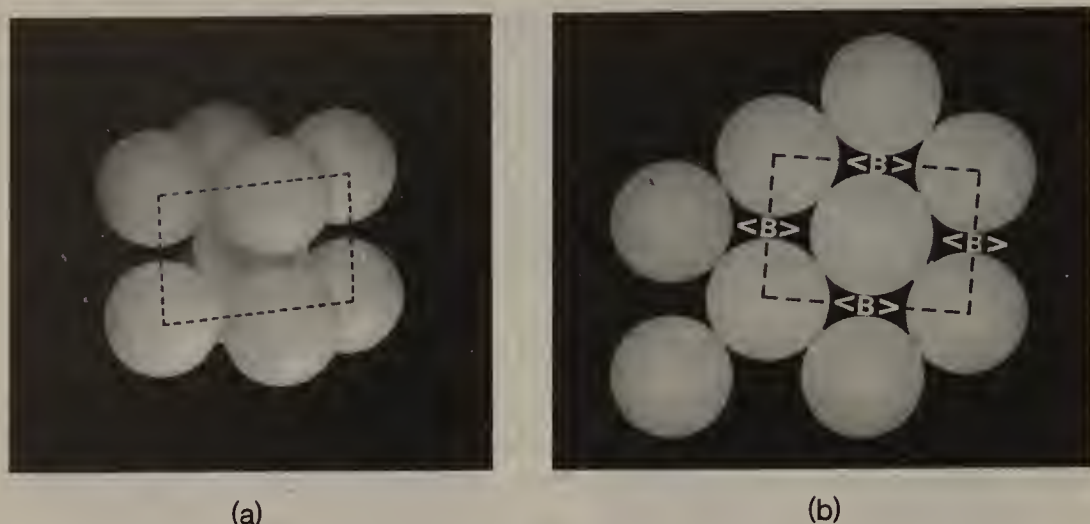


(b)



(c)

**Fig. 1.8.** (a) 'Square' layers of atoms with interstices marked X; (b) stacking the layers so that the atoms fall into these interstices, showing the development of the close-packed layers; (c) stacking the layers directly above one another, showing the development of the simple cubic structure.



**Fig. 1.9.** (a) Unit cell of the bcc structure, showing a face-diagonal plane in which the atoms are most closely packed; (b) a plan view of this 'closest-packed' plane of atoms; the positions of atoms in alternate layers are marked B. The arrows indicate possible slip directions from these positions.

## 1.5 Constructing body-centred cubic crystals

The important and commonly occurring **body-centred cubic (bcc)** structure differs from those already discussed in that it cannot be constructed either from hexagonal close-packed or square-packed layers of atoms (Fig. 1.3). The unit cell of the bcc structure is shown in Fig. 1.9. Notice how the body-centring atom 'pushes' the corner ones apart so that, on the basis of the 'hard sphere' model of atoms discussed above, they are not 'in contact' along the edges (in comparison with the simple cubic structure of Fig. 1.8(c), where they are in contact). In the bcc structure the atoms are in contact only along the body-diagonal directions. The planes in which the atoms are most (not fully) closely packed is the face-diagonal plane, as shown in Fig. 1.9(a), and in plan view, showing more atoms, in Fig. 1.9(b). The atom centres in the next layer go over the interstices marked B, then the third layer goes over the first layer, and so on—an ABAB... type of stacking sequence. The interstices marked B have a slight 'saddle' configuration, and model building will suggest that the atoms in the second layer might slip a small distance to one side or the other (indicated by arrows), leading to a distortion in the cubic structure. Whether such a situation can arise in real crystals, even on a small scale, is still a matter of debate. Metals such as chromium, molybdenum, the high-temperature form of titanium and the low-temperature form of iron have the bcc structure.

Finally, notice the close similarity between the layers of atoms in Figs 1.3(a) and 1.9(b). With only small distortions, e.g. closing of the gaps in Fig. 1.9(b), the two layers become geometrically identical and some important  $\text{bcc} \rightleftharpoons \text{ccp}$  and  $\text{bcc} \rightleftharpoons \text{hcp}$  transformations are thought to occur as a result of distortions of this kind. For example, when iron is quenched from its high-temperature form (ccp



above 910°C) to transform to its low-temperature (bcc) form, it is found that the set of the close-packed and closest-packed layers and close-packed directions are approximately parallel.

## 1.6 Interstitial structures

The different stacking sequences of one size of atom discussed in Sections 1.2 and 1.5 are not only useful in describing the crystal structures in many of the elements, where all the atoms are identical to one another, but can also be used to describe and explain the crystal structures of a wide range of compounds of two or more elements, where there are atoms of two or more different sizes. In particular, they can be applied to those compounds in which 'small' atoms or cations fit into the interstices between 'large' atoms or anions. The different structures of very many compounds arise from the different numbers and sizes of interstices which occur in the simple hexagonal, hcp, ccp, simple cubic and bcc structures and also from the ways in which the small atoms or cations distribute themselves among these interstices. These ideas can, perhaps, be best understood by considering the types, sizes and numbers of interstices which occur in the ccp and simple cubic structures.

In the ccp structure there are two types and sizes of interstice into which small atoms or cations may fit. They are best seen by fitting small spheres into the interstices between two-close-packed atom layers (Fig. 1.4). Consider an atom in a B layer which fits into the hollow or interstice between three A layer atoms: beneath the B atom is an interstice which is surrounded at equal distances by four atoms—three in the A layer and one in the B layer. These four atoms surround or 'coordinate' the interstice in the shape of a tetrahedron, hence the name **tetrahedral interstice** or **tetrahedral interstitial site**, i.e. where a small interstitial atom or ion may be situated. The position of one such site in the ccp unit cell is shown in Fig. 1.10(a) and diagrammatically in Fig. 1.10(b).

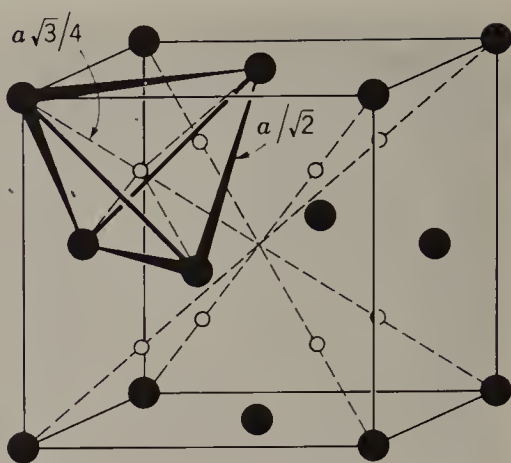
The other interstices between the A and B layers (Fig. 1.4) are surrounded or coordinated by six atoms, three in the A layer and three in the B layer. These six atoms surround the interstice in the shape of an octahedron; hence the name **octahedral interstice** or **octahedral interstitial site**. The positions of several atoms or ions in octahedral sites in a ccp unit cell are shown in Fig. 1.11(a) and diagrammatically, showing one octahedral site, in Fig. 1.11(b).

In the simple cubic structure (Fig. 1.8(c)) there is an interstice at the centre of the unit cell which is surrounded or coordinated by the eight atoms at the corners of the cube (Fig. 1.12(a)), hence the name **cubic interstitial site**. Caesium chloride, CsCl, has this structure, as shown diagrammatically in Fig. 1.12(b).

Now the diameters, or radii, of atoms or ions which can just fit into these interstices may easily be calculated on the basis that atoms or ions are spheres of fixed diameter—the 'hard sphere' model. The results are usually expressed as a **radius ratio**,  $r_X/r_A$ ; the ratio of the radius (or diameter) of the interstitial atoms, X, to that of the large atoms, A, with which they are in contact. In the



(a)



● Metal atoms

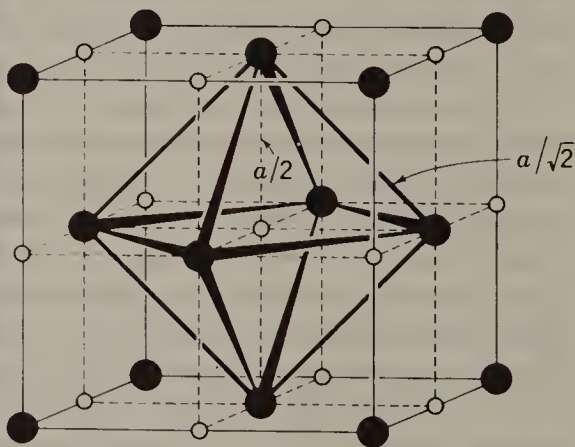
(b) ○ Tetrahedral interstices

**Fig. 1.10.** (a) An atom in a tetrahedral interstitial site,  $r_X/r_A = 0.225$  within the ccp unit cell and (b) geometry of a tetrahedral site, showing the dimensions of the tetrahedron in terms of the unit cell edge length  $a$  (from *The Structure of Metals*, 3rd edn, by C. S. Barrett and T. B. Massalski, Pergamon, 1980).

ccp structure,  $r_X/r_A$  for the tetrahedral sites is 0.225 and for the octahedral sites it is 0.414; in the simple cubic structure,  $r_X/r_A$  for the cubic sites is 0.732. As well as being of different relative sizes, there are different numbers, or proportions, of these interstitial sites. For both the octahedral sites in ccp, and the cubic sites in the simple cubic structure, the proportion is one interstitial site to



(a)



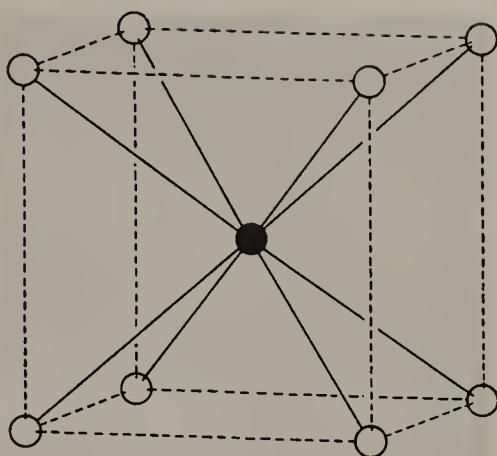
● Metal atoms

(b) ○ Octahedral interstices

**Fig. 1.11.** (a) Atoms or ions in some of the octahedral interstitial sites,  $r_X/r_A = 0.414$  within the ccp unit cell and (b) geometry of an octahedral site, showing the dimensions of the octahedron in terms of the unit cell edge length  $a$  (from Barrett and Massalski, loc. cit.).



(a)

(b) ● : Cs<sup>+</sup>○ : Cl<sup>-</sup>

**Fig. 1.12.** (a) Cubic interstitial site,  $r_X/r_A = 0.732$ , within the simple cube unit cell and (b) the CsCl structure (ions not to scale).

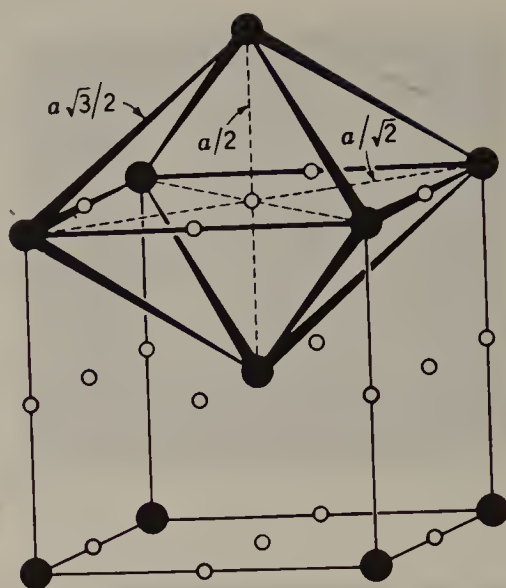
one (large) atom or ion, but for the tetrahedral interstitial sites in ccp the proportion is two sites to one atom. These proportions will be evident from model building or, if preferred, by geometrical reasoning. In the simple cubic structure (Fig. 1.12) there is one interstice per unit cell (at the centre) and eight atoms at each of the eight corners. As each corner atom or ion is 'shared' by seven other cells, there is therefore one atom per cell—a ratio of 1:1. In the unit cell of the ccp structure (Fig. 1.11), the octahedral sites are situated at the midpoints of each edge and in the centre. As each edge is shared by three other cells there are four octahedral sites per cell, i.e. twelve edges divided by four (number shared), plus one (centre). There are also four atoms per cell, i.e. eight corners divided by eight (number shared), plus six faces divided by two (number shared), again giving a ratio of 1:1. The tetrahedral sites in the ccp structure (Fig. 1.10) are situated between a corner and three face-centring atoms, i.e. eight tetrahedral sites per unit cell, giving a ratio of 1:2.

It is a useful exercise to determine also the types, sizes and proportions of interstitial sites in the hcp, bcc and simple hexagonal structures. The hcp structure presents no problem; for the 'hard sphere' model with an interlayer to in-layer atomic ratio of  $\sqrt{2/3}$  (Section 1.2) the interstitial sites are identical to those in ccp. It is only the distribution or 'stacking sequence' of the sites, like that of the close-packed layers of atoms, which is different. In the bcc structure there are octahedral sites at the centres of the faces and mid-parts of the edges (Figs. 1.13(a) and (b)) and tetrahedral sites situated between the centres of the faces and mid-points of each edge (Figs. 1.13(c) and (d)). Note, however, that both the octahedron and tetrahedron of the coordinating atoms do not have edges of equal length. The octahedron, for example, is 'squashed' in one direction and two of the coordinating atoms are closer to the centre of the interstice than are the other four. The radius ratios for the octahedral and tetrahedral interstitial sites are 0.154 and 0.291, respectively.





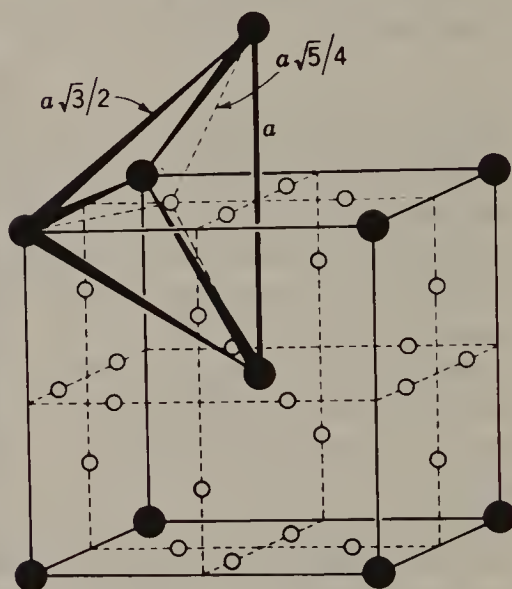
(a)



● Metal atoms  
○ Octahedral interstices



(c)



● Metal atoms  
○ Tetrahedral interstices

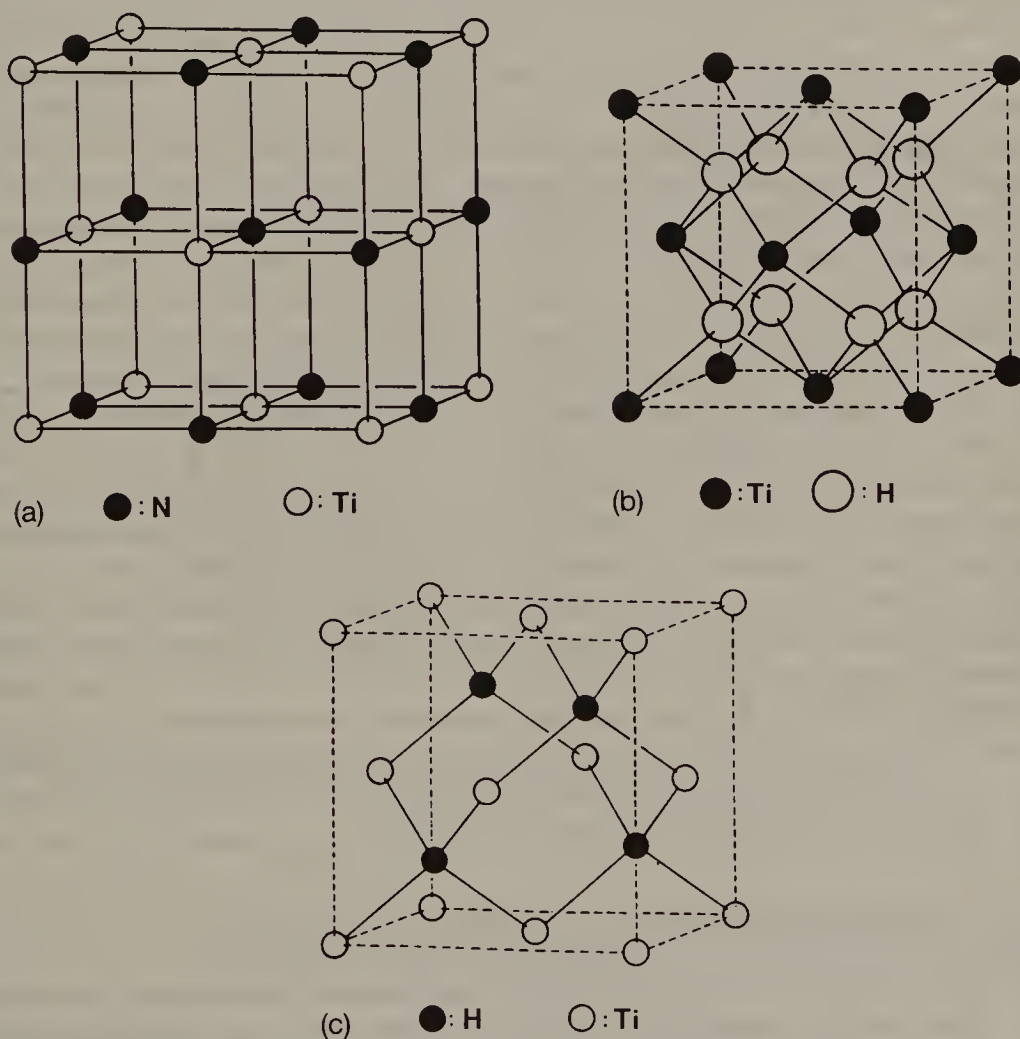
**Fig. 1.13.** (a) Octahedral interstitial sites,  $r_X/r_A = 0.154$ , (b) geometry of the octahedral interstitial sites, (c) tetrahedral interstitial sites  $r_X/r_A = 0.291$ , and (d) geometry of the tetrahedral interstitial sites in the bcc structure. (b) and (d) show the dimensions of the octahedron and tetrahedron in terms of the unit cell edge length  $a$  (from Barrett and Massalski, loc. cit.).

The radius ratios of interstitial sites and their proportions provide a very rough guide in interpreting the crystal structures of some simple, but important, compounds. The first problem, however, is that the 'radius' of an atom is not a



fixed quantity but depends on its state of ionization (i.e. upon the nature of the chemical bonding in a compound) and coordination (the number and type of the surrounding atoms or ions). For example, the atomic radius of Li is about 156 pm but the ionic radius of the  $\text{Li}^+$  cation is about 60 pm. The atomic radius of Fe in the ccp structure, where each atom is surrounded by twelve others, is about 258 pm but that in the bcc structure, where each atom is surrounded by eight others, is about 248 pm—a contraction in going from twelve- to eight-fold coordination of about 4 per cent.

Metal hydrides, nitrides, borides, carbides, etc., in which the radius ratio of the (small) non-metallic or metalloid atoms to the (large) metal atoms is small, provide good examples of interstitial compounds. However, in almost all of these compounds the interstitial atoms are 'oversize' (in terms of the exact radius ratios) and so, in effect, 'push apart' or separate the surrounding atoms such that they are no longer strictly close-packed although their pattern or distribution remains unchanged. For example, Fig. 1.14(a) shows the structure of TiN;



**Fig. 1.14.** (a) TiN structure (isomorphous with  $\text{NaCl}$ ), (b)  $\text{TiH}_2$  (isomorphous with  $\text{CaF}_2$ ) and (c) TiH structure (isomorphous with sphalerite or zinc blende,  $\text{ZnS}$ ) (from *An Introduction to Crystal Chemistry*, 2nd edn, by R. C. Evans, Cambridge University Press, 1964).

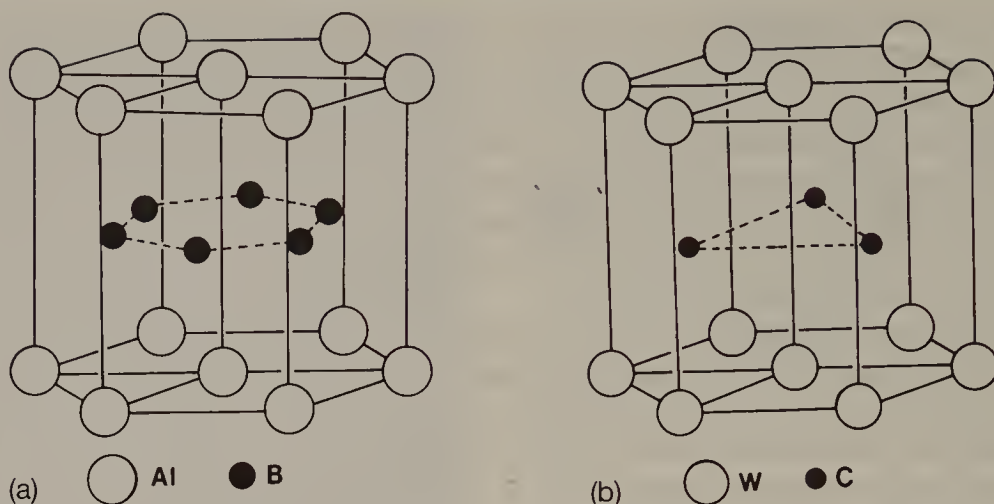


Fig. 1.15. (a)  $\text{AlB}_2$  structure, (b) WC structure.

the nitrogen atoms occupy all the octahedral interstitial sites and, because they are oversized, the titanium atoms are separated but still remain situated at the corners and face centres of the unit cell. This is described as a **face-centred cubic (fcc) array**, rather than a ccp array of titanium atoms, and TiN is described as a **face-centred cubic structure**. This description also applies to all compounds in which some of the atoms occur at the corners and face centres of the unit cell. The ccp structure may therefore be regarded as a special case of the fcc structure in which the atoms are in contact along the face diagonals.

In  $\text{TiH}_2$  (Fig. 1.14(b)), the titanium atoms are also in an fcc array and the hydrogen atoms occupy all the tetrahedral sites, the ratio being of course 1 : 2. In TiH (Fig. 1.14(c)) the hydrogen atoms are again situated in the tetrahedral sites, but only half of these sites are occupied.

Although, as mentioned in Section 1.2, no elements have the simple hexagonal structure in which the close-packed layers are stacked in an AAA... sequence directly on top of one another (Fig. 1.5(a)), the metal atoms in some metal carbides, nitrides, borides, etc., are stacked in this way, the carbon, nitrogen, boron, etc., atoms being situated in some or all of the interstices between the metal atoms. The interstices are halfway between the close-packed (or nearly close-packed) layers and are surrounded or coordinated by six atoms—not, however, in the form of an octahedron but in the form of a triangular prism. In the  $\text{AlB}_2$  structure all these sites are occupied (Fig. 1.15(a)) and in the WC structure only half are occupied (Fig. 1.15(b)).

## 1.7 Some simple ionic and covalent structures

The ideas presented in Section 1.6 above can be used to describe and explain the crystal structures of many simple but important ionic and covalent compounds, in particular many metal halides, sulphides and oxides. Although the metal atoms or cations are smaller than the chlorine, oxygen, sulphur, etc. atoms

or anions, radius ratio considerations are only one factor in determining the crystal structures of ionic and covalent compounds and they are not usually referred to as interstitial compounds even though the pattern or distribution of atoms in the unit cells may be exactly the same. For example, the TiN structure (Fig. 1.14(a)) is isomorphous with the NaCl structure. Similarly, the  $\text{TiH}_2$  structure (Fig. 1.14(b)) is identical to the  $\text{Li}_2\text{O}$  structure and the TiH structure (Fig. 1.14(c)) is isomorphous with ZnS (zinc blende or sphalerite) structure.

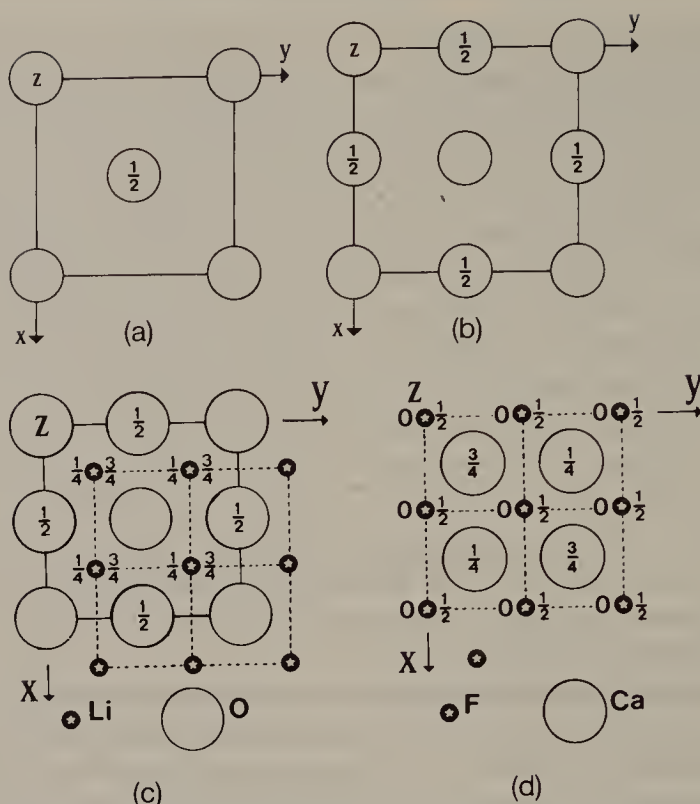
The differences in stacking discussed in Sections 1.2 and 1.6 also explain the different crystal structures or different crystalline polymorphs sometimes shown by one compound. As mentioned above, zinc blende has an fcc structure, the sulphur atoms being stacked in the ABCABC... sequence. In wurtzite, the other crystal structure or polymorph of zinc sulphide, the sulphur atoms are stacked in the hexagonal ABABAB... sequence, giving a hexagonal structure. In both cases the zinc atoms occupy half the tetrahedral interstitial sites between the sulphur atoms. As in the case of cobalt, stacking faults may arise during crystal growth or under conditions of deformation, giving rise to 'mixed' sphalerite-wurtzite structures.

Examples of ionic structures based on the simple cubic packing of anions are CsCl and  $\text{CaF}_2$  (fluorite). In CsCl all the cubic interstitial sites are occupied by caesium cations (Fig. 1.12(b)) but in fluorite only half the sites are occupied by the calcium cations. The resulting unit cell is not just one simple cube of fluorine anions, but a larger cube with a cell side double that of the simple cube and containing therefore  $2 \times 2 \times 2 = 8$  cubes, four of which contain calcium cations and four of which are empty.

The distribution of the small calcium cations in the cubic sites is such that they form an fcc array and the fluorite structure can be represented alternatively as an fcc array of calcium cations with all the tetrahedral sites occupied by fluorine anions. It is identical, in terms of the distribution of ionic sites, to the structure of  $\text{TiH}_2$  or  $\text{Li}_2\text{O}$  (Fig. 1.14(b)), except that the positions of the cations and anions are reversed; hence  $\text{Li}_2\text{O}$  is said to have the *antifluorite* structure. However, these differences, although in principle quite simple, may not be clear until we have some better method of representing the atom/ion positions in crystals other than the sketches (or clinographic projections) used in Figs. 1.10–1.15.

## 1.8 Representing crystals in projection: crystal plans

The more complicated the crystal structure and the larger the unit cell, the more difficult it is to visualize the atom or ion positions from diagrams or photographs of models—atoms or ions may be hidden behind others and therefore not seen. Another form of representation, the **crystal plan** or **crystal projection**, is needed, which shows precisely the atomic or ionic positions in the unit cell. The first step is to specify axes  $x$ ,  $y$  and  $z$  from a common origin and along the sides of the cell (see Chapter 5). By convention the 'back left-hand corner' is chosen as the origin, the  $z$ -axis 'upwards', the  $y$ -axis to the right and



**Fig. 1.16.** Plans of (a) bcc structure, (b) ccp or fcc structure, (c)  $\text{Li}_2\text{O}$  (antifluorite) structure, (d)  $\text{CaF}_2$  (fluorite) structure.

the  $x$ -axis 'forwards', out of the page. The atomic/ionic positions or coordinates in the unit cell are specified as fractions of the cell edge lengths in the order  $x, y, z$ . Thus in the bcc structure the atomic/ionic coordinates are (000) (the atom/ion at the origin) and  $(\frac{1}{2}\frac{1}{2}\frac{1}{2})$  (the atom/ion at the centre of the cube). As all eight corners of the cube are *equivalent positions* (i.e. any of the eight corners can be chosen as the origin), there is no need to write down atomic/ionic coordinates (100), (110), etc.; (000) specifies *all* the corner atoms, and the two-coordinates (000) and  $(\frac{1}{2}\frac{1}{2}\frac{1}{2})$  represent the two atoms/ions in the bcc unit cell. In the fcc structure, with four atoms/ions per unit cell, the coordinates are (000),  $(\frac{1}{2}\frac{1}{2}0)$ ,  $(\frac{1}{2}0\frac{1}{2})$ ,  $(0\frac{1}{2}\frac{1}{2})$ .

Crystal projections or plans are usually drawn perpendicular to the  $z$ -axis, and Fig. 1.16(a) and (b) are plans of the bcc and fcc structure, respectively. Note that only the  $z$  coordinates are indicated in these diagrams; the  $x$  and  $y$  coordinates need not be written down because they are clear from the plan. Similarly, no  $z$  coordinates are indicated for all the corner atoms because all eight corners are equivalent positions in the structure, as mentioned above.

Figure 1.16(c) shows a projection of the antifluorite ( $\text{Li}_2\text{O}$ ) structure; the oxygen anions in the fcc positions and the lithium cations in all the tetrahedral interstitial sites with  $z$  coordinates one-quarter and three-quarters between the oxygen anions are clearly shown. Notice that the lithium cations are in a simple cubic array, i.e. equivalent to the fluorine anions in the fluorite structure. The



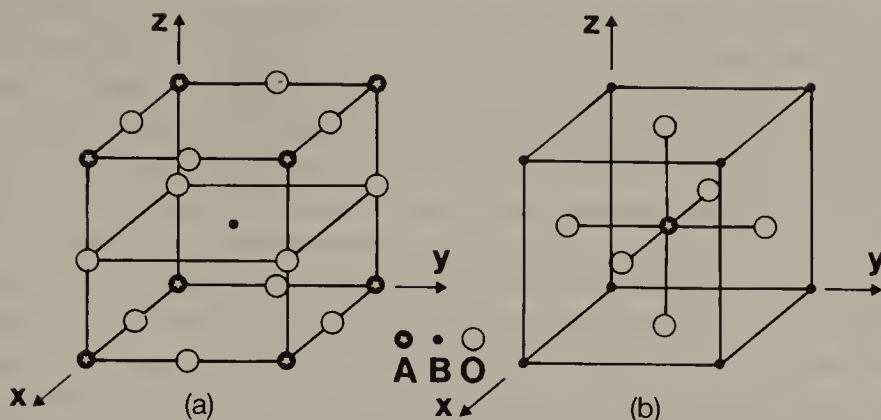


Fig. 1.17. Alternative unit cells of the perovskite  $\text{ABO}_3$  structure.

alternative fluorite unit cell, made up of eight simple cubes (see Section 1.7), is drawn by shifting the origin of the axes in Fig. 1.16(c) to the ion at the  $(\frac{1}{4}\frac{1}{4}\frac{1}{4})$  site and relabelling the coordinates. The result is shown in Fig. 1.16(d).

Sketching crystal plans helps you to understand the similarities and differences between structures; in fact, it is very difficult to understand them otherwise! For example, Fig. 1.17(a) and (b) show the same crystal structure (perovskite,  $\text{CaTiO}_3$ ). They look different because the origins of the cells have been chosen to coincide with different atoms/ions.

## 1.9 Stacking faults and twins

As pointed out in Sections 1.2 and 1.7, the close packing of atoms (in metals and alloys) and anions (in ionic and covalent structures) may depart from the ABCABC... (ccp or fcc) or ABAB... (hcp or hexagonal) sequences: 'nature makes mistakes' and may do so in a number of ways. First, stacking faults may occur during crystallization from the melt or magma: second, they may occur during the solid state processes or recrystallization, phase transitions and crystal growth (i.e. during the heating and cooling of metals and alloys, ceramics and rocks); and third, they may occur during deformation. The mechanisms of faulting have been most widely studied, and are probably most easily understood in the simple case of metals in which there is no (interstitial) distribution of cations to complicate the picture. It is a study of considerable importance in metallurgy because of the effects of faulting on the mechanical and thermal properties of alloys—strength, work-hardening, softening temperatures and so on. However, this should not leave the impression that faulting is of lesser importance in other materials.

Consider first the ccp structure (or, better, have your close-packed raft models to hand). Three layers are stacked ABC (Fig. 1.4). Now the next layer should again be A; instead place it in the B layer position, where it fits equally well into the 'hollows' between the C layer atoms. This is the only alternative choice and the stacking sequence is now ABCB. Now, when we add the next layer we have

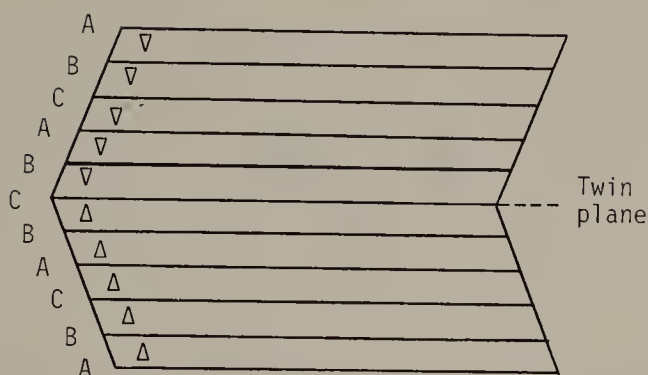
two choices: either to place it in an A layer or in a C layer position. Now continue with our interrupted ABC... stacking sequence. In the first case we have the sequence ABCBABC... and in the second sequence ABCBCABC.... In both cases it can be seen that there are layers which are in an hcp type of stacking sequence—but is there any difference between them, apart from the mere labelling of atom layers? Yes, there is a difference, which may be explained in two ways. If you examine the first sequence you will see that it is as if the mis-stacked B layer had been *inserted* into the ABCABC... sequence and this is called an *extrinsic* stacking fault, whereas in the second case it is as if an A layer had been *removed* from the ABCABC... sequence, and this is called an *intrinsic* stacking fault. However, this explanation, although it is the basis of the names *intrinsic* and *extrinsic*, is not very satisfactory. In order to understand better the distinction between stacking faults of different types (and indeed different stacking sequences in general), a completely different method of representing stacking sequences needs to be used.

You will recall (Section 1.2) that the labels for the layers are arbitrary and that it is the stacking *sequence* which is important; clearly then, some means of representing the sequence, rather than the layers themselves, is required. This requirement has been provided by William Shockley\* and is named after him—the Shockley notation. Shockley proposed that each step in the stacking sequence  $A \rightarrow B \rightarrow C \rightarrow A \dots$  should be represented by a little ‘upright’ triangle  $\Delta$ , and that each step in the stacking sequence,  $C \rightarrow B \rightarrow A \rightarrow C \dots$  should be represented by a little ‘inverted’ triangle  $\nabla$ . Here are some examples, showing both the ABC... etc. type of notation for the layers and the Shockley notation for the sequence of stacking of the layers. Note that the triangles come *between* the close packed layers, representing the stacking *sequence* between them.

A B C A B C A B C	C B A C B A C B A	two fcc sequences
$\Delta \Delta \Delta \Delta \Delta \Delta \Delta \Delta$	$\nabla \nabla \nabla \nabla \nabla \nabla \nabla \nabla$	
A B A B A B A B	C B C B C B C B	two hcp sequences
$\Delta \nabla \Delta \nabla \Delta \nabla \Delta$	$\nabla \Delta \nabla \Delta \nabla \Delta \nabla$	
A B C B A B C	A B C B C A B C	extrinsic (left) and intrinsic (right) stacking faults.
$\Delta \Delta \nabla \nabla \Delta \Delta$	$\Delta \Delta \Delta \nabla \Delta \Delta \Delta$	

Notice that the ccp (or fcc) stacking sequence is represented either by a sequence of upright triangles, or by a sequence of inverted ones—you could of course convert one to the other by simply turning your stack of close-packed layers upside down. However, the distinction is less arbitrary than this. An fcc crystal may grow, or be deformed (as explained below), such that the stacking sequence reverses, as indicated in Fig. 1.18 which shows the close-packed layers ‘edge on’ and both their ABC... etc. and  $\Delta$  or  $\nabla$  labels. Such a crystal is said to be twinned and the twin plane is that at which the stacking sequence reverses.

\* Denotes biographical notes available in Appendix 3.



**Fig. 1.18.** Representation of the close-packed layers of a twinned fcc crystal indicating the atom layers 'edge on'. Notice that the stacking sequence reverses across the twin plane, such that the crystal on one side of the twin plane is a mirror reflection of the other.

Note that the crystal on one side of the twin plane is a mirror reflection of the other, just like the pair of hands in Fig. 4.4(b).

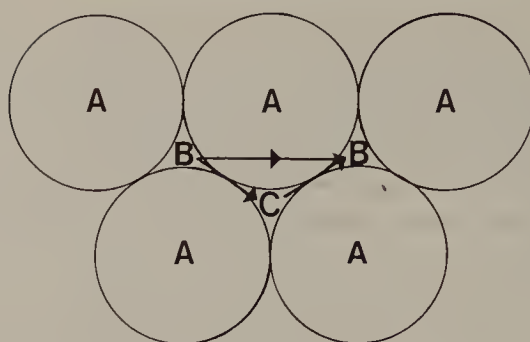
The hcp stacking sequence is represented by alternate upright and inverted triangles—and the sequence is unchanged if the stack of close-packed layers is turned upside down. Hence twinning on the close-packed planes is not possible in the hcp structure—it is as if the backs and palms of your hands were identical, in which case, of course, your right hand would be indistinguishable from your left!

The Shockley notation shows very well the distinction between extrinsic and intrinsic stacking faults; in the former case there are two inversions from the fcc stacking sequence, and in the latter case, one.

So far we have only considered stacking of close-packed layers of atoms and stacking faults in terms of the simple 'hard sphere' model. This model, given the criterion that the atoms should fit into the 'hollows' of the layers below (Fig. 1.4), would indicate that any stacking sequence is equally likely. We know that this is not the case—the fact that (except for the occurrence of stacking faults) the atoms, for example, of aluminium, gold, copper etc. form the ccp structure, and zinc, magnesium etc., form the hcp structure, indicates that other factors have to be considered. These factors are concerned with the minimization of the energies of the nearest and second nearest neighbour configuration of atoms round an atom. It turns out that it is the configuration of the second nearest neighbours which determines whether the most stable structure is ccp or hcp. In one metal (cobalt) and in many alloys (e.g.  $\alpha$ -brass) the energy differences between the two configurations is less marked and varies with temperature. Cobalt undergoes a phase change  $\text{ccp} \rightleftharpoons \text{hcp}$  at  $25^\circ\text{C}$ , but the structure both above and below this temperature is characterized by many stacking faults. In  $\alpha$ -brass the occurrence of stacking faults (and twins) increases with zinc content.

A detailed consideration of the stability of metal structures properly belongs to solid state physics. However, in practice we need to invoke some parameter which provides a measure of the occurrence of stacking faults and twins, and this is provided by the concept of the stacking fault energy (units  $\text{mJ m}^{-2}$ ); it is





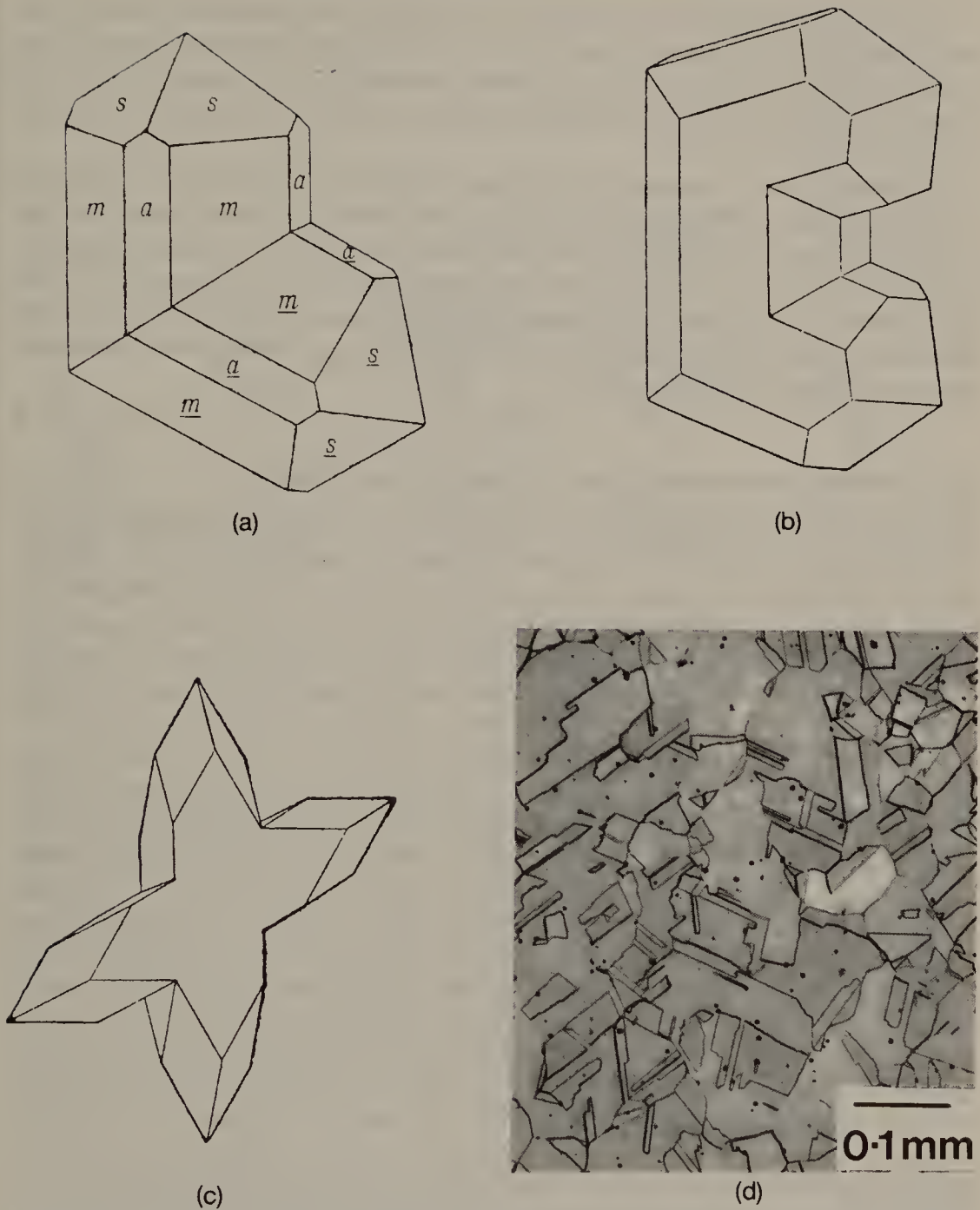
**Fig. 1.19.** On deformation, a B layer atom glides not in a straight line, e.g.  $B \rightarrow B$  (left to right) but in two steps via a C site across the 'saddle points' between the underlying A layer atoms, i.e.  $B \rightarrow C$  (first step),  $C \rightarrow B$  (second step).

simply the increased energy (per unit area) above that of the normal (unfaulted) stacking sequence. Hence the lower the stacking fault energy, the greater the occurrence of stacking faults. On this basis the energy of a twin boundary will be about half that of an intrinsic stacking fault, and the energy of an extrinsic stacking fault will be about double that of an intrinsic stacking fault.

As mentioned above, stacking faults, and the concept of stacking fault energy, play a very important role in the deformation of metals. During deformation—rolling, extrusion, forging and so on—the regular, crystalline arrangement of atoms is not destroyed. Metals do not, as was once supposed, become amorphous. Rather, the deformation is accomplished by the gliding or sliding of close-packed layers over each other. The overall gliding directions are those in which the rows of atoms are close-packed, but, as will also be evident from the models, the layers glide in a zig-zag path, from 'hollow to hollow' and passing across the 'saddle-points' between them. This is shown in Fig. 1.19, which is similar to Fig. 1.4, but re-drawn showing fewer atoms for simplicity. The overall glide direction of the B layer is along a close-packed direction, e.g. left to right, but the path from one B position to the next is over the saddle-points via a C position, as shown by the arrows. But the B layer may stop at a C position (partial slip), in which case we have an (intrinsic) stacking fault (Exercise 1.7). This partial slip, represented by the arrow or vector  $B \rightarrow C$  or  $C \rightarrow B$  is also named after Shockley. Extrinsic stacking faults, twins and the ccp  $\rightarrow$  hcp transformation may be accomplished by mechanisms involving the partial slip of close-packed layers.

The twinned crystal shown diagrammatically in Fig. 1.18 is just one particular example of very general phenomenon, which occurs in crystals with much more complex structures and in which the two parts of the twinned crystal may not simply be related by reflection across the twin plane (reflection twins). Some examples of twinned crystals from geology and metallurgy are shown in Fig. 1.20. The left-right-hand character of the twinned crystal in Fig. 1.20(a) is easily seen; in practice the twins may be interpenetrated and twinning may occur not just in one but in several different planes, as shown in Figs. 1.20(b) and (c). In metals and alloys, the presence of twins may be seen in polished and etched surfaces





**Fig. 1.20.** Examples of twinned crystals: (a) rutile ( $\text{TiO}_2$ ) twinned on a  $\{101\}$  plane (from Rutley's *Elements of Mineralogy*, 25th edn, revised by H. H. Read, George Allen and Unwin Ltd, 1962); (b) multiple twinning in rutile (from *Introduction to Crystallography*, 3rd edn, by F. C. Phillips, Longman, 1977); (c) interpenetrant twin in mercurous chloride ( $\text{HgCl}_2$ ), twin plane  $\{101\}$  (from F. C. Phillips loc. cit.); (d) a photomicrograph of the etched surface of  $\alpha$ -brass showing grain boundaries and (straight-sided) annealing twins, twin plane  $\{111\}$ .

(Fig. 1.20(d)). Old cast brass doorknobs provide a good and homely example. The stacking fault energy of  $\alpha$ -brass ( $\text{Cu} \sim 30\% \text{ Zn}$ ) is very low ( $30 \text{ mJ m}^{-2}$ )

and almost all the grains or crystals will contain recrystallization twins. The corrosive contact of human hands reveals the irregular outlines or boundaries between the grains and also the perfectly straight lines or traces of the twin boundaries which terminate (unlike scratches) at the grain boundaries, as shown in Fig. 1.20(d).

Twinning is very common in minerals, frequently occurring as a result of phase transitions during cooling. They may be observed, like the brass, on the polished surfaces of minerals, where they may give rise to beautiful iridescent textures as a result of the diffraction and interference of light (Chapter 7). They may be more readily seen in petrographic thin sections under the polarizing light microscope. For the petrologist they constitute one of the most important means of mineral identification.

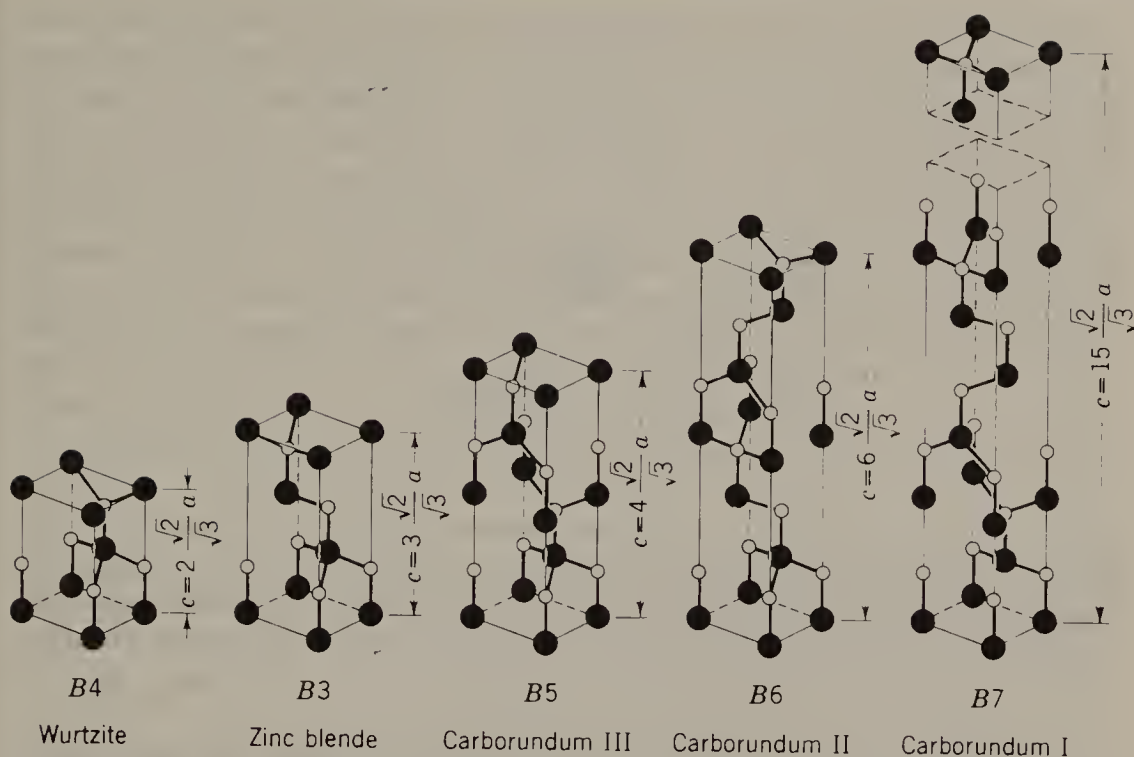
## 1.10 Some more complex crystal structures

The newcomer to crystallography is often dismayed by the immensity of all the different crystal structures—not only inorganic but also organic. The subject may seem worse than French vocabulary! The subject is certainly immense and only a fraction of it can be learnt. However, it is not arbitrary and a knowledge of the rules or criteria determining the simplest structures, described in Sections 1.2–1.7 above, are the stepping stones to an understanding of more complex structures.

Consider, for example, the crystal structures which consist of close-packed layers of large atoms or ions, with the smaller atoms or ions occupying some or all of the tetrahedral interstitial sites. Zinc blende and wurtzite are two such structures (Section 1.7) which are drawn in Fig. 1.21 so as to emphasize the  $\Delta\nabla\Delta\dots$  stacking of the S (or Zn) atoms in wurtzite and the  $\Delta\Delta\Delta\dots$  stacking of the S (or Zn) atoms in zinc blende. Many carbides also possess such close-packed structures, with the carbon atoms occupying the tetrahedral interstitial sites and the metal or metalloid atoms stacked in various combinations of  $\Delta\nabla\Delta\dots$  and  $\Delta\Delta\Delta\dots$  sequences. Five forms of carborundum, SiC, are shown in Fig. 1.21, in which the silicon atoms are represented as solid spheres and the carbon atoms as open spheres. As can be seen, two of these structures, B4 and B3, are isomorphous with wurtzite and zinc blende, respectively. The other forms of carborundum have more complex stacking sequences, resulting in longer unit cell repeat distances. For example, the stacking sequence of the silicon atoms in carborundum III (B5) is (reading up) ABACABAC... giving a four-layer repeat distance. In the Shockley notation this is represented by  $\Delta\nabla\nabla\Delta\Delta\nabla\nabla\dots$ , i.e. by inversions in the stacking sequence every two layers, not every layer as in B4, the wurtzite structure.

Silicates—which constitute by far the most important minerals in the Earth's crust—are based on the different ways in which  $\text{SiO}_4$  tetrahedra\* may be joined

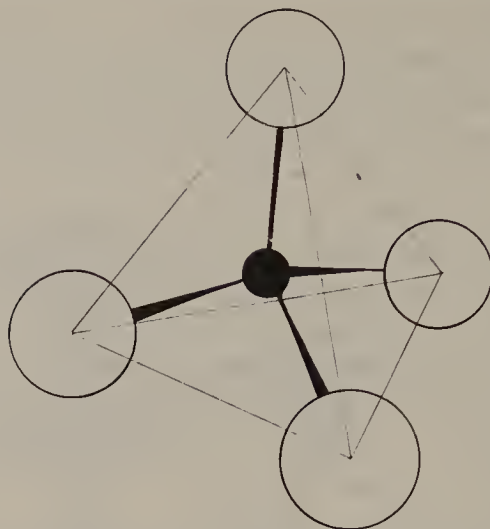
\* The  $\text{SiO}_4$  tetrahedra may be referred to more generally as Si–O tetrahedra since, as described in sub-sections (a)–(g), the silicon–oxygen ratio depends on how they are linked.



**Fig. 1.21.** Five common tetrahedral structure types (after E. Parthe, *Crystal Chemistry of Tetrahedral Structures*, Gordon and Breach, New York, 1964, reproduced from *The Structure of Metals*, 3rd edn, C. S. Barrett and T. B. Massalski, Pergamon, 1980).

together, each tetrahedron being made up of four oxygen anions with the silicon cation in the tetrahedral interstice in the centre (Fig. 1.22). Silicate chemistry is based on the linking of the  $\text{SiO}_4$  tetrahedra, i.e. whether they occur separately, or whether they are linked by common oxygen anions to form chains, rings, sheets or complete frameworks. This provides the initial basis for the classification of silicate structures. If the Si–O bond is considered to be purely ionic, there are four positive charges associated with each silicon cation and two negative charges associated with each oxygen anion; hence there are four net negative charges associated with each  $\text{SiO}_4$  tetrahedron. The ‘charge balance’ in silicates may be achieved in seven possible ways (see Fig. 1.23):

- Separate  $\text{SiO}_4$  tetrahedra (*nesosilicates*): the charge balance (four net negative charges) is achieved with metal cations, e.g.  $\text{Mg}^{2+}$ ,  $\text{Fe}^{2+}$ , which also link the tetrahedra together. Typical minerals are forsterite,  $\text{Mg}_2(\text{SiO}_4)$ , or fayalite,  $\text{Fe}_2(\text{SiO}_4)$ , the end-members of the olivine group,  $\text{MgFe}(\text{SiO}_4)$ .
- Two tetrahedra linked together sharing one oxygen anion (*sorosilicates*): the Si:O ratio is now  $\text{Si}_2\text{O}_7$  giving six net negative charges which are balanced with metal cations. Typical minerals are melilite,  $\text{Ca}_2\text{Mg}(\text{Si}_2\text{O}_7)$ , or hemimorphite,  $\text{Zn}_4(\text{OH})\text{H}_2\text{O}(\text{Si}_2\text{O}_7)$ .
- Three or more tetrahedra linked together to form rings, each tetrahedron



**Fig. 1.22.** A perspective of the  $\text{SiO}_4$  tetrahedron. The oxygen anions at the corners of the tetrahedron are nearly close packed, as shown in the models, e.g. in Fig. 1.7 (the radius of the oxygen anion,  $r_n = 0.132$  nm and that of the silicon cation,  $r_x = 0.039$  nm, give a radius ratio,  $r_x/r_n = 0.296$ , slightly greater than the ideal value  $r_x/r_n = 0.225$ , Fig. 1.10).

sharing two oxygen anions (*cyclosilicates*): the Si:O ratio is  $\text{Si}_n\text{O}_{3n}$  where  $n$  is the number of tetrahedra in the ring. A typical mineral is beryl, with a ring of six tetrahedra,  $\text{Be}_3\text{Al}_2(\text{Si}_6\text{O}_{18})$ .

- (d) Many tetrahedra linked together to form single chains (*inosilicates*): each tetrahedron shares two oxygen anions, as in the ring structures above, and which therefore give rise to the same Si:O ratio. This is the basis of the group of minerals called the pyroxenes. Typical examples are enstatite,  $\text{Mg}_2(\text{Si}_2\text{O}_6)$ , or diopside,  $\text{CaMg}(\text{Si}_2\text{O}_6)$ .
- (e) Tetrahedra linked together to form double chains (*inosilicates*), each tetrahedron sharing alternately two and three oxygen anions, giving the Si:O ratio  $\text{Si}_4\text{O}_{11}$ . This is the basis of the group of minerals called the amphiboles. Typical examples are anthophyllite,  $\text{Mg}_7(\text{OH})_2(\text{Si}_4\text{O}_{11})_2$ , or tremolite,  $\text{Ca}_3\text{Mg}_5(\text{OH})_2(\text{Si}_4\text{O}_{11})_2$ .
- (f) Tetrahedra linked together to form sheets (*phyllosilicates*), each tetrahedron sharing three oxygen anions giving the Si:O ratio  $\text{Si}_2\text{O}_5$ . This is the basis of the micas, chlorites and the clay minerals.
- (g) Tetrahedra linked together such that all the oxygen anions are shared giving a three-dimensional framework (*tectosilicates*). The Si:O ratio is now  $\text{SiO}_2$  and there is an overall charge balance without the necessity of any linking cations.

Figure 1.23 shows the arrangements of  $\text{SiO}_4$  tetrahedra in these seven silicate structures. However, having established the basic pattern there are very important complications both in the chemistry and the arrangements of the tetrahedra



which must not be overlooked. In all the silicates, and in the chain, sheet and framework silicates in particular, the silicon in the centre of the tetrahedron can be substituted by aluminium—a trivalent rather than a tetravalent ion. For each such substitution an additional positive charge by way of a ‘linking cation’ is required. All sheet silicates or phyllosilicates show such substitution to a greater or lesser extent, for example phlogopite in which one silicon is replaced by one aluminium cation giving the formula  $\text{KMg}_3(\text{OH})_2(\text{Si}_3\text{AlO}_{10})$ . In framework silicates (tectosilicates), substitution gives rise to an important new class of minerals—the feldspars, the most abundant minerals in the Earth’s crust, e.g. albite,  $\text{Na}(\text{Si}_3\text{AlO}_8)$ , or orthoclase,  $\text{K}(\text{Si}_3\text{AlO}_8)$  (one silicon cation substituted), or anorthite,  $\text{Ca}(\text{Si}_2\text{Al}_2\text{O}_8)$  (two silicon cations substituted).

With respect to the arrangements of the tetrahedra, one example—that of the inosilicates—will suffice to show the principles involved. Figure 1.24 shows nine possible patterns (a)–(i) or conformations of the (unbranched) single chains, giving rise to different repeat distances as indicated: (a) (the simplest—known as zweier single chains because there are two tetrahedra in the repeat distance) is that for diopside and enstatite; (b) (drier single chains with three tetrahedra in the repeat distance) is that for wollastonite,  $\text{Ca}_3(\text{Si}_3\text{O}_9)$ , and so on.

Clearly, there are also many possible arrangements of the tetrahedra in the cyclosilicates, phyllosilicates and tectosilicates, and it is these which give rise (in part) to the many structural differences in silicate minerals. For example, in the tectosilicates the three different crystallographic forms of silica—quartz, tridymite and cristobalite—simply correspond to different ways in which the  $\text{SiO}_4$  tetrahedra are linked together, and the  $\alpha$  and  $\beta$  forms of these structures (with slightly different densities) arise from small relative rotations of the tetrahedra.

## Exercises

- 1.1 Draw crystal plans of the perovskite structure shown in Fig. 1.17, relocate the origin of one cell, relabel the ionic coordinates and show that these two cells do represent the same crystal structure.
- 1.2 With reference to Figs. 1.10(b), 1.11(b), 1.13(b) and 1.13(d) (or your crystal models) check the radius ratios stated in the text for the tetrahedral and octahedral interstitial sites in the ccp and bcc structures.  
(*Hint:* These figures show the dimensions of the coordination polyhedra in terms of  $a$ , the cell edge lengths.)
- 1.3 Examine your crystal models and find:
  - (a) the number of different (non-parallel) close-packed planes and close-packed directions in the ccp and hcp structures; and
  - (b) the number of closest-packed planes and close-packed directions in the bcc structure.
- 1.4 In the deformation of ccp and bcc metals, slip generally occurs on the close- or closest-packed planes and in close-packed directions. Each combination of slip plane and direction is called a **slip system**. How many slip systems are there in these metals?

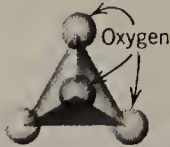
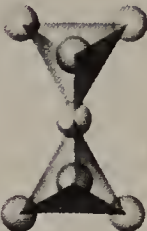



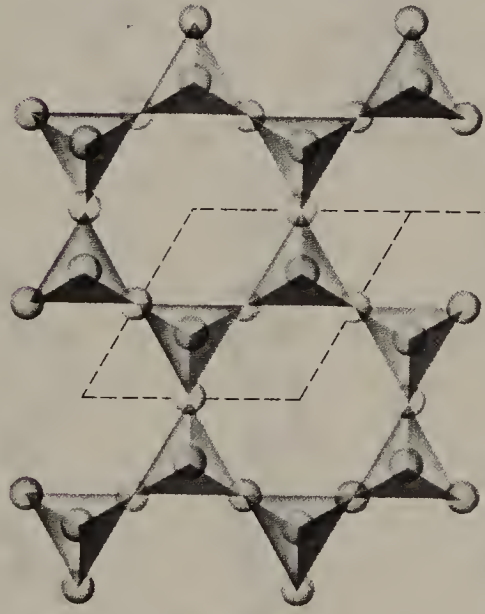

Class	Arrangement of SiO <sub>4</sub> tetrahedra (central Si <sup>4+</sup> not shown)	Unit composition	Mineral example
(a) Nesosilicates		(SiO <sub>4</sub> ) <sup>4-</sup>	Olivine, (Mg, Fe) <sub>2</sub> SiO <sub>4</sub>
(b) Sorosilicates		(Si <sub>2</sub> O <sub>7</sub> ) <sup>6-</sup>	Hemimorphite, Zn <sub>4</sub> Si <sub>2</sub> O <sub>7</sub> (OH)•H <sub>2</sub> O
(c) Cyclosilicates		(Si <sub>6</sub> O <sub>18</sub> ) <sup>12-</sup>	Beryl, Be <sub>3</sub> Al <sub>2</sub> Si <sub>6</sub> O <sub>18</sub>
(d) Inosilicates (single chain)		(Si <sub>2</sub> O <sub>6</sub> ) <sup>4-</sup>	Pyroxene e.g. Enstatite, MgSiO <sub>3</sub>

Fig. 1.23. The arrangements of the SiO<sub>4</sub> tetrahedra and Si:O ratios in the seven main types of silicate structures, with examples of typical minerals (from *Manual of Mineralogy*, 21st edn,

(e) Inosilicates (double chain)		$(\text{Si}_4\text{O}_{11})^{6-}$	Amphibole e.g. Anthophyllite, $\text{Mg}_7\text{Si}_8\text{O}_{22}(\text{OH})_2$
(f) Phyllosilicates		$(\text{Si}_2\text{O}_5)^{2-}$	Mica e.g. Phlogopite, $\text{KMg}_3(\text{AlSi}_3\text{O}_{10})(\text{OH})_2$
(g) Tectosilicates		$(\text{SiO}_2)^0$	High cristobalite, $\text{SiO}_2$



**Fig. 1.24.** The arrangements of the tetrahedra in the inosilicates. They are described (in German) according to the number of the tetrahedra in the repeat distance: a (zweier); b (dreier); c (vierer); d (fünfer); e (sechser); f (siebener); g (neuner); h (zwölfer); i (24er) (from *Structural Chemistry of Silicates* by F. Liebau, Springer-Verlag, 1985).



- 1.5 With reference to Fig. 1.5(b), calculate the  $c/a$  ratio for the hcp structure.  
(*Hint:  $a$  is equal to  $d$ , the atomic diameter and edge length of the tetrahedron, and  $c$  is twice the height of the tetrahedron.*)
- 1.6 Draw a plan or crystal projection of the hcp structure perpendicular to the  $z$ - or  $c$ -axis. Assign axes  $x$  and  $y$  (at  $120^\circ$  to each other) and outline a primitive hexagonal cell (one atom at each corner and one within the cell). What are the atomic coordinates of the atoms in the cell?
- 1.7 Sketch a sequence of close-packed layers stacked in the ABCABC... sequence as shown in the lower half of Fig. 1.18. Fault an A layer in this sequence such that it becomes a B layer; in so doing, all the layers above are shifted together and need to be relabelled, i.e.  $B \rightarrow C$ ,  $C \rightarrow A$ ,  $A \rightarrow B$  and so on. What type of stacking fault—intrinsic or extrinsic—is produced? Now fault the next layer above and repeat the relabelling of the layers above that. What type of fault is produced? What faulting sequence would you need to carry out to produce (a) a twin (as in Fig. 1.18) and (b) the hcp stacking sequence?
- 1.8 Determine the stacking sequence of the atoms or ions represented by the solid circles in the structures B6 and B7 (carborundum II and I) using both the ABC... and Shockley notations.  
(*Hint: in carborundum I, the sequence, which is omitted to save space, is (reading up) CBABCBA.*)

---

# Two-dimensional patterns, lattices and symmetry

## 2.1 Approaches to the study of crystal structures

In Chapter 1 we developed an understanding of simple crystal structures by first considering the ways in which atoms or ions could pack together and then introducing smaller atoms or ions into the interstices between the larger ones. This is a pragmatic approach as it not only provides us with an immediate and straightforward understanding of the atomic/ionic arrangements in some simple compounds, but also suggests the ways in which more complicated compounds can be built up.

However, it is not a systematic and rigorous approach, as all the possibilities of atomic arrangements in all crystal structures are not explored. The rigorous, and essentially mathematical, approach is to analyse and classify the geometrical characteristics of quite general two-dimensional patterns and then to extend the analysis to three dimensions to arrive at a completely general description of all the patterns to which atoms or molecules or groups of atoms or molecules might conform in the crystalline state.

These two distinct approaches—or strands of crystallographic thought—are apparent in the literature of the nineteenth and early twentieth centuries. In general, it was the metallurgists and chemists, such as Tammann\* and Pope\*, who were the pragmatists, and the theoreticians and geometers, such as Fedorov\* and Schoenflies\*, who were the analysts. It might be thought that the analytical is necessarily superior to the pragmatic approach because its generality and comprehensiveness provides a much more powerful starting point for progress to be made in the discovery and interpretation of the crystal structures of more and more complex substances. But this is not so. It was, after all, the simple models of sodium chloride and zinc blende of Pope (such as we also constructed in Chapter 1) that helped to provide the Braggs\* with the necessary insight into crystal structures to enable them to make their great advances in the interpretation of X-ray diffraction photographs. In the same way, 40 years later, the discovery of the structure of DNA by Watson and Crick was based as much upon structural and chemical knowledge and intuition, together with model building, as upon formal crystallographic theory.

However, a more general appreciation of the different patterns into which atoms and molecules may be arranged is essential, because it leads to an understanding of the important concepts of symmetry, motifs and lattices. The

\* Denotes biographical notes available in Appendix 3.

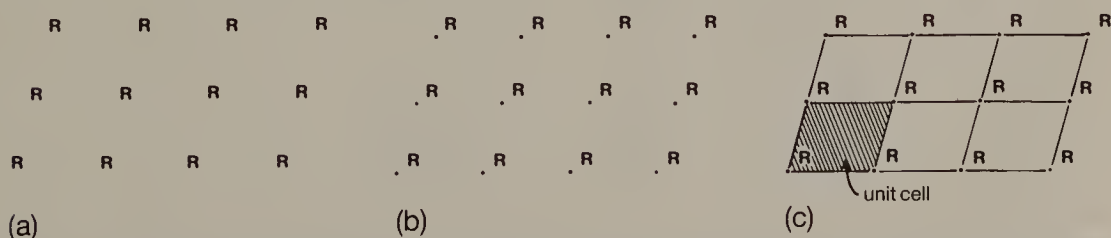
topic need not be pursued rigorously—in fact it is unwise to do so because we might quickly ‘lose sight of the wood for the trees!’ The essential ideas can be appreciated in two dimensions, the subject of this chapter. The extension to three dimensions (Chapters 3 and 4) which relates to ‘real crystal structures’, should then present no conceptual difficulties.

## 2.2 Two-dimensional patterns and lattices

Consider the pattern of Fig. 2.1(a), which is made up of the letter **R** repeated indefinitely. What does **R** represent? Anything you like—a ‘two-dimensional molecule’, a cluster of atoms or whatever. Representing the ‘molecule’ as an **R**, an *asymmetric* shape, is in effect representing an *asymmetric* molecule. We shall discuss the different types or elements of symmetry in detail in Section 2.3 below, but for the moment our general everyday knowledge is enough. For example, consider the symmetry of the letters **RMS**. **R** is asymmetrical. **M** consists of two equal sides, each of which is a reflection or mirror image of the other, there is a **mirror line** of symmetry down the centre indicated by the letter m, thus **M** <sub>← m</sub>. There is no mirror line in the **S**, but if it is rotated 180° about a point in its centre, an identical **S** appears; there is a **two-fold rotation axis** usually called a **diad axis** at the centre of the **S**. This is represented by a little lens-shape at the axis of rotation: **S**.

In Fig. 2.1(a) **R**, the repeating ‘unit of pattern’ is called the **motif**. These motifs may be considered to be situated at or near the intersections of an (imaginary) grid. The grid is called the **lattice** and the intersections are called **lattice points**.

Let us now draw this underlying lattice in Fig. 2.1(a). First we have to decide where to place each lattice point in relation to each motif: anywhere will do—above, below, to one side, in the ‘middle’ of the motif—the only requirement is that the *same* position with respect to the motif is chosen every time. We shall choose a position a little below the motif, as shown in Fig. 2.1(b). Now there are an infinite number of ways in which the lattice points may be ‘joined up’ (i.e. an infinite number of ways of drawing a lattice or grid of lines through lattice points). In practice, a grid is usually chosen which ‘joins up’ adjacent lattice points to give the lattice as shown in Fig. 2.1(c), and a unit cell of the lattice may also be outlined. Clearly, if we know (1) the size and shape of the



**Fig. 2.1.** (a) A pattern with the motif **R**, (b) with the lattice points indicated and (c) the lattice and a unit cell outlined.

unit cell and (2) the motif which each lattice point represents, including its orientation with respect to the lattice point, we can draw the whole pattern or build up the whole structure indefinitely. The unit cell of the lattice and the motif therefore define the whole pattern or structure. This is very simple: but observe an importance consequence. Each motif is identical and, for an infinitely extended pattern, the environment (i.e. the spatial distribution of the surrounding motifs, and their orientation) around each motif is identical. This provides us with the definition of a lattice (which applies equally in two and three dimensions): *a lattice is an array of points in space in which the environment of each point is identical*. Again it should be stressed that by environment we mean the spatial distribution and orientation of the surrounding points.

Like all simple definitions (and indeed ideas), this definition of a lattice is often not fully appreciated; there is, to use a colloquial expression, 'more to it than meets the eye!' This is particularly the case when we come to three-dimensional lattices (Chapter 4), but, for the two-dimensional case, consider the patterns of points in Fig. 2.2 (which should be thought of as extending infinitely). Of these only (a) and (d) constitute a lattice; in (b) and (c) the points are certainly in a *regular* array, but the surroundings of each point are *not* all identical.

Figures 2.2(a) and (d) represent two two-dimensional lattice types, named **oblique** and **rectangular**, respectively, in view of the shapes of their unit cells. But what is the distinction between the oblique and rectangular lattices? Surely the rectangular lattice is just a special case of the oblique, i.e. with a  $90^\circ$  angle?

The distinction arises from different symmetries of the two lattices, and requires us to extend our everyday notions of symmetry and to classify a series of symmetry elements. This precise knowledge of symmetry can then be applied

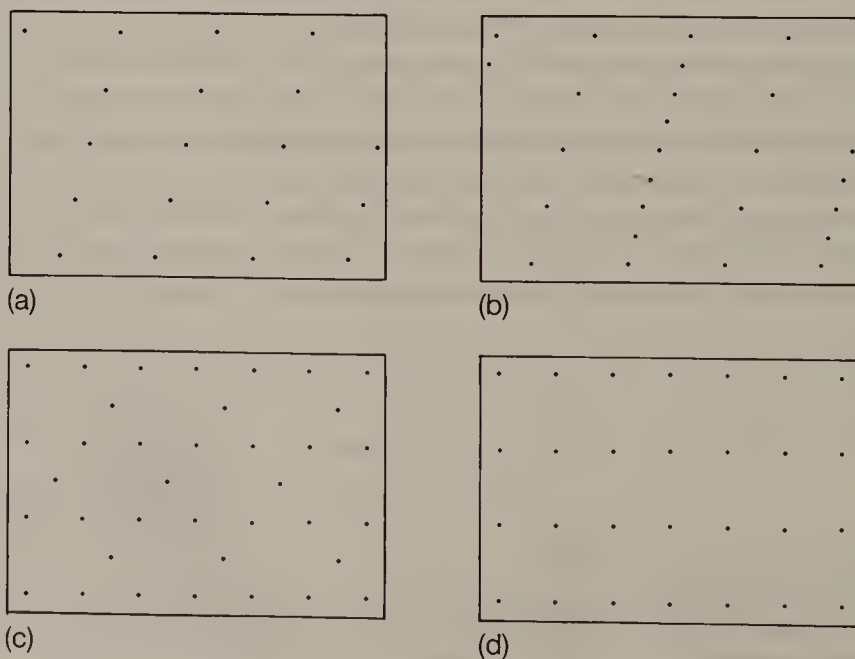


Fig. 2.2. Patterns of points. Only (a) and (d) constitute lattices.



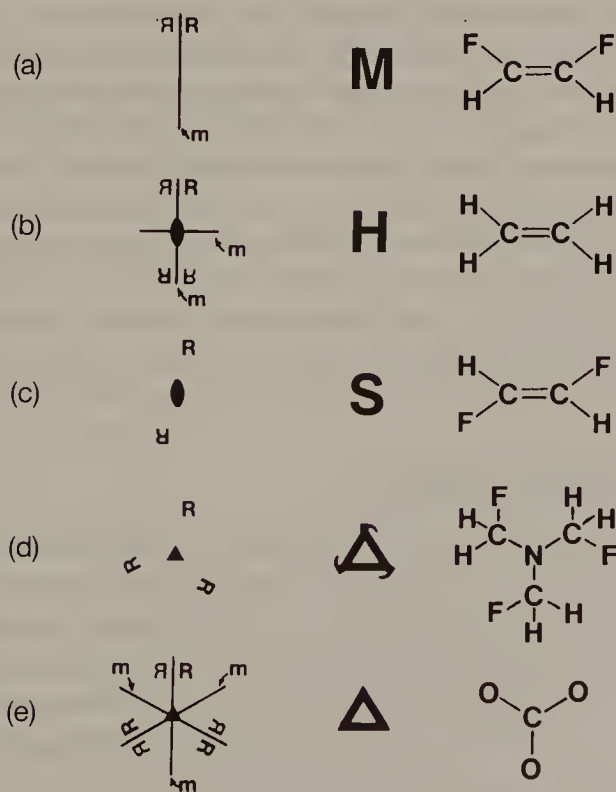
to both the motif and the lattice and will show that there are a limited number of patterns with different symmetries (only seventeen) and a limited number of two-dimensional lattices (only five).

## 2.3 Two-dimensional symmetry elements

The clearest way of developing the concept of symmetry is to begin with an asymmetrical 'object'—say the **R** of Fig. 2.1—then to add successively mirror lines and axes of symmetry and to see how the **R** is repeated to form different patterns or groups. The different patterns or groups of **R**s which are produced correspond, of course, to objects or projections of molecules (i.e. 'two-dimensional molecules') with different symmetries which are not possessed by the **R** alone.

For example, consider Fig. 2.3(a). 'Right-' and 'left-'handed **R**s are reflected in the 'vertical' mirror line between them. This pair of **R**s has the same mirror symmetry as the letter **M**, or the projection of the *cis*-difluoroethene molecule. Now add another 'horizontal' mirror line as in Fig. 2.3(b). A group of four **R**s—two right and two left handed—is produced. This group has the same symmetry as the single letter **H** or the projection of the ethene molecule.

The **R** may also be repeated with a diad (two-fold rotation) axis, as in Fig.



**Fig. 2.3.** Generation of motifs (a)–(e) with different symmetries (five out of the ten plane point groups) and examples of two-dimensional symbols and (right) molecules and ions. (a) *Cis*-difluoroethene, (b) ethene, (c) *trans*-difluoroethene, (d) tri(fluoroalkyl)ammonia molecule and (e) carbonate ion.

2.3(c). The two **R**s—both right handed—have the same symmetry as the letter **S** as we saw above, or the *trans*-difluoroethene molecule. Now look back to the group of **R**s in Fig. 2.3(b); notice that they are also related by a diad (two-fold rotation axis) at the intersection of the mirror lines: the action of reflecting the **R**s across two perpendicular mirror lines ‘automatically’ generates the two-fold symmetry as well. This effect, where the action of one symmetry element generates another, is quite general, as we shall see below.

Mirror lines and diad axes of symmetry are just two of the symmetry elements in two dimensions. In addition, there are three-fold, rotation or **triad** axes (represented by a little triangle ▲), four-fold rotation or **tetrad** axes (represented by a little square ■) and six-fold rotation or **hexad** axes (represented by a little hexagon ●). Figure 2.3(d) shows the **R** related by a triad (three-fold) axis. This paper windmill and the projection of the trifluoralkylammonia molecule also have this same symmetry. Now add a ‘vertical’ mirror line as in Fig. 2.3(e). Three more (left-handed) **R**s are generated, and at the same time, the **R**s are mirror related not just in the vertical line but also in two lines inclined at 60° as shown, another example of additional symmetry elements—in this case mirror lines—being automatically generated.

This procedure—of generating groups of **R**s which represent motifs with different symmetries—may be repeated with tetrad (four-fold) and hexad (six-fold) rotation axes of symmetry. Altogether there are ten such symmetries in two dimensions or **ten plane point groups**\*, so called because all the symmetry elements pass through one point. The ten plane point groups are labelled with ‘shorthand’ symbols which indicate the symmetry elements present; *m* for one mirror plane, *mm* or *mm2* for two mirror planes (plus diad), 2 for a diad, 3 for a triad, *3m* for a triad and three mirror planes and so on. The assiduous reader should complete Fig. 2.3 for himself or herself including, as well as the **R**s, common objects and molecules with the appropriate symmetries. In addition, it will become obvious why it is not possible to have five-, seven-, eight-, etc., fold rotation axes of symmetry. A five-fold ‘pentad’ axis, for example, would require five lattice points to be equally arranged about the axis, but such an arrangement of points could not be put together to form a lattice. Try it and see!

## 2.4 The five plane lattices

Having examined some of the types of symmetry which a two-dimensional motif can possess (Fig. 2.3), we can now determine how many two-dimensional or plane lattices there are. The important criterion is this: the lattice itself must possess at least the symmetry of the motif; it may possess more symmetry elements but it cannot possess fewer. Or, put another way, the symmetry of the arrangement of lattice points around each lattice point must be the same as, or

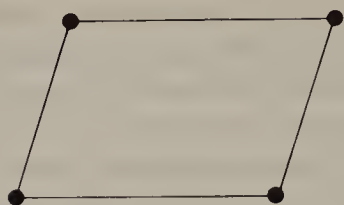
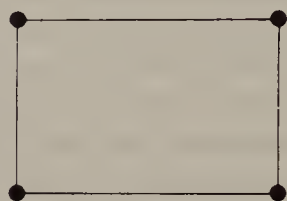
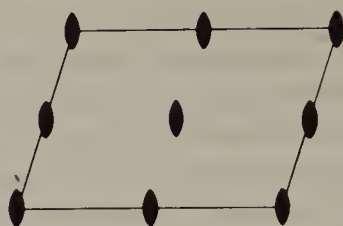
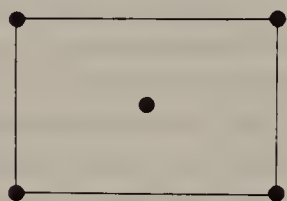
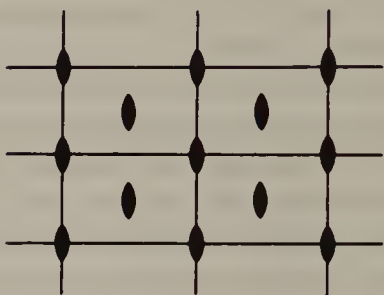
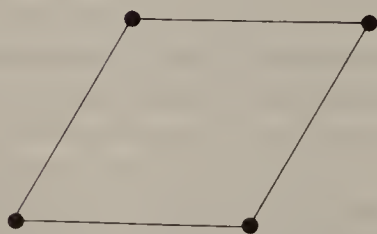
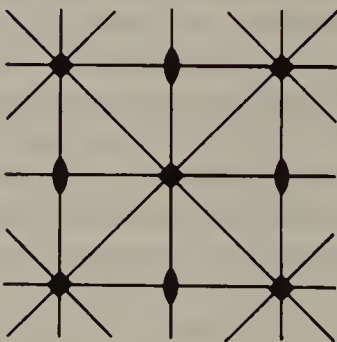
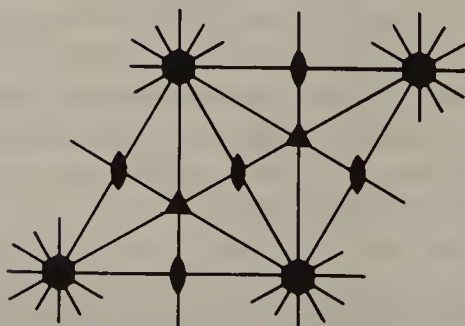
\* This is only true for the case of repeating patterns. Separate objects in nature may have five-fold (pentagonal) symmetry (a starfish for example), or higher order axes of symmetry, but these do not occur in repeating patterns. The ten plane point groups which occur in plane patterns as discussed below are 1 (asymmetric), 2, 3, 4, 6, *m*, *mm*, *3m*, *4m*, and *6m*.

greater than, the symmetry of the motif. A few examples will make this clear. Consider the rectangular lattice of Fig. 2.2(d). Through each lattice point and halfway between there are vertical and horizontal lines of symmetry intersecting at diad axes. The motif of Fig. 2.3(b) also has this symmetry and therefore it follows that a pattern with such a motif will have a rectangular lattice. The motif of Fig. 2.3(a) has one mirror line, and a pattern with this motif will also have a rectangular lattice—in this case the symmetry of the lattice is greater than that of the motif. Note, on the other hand, that the motifs with one or two mirror lines of symmetry (Figs. 2.3(a) and (b)) cannot occur in a pattern with the oblique lattice because the oblique lattice does not itself have any mirror lines of symmetry.

This procedure can be applied to all the other motifs. For example, a motif with tetrad (four-fold) symmetry applies to a pattern with a square lattice and a motif with triad (three-fold) symmetry (Figs 2.3(d) and (e)) and hexad (six-fold) symmetry will apply to a pattern with an hexagonal lattice. Altogether, five two-dimensional or plane lattices may be worked out, as shown in Fig. 2.4(a). They are described by the shapes of the unit cells which are drawn between lattice points—oblique *p*, rectangular *p*, rectangular *c* (which is distinguished from rectangular *p* by having an additional lattice point in the centre of the cell), square *p* and hexagonal *p*. Notice again that additional symmetry elements are generated 'in between' the lattice points as shown in Fig. 2.4(a) (right). For example, in the square lattice there is a tetrad at the centre of the cell, diads halfway along the edges and vertical, horizontal and diagonal mirror lines as well as the tetrads situated at the lattice points.

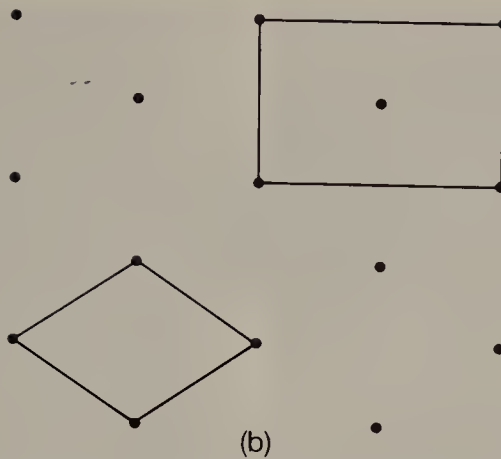
All two-dimensional patterns must be based upon one of these five plane lattices; no others are possible. This may seem very surprising—surely other shapes of unit cells are possible? The answer is 'yes', a large number of unit cell shapes are possible, but the pattern of lattice points which they describe will always be one of the five of Fig. 2.4(a). For example, the rectangular *c* lattice may also be described as a rhombic *p* or diamond *p* lattice, depending upon which unit cell is chosen to 'join up' the lattice points (Fig. 2.4(b)). These are just two alternative descriptions of the *same* arrangement of lattice points. So the choice of unit cell is arbitrary: *any* four lattice points can be joined up to form a unit cell. In practice we take a sensible course and mostly choose a unit cell that is as small as possible—or 'primitive' (symbol *p*)—which does not contain other lattice points within it. Sometimes a larger cell is more useful because the axes joining up the sides are at 90°. Examples are the rhombic or diamond lattice which is identical to the rectangular centred lattice described above and, to take an important three-dimensional case, the cubic cell (Fig. 1.6(c)) which is used to describe the ccp structure in preference to the primitive rhombohedral cell (Fig. 1.7(c)).

Now as there are ten point group symmetries which a motif can possess (five of which are shown in Fig 2.3), it may be thought that there are therefore only ten different types of two-dimensional patterns, distributed among the five plane lattices. However, there is a complication: the combination of a point group

The oblique  $p$ -latticeThe rectangular  $p$ -latticeThe rectangular  $c$ -latticeThe square  $p$ -latticeThe hexagonal  $p$ -lattice

(a)

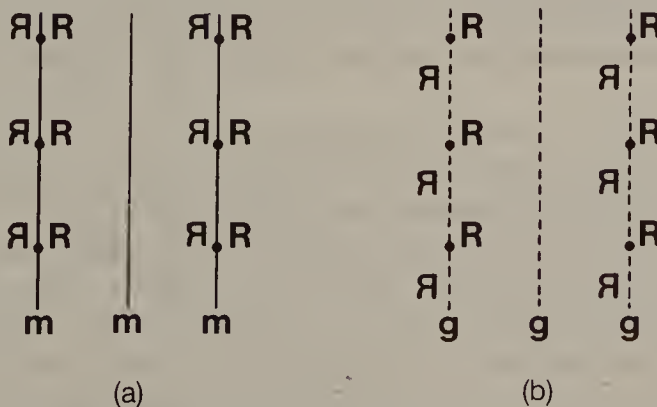




**Fig. 2.4.** (a) Unit cells of the five plane lattices (left), showing (right) the symmetry elements present (from *Essentials of Crystallography*, by D. McKie and C. McKie, Blackwell, 1986). (b) The rectangular *c* lattice, showing the alternative primitive (rhombic *p* or diamond *p*) unit cell.

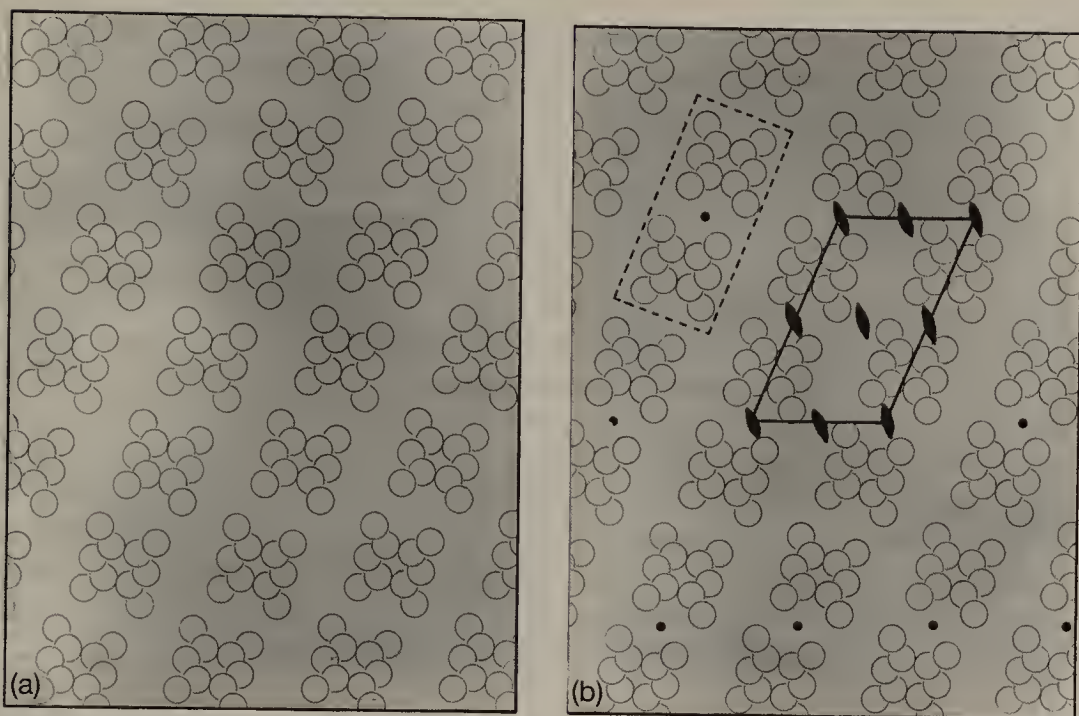
symmetry with a lattice can give rise to an additional symmetry element called a **glide line**. Consider the two patterns in Fig. 2.5, both of which have a rectangular lattice. In Fig. 2.5(a) the motif has mirror symmetry as in Fig. 2.3(a); it consists of a pair of right- and left-handed **Rs**. In Fig. 2.5(b) there is still a reflection—still pairs of right- and left-handed **Rs**—but one set of **Rs** has been translated, or glided half a lattice spacing. This symmetry is called a **reflection glide** or simply a **glide line of symmetry**. Notice that glide lines also arise automatically in the centre of the unit cell of Fig. 2.5(b) as do mirror lines in Fig. 2.5(a).

The presence of the glide lines also has important consequences regarding the symmetry of the motif. In Fig. 2.5(a) the motif has mirror symmetry but in Fig. 2.5(b) it does not: the pair of right- and left-handed **Rs** is asymmetric. It is the repetition of the translational symmetry elements—the glide lines—that determines the overall rectangular symmetry of the pattern.



**Fig. 2.5.** Patterns with (a) reflection symmetry and (b) glide-reflection symmetry. The mirror lines (*m*) and glide lines (*g*) are indicated.





**Fig. 2.7.** Projection (a) of the structure of  $\text{C}_6\text{H}_2(\text{CH}_3)_4$  (from *Contemporary Crystallography*, by M. J. Buerger, McGraw-Hill, 1970), with (b) the motif, lattice and symmetry elements indicated.

## 2.5 The seventeen plane groups

Glide lines give seven more two-dimensional patterns, giving seventeen in all—the seventeen **plane groups**. On a macroscopic scale the glide symmetry in a crystal would appear as simple mirror symmetry—the shift between the mirror-related parts of the motif would only be observable in an electron microscope which was able to resolve the individual mirror-related parts of the motif, i.e. distances of the order of  $0.5\text{--}2\text{ \AA}$  ( $50\text{--}200\text{ pm}$ ).

The seventeen plane groups are shown in Fig. 2.6. They are labelled by ‘shorthand’ symbols which indicate the type of lattice ( $p$  for primitive,  $c$  for centred) and the symmetry elements present,  $m$  for mirror lines,  $g$  for glide lines,  $4$  for tetrads and so on.

It is essential to practice recognizing the motifs, symmetry elements and lattice types in two-dimensional patterns and therefore to find to which of the seventeen plane groups they belong. Any regular patterned object will do—wallpapers, fabric designs, or the examples at the end of this chapter. Figure 2.7 indicates the procedure you should follow. Cover up Fig. 2.7(b) and examine only Fig. 2.7(a); it is a projection of molecules of  $\text{C}_6\text{H}_2(\text{CH}_3)_4$ . You should recognize that the molecules or groups of atoms are *not* identical in this two-dimensional projection. The motif is a *pair* of such molecules and this is the ‘unit of pattern’ that is repeated. Now look for symmetry elements and (using a



piece of tracing paper) indicate the positions of all of these on the pattern. Compare your pattern of symmetry elements with those shown in Fig. 2.7(b). If you did not obtain the same result you have not been looking carefully enough! Finally, insert the lattice points—one for each motif. Anywhere will do, but it is convenient to have them coincide with a symmetry element, as has been done in Fig. 2.7(b). The lattice is clearly oblique and the plane group is  $p2$  (see Fig. 2.6).

The motifs of the seventeen patterns in Fig. 2.6 should be identified by circling them (lightly in pencil in case you make a mistake). You will find that, as a result of the presence of glide lines of symmetry, there are three plane groups ( $pg$ ,  $p2gg$  and  $p4gm$ ) in which the motif is asymmetric and one ( $p2mg$ ) in which it has only one mirror-line of symmetry.

Another systematic way of identifying a plane pattern is to follow the ‘flow diagram’ shown in Fig. 2.8. The first step is to identify the highest order of rotation symmetry present, then to determine the presence or absence of reflection symmetry and so on through a series of ‘yes’ and ‘no’ answers, finally identifying one of the seventeen plane patterns whose plane group symbols are indicated ‘in boxes’, corresponding to those given in Fig. 2.6.

## 2.6 One-dimensional symmetry: border or frieze patterns

Identifying the number of one-dimensional patterns provides us with a good exercise in applying our more general knowledge of plane patterns. It is also a useful exercise in that it tells us about the different types of patterns that can be designed for the borders of wallpapers, edges of dress fabrics, friezes and cornices in buildings, and so on.

In plane patterns the symmetry operations and symmetry elements are (clearly) repeated in a plane; in one-dimensional patterns they can only be repeated in or along a line—i.e. the line or long direction of the border or frieze. This restriction immediately rules out all rotational symmetry elements with the exception of diads: two-fold symmetry alone can be repeated in a line: three-, four-, and six-fold symmetry elements require the repetition of a motif in directions other than the line of the border. For the same reason glide-reflection lines of symmetry, other than that along the line of the border, are ruled out. Mirror lines of symmetry are restricted to those along, and perpendicular to, the line of the border.

These restrictions result in seven one-dimensional groups, shown in Fig. 2.9. It is a good and satisfying exercise for you to derive these from first principles as outlined above. It is also useful to compare Fig. 2.9 with Fig. 2.6; the bracketed symbols in Fig. 2.9 indicate from which plane pattern the one-dimensional pattern may be derived. Notice that in one case two one-dimensional patterns—these with ‘horizontal’ and ‘vertical’ mirror planes—are derived from one plane pattern ( $pm$ ). This is because the mirror lines in the plane group  $pm$  can be oriented either along, or perpendicular to, the line of the one-dimensional pattern.



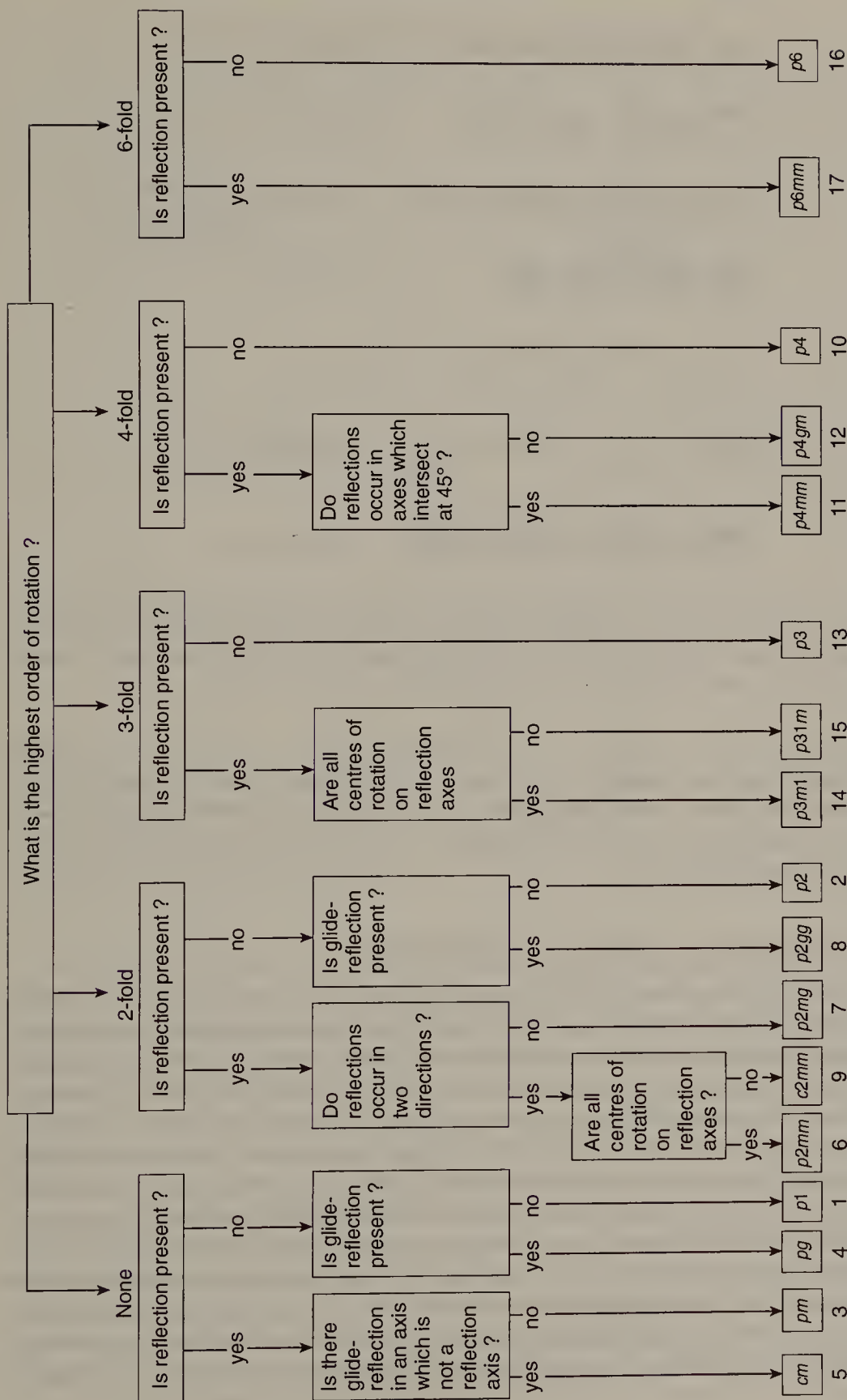
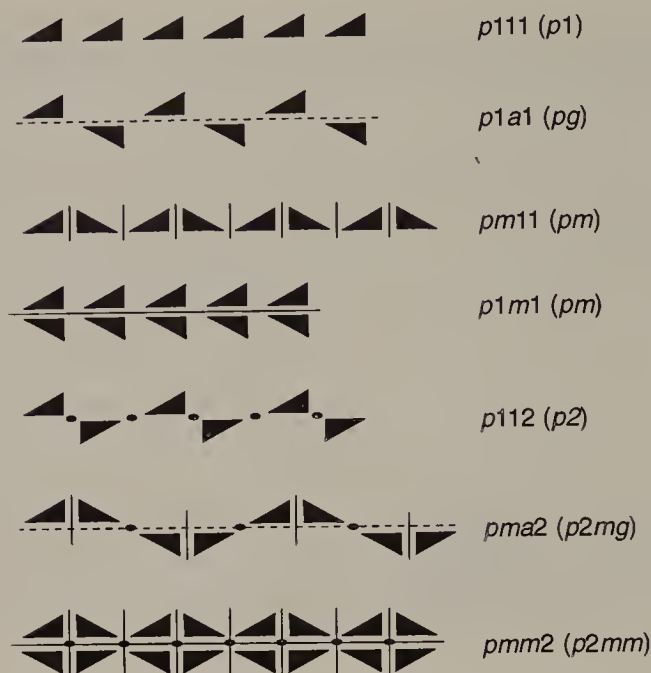


Fig. 2.8. Flow diagram for identifying one of the seventeen plane patterns (redrawn from *The Geometry of Regular Repeating Patterns* by M. A. Hann and G. M. Thomson, the Textile Institute, Manchester, 1992). The numbering is that which is arbitrarily assigned in the International Tables (see Fig 2.6).



**Fig. 2.9.** The seven one-dimensional groups or seven classes of border or frieze patterns with their symmetry symbols (bracketed), the plane pattern symbols from which they may be derived. Solid lines indicate mirror lines, dotted lines indicate glide lines and symbols indicate diads (redrawn from *The Geometry of Regular Repeating Patterns*, loc. cit.).

Figure 2.15 (see Exercise 2.6) also shows examples of some of the border patterns. You can practice recognizing such patterns either by overlaying the pattern with a piece of tracing paper, and indicating the positions of the diads, mirror and glide lines as described above for plane patterns or by following the flow diagram (Fig. 2.10).

## 2.7 Symmetry, patterns and cultures

We have a rich inheritance of plane and border patterns in printed and woven textiles, wallpapers, bricks and tiles which have been designed and made by countless craftsmen and artisans in the past ‘without benefit of crystallography’. The question we may now ask is: ‘Have all the seventeen plane groups and seven one-dimensional groups been utilized in pattern design or are some patterns and some symmetries more evident than others? If so, is there any relationship between the preponderance or absence of certain types of symmetry elements in patterns and the civilization or culture which produced them?’

Questions such as these have exercised the minds of archaeologists, anthropologists and historians of art and design. They are, to be sure, questions more of cultural than crystallographic significance, but patterns play such a large part in our everyday experience that a crystallographer can hardly fail to be absorbed by them, just as he or she is absorbed by the three-dimensional patterns of crystals.

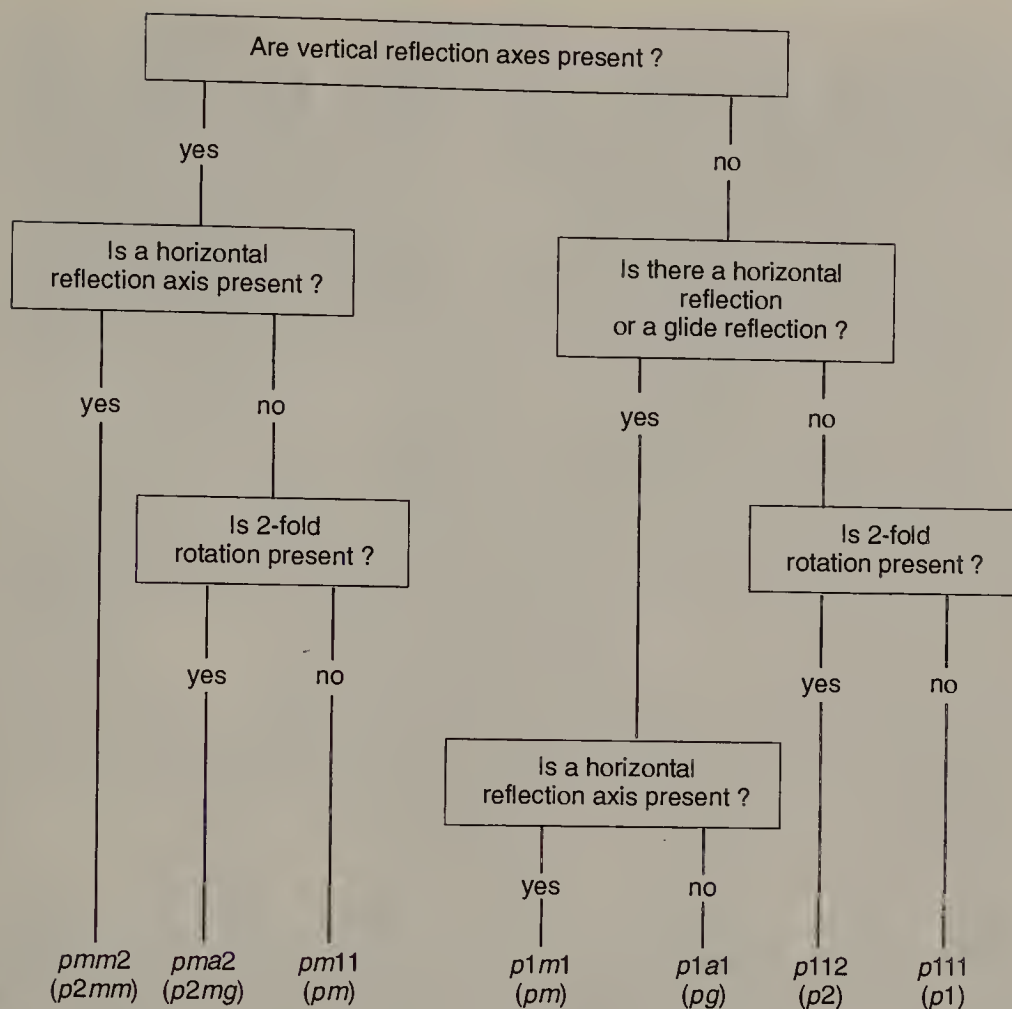


Fig. 2.10. Flow diagram for identifying one of the seven border patterns (from *The Geometry of Regular Repeating Patterns*, loc. cit.).

The study of plane and one-dimensional patterns (and indeed three-dimensional (space) patterns) is complicated by the question of colour—‘real’ colours in the case of plane and one-dimensional patterns, or colours representing some property, such as electron spin direction or magnetic moment, in space patterns (Chapter 4). Colour changes may also be analysed in terms of symmetry elements in which colours are alternated in a systematic way. Clearly, the greater the number of colours, the greater the complexity. The simplest cases to consider are two-colour (e.g. black and white) patterns. Figure 2.11 shows the generation of plane motifs through the operation of what are called counterchange or colour symmetry elements, which are distinguished from ordinary (rotation) axes and mirror lines of symmetry by a prime superscript. For example, the operation of a  $2'$  axis is a twice repeated rotation of an asymmetric object by  $180^\circ$  plus a colour change at each rotation; the operation of an  $m'$  mirror line is a reflection plus colour change. Figure 2.11 shows the operation of all the two-dimensional counterchange point symmetry elements.

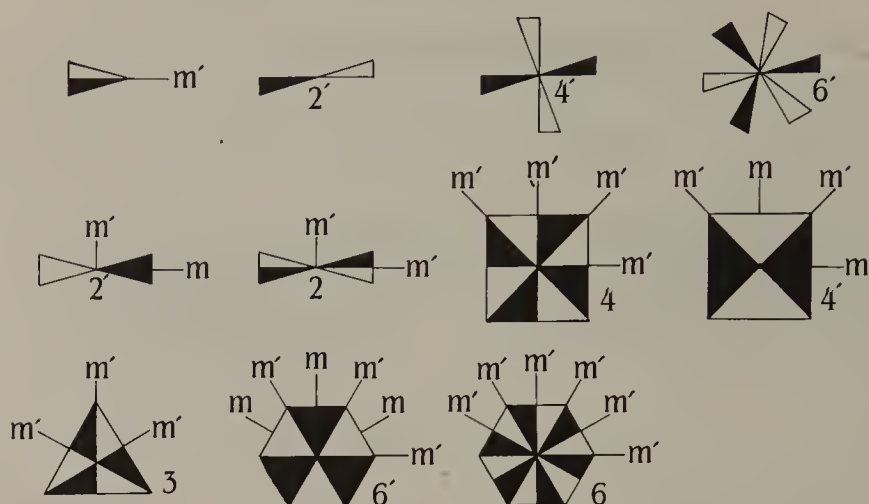


Fig. 2.11. The operation of two-colour (black/white) counterchange symmetry elements (denoted by prime superscripts).

Accounting for two-colour symmetry gives rise to a total of forty-six (rather than seventeen) plane patterns and seventeen (rather than seven) one-dimensional patterns.

Probably the most influential and pioneering study of patterns was *The Grammar of Ornament* by Owen Jones, first published in 1856\*. Owen Jones attempted to categorize both plane and border patterns in terms of the different cultures that produced them, and although the symmetry aspects of patterns are touched on in the most fragmentary way, there is no doubt that the superb illustrations and encyclopaedic character of the book provided later writers with material which could be classified and analysed in crystallographic terms. Perhaps the best known of these was M. C. Escher (1898–1971) who drew inspiration for his drawings of tessellated figures from visits to the Alhambra in the 1930s, and also presumably from Owen Jones' chapter on 'Moresque Ornament' in which he describes the Alhambra as 'the very summit of Moorish art, as the Parthenon is of Greek art'. Escher's patterns encompass all the seventeen plane groups, eleven of which are represented in the Alhambra.

More recent work has identified clear preponderances of certain plane symmetry groups, and the absences of others†. For example, nearly 50% of traditional Javanese batik (wax-resist textile) patterns belong to plane group  $4mm$  (Fig. 2.6), others, such as  $p3$ ,  $p3m1$ ,  $p31m$  and  $p6$  are wholly absent. In Jacquard-woven French silks of the last decade of the nineteenth century, nearly 80% of the patterns belong to plane group  $pg$ . In Japanese textile designs of the Edo period *all* plane groups are represented, with a marked preponderance for groups  $p2mm$  and  $c2mm$ . What these differences mean, or tell us about the cultures which gave rise to them, is, as the saying goes, 'another question'.

\* Owen Jones. *The Grammar of Ornament*, Day & Sons Ltd., London, reprinted by Studio Editions, London (1986).

† M. A. Hann. *Symmetry of Regular Repeating Patterns: Case studies from various cultural settings*. Journal of the Textile Institute (1992), Vol. 83, pp. 579–580.





**Fig. 2.12.** A plane pattern (from *Symmetry Aspects of M. C. Escher's Periodic Drawings*, 2nd edn, by C. H. MacGillavry. Published for the International Union of Crystallography by Bohn, Scheltema and Holkema, Utrecht, 1976).

## Exercises

- 2.1 Lay tracing paper over the plane patterns in Fig. 2.6. Outline a unit cell in each case and indicate the positions of all the symmetry elements within the unit cell. Notice in particular the differences in the distribution of the triad axes and mirror lines in the plane groups  $p31m$  and  $p3m1$ .
- 2.2 Figure 2.12 is a design by M. C. Escher. Using a tracing paper overlay, indicate the positions of all the symmetry elements. With the help of the flow diagram (Fig. 2.8), determine the plane lattice type.



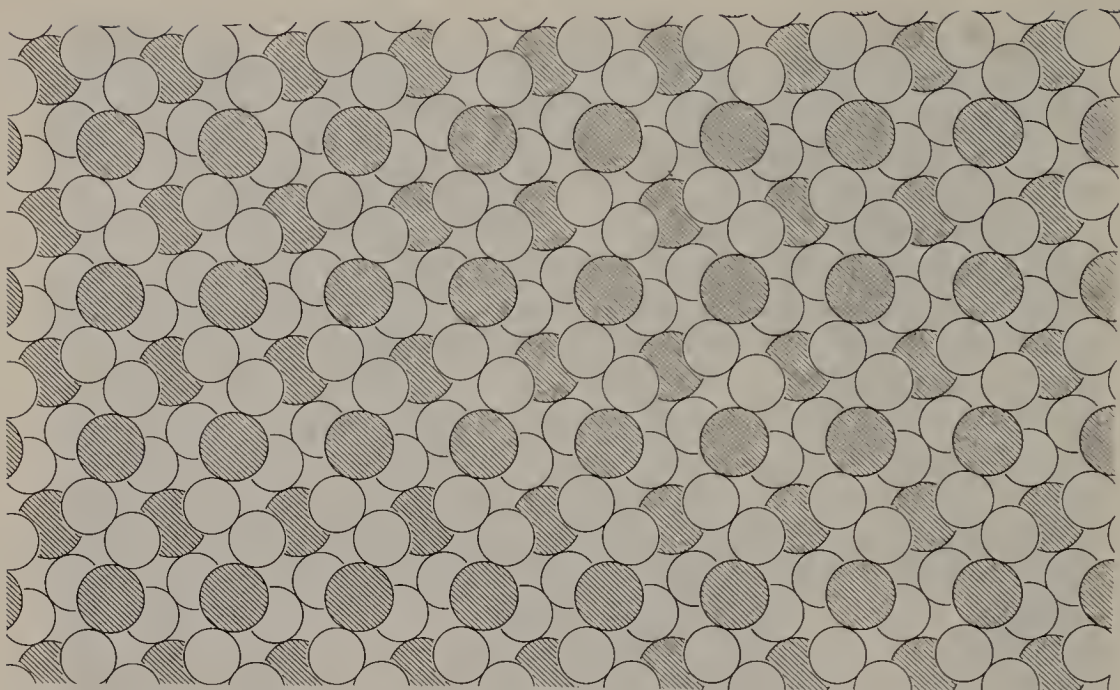
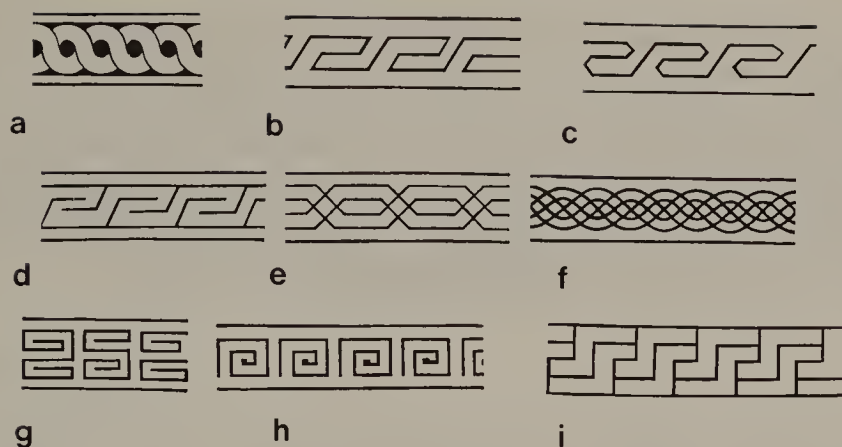


Fig. 2.13. A projection of the structure of  $\text{FeS}_2$  (from *Contemporary Crystallography* by M. J. Buerger, McGraw-Hill, New York, 1970).



Fig. 2.14. A plane pattern (from C. H. MacGillavry, loc. cit.).



**Fig. 2.15.** Examples of border or frieze patterns (from *The Grammar of Ornament* by Owen Jones, Day & Son, London 1856, reprinted by Studio Editions, London, 1986). a, b, Greek; c, d, Arabian; e, Moresque; f, Celtic; g, h, Chinese; i, Mexican.

- 2.3 Figure 2.13 is a projection of the structure of  $\text{FeS}_2$  (shaded atoms Fe, unshaded atoms S). Using a tracing paper overlay, indicate the positions of the symmetry elements, outline a unit cell and, with the help of the flow diagram in Fig. 2.8, determine the plane pattern type.
- 2.4 Figure 2.14 is a design by M. C. Escher. Can you see that the two sets of men are related by glide lines of symmetry? Draw in the positions of these glide lines, and determine the plane lattice type.
- 2.5 Determine (with reference to Fig. 2.11) the counterchange (black-white) point group symmetry of a chessboard.
- 2.6 Figure 2.15 shows examples of border or frieze patterns from *The Grammar of Ornament* by Owen Jones. Using a tracing paper overlay, indicate the positions of the symmetry elements and, with the help of the flow diagram (Fig. 2.10), determine the one-dimensional lattice types.



**Fig. 2.16.** Examples of motifs, representing the ten plane point groups (from *The Geometry of Regular Repeating Patterns*, loc. cit.).

- 2.7 Figure 2.16 shows examples of motifs representing the ten plane point groups (five of which are shown in Fig. 2.3). Indicate the point symmetry elements present in each case.
- 2.8 Compare the symmetries of the eleven motifs generated by the black/white point counterchange symmetry elements (Fig. 2.11) with the ten plane point groups (Fig. 2.16). If the black/white symmetry in Fig. 2.11 is ignored, i.e.  $m'$  becomes  $m$  and  $2'$  becomes  $2$  etc., then these motifs reduce to the ten plane point groups: all the ten plane point groups are represented, except two. Which are they?



---

# Bravais lattices and crystal systems

## 3.1 Introduction

The definitions of the motif, the repeating ‘unit of pattern’, and the lattice, an array of points in space in which each point has an identical environment, hold in three dimensions exactly as they do in two dimensions. However, in three dimensions there are additional symmetry elements that need to be considered: both **point symmetry elements** to describe the symmetry of the three-dimensional motif (or indeed any crystal or three-dimensional object) and also **translational symmetry elements**, which are required (like glide lines in the two-dimensional case) to describe all the possible patterns which arise by combining motifs of different symmetries with their appropriate lattices. Clearly, these considerations suggest that the subject is going to be rather more complicated and ‘difficult’; it is obvious that there are going to be many more three-dimensional patterns (or space groups) than the seventeen two-dimensional patterns (or plane groups—Chapter 2), and to work through all of these systematically would take up many pages! However, it is not necessary to do so; all that is required is an understanding of the principles involved (Chapter 2), the operation and significance of the additional symmetry elements, and the main results. These main results may be stated straight away. The additional point symmetry elements required are centres of symmetry, mirror planes (instead of lines) and inversion axes; the additional translational symmetry elements are glide planes (instead of lines) and screw axes. The application and permutation of all symmetry elements to patterns in space give rise to 230 **space groups** (instead of seventeen plane groups) distributed among fourteen space lattices (instead of five plane lattices) and thirty-two point group symmetries (instead of ten plane point group symmetries).

In this chapter the concept of space (or Bravais) lattices and their symmetries is discussed and, deriving from this, the classification of crystals into seven systems.

## 3.2 The fourteen space (Bravais) lattices

The systematic work of describing and enumerating the space lattices was done initially by Frankenheim\* who, in 1835, proposed that there were fifteen in all. Unfortunately for Frankenheim, two of his lattices were identical, a fact first pointed out by Bravais\* in 1848. It was, to take a two-dimensional analogy, as if

\* Denotes biographical notes available in Appendix 3.

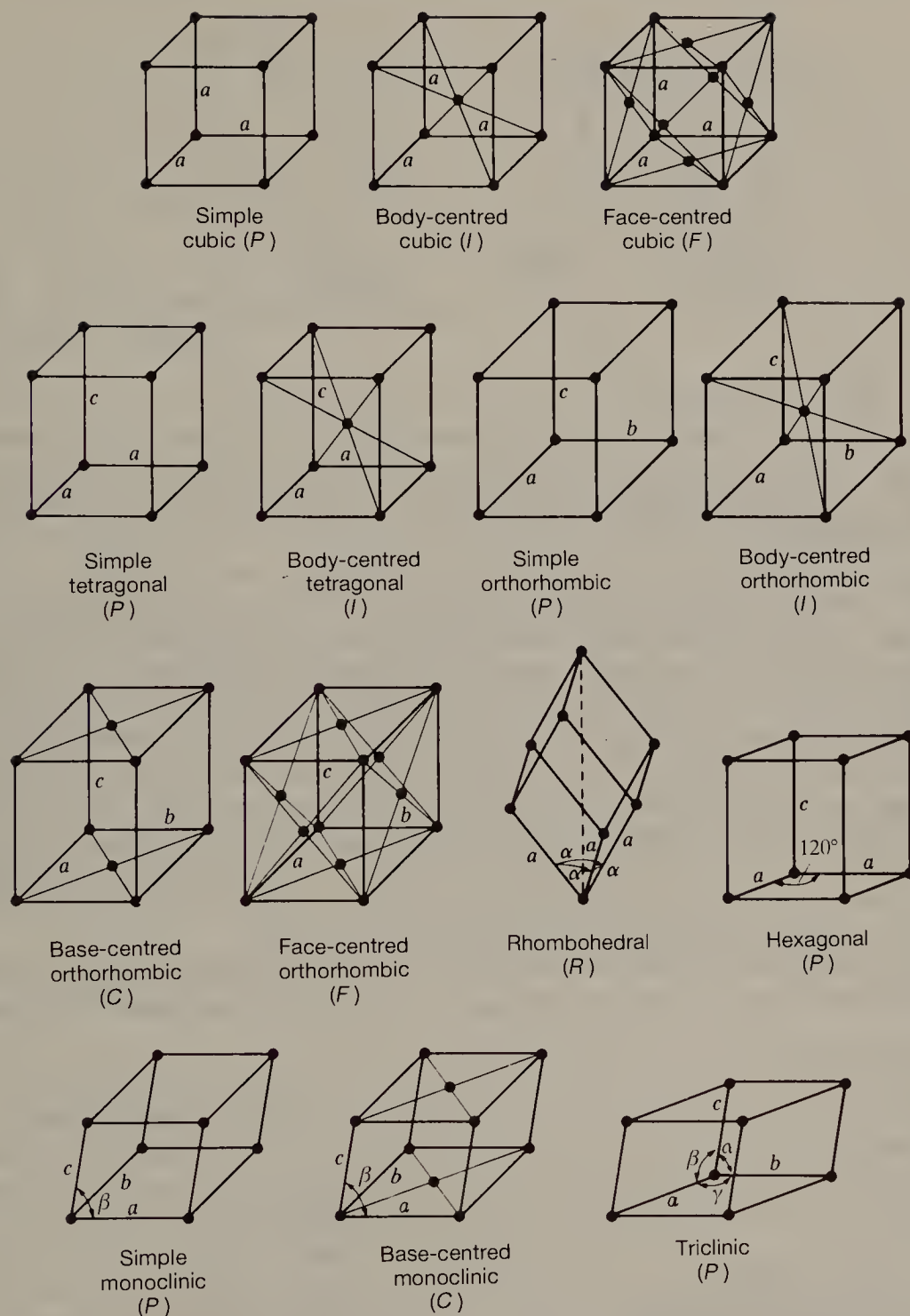
Frankenheim had failed to notice (see Fig. 2.4(b)) that the rhombic or diamond and the rectangular centred plane lattices were identical! Hence, to this day, the fourteen space lattices are usually, and perhaps unfairly, called Bravais lattices.

The unit cells of the Bravais lattices are shown in Fig. 3.1. The different shapes and sizes of these cells may be described in terms of three cell edge lengths or axial distances,  $a$ ,  $b$ ,  $c$ , or lattice vectors  $\mathbf{a}$ ,  $\mathbf{b}$ ,  $\mathbf{c}$  and the angles between them,  $\alpha$ ,  $\beta$ ,  $\gamma$ , where  $\alpha$  is the angle between  $\mathbf{b}$  and  $\mathbf{c}$ ,  $\beta$  the angle between  $\mathbf{a}$  and  $\mathbf{c}$ , and  $\gamma$  the angle between  $\mathbf{a}$  and  $\mathbf{b}$ . The axial distances and angles are measured from one corner to the cell, i.e. a common origin. It does not matter where we take the origin—any corner will do—but, as pointed out in Chapter 1, it is a useful convention (and helps to avoid confusion) if the origin is taken as the ‘back left-hand corner’ of the cell, the  $a$ -axis pointing forward (out of the page), the  $b$ -axis towards the right and the  $c$ -axis upwards. This convention also gives a right-handed axial system. If any one of the axes is reversed (e.g. the  $b$ -axis towards the left instead of the right), then a left-handed axial system results. The distinction between them is that, like left and right hands, they are mirror images of one another and cannot be brought into coincidence by rotation.

The drawings of the unit cells of the Bravais lattices in Fig. 3.1 can be misleading because, as shown in Chapter 2, it is the *pattern* of lattice points which distinguishes the lattices. The unit cells simply represent arbitrary, though convenient, ways of ‘joining up’ the lattice points. Consider, for example, the three cubic lattices; cubic  $P$  (for *Primitive*, one lattice point per cell, i.e. lattice points only at the corners of the cell), cubic  $I$  (for ‘*Innenzentrierte*’, which is German for ‘body-centred’, an additional lattice point at the centre of the cell, giving two lattice points per cell) and cubic  $F$  (for *Face-centred*, with additional lattice points at the centres of each face of the cell, giving four lattice points per cell). It is possible to outline alternative primitive cells (i.e. lattice points only at the corners) for the cubic  $I$  and cubic  $F$  lattices, as is shown in Fig. 3.2. As mentioned in Chapter 1, these primitive cells are not often used (1) because the inter-axial angles are not the convenient  $90^\circ$  (i.e. they are not orthogonal) and (2) because they do not reveal very clearly the cubic symmetry of the cubic  $I$  and cubic  $F$  lattices. (The symmetry of the Bravais lattices, or rather the point group symmetries of their unit cells, will be described in Section 3.3.)

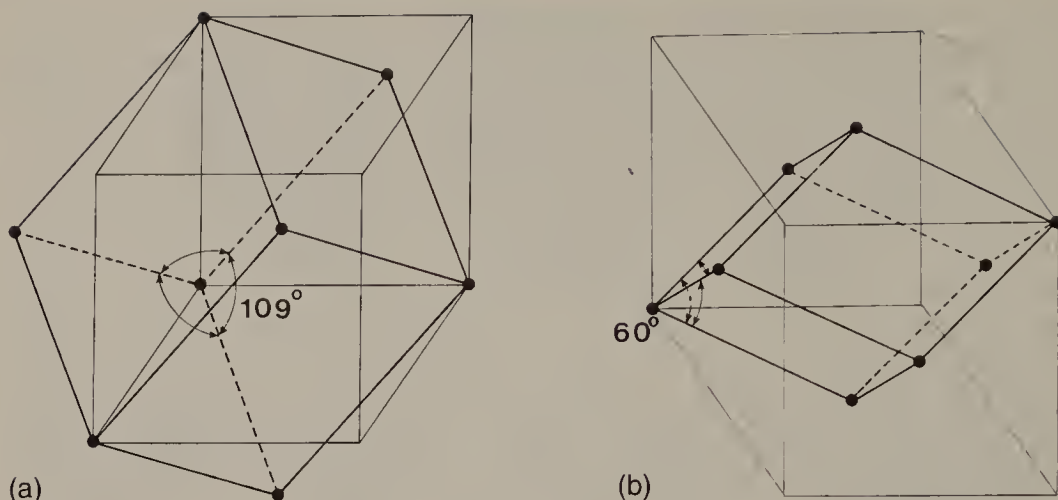
Similar arguments concerning the use of primitive cells apply to all the other centred lattices. Notice that the unit cells of two of the lattices are centred on the ‘top’ and ‘bottom’ faces. These are called base-centred or  $C$ -centred because these faces are intersected by the  $c$ -axis.

The Bravais lattices may be thought of as being built up by stacking ‘layers’ of the five plane lattices, one on top of another. The cubic and tetragonal lattices are based on the stacking of square lattice layers; the orthorhombic  $P$  and  $I$  lattices on the stacking of rectangular layers; the orthorhombic  $C$  and  $F$  lattices on the stacking of rectangular centred layers; the rhombohedral and hexagonal lattice on the stacking of hexagonal layers and the monoclinic and triclinic lattices on the stacking of oblique layers. These relationships between the plane



**Fig. 3.1.** The fourteen Bravais lattices (from *Elements of X-Ray Diffraction*, (2nd edn), by B. D. Cullity, Addison-Wesley, 1978). In the two monoclinic cells the origin is located at the 'front left-hand corner' to show clearly the angle  $\beta$  between the  $a$  and  $c$  axes.

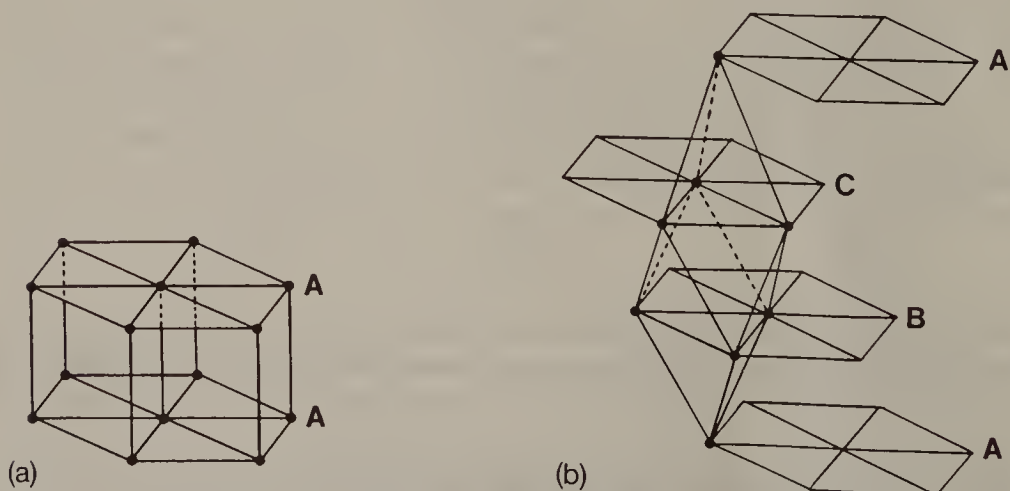
and the Bravais lattices are easy to see, except perhaps for the rhombohedral lattice. The rhombohedral unit cell has axes of equal length and with equal



**Fig. 3.2.** (a) The cubic *I* and (b) the cubic *F* lattices with the primitive rhombohedral cells and inter-axial angles indicated.

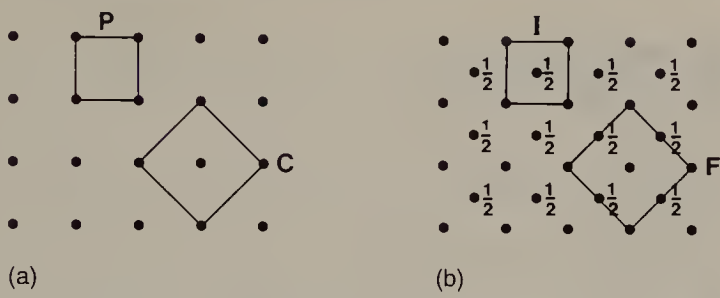
angles ( $\alpha$ ) between them. Notice that the layers of lattice points, perpendicular to the 'vertical' direction (shown dotted in Fig. 3.1) form triangular, or equivalently, hexagonal layers. The hexagonal and rhombohedral lattices differ in the ways in which the hexagonal layers are stacked. In the hexagonal lattice they are stacked directly one on top of the other (Fig. 3.3(a)) and in the rhombohedral lattice they are stacked such that the next two layers of points lie above the triangular 'hollows' or interstices of the layer below, giving a three layer repeat (Fig. 3.3(b)). These hexagonal and rhombohedral stacking sequences have been met before in the stacking of close-packed layers (Chapter 1); the hexagonal lattice corresponds to the simple hexagonal AAA... sequence and the rhombohedral lattice corresponds to the fcc ABCABC... sequence.

Now observant readers will notice that the rhombohedral and cubic lattices are therefore related. The primitive cells of the cubic *I* and cubic *F* lattices



**Fig. 3.3.** Stacking of hexagonal layers of lattice points in (a) the hexagonal lattice and (b) the rhombohedral lattice.





**Fig. 3.4.** Plans of tetragonal lattices showing (a) the tetragonal  $P = C$  lattice and (b) the tetragonal  $I = F$  lattice.

(Fig. 3.2) are rhombohedral—the axes are of equal length and the angles ( $\alpha$ ) between them are equal. As in the two-dimensional cases, what distinguishes the cubic lattices from the rhombohedral is their symmetry. When the angle  $\alpha$  is  $90^\circ$  we have a cubic  $P$  lattice, when it is  $60^\circ$  we have a cubic  $F$  lattice and when it is  $109.47^\circ$  we have a cubic  $I$  lattice (Fig. 3.2). Or, alternatively, when the hexagonal layers of lattice points in the rhombohedral lattice are spaced apart in such a way that the angle  $\alpha$  is  $90^\circ$ ,  $60^\circ$  or  $109.47^\circ$ , then cubic symmetry results.

Finally, compare the orthorhombic lattices (all sides of the unit cell of different lengths) with the tetragonal lattices (two sides of the cell of equal length). Why are there four orthorhombic lattices,  $P$ ,  $C$ ,  $I$  and  $F$ , and only two tetragonal lattices,  $P$  and  $I$ ? Why are there not tetragonal  $C$  and  $F$  lattices as well? The answer is that there *are* tetragonal  $C$  and  $F$  lattices, but by redrawing or outlining different unit cells, as shown in Fig. 3.4, it will be seen that they are identical to the tetragonal  $P$  and  $I$  lattices, respectively. In short, they represent no new arrangements of lattice points.

**3.3 The symmetry of the fourteen Bravais lattices: crystal systems**

The unit cells of the Bravais lattices may be thought of as the ‘building blocks’ of crystals, precisely as Haüy envisaged (Fig. 1.2). Hence it follows that the habit or external shape, or the observed symmetry of crystals, will be based upon the shapes and symmetry of the Bravais lattices, and we now have to describe the point symmetry of the unit cells of the Bravais lattices just as we described the point symmetry of plane patterns and lattices. The subject is far more readily understood if simple models are used (Appendix 1).

First, mirror lines of symmetry become mirror planes in three dimensions. Second, axes of symmetry (diads, triads, tetrads and hexads) also apply to three dimensions. The additional complication is that, whereas a plane motif or object can only have one such axis (perpendicular to its plane), a three-dimensional object can have several axes running in different directions (but always through a point in the centre of the object).

Consider, for example, a cubic unit cell (Fig. 3.5(a)). It contains a total of nine mirror planes, three parallel to the cube faces and six parallel to the face diagonals. There are three tetrad (four-fold) axes perpendicular to the three sets

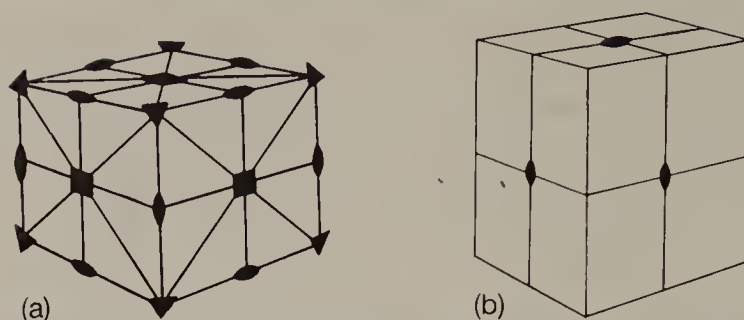


Fig. 3.5. The point symmetry elements in (a) a cube (cubic unit cell) and (b) an orthorhombic unit cell.

of cube faces, four triad (three-fold) axes running between opposite cube corners, and six diad (two-fold) axes running between the centres of opposite edges. This 'collection' of symmetry elements is called the **point group symmetry** of the cube because all the elements—planes and axes—pass through a point in the centre.

Why should there be these particular numbers of mirror planes and axes? It is because all the various symmetry elements operating at or around the point must be consistent with one another. Self-consistency is a fundamental principle, underlying all the two-dimensional plane groups, all the three-dimensional point groups and all the space groups that will be discussed in Section 4.6. If there are two diad axes, for example, then they *have* to be mutually orthogonal, otherwise chaos would result; by the same token they also *must* generate a third diad perpendicular to both of them. It is the necessity for self-consistency which governs the construction of every one of the different combinations of symmetry, controlling the nature of each combination; it is this, also, which limits the total numbers of possible combinations to quite definite numbers such as thirty-two, in the case of the crystallographic point groups (the crystal classes), the fourteen Bravais lattices, and so on.

The cubic unit cell has more symmetry elements than any other: its very simplicity makes its symmetry difficult to grasp. More easy to follow is the symmetry of an orthorhombic cell. Figure 3.5(b) shows the point group symmetry of an orthorhombic unit cell. It contains, like the cube, three mirror planes parallel to the faces of the cell but no more—mirror planes do not exist parallel to the face diagonals. The only axes of symmetry are three diads perpendicular to the three faces of the unit cell.

In both cases it can be seen that the point group symmetry of these unit cells (Figs. 3.5(a) and 3.5(b)) is independent of whether the cells are centred or not. All three cubic lattices, *P*, *I* and *F*, have the same point group symmetry; all four orthorhombic lattices, *P*, *I*, *F* and *C*, have the same point group symmetry and so on. This simple observation leads to an important conclusion: it is not possible, from the observed symmetry of a crystal, to tell whether the underlying Bravais lattice is centred or not. Therefore, in terms of their point group symmetries, the Bravais lattices are grouped, according to the shapes of their unit cells, into seven **crystal systems**. For example, crystals with cubic *P*, *I* or *F*

Table 3.1 The seven crystal systems, their corresponding Bravais lattices and symmetries

System	Bravais lattices	Axial lengths and angles	Characteristic (minimum) symmetry	Point groups <sup>1</sup>	
				Enantiomorphous <sup>2</sup>	Non-enantiomorphous <sup>3,4</sup>
Cubic	<i>P I F</i>	$a = b = c$ $\alpha = \beta = \gamma = 90^\circ$	4 triads equally inclined at $109.47^\circ$	23, 432	$*m\bar{3}, \bar{4}3m, *m\bar{3}m$
Tetragonal	<i>P I</i>	$a = b \neq c$ $\alpha = \beta = \gamma = 90^\circ$	1 rotation tetrad or inversion tetrad	4, 422	$\bar{4}, *4/m, *4/mmm$ $4mm, \bar{4}2m$
Orthorhombic	<i>P I C F</i>	$a \neq b \neq c$ $\alpha = \beta = \gamma = 90^\circ$	3 diads equally inclined at $90^\circ$	222	$mm2, *mmm$
Trigonal <sup>5</sup>	<i>P R</i>	$a = b = c$ $\alpha = \beta = \gamma \neq 90^\circ$	1 rotation triad or inversion triad (= triad + centre of symmetry)	3, 32	$*\bar{3}, 3m, *3m$
Hexagonal	<i>P</i>	$a = b \neq c$ $\alpha = \beta = 90^\circ, \gamma = 120^\circ$	1 rotation hexad or inversion hexad (= triad + perp. mirror plane)	6, 622	$\bar{6}, *6/m, *6/mmm$ $6mm, \bar{6}m2$
Monoclinic	<i>P C</i>	$a = b \neq c$ $\alpha = \gamma = 90^\circ \neq \beta > 90^\circ$	1 rotation diad or inversion diad (= mirror plane)	2	$m, *2/m$
Triclinic	<i>P</i>	$a \neq b \neq c$ $\alpha \neq \beta \neq \gamma \neq 90^\circ$	None	1	$*\bar{1}$

<sup>1</sup> The ten polar point groups possess a unique axis not related by symmetry; they are a sub-group of the point groups which do not possess a centre of symmetry and are equally divided between the enantiomorphous point groups (1, 2, 3, 4, 6) and non-enantiomorphous point groups ( $m, mm2, 3m, 4mm, 6mm$ ).

<sup>2</sup> The eleven enantiomorphous point groups are those which do not possess a plane or a centre of symmetry. Hence enantiomorphous crystals can exist in right- or left-handed forms.

<sup>3</sup> The twenty-one non-enantiomorphous point groups are these which possess a centre and/or a plane of symmetry.

<sup>4</sup> Eleven of the twenty-one non-enantiomorphous point groups possess a centre of symmetry (indicated by a \*). Crystals which have a centre of symmetry do not exhibit certain properties, e.g. the piezoelectric effect.

<sup>5</sup> Trigonal crystals may be represented either by the hexagonal *P* lattice or the rhombohedral *R* lattice.

lattices belong to the **cubic system**, crystals with orthorhombic *P*, *I*, *F* or *C* lattices belong to the **orthorhombic system**, and so on. However, a complication arises in the case of crystals with a hexagonal lattice. One might expect that all crystals with a hexagonal lattice should belong to the hexagonal system, but, as shown in Chapter 4, the external symmetry of crystals may not be identical (and usually is not identical) to the symmetry of the underlying Bravais lattice. Some crystals with a hexagonal lattice, e.g. quartz, do not show hexagonal (hexad) symmetry but have triad symmetry. Such crystals are assigned to the **trigonal system** rather than to the hexagonal system. Hence the trigonal system includes crystals with both hexagonal and rhombohedral Bravais lattices. There is yet another problem which is particularly associated with the trigonal system, which is that the rhombohedral unit cell outlined in Figs 3.1 and 3.3 is not always used—a larger (non-primitive) unit cell of three times the size is sometimes more convenient. The problem of transforming axes from one unit cell to another is addressed in Chapter 5.

The crystal systems and their corresponding Bravais lattices are shown in Table 3.1. Notice that there are no axes or planes of symmetry in the **triclinic system**. The only symmetry that the triclinic lattice possesses (and which is possessed by all the other lattices) is a **centre of symmetry**. This point symmetry element and inversion axes of symmetry are explained in Chapter 4.

## Exercises

- 3.1 The drawings in Fig. 3.6 show patterns of points distributed in orthorhombic-shaped unit cells. Identify to which (if any) of the orthorhombic Bravais lattices, *P*, *C*, *I* or *F*, each pattern of points corresponds.  
(*Hint*: It is helpful to sketch plans of several unit cells, which will show more clearly the patterns of points, and then to outline (if possible) a *P*, *C*, *I* or *F* unit cell.)
- 3.2 The unit cells of several **orthorhombic** structures are described below. Draw *plans* of each and identify the Bravais lattice, *P*, *C*, *I* or *F*, in each case.
- One atom per unit cell located at  $(x'y'z')$ .
  - Two atoms per unit cell of the *same* type located at  $(0\frac{1}{2}0)$  and  $(\frac{1}{2}0\frac{1}{2})$ .
  - Two atoms per unit cell, one type located at  $(00z')$  and  $(\frac{1}{2}\frac{1}{2}z')$  and the other type at  $(00(\frac{1}{2} + z'))$  and  $(\frac{1}{2}\frac{1}{2}(\frac{1}{2} + z'))$ .
- (*Hint*: Draw plans of several unit cells and relocate the origin of the axes.  $x'$ ,  $y'$ ,  $z'$  should be taken as small (non-integral) fractions of the cell edge lengths.)

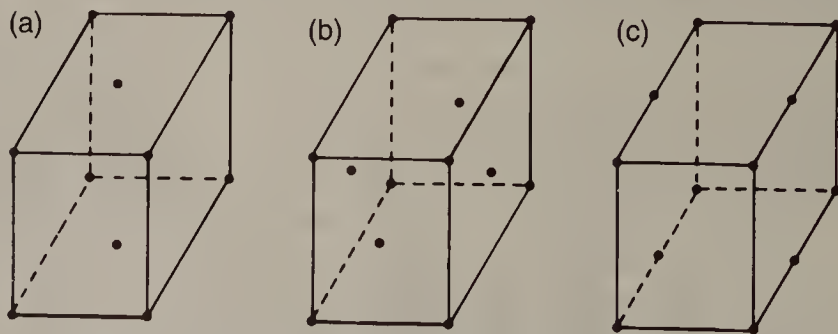


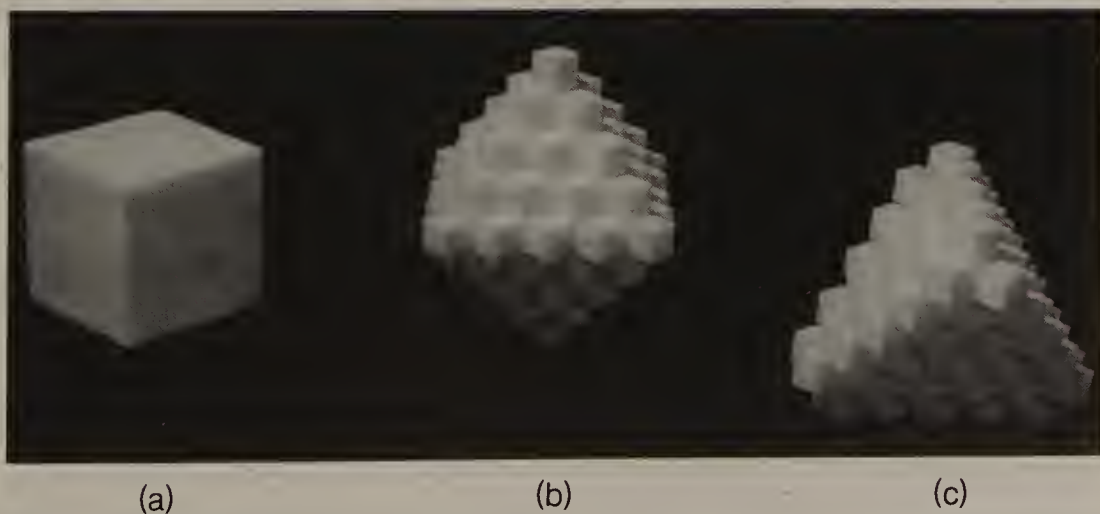
Fig. 3.6. Patterns of points in orthorhombic unit cells.



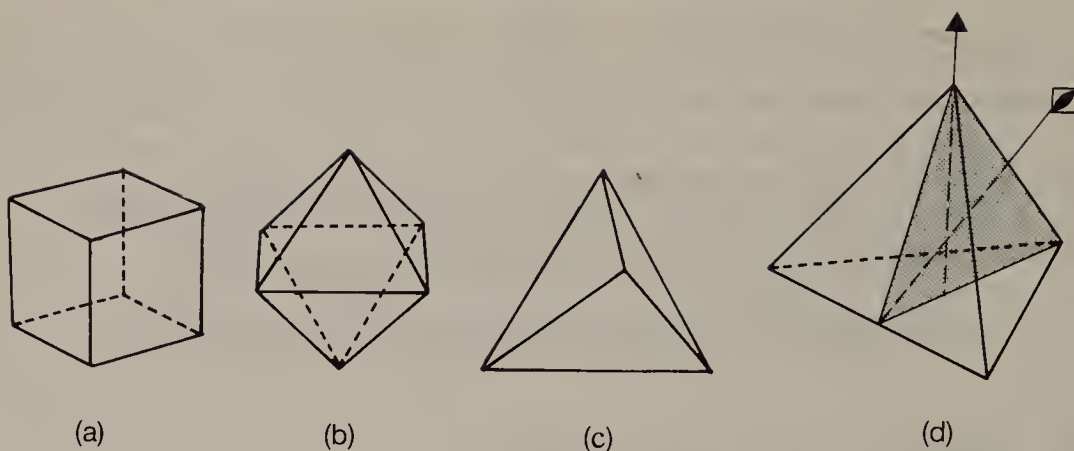
# Crystal symmetry, point groups and crystal structures: the external symmetry of crystals

## 4.1 Symmetry and crystal habit

As indicated in Chapter 3, the system to which a crystal belongs may be identified from its observed or external symmetry. Sometimes this is a very simple procedure. For example, crystals which are found to grow or form as cubes obviously belong to the cubic system: the external point symmetry of the crystal and that of the underlying unit cell are identical. However, a crystal from the cubic system may not grow or form with the external shape of a cube; the unit cells may stack up to form, say, an octahedron, or a tetrahedron, as shown in the models constructed from sugar-cube unit cells (Fig. 4.1). These are just two examples of a very general phenomenon throughout all the crystal systems: only very occasionally do crystals grow with the same shape as that of the underlying unit cell. The different shapes or **habits** adopted by crystals are determined by chemical and physical factors which do not, at the moment, concern us; what does concern us as crystallographers is to know how to recognize to which system a crystal belongs even though its habit may be quite different from, and therefore conceal, the shape of the underlying unit cell.



**Fig. 4.1.** Stacking of 'sugar-cube' unit cells to form (a) a cube, (b) an octahedron and (c) a tetrahedron. Note that the cubic cells in all three models are in the same orientation.



**Fig. 4.2.** (a) A cube, (b) an octahedron and (c) a tetrahedron drawn in the same orientation as the models in Fig. 4.1. (d) A tetrahedron showing the positions of one variant of the point symmetry elements: mirror plane (shaded) ( $\times 6$ ), triad ( $\times 4$ ) and inversion tetrad (which includes a diad) ( $\times 3$ ).

The clue to the answer lies in the point group symmetry of the crystal. Consider, for example, the symmetry of the cubic crystals which have the shape or habit of a cube, an octahedron or a tetrahedron (Figs 4.1 and 4.2) or construct models of them (Appendix 1). The cube and octahedron, although they are different shapes, possess the same point group symmetry. The tetrahedron, however, has less symmetry: only six mirror planes instead of nine: only three diads running between opposite edges (i.e. along the directions perpendicular to the cube faces in the underlying cubes) and, as before, four triads running through each corner. The common, unchanged symmetry elements are the four (equally inclined) triads, and it is the presence of these four triads which characterizes crystals belonging to the cubic system. Cubic crystals usually possess additional symmetry elements—the most symmetrical cubic crystals being those with the full point group symmetry of the underlying unit cell. But it is the four triads—not the three tetrads or the nine mirror planes—which are the ‘hallmark’ of a cubic crystal.

Similar considerations apply to all the other crystal systems. For example, Fig. 4.3 shows three orthorhombic crystals. Figure 4.3(a) shows a crystal with the full symmetry of the underlying unit cell—three perpendicular mirror planes and three perpendicular diads. Figure 4.3(b) shows a crystal with only two mirror planes and one diad along their line of intersection. Figure 4.3(c) shows a crystal with three perpendicular diads but no mirror planes.

## 4.2 The thirty-two crystal classes

The examples shown in Figs 4.1–4.3 are of crystals with different point group symmetries: they are said to belong to different **crystal classes**. Crystals in the same class have the same point group symmetry, so in effect the terms are synonymous. Notice that crystals in the same class do not necessarily have the same shape. For example, the cube and octahedron are obviously different

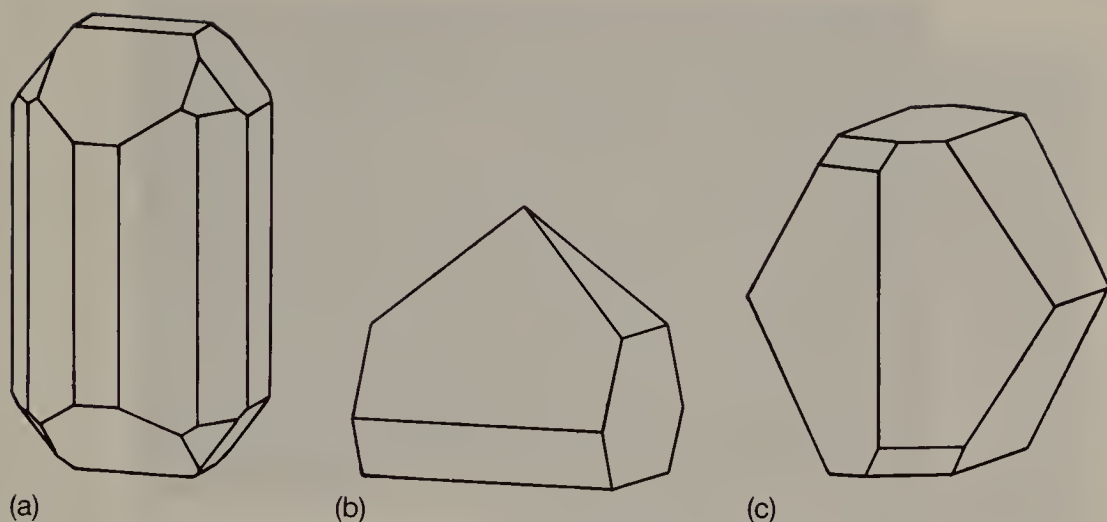


Fig. 4.3. Orthorhombic crystals (a)  $\text{PbSO}_4$  ( $mmm$ ), (b)  $\text{NH}_4\text{MgPO}_4 \cdot 6\text{H}_2\text{O}$  ( $mm2$ ), (c)  $\text{MgSO}_4 \cdot 7\text{H}_2\text{O}$  ( $222$ ) (from *Introduction to Crystallography*, 3rd edn, by F. C. Phillips, Longman, 1977).

shapes but belong to the same class because their point group symmetry is the same.

In two dimensions (Chapter 2) we found that there were ten plane point groups; in three dimensions there are thirty-two three-dimensional point groups. One of the great achievements of the science of mineralogy in the nineteenth century was the systematic description of the thirty-two point groups or crystal classes and their division into the seven crystal systems. Particular credit is due to J. F. C. Hessel\*, whose contributions to the understanding of point group symmetry were unrecognized until after his death. The concept of seven different types or shapes of underlying unit cells then links up with the concept of the fourteen Bravais lattices; in other words, it establishes the connection between the external crystalline form or shape and the internal molecular or atomic arrangements.

It is not necessary to describe all the thirty-two point groups systematically; only the nomenclature for describing their important distinguishing features needs to be considered. This requires a knowledge of additional symmetry elements—centres and inversion axes.

### 4.3 Centres and inversion axes of symmetry

If a crystal, or indeed any object, possesses a **centre of symmetry**, then any line passing through the centre of the crystal connects equivalent faces, or atoms, or molecules. A familiar example is a right hand and a left hand placed palm-to-palm but with the fingers pointing in opposite directions, as in Fig. 4.4(a). Lines joining thumb to thumb or fingertip to fingertip all pass through a centre of symmetry between the hands. When the hands are placed palm-to-palm but with the fingers pointing in the same direction, as in prayer, then there is no centre

\* Denotes biographical notes available in Appendix 3.



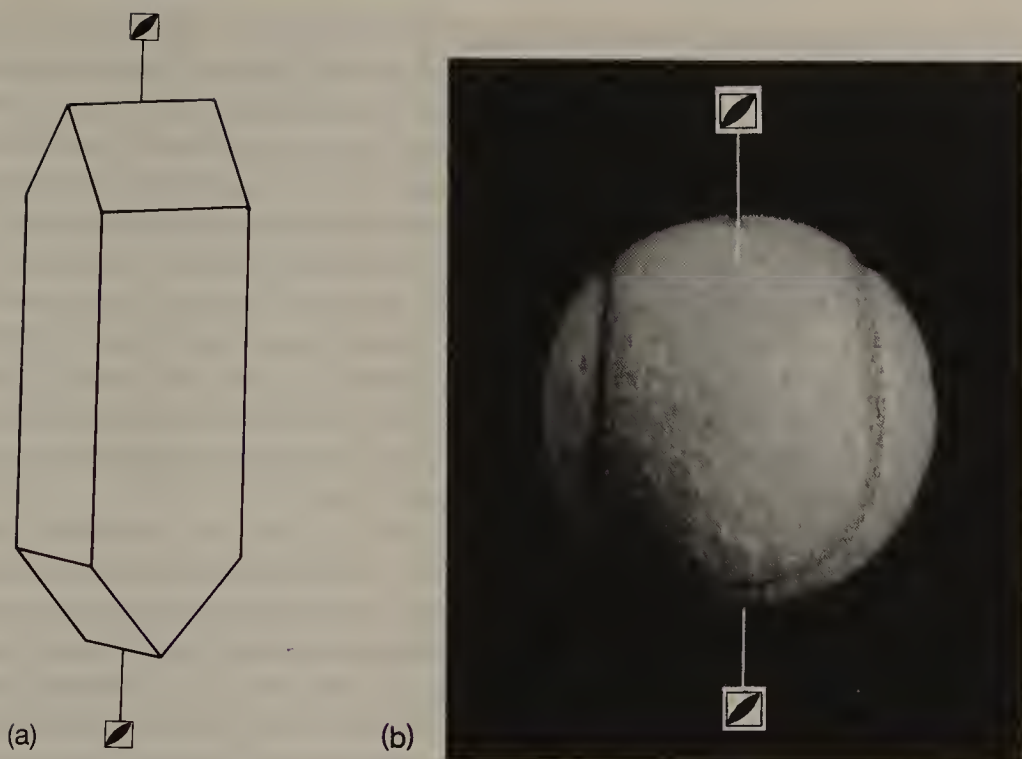
Fig. 4.4. Right and left hands (a) disposed with a centre of symmetry between them and (b) disposed with a mirror plane between them.

of symmetry but a mirror plane of symmetry instead, as in Fig. 4.4(b). In two dimensions a centre of symmetry is equivalent to diad symmetry. (See, for example, the motif and plane molecule shown in Fig. 2.3(c), which may be described as showing diad symmetry or a centre of symmetry.) In three dimensions this is not the case, as an inspection of Fig. 4.4(a) will show.

**Inversion axes of symmetry** are rather difficult to describe (and therefore difficult for the reader to understand) without the use of the stereographic projection—a method of representing a three-dimensional pattern of planes in a crystal on a two-dimensional plan. Geographers have the same problem when trying to represent the surface of the Earth on a two-dimensional map, and they too make use of the stereographic projection. In atlases, the circular maps of the world (usually with the North or South Poles in the centre) are often stereographic projections.

**Inversion axes** are *compound* symmetry elements, consisting of a rotation followed by an inversion. For example, as described in Chapter 2, the operation





**Fig. 4.5.** Examples of a crystal and an object which have inversion tetrad axes (both point group  $\bar{4}2m$ ). (a) Urea  $\text{CO}(\text{NH}_2)_2$  and (b) a tennis ball.

of a tetrad (four-fold) rotation axis is to repeat a crystal face or pattern every  $90^\circ$  rotation, e.g. in two dimensions giving four repeating **R**s or the four-fold pattern of faces in a cube. The operation of an inversion tetrad, symbol  $\square$  or  $\bar{4}$ , is to repeat a crystal face or pattern every  $90^\circ$  rotation-plus-inversion through a centre. What results is a four-fold pattern of faces around the inversion axis, but with each alternate face inverted. Examples of a crystal and an object with inversion tetrad axes are shown in Figs 4.5(a) and (b). The tennis ball has, in fact, the same point group symmetry as the crystal. Notice that when it is rotated  $90^\circ$  about the axis indicated, the 'downwards' loop in the surface pattern is replaced by an 'upwards' loop. Another  $90^\circ$  rotation brings a 'downwards' loop and so on for the full  $360^\circ$  rotation. Notice also that the inversion tetrad includes a diad, as is indicated by the diad (lens) symbol in the inversion tetrad (open square) symbol,  $\square$  or  $\bar{4}$ .

Finally, compare the symmetry of the tetragonal crystal in Fig. 4.5(a) with that of the tetrahedron (Fig. 4.2(d)): the diad axes which we recognized passing through the centres of opposite edges in the tetrahedron are, in fact, inversion tetrad axes or, to develop one of the points made in Section 4.1, stacking the cubes into the form of a tetrahedron reduces the symmetry element along the cube axis directions from rotation to inversion tetrad.

There are also inversion axes corresponding to rotation diads, triads and hexads. The operation of an inversion hexad, for example, is a rotation of  $60^\circ$  plus an inversion, this compound operation being repeated a total of six times

until we return to the beginning. However, for a beginner to the subject, these axes may perhaps be regarded as being of lesser importance than the inversion tetrads because they can be represented by combinations of other (better-understood) symmetry elements. The inversion diad is equivalent to a perpendicular mirror plane. The inversion triad is equivalent to a rotation triad plus a centre of symmetry—which is the symmetry of a rhombohedral lattice (see Fig. 3.1). Notice that the ‘top’ three faces of the rhombohedron are related to the ‘bottom’ three faces by a centre of symmetry. An inversion hexad is equivalent to a triad with a perpendicular mirror plane. Again, these equivalences are best understood with the use of the stereographic projection. The important point is that only inversion tetrads are unique (i.e. they cannot be represented by a combination of rotation axes, centres or mirror planes) and therefore need to be considered separately.

The point group symmetries of the thirty-two classes are described by a ‘short-hand’ notation or **point group symbol** which lists the main (but not necessarily all) symmetry elements present. For example, the presence of centres of symmetry is not recorded because they may arise ‘automatically’ from the presence of other symmetry elements, e.g. the presence of an inversion triad mentioned above. This notation for the thirty-two crystal classes or point groups, and their distribution among the seven crystal systems, is fully worked out in the *International Tables for Crystallography* published for the International Union of Crystallography and in F. C. Phillips’ *Introduction to Crystallography* (3rd edn) (Longman, 1977). Altogether there are five cubic classes, three orthorhombic classes, three monoclinic classes and so on. They are all listed in Table 3.1 (p. 57). The order in which the symmetry elements are written down in the point group symbol depends upon the crystal system.

In the cubic system the first place in the symbol refers to the axes parallel to, or planes of symmetry perpendicular to, the  $x$ -,  $y$ - or  $z$ -axes, the second refers to the four triads and the third the axes parallel to, or planes of symmetry perpendicular to, the face diagonal directions. Hence the point group symbol for the cube or the octahedron—the most symmetrical of the cubic crystals—is  $4/m\bar{3}2/m$ . This full point group symbol is usually (and rather unhelpfully) contracted to  $m\bar{3}m$  because the operation of the four triads and nine mirror planes (three parallel to the cube faces and six parallel to the face diagonals) ‘automatically’ generates the three tetrads and six diads. The symbol for the tetrahedron is  $\bar{4}3m$ , the  $\bar{4}$  referring to the three inversion tetrad axes along the  $x$ -,  $y$ - and  $z$ -axes together with the  $m$  referring to the face-diagonal mirror planes. The least symmetric cubic class has point group symbol  $23$ , i.e. it only has diads along the  $x$ -,  $y$ - and  $z$ -axes and the characteristic four triads.

In the orthorhombic system the three places in the point group symbol refer to the symmetry elements associated with the  $x$ -,  $y$ - and  $z$ -axes. The most symmetrical class (Fig. 4.3(a)), which has the full point group symmetry of the underlying orthorhombic unit cell (Fig. 3.5), has the full point group symbol  $2/m2/m2/m$ , but this is usually abbreviated to  $mmm$  because the presence of the three mirror planes perpendicular to the  $x$ -,  $y$ - and  $z$ -axes ‘automatically’

generates the three perpendicular diads. The other two classes are  $mm2$  (Fig. 4.3(b))—a diad along the intersection of two mirror planes—and  $222$  (Fig. 4.3(c))—three perpendicular diads.

In the monoclinic system the point group symbol simply refers to the symmetry elements associated with the  $y$ -axis. This may be a diad (class 2), an inversion diad (equivalent to a perpendicular mirror plane (class  $\bar{2}$  or  $m$ )), or a diad plus a perpendicular mirror plane (class  $2/m$ ).

In the tetragonal, hexagonal and trigonal systems, the first position in the point group symbol refers to the 'unique'  $z$ -axis. For example, the tetragonal crystals in Fig. 4.5 have point group symmetry  $\bar{4}2m$ ;  $\bar{4}$  referring to the inversion tetrad along the  $z$ -axis, 2 referring to the diads along the  $x$ - and  $y$ -axes and  $m$  to the mirror planes which bisect the  $x$ - and  $y$ -axes (which you will find by examining the model!). One of the trigonal classes has point group symbol  $32$  (not to be confused with cubic class  $23!$ ), i.e. a single triad along the  $z$ -axis and (three) perpendicular diads.

Not all classes are of equal importance; in two of them ( $432$  and  $\bar{6} = 3/m$ ) there may be no examples of real crystals at all! On the other hand, the two monoclinic classes  $m$  and  $2/m$  contain about 50 per cent of all inorganic crystalline materials on a 'crystal counting' basis, including feldspar, the commonest mineral in nature, and many other economically important minerals. As for the crystals of organic compounds, class  $2/m$  is by far the most important, while crystals of biologically important substances which contain chiral (right- or left-handed enantiomorphic molecules) have a predilection for class 2. The commonest class in any system is the **holosymmetric** class, i.e. the class which shows the highest symmetry. The holosymmetric cubic class  $m\bar{3}m$ , the most symmetrical of all, contains only a few per cent of all crystals on this basis, but these also include many materials and ceramics of economic and commercial importance.

## 4.4 Crystal symmetry and properties

The quantities which are used to describe the properties of materials are, as we know, simply represented as *coefficients*, i.e. as one measured (or measurable) quantity divided by another. For example, the property (coefficient) of electrical conductivity is given by the amount of electrical current flowing between two points (which may be measured in various ways) divided by the electrical potential gradient; the pyroelectric effect—the property of certain crystals of developing electrical polarization when the temperature is changed—is given by the polarization divided by the temperature change; the heat capacity is given by the quantity of heat absorbed or given out divided by the temperature change, and so on.

In many (in fact most) cases the measured quantities depend on direction and are called **vectors**\*. In the examples above, electrical current flow, potential

\* See Appendix 5.



gradient and polarization are all vectors. The other quantities in the examples above, temperature change, quantity of heat, do not depend on direction and are called **scalars**.

The important point is that, in those cases where one or more of the measured quantities vary with direction, so also do the crystal properties; they are said to be *anisotropic* (from the Greek tropos, direction or turn; (an)iso, (not the) same). Anisotropy clearly arises because the arrangements of atoms in crystals vary in different directions—you would intuitively *expect* crystals to be anisotropic, the only exceptions being those properties (the heat capacity) which are direction independent. You would also intuitively expect cubic crystals to be 'less anisotropic' than, say, monoclinic ones because of their greater symmetry, and this intuition would also be correct. For many properties, but not all, cubic crystals are isotropic—the property (and property coefficient) is direction independent. In the example given above, cubic crystals are isotropic with respect to electrical conductivity. They are also isotropic with regard to the pyroelectric effect, i.e. cubic crystals do not exhibit electrical polarization when the temperature is changed; the pyroelectric coefficient is zero. But cubic crystals are not isotropic with respect to all properties. For example, their elastic properties, which determine the mechanical properties of stiffness, shear and bulk moduli, are direction dependent and these are very important factors with respect to the properties of metals and alloys.

Hence, one major use of point groups is in relating crystal symmetry and properties; as the external symmetry of crystals arises from the symmetry of the internal molecular or atomic arrangements, so also do these in turn determine or influence crystal properties. Some examples have already been alluded to. For example, the pyroelectric effect cannot exist in a crystal possessing a centre of symmetry, and the pyroelectric polarization can only lie along a direction in a crystal that is *unique*, in the sense that it is not repeated by any symmetry element. There are only ten point groups or crystal classes which fulfil these conditions and they are called the **ten polar point groups**:

1	2	3	4	6
<i>m</i>	<i>mm2</i>	<i>3m</i>	<i>4mm</i>	<i>6mm</i> .

Hence, pyroelectricity or the pyroelectric effect can only occur in these ten polar point groups or classes.

A very closely related property to pyroelectricity, and of great importance in electroceramics, is ferroelectricity. A ferroelectric crystal, like a pyroelectric crystal, can also show polarization, but in addition the direction of polarization may be reversed by the application of an electric field. Most ferroelectric crystals have a transition temperature (Curie point) above which their symmetry is non-polar and below which it is polar.

One such example is barium titanate,  $\text{BaTiO}_3$ , which has the perovskite structure (Fig. 1.17). Above the Curie temperature barium titanate has the fully symmetric cubic structure, point group  $m3m$ , but below the Curie temperature, when the crystal becomes ferroelectric, distortions occur—a small expansion

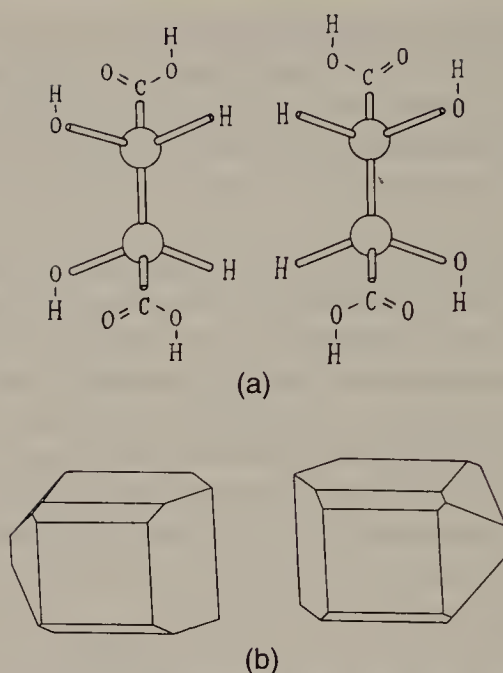


occurs along one cell edge and small contractions along the other two, changing the crystal system symmetry from cubic to tetragonal and the point group symmetry from  $m\bar{3}m$  to  $4mm$ . As the temperature is further lowered below the Curie point, further distortions occur and the point group symmetry changes successively to  $mm2$  and  $3m$ —all of them, of necessity, being polar point groups.

Another very important crystal property is piezoelectricity—the development of an electric dipole when a crystal is stressed, or conversely, the change of shape of a crystal when it is subjected to an electrical field. At equilibrium the applied stress will be centrosymmetrical, so if a crystal is to develop a dipole, i.e. develop charges of opposite sign at opposite ends of a line through its centre, it cannot have a centre of symmetry. There are twenty-one non-centrosymmetric point groups (Table 3.1), all of which, except one, point group 432, may exhibit piezoelectricity. It is the presence of the equally inclined triads, tetrads and diads in this cubic point group which in effect cancel out the development of a unidirectional dipole.

The optical properties of crystals—the variation of refractive index with the vibration and propagation direction of light (double refraction or birefringence), the variation of refractive index with wavelength or colour of the light (dispersion), or the associated variations of absorption of light (pleochroism)—are all symmetry dependent. The complexity of the optical properties increases as the symmetry decreases. Cubic crystals are optically isotropic—the propagation of light is the same in all directions and they have a single refractive index. Tetragonal, hexagonal and trigonal crystals are characterized by two refractive indices. For light travelling in a direction *perpendicular* to the principal (tetrad, hexad or triad) axis, such crystals exhibit two refractive indices—one for light vibrating along the principal axis, and another for light vibrating in a plane perpendicular to the principal axis. For light travelling *along* the principal axis (and therefore vibrating in the plane perpendicular to it), the crystal exhibits only one refractive index, and therefore behaves, for this direction only, as an optically isotropic crystal. Such crystals are called *uniaxial* with respect to their optical properties, and their principal symmetry axis is called the *optic axis*. Crystals belonging to the remaining crystal systems—orthorhombic, monoclinic and triclinic—are characterized by three refractive indices and two, not one, optic axes. Hence they are said to be biaxial since there are two, not one, directions for the direction of propagation of light in which they appear to be optically isotropic. It should be noted, however, that unlike uniaxial crystals, there is no simple relationship between the two optic axes of biaxial crystals and the principal symmetry elements; nor are they fixed, but vary as a result of dispersion, i.e. the variations in the values of the refractive indices with wavelength.

Finally, there is the phenomenon or property of optical activity or rotatory polarization, which should not be confused with double refraction. It is a phenomenon in which, in effect, the vibrational direction of light rotates such that it propagates through the crystal in a helical manner either to the right



**Fig. 4.6.** (a) (above) Left- and right-handed forms of tartaric acid molecules (from *Crystals: their Role in Nature and Science* by C. W. Bunn, Academic Press, New York, 1964); and (b) (below) the left- and right-handed forms of tartaric acid crystals (from F. C. Phillips, loc. cit.).

(dextrorotatory) or the the left (laevorotatory). Now right-handed and left-handed helices are distinct in the same way as a right and left hand (Fig. 4.4) or the two parts of a twinned crystal (Fig. 1.20(a)) and therefore optical activity would be expected to occur only in those crystals which occur in right-handed or left-handed forms, i.e. those which do not possess a mirror plane or a centre (or inversion axis) of symmetry. Such crystals are said to be enantiomorphous and there are altogether eleven enantiomorphous classes of point group symmetries (Table 3.1).

A famous example is tartaric acid (Fig. 4.6). In 1848 Louis Pasteur\* first noticed these two forms 'hemihedral to the right' and 'hemihedral to the left' under the microscope and, having separated them, found that their solutions were optically active in opposite senses.

## 4.5 Translational symmetry elements

The thirty-two point group symmetries (Table 3.1) may be applied to three-dimensional patterns just as the ten plane point group symmetries are applied to two-dimensional patterns (Chapter 2). As in two dimensions where translational symmetry elements or glide lines arise, so also in three dimensions do **glide planes** and also **screw axes** arise. It is only necessary to state the symmetry properties of patterns that are described by these translational symmetry elements. Glide planes are the three-dimensional analogues of glide lines; they

\* Denotes biographical notes available in Appendix 3.

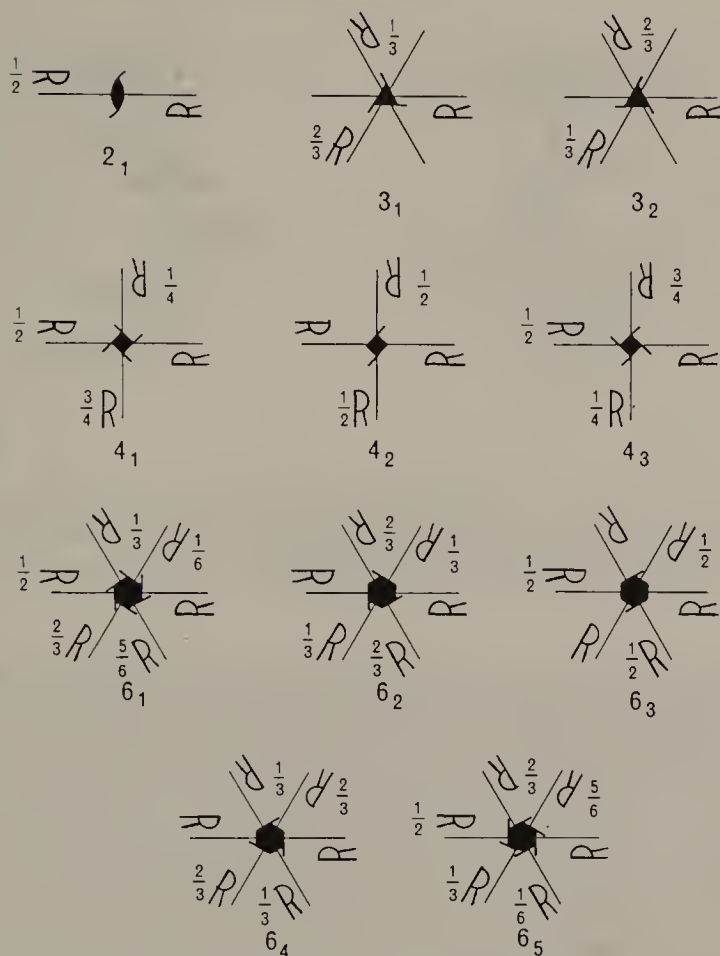
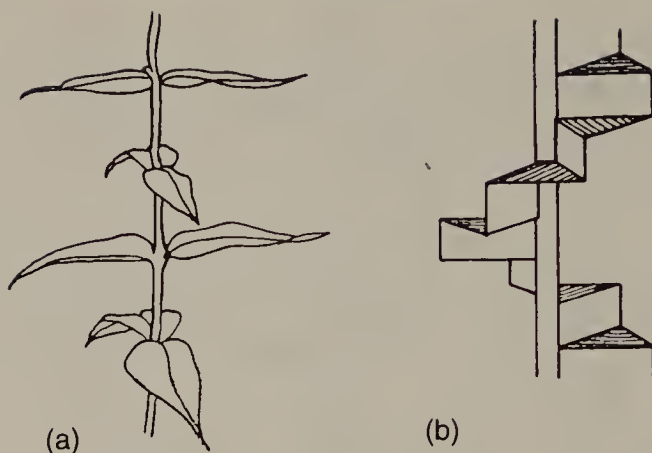


Fig. 4.7. The operation of screw axes on an asymmetrical motif,  $R$ . The fractions indicate the 'heights' of each motif as a fraction of the repeat distance.

define the symmetry in which mirror-related parts of the motif are shifted half a lattice spacing. In Fig. 2.9 the figures are related by glide lines, which can easily be visualized as glide-plane symmetry. Glide planes are symbolized as  $a$ ,  $b$ ,  $c$  (according to whether the translation is along the  $x$ -,  $y$ - or  $z$ -axes),  $n$  or  $d$  (diagonal or diamond glide—special cases involving translations along more than one axis).

Screw axes (for which there is no two-dimensional analogue) essentially describe helical patterns of atoms or molecules, or the helical symmetry of motifs. Several types of helices are possible and they are all based upon different combinations of rotation axes and translations. Figure 4.7 shows the possible screw axes (the direction of translation out of the plane of the page) with the heights  $R$  of the asymmetrical objects represented as fractions of the lattice repeat distance (compare to Fig. 2.3). Screw axes are represented in writing by the general symbol  $N_m$ ,  $N$  representing the rotation (2, 3, 4, 6) and the subscript  $m$  representing the pitch in terms of the number of lattice translation or repeat distances for one complete rotation of the helix.  $m/N$



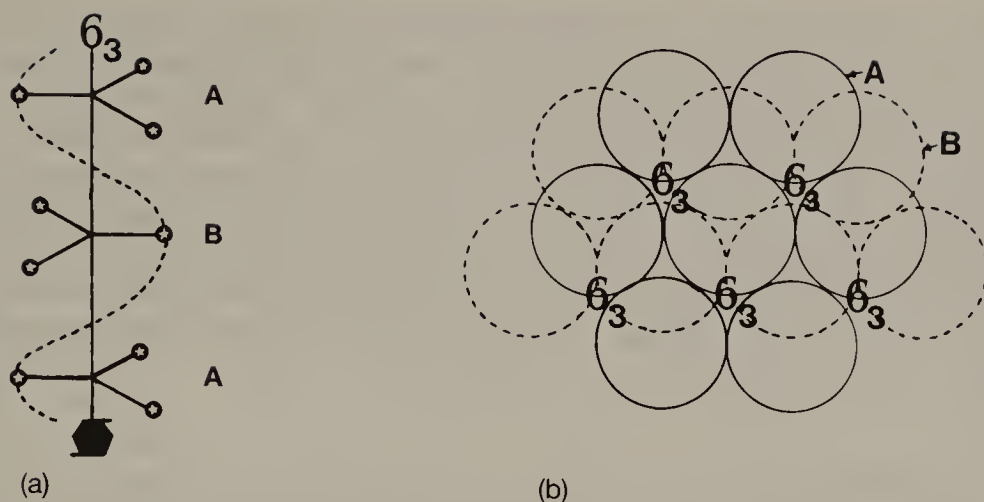
**Fig. 4.8.** (a) The  $4_2$  screw axis arrangement of leaves round a stem of pentstemon (after Walter Crane); and (b) a  $6_1$  screw axis spiral (helical) staircase (from *The Third Dimension in Chemistry* by A. F. Wells, Clarendon Press, Oxford, 1968).

therefore represents the translation for each rotation around the axis. Thus the  $4_1$  screw axis represents a rotation of  $90^\circ$  followed by a translation of  $\frac{1}{4}$  of the repeat distance, which repeated three times brings **R** to an identical position but displaced one lattice repeat distance; the  $4_3$  screw axis represents a rotation of  $90^\circ$  followed by a translation of  $\frac{3}{4}$  of the lattice repeat distance, which repeated three times gives a helix with a pitch of three lattice repeat distances. This is equivalent to the  $4_1$  screw axis but of opposite sign: the  $4_1$  axis is a right-handed helix and  $4_3$  axis is a left-handed helix. In short they are enantiomorphs of each other. Similarly the  $3_1$  and  $3_2$  axes, the  $6_1$  and  $6_5$  axes, and the  $6_2$  and  $6_4$  axes are enantiomorphs of each other. In diagrams, screw axes are represented by the symbol for the rotation axis with little 'tails' indicating (admittedly not very satisfactorily) the pitch and sense of rotation (see Fig. 4.7). Screw axes have, of course, their counterparts in nature and design—the distribution of leaves around the stem of a plant, for example, or the pattern of steps in a spiral (strictly helical) staircase. Figure 4.8 shows two such examples. Figure 4.9 shows the  $6_3$  screw hexads which occur in the hcp structure; notice that they run parallel to the *c*-axis and are located in the 'unfilled' channels which occur in the hcp structure. They do not pass through the atom centres of either the A layer or the B layer atoms; these are the positions of the triad (not hexad) axes in the hcp structure.

Just as the external symmetry of crystals does not distinguish between primitive and centred Bravais lattices, so also it does not distinguish between glide and mirror planes, or screw and rotation axes. For example, the six faces of an hcp crystal show hexad, six-fold symmetry, whereas the underlying structure possesses only screw hexad,  $6_3$ , symmetry.

In many crystals, optical activity arises as a result of the existence of enantiomorphic screw axes. For example, in quartz (enantiomorphic class 32), the  $\text{SiO}_2$  structural units which are not themselves asymmetric are arranged

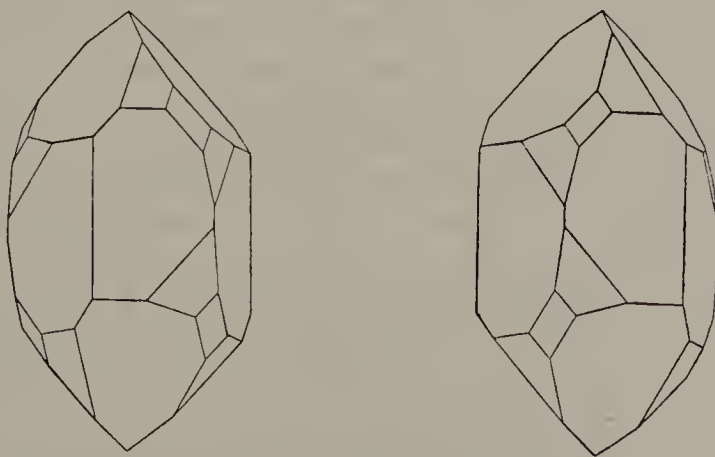




**Fig. 4.9.** (a) A screw hexad ( $6_3$ ) axis; and (b) location of these axes in the hcp structure. Notice that they pass through the 'unfilled channels' between the atoms in this structure.

along the  $c$ -axis (which is also the optic axis) in either a  $3_1$  or a  $3_2$  screw orientation. This gives rise to the two enantiomorphic crystal forms of quartz (class 32, Fig. 4.10). The plane of polarization of plane-polarized light propagating along the optic axis is rotated to right or left, the angle of rotation depending on the wavelength of the light and the thickness of the crystal. This is not, to repeat, the same phenomenon as birefringence; for the light travelling along the optic axis the crystal exhibits (by definition) one refractive index. If the  $3_1$  or  $3_2$  helical arrangement of the  $\text{SiO}_2$  structural units in quartz is destroyed (e.g. if the crystal is melted and solidified as a glass), the optical activity will also be destroyed.

However, in other crystals such as tartaric acid (Fig. 4.6) and its derivatives, the optical activity arises from the asymmetry—the lack of a mirror plane or centre of symmetry—of the molecule itself (Fig. 4.6(a)). In such cases the optical



**Fig. 4.10.** The enantiomorphic (right- and left-handed) forms of quartz. The optic axis is in the vertical (long) direction in each crystal (from F. C. Phillips, loc. cit.).

activity is not destroyed if the crystal is melted or dissolved in a liquid. The left or right handedness of the molecules, even though they are randomly orientated in a solution, is communicated at least in part, to the plane-polarized light passing through it. Unlike quartz, in which the optical activity depends on the direction of propagation of the light with respect to the optic axis, the optical activity of a solution such as tartaric acid is unaffected by the direction of propagation of the light. In summary, the optical activity of solutions arises from the asymmetry of the molecule itself; the optical activity which is shown in crystals, but not their solutions or melts, arises from the enantiomorphic screw symmetry of the arrangement of molecules in the crystal.

## 4.6 Space groups

In Section 2.4 it is shown how the seventeen possible two-dimensional patterns or plane groups (Fig. 2.6) can be described as a combination of the five plane lattices with the appropriate point and translational symmetry elements. Similarly, in three dimensions, it can be shown that there are 230 possible three-dimensional patterns or **space groups**, which arise when the fourteen Bravais lattices are combined with the appropriate point and translational symmetry elements. It is easy to see why there should be a substantially larger number of space groups than plane groups. There are fourteen space lattices compared with only five plane lattices, but more particularly there is a greater number of combinations of point and translational symmetry elements in three dimensions, particularly the presence of inversion axes (point) and screw axes (translational) which do not occur in two-dimensional patterns.

The first step in the derivation of 230 space groups was made by L. Sohncke\* (who also first introduced the notion of screw axes and glide planes described in Section 4.5). Essentially, Sohncke relaxed the restriction in the definition of a Bravais lattice—that the environment of each point is identical—by considering the possible arrays of points which have identical environments when viewed from *different* directions, rather than from the *same* direction as in the definition of a Bravais lattice. This is equivalent to combining the fourteen Bravais lattices with the appropriate translational symmetry elements, and gives rise to a total of sixty-five space groups or Sohncke groups.

The second, final, step was to account for inversion axes of symmetry which gives rise to a further 165 space groups. They were first worked out by Fedorov\* in Moscow in 1890 (who drew heavily on Sohncke's work) and independently by Schoenflies\* in Göttingen in 1891 and Barlow\* in London in 1894—an example of the frequently occurring phenomenon in science of progress being made almost at the same time by people approaching a problem entirely independently. The 230 space groups are systematically described in the *International Tables for Crystallography*. The short-hand representation now most generally adopted is that due to Hermann\* and Mauguin\*. However, not all the 230

\* Denotes biographical notes available in Appendix 3.

Hermann–Mauguin space group symbols will be described; only their most salient characteristics will be covered together with one example.

The Hermann–Mauguin space group symbol consists first of a letter  $P$ ,  $C$ ,  $I$ ,  $F$  or  $R$ , which describes the Bravais lattice type; then a statement, rather like a point group symbol, of the essential (not all) symmetry elements present. For example, the space group symbol  $Pba2$  represents a space group which has a primitive ( $P$ ) Bravais lattice and whose point group is  $mm2$  (the  $a$  and  $b$  glide planes being simple mirror planes in point group symmetry). This is one of the point groups of the orthorhombic system (Fig. 4.3(b)) and the lattice type is orthorhombic  $P$ .

The space group itself is represented by means of two diagrams, usually plotted as projections or plans in the  $x$ - $y$  plane (i.e. the  $z$ -axis is out of the plane of the paper). One of these plans shows the positions of all the symmetry elements present. The other shows the operation of these symmetry elements on an asymmetrical 'unit of pattern' represented as the symbol  $\odot$  (i.e. corresponding to the  $\mathbf{R}$  in our two-dimensional case), as shown in Fig. 2.1. In other words, the symbol  $\odot$  may represent an asymmetric molecule, a group of molecules or, indeed, any asymmetrical structural unit. It is placed at small fractions of the cell edge lengths  $x'y'z'$  away from the origin of the lattice, the  $z'$  parameter being represented by a plus sign in a projection along the  $z$ -axis (see Exercise 3.2); this is called a 'general position' because it does not lie on a non-translational symmetry element, i.e. at a centre of symmetry, on a mirror plane, or on an axis (rotational or inversion) of symmetry. The resulting set of atomic positions is known as the 'general equivalent positions'.

Figure 4.11 gives the two diagrams for space group  $Pba2$ . In Fig. 4.11(b) the diad axes are shown parallel to the  $z$ -axis and passing through every corner of the cell (i.e. through rows of lattice points), and the  $a$  and  $b$  glide planes are shown by dashed lines. Again, they run parallel to the  $z$ -axis but lie between the diad axes. The operation of these symmetry elements on the pattern unit  $\odot$  is shown in Fig. 4.11(a); the operation of the diads is to repeat the  $\odot$  after  $180^\circ$  rotation in exactly the same way as in the two-dimensional case (see Fig. 2.3).

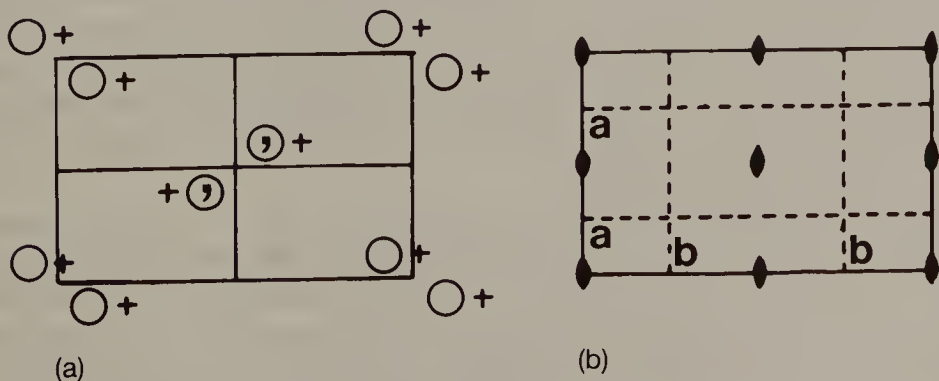


Fig. 4.11. Space group  $Pba2$  shown projected down the  $z$ -axis. (a) General equivalent positions within the unit cell and (b) positions of the symmetry elements.



The operation of the glide planes is to reflect the  $\bigcirc$  to give its mirror image, which is represented by the symbol  $\ominus$ , i.e. corresponding to the  $\bar{\mathbf{A}}$  in our two-dimensional case (Fig. 2.1), and then to translate it half a lattice spacing along the  $y$ - or  $x$ -axis. Hence we arrive at the pattern of right- and left-handed asymmetrical units,  $\bigcirc$  and  $\ominus$ , shown in Fig. 4.11(a) which is the space group *Pba*2. Notice that the operation of the diads through the corners of the unit cell 'automatically' generates additional diads in between. *All* the symmetry elements which arise in the space group are shown in Fig. 4.11(b). Notice too that if the pattern unit  $\bigcirc$  were to be placed not in a general position but in a 'special position', on a diad axis in this example, then a simpler pattern, with fewer general equivalent positions, results.

All the other 229 space groups can be built up in the same way, although it will be clear that the more symmetrical the crystal, the greater the number and types of symmetry elements present, the more complicated the pattern will be. Cubic space groups are therefore the most 'complicated', as a glance at the *International Tables* will show. However, remember that these complicated patterns of structural or pattern units do not mean that cubic crystals have necessarily more complicated structures. The space groups as drawn represent the most general case. As we saw above for space group *Pba*2, when the pattern unit, the  $\bigcirc$ , is placed on a diad axis of symmetry, i.e. a 'special position', a simpler pattern results. So also when the atoms are in special positions in the higher-symmetry crystals, and the greater the number of symmetry elements, the greater the simplification.

## 4.7 Bravais lattices, motifs and crystal structures

In the simple cubic, bcc and ccp structures of the elements, the three cubic lattices (Fig. 3.1) have exactly the same arrangement of lattice points as the atoms, i.e. in these examples the motif is just one atom. In more complex crystals the motif consists of more than one atom and, to determine the Bravais lattice of a crystal, it is necessary first to identify the motif and then to identify the arrangement of the motifs. In crystals consisting of two or more different types of atoms this procedure may be quite difficult, but fortunately simple examples best illustrate the procedure and the principles involved. For example, in NaCl (isomorphous with TiN; see Fig. 1.14(a)), the motif is one sodium and one chlorine ion and the motifs are arranged in an fcc array. Hence the Bravais lattice of NaCl and TiN is cubic *F*.

In  $\text{Li}_2\text{O}$  (isomorphous with  $\text{TiH}_2$ ; see Fig. 1.14(b)) the motif is one oxygen and two lithium atoms; the motifs are arranged in an fcc array and the Bravais lattice of these compounds is cubic *F*. In ZnS (isomorphous with  $\text{TiH}$ ; see Fig. 1.14(c)) the motif is one zinc and one sulphur atom; again, these are arranged in an fcc array and Bravais lattice of these compounds is cubic *F*. All the crystal structures illustrated in Fig. 1.14 have the cubic *F* Bravais lattice. They are called face-centred cubic structures not because the arrangements of atoms are the same—clearly they are not—but because they all have the cubic *F* lattice.



In CsCl (Fig. 1.12(b)), the motif is one caesium and one chlorine ion; the motifs are arranged in a simple cubic array and the Bravais lattice is cubic  $P$ . To be sure, the arrangement of ions in CsCl (and compounds isomorphous with it) is such that there is an ion or atom at the body-centre of the unit cell, but the Bravais lattice is *not* cubic  $I$  because the ions or atoms at the corners and centre of the unit cell are different. Nor, for the same reason, should CsCl and compounds isomorphous with it be described as having a body-centred cubic structure.

In the case of hexagonal structures the arrangements of lattice points in the hexagonal  $P$  lattice (Fig. 3.1) corresponds to the arrangement of atoms in the simple hexagonal structure (Fig. 1.5(a)) and *not* the hcp structure (Fig. 1.5(b)). In the simple hexagonal structure the environment of all the atoms is identical and the motif is just one atom. In the hcp structure the environment of the atoms in the A and B layers is different. The motif is a pair of atoms, i.e. an A layer and a B layer atom per lattice point. The environment of these pairs of atoms (as for the pairs of ions or atoms in the NaCl, or CsCl or ZnS structures) is identical and they are arranged on a simple hexagonal lattice. Notice that in these examples the motif is either asymmetric or has only one mirror line of symmetry. These are further instances of the situation which we found in two-dimensional patterns (Section 2.5). It is the repetition of the motif by the lattice which generates the crystal structures.

## Exercises

4.1 Draw the space group  $Pba2$  with the pattern unit  $\bigcirc$  at the following positions:

- (a) on the  $b$  glide plane, i.e. at  $(x'\frac{1}{4}z')$ ;
- (b) at the intersections of the  $a$  and  $b$  glide planes, i.e. at  $(\frac{1}{4}\frac{1}{4}z')$ ;
- (c) on a diad axis through the origin, i.e. at  $(00z')$ ;
- (d) on a diad axis through the mid-points of the cell edges, i.e. at  $(\frac{1}{2}0z')$ .

Hence, show that only (c) and (d) constitute special positions.

4.2 Make and examine the crystal models of NaCl, CsCl, diamond, ZnS (sphalerite), ZnS (wurtzite),  $\text{Li}_2\text{O}$  or  $\text{CaF}_2$  (fluorite),  $\text{CaTiO}_3$  (perovskite). Identify the Bravais lattice and describe the motif of each structure.

# Describing lattice planes and directions in crystals: Miller indices and zone axis symbols

## 5.1 Introduction

In previous chapters we have described the distributions of atoms in crystals, the symmetry of crystals, and the concept of Bravais lattices and unit cells. We now introduce what are essentially shorthand notations for describing directions and planes in crystals (whether or not they correspond to axes or planes of symmetry). The great advantages of these notations are that they are short, unambiguous and easily understood. For example, the direction (or zone axis) symbol for the ‘corner-to-corner’ (or triad axis) directions in a cube is simply  $\langle 111 \rangle$ . The plane index (or Miller index) for the faces of a cube is simply  $\{100\}$  or of an octahedron  $\{111\}$  (Fig. 4.1). The various faces and the directions of their intersections in crystals such as those illustrated in Fig. 4.3 can also be precisely described using these notations. Without them one would have to resort to carefully scaled drawings or projections.

Now direction symbols and plane indices are based upon the crystal axes or lattice vectors which outline or define the unit cell (see Section 3.2) and the only ambiguities which can arise occur in those cases in which different unit cells may be used. For example, crystals with the cubic  $F$  Bravais lattice may be described in terms of the ‘conventional’ face-centred cell (Fig. 1.6) or in terms of the primitive rhombohedral cell (Fig. 1.7). Because the axes are different, the direction symbols and plane indices will also be different. Hence it is important to know (1) which set of crystal axes, or which unit cell, is being used and (2) how to change or transform direction symbols and plane indices when the set of crystal axes or the unit cell is changed. This topic is covered in Section 5.8. It is a serious problem only in the case of the trigonal system for crystals with a rhombohedral lattice where there are two almost equally ‘popular’ unit cells—unlike, say, the rhombohedral cells for the cubic  $F$  and cubic  $I$  lattices which are rarely used. In addition, in the trigonal and hexagonal systems it is possible to introduce, because of symmetry considerations, a fourth axis, giving rise to ‘Miller–Bravais’ plane indices and ‘Weber’ direction symbols, each of which consist of four, rather than three, numbers. This topic is covered in Section 5.7, but first the concept of a zone and zone axis needs to be explained, a topic which is covered in more detail in Section 5.6.

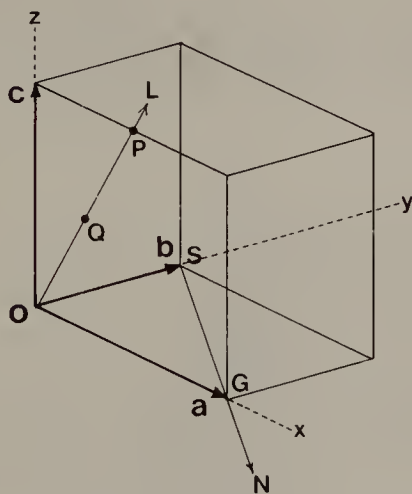
A **zone** may be defined as ‘a set of faces or planes in a crystal whose intersections are all parallel’. The common direction of the intersections is

called the **zone axis**. All directions in crystals are zone axes, so the terms 'direction' and 'zone axis' are synonymous. So much for the definition. The concept of a zone is readily understood by examining an ordinary pencil. The six faces of a pencil all form or lie in a zone because they all intersect along one direction—the pencil lead direction—which is the zone axis for this set of faces. The number of faces in a zone is not restricted and the faces need not be crystallographically equivalent. For example, the edges of a pencil may be shaved flat to give a 12-sided pencil, i.e. an additional six faces in the zone. Or consider an orthorhombic crystal (Fig. 3.5(b)), or a matchbox. Each crystal axis is the zone axis for four faces, or two crystallographically equivalent pairs of faces. Each face lies in two zones; for example, the 'top' and 'bottom' faces of Fig. 3.5(b) lie in the zones which have the  $x$ - and  $y$ -directions as zone axes. In general, a face or plane in a crystal belongs to a whole 'family' of zones, the zone axes of which lie in or are parallel to the face.

Verbal definitions are frequently rather clumsy in relation to the simple concepts which they seek to express. Take a piece of paper and draw on it some parallel lines. Fold the paper along the lines—and there you have a zone!

## 5.2 Indexing lattice directions—zone axis symbols

First, the direction whose symbol is to be determined must pass through the origin of the unit cell. Consider the unit cell shown in Fig. 5.1, which has unit cell edge vectors  $\mathbf{a}$ ,  $\mathbf{b}$ ,  $\mathbf{c}$  (which are not necessarily orthogonal or equal in length)\*. The steps for determining the zone axis symbol for the direction OL are as follows. Write down the coordinates of a point—any point—in this direction—say P—in terms of fractions of the lengths  $a$ ,  $b$  and  $c$ , respectively.



**Fig. 5.1.** Primitive unit cell of a lattice defined by unit cell vectors  $\mathbf{a}$ ,  $\mathbf{b}$ ,  $\mathbf{c}$ . OL and SN are directions  $[102]$  and  $[1\bar{1}0]$  respectively.

\* See Appendix 5 for a simple introduction to vectors.

The coordinates of P are  $\frac{1}{2}$ , 0, 1. Now express these fractions as the ratio of whole numbers and insert them into [square] brackets without commas; hence [102]. This is then the direction or zone axis symbol for OL. Notice that if we had chosen a different point along OL—say Q—with coordinates  $\frac{1}{4}$ , 0,  $\frac{1}{2}$ , we would have obtained the same result.

Now consider the direction SN. To find its direction symbol the origin must be shifted from O to S. Proceeding as before (e.g. finding the coordinates of G with respect to the origin at S) gives the direction symbol  $[\bar{1}10]$  (pronounced one bar-one oh), the bar or minus sign referring to a coordinate in the negative sense along the crystal axis.

Directions in crystals are, of course, vectors, which may be expressed in terms of components on the three unit cell edge or 'base' vectors **a**, **b** and **c**. In the above example the direction OL is written

$$\mathbf{r}_{102} = 1\mathbf{a} + 0\mathbf{b} + 2\mathbf{c}.$$

The general symbol for a direction is  $[uvw]$  or, written as a vector,

$$\mathbf{r}_{uvw} = u\mathbf{a} + v\mathbf{b} + w\mathbf{c}.$$

The direction symbols for the unit cell edge vectors **a**, **b** and **c** are [100], [010] and [001], and very often these symbols are used in preference to the terms *x*-axis, *y*-axis and *z*-axis.

### 5.3 Indexing lattice planes—Miller indices

First, for reasons which will be apparent shortly, the lattice plane whose index is to be determined must not pass through the origin of the unit cell, or rather the origin must be shifted to a corner of the cell which does not lie in the plane. Consider the unit cell in Fig. 5.2 (identical to Fig. 5.1 but drawn separately to avoid confusion). We shall determine the index of the lattice plane which is

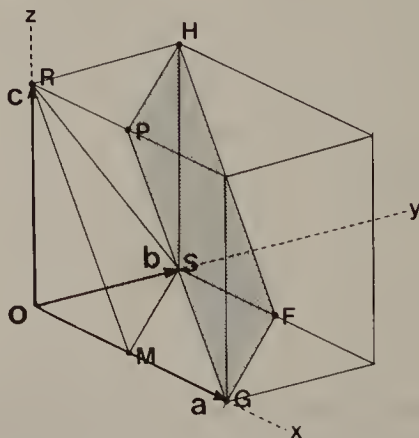


Fig. 5.2. Primitive unit cell (identical to Fig. 5.1), showing the first two planes, RMS and PGFH, in the family. These planes are shaded within the confines of the unit cell.



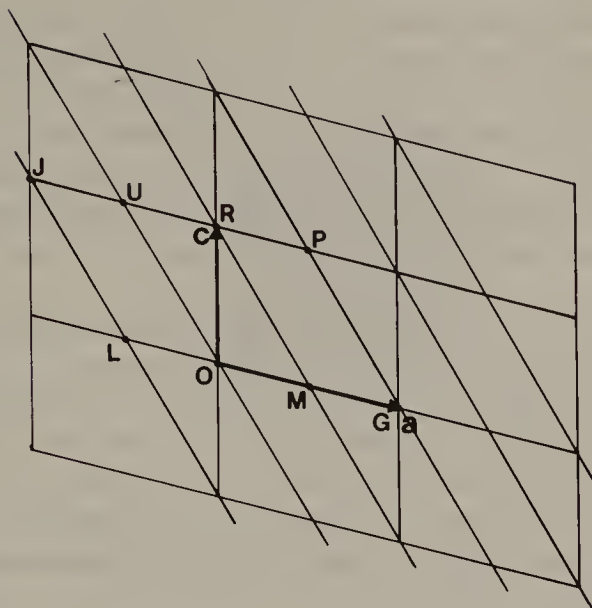


Fig. 5.3. Sketch of Fig. 5.2 with the  $\mathbf{a}$  and  $\mathbf{c}$  unit cell vectors in the plane of the paper ( $\mathbf{b}$  into the plane of the paper) showing traces JL, UO, RM, PG of a family of planes.

shaded and outlined by the letters RMS. It is important first to realize that this plane extends indefinitely through the crystal; the shaded area is simply that portion of the plane that lies within the unit cell of Fig. 5.2. It is also important to realize that we are not just considering *one* plane but a whole *family* of identical, parallel planes passing through the crystal. The next plane 'up' in the family is also shaded within the confines of the unit cell and is outlined by the letters PGFH. There is a whole succession of such planes, including one which passes through the origin of the unit cell.

A two-dimensional sketch (Fig. 5.3) of Fig. 5.2, with the  $x$ - and  $z$ -axes in the plane of the paper, and showing the traces of these planes extending into neighbouring cells, will make this clear. Figure 5.3 also shows that all the planes in the family are identical in that they contain the same number or sequence of lattice points.

For RMS, the plane in the family nearest the origin, write down the *intercepts* of the plane on the axes or unit cell vectors  $\mathbf{a}$ ,  $\mathbf{b}$ ,  $\mathbf{c}$ , respectively; they are  $\frac{1}{2}\mathbf{a}$ ,  $1\mathbf{b}$ ,  $1\mathbf{c}$ . Expressed as fractions of the cell edge lengths we have  $\frac{1}{2}$ , 1, 1. Now take the *reciprocals* of these fractions, and put the whole numbers into (round) brackets without commas; hence (211). This is the **Miller index** of the plane, so-called after the crystallographer, W. H. Miller\*, who first devised the notation. Proceeding similarly for the next plane in the family, PGFH (and considering its extension beyond the confines of the unit cell), we have intercepts  $1\mathbf{a}$ ,  $2\mathbf{b}$ ,  $2\mathbf{c}$ , which expressed as fractions becomes 1, 2, 2; the reciprocals of which are  $1$ ,  $\frac{1}{2}$ ,  $\frac{1}{2}$ , which expressed as whole numbers again gives the Miller index

\* Denotes biographical notes available in Appendix 3.

(211). The plane through the origin, OU (Fig. 5.3), has intercepts 0, 0, 0 which gives an indeterminate 'Miller index' ( $\infty\infty\infty$ ), but this is merely expressive of the fact that another corner of the unit cell must be selected as the origin. The plane JL (Fig. 5.3) in the same family lies on the opposite side of the origin from RM and has intercepts  $-\frac{1}{2}a, -1b, -1c$ , which gives the Miller index ( $\bar{2}\bar{1}\bar{1}$ ) (pronounced bar-two, bar-one, bar-one), the bar signs simply being expressive of the fact that the planes are recorded from the opposite (negative axis) side of the origin.

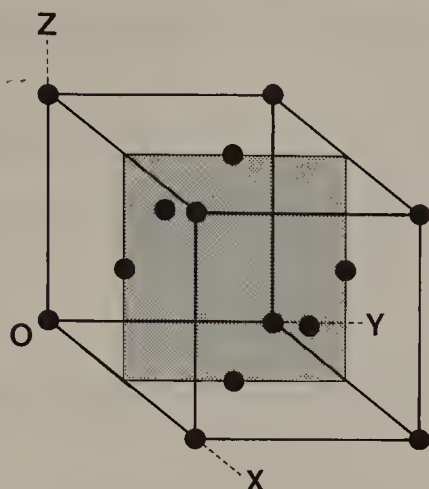
The general index for a lattice plane is  $(hkl)$ , i.e. (working backwards), the first plane in the family from the origin makes intercepts  $a/h, b/k, c/l$  on the axes. This provides us with an alternative method for determining the Miller index of a family of planes. Count the number of planes intercepted in passing from one corner of the unit cell to the next. For the family of planes  $(hkl)$  the first plane intercepts the  $x$ -axis at a distance  $a/h$ , the second at  $2a/h$ , and so on; i.e. a total of  $h$  planes are intercepted in passing from one corner of the unit cell to the next along the  $x$ -axis. Similarly,  $k$  planes are intercepted along the  $y$ -axis and  $l$  planes along the  $z$ -axis.

Miller indices apply not only to lattice planes, as sketched in Fig. 5.2 and 5.3, but also to the external faces of crystals, where the origin is conventionally taken to be at the centre of the crystal. The intercepts of a crystal face will be many millions of lattice spacings from the origin, depending of course on the size of the crystal but the *ratios* of the fractional intercepts, and therefore the Miller indices, will be simple whole numbers as before. This is sometimes expressed as 'The Law of Rational Indices', the germ of which can be traced back to Haüy—see, for example, his representation of the relationship between the crystal faces and the unit cell in dog-tooth spar (Fig. 1.2).

When a crystal plane lies parallel to an axis its intercept on that axis is infinity, the reciprocal of which is zero. For example, the 'front' face of a crystal, i.e. the face which intersects the  $x$ -axis only and is parallel to the  $y$ - and  $z$ -axes, has Miller index (100); the 'top' face, which intersects the  $z$ -axis is (001) and so on. It is useful to remember that a zero Miller index means that the plane (or face) is parallel to the corresponding unit cell axis.

Although Miller indices never include fractions they may, when used to describe lattice planes, have common denominators and this occurs when the unit cell is non-primitive. Consider, for example, the lattice planes perpendicular to the  $x$ -axis in the cubic  $F$  unit cell (Fig. 5.4). Because of the presence of the face-centring lattice points, lattice planes are intersected every  $\frac{1}{2}a$  distance along the  $x$ -axis. The first lattice plane in the family, shown shaded in Fig. 5.4, makes fractional intercepts  $\frac{1}{2}, \infty, \infty$  on the  $x$ -,  $y$ - and  $z$ -axes. The Miller index of this family of planes is therefore (200). To refer to them as (100) would be to ignore the 'interleaving' lattice planes within the unit cell. This distinction does not apply to the Miller indices of the external crystal faces, which are many millions of lattice planes from the origin.

The procedure described above for defining plane indices may seem rather odd—why not simply express indices as fractional intercepts without taking



**Fig. 5.4.** A cubic  $F$  unit cell showing (shaded) the first plane from the origin of a family of planes perpendicular to the  $x$ -axis but with interplanar spacing  $a/2$ .

reciprocals? The Law of Rational Indices gives half a clue, but the full significance can only be appreciated in terms of the reciprocal lattice (Chapter 6).

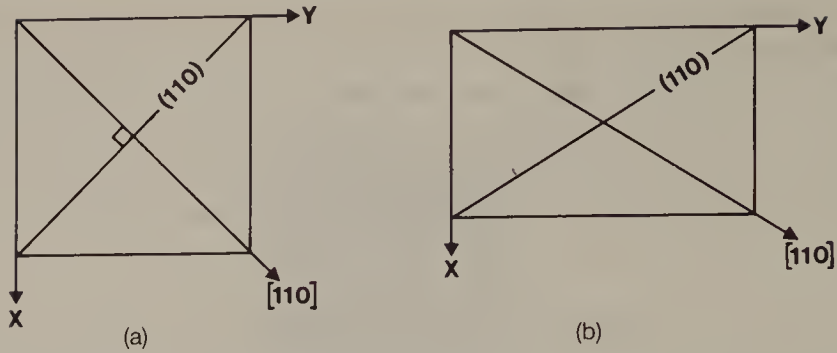
## 5.4 Miller indices and zone axis symbols in cubic crystals

Miller indices and zone axis symbols may be used to express the symmetry of crystals. This applies to crystals in all the seven systems, but the principles are best explained in relation to cubic crystals because of their high symmetry.

The positive and negative directions of the crystal axes  $x, y, z$  can be expressed by the direction symbols (Section 5.2) as  $[100]$ ,  $[\bar{1}00]$ ,  $[010]$ ,  $[0\bar{1}0]$ ,  $[001]$ ,  $[00\bar{1}]$ . Because, in the cubic system, the axes are crystallographically equivalent and interchangeable, so also are all these six direction symbols. They may be expressed collectively as  $\langle 100 \rangle$ , the  $\langle$ triangular $\rangle$  brackets implying all six permutations or variants of 1, 0, 0. Similarly, the triad axis corner-to-corner directions are expressed as  $\langle 111 \rangle$ , of which there are eight (four pairs) of variants, namely,  $[11\bar{1}]$ ,  $[\bar{1}11]$ ;  $[\bar{1}\bar{1}1]$ ,  $[\bar{1}1\bar{1}]$ ;  $[\bar{1}11]$ ,  $[1\bar{1}\bar{1}]$ ;  $[111]$ ,  $[1\bar{1}\bar{1}]$ . The diad axis (edge-to-edge) directions are  $\langle 110 \rangle$ , of which there are twelve (six pairs) of variants. For the general direction  $\langle uvw \rangle$  there are forty-eight (twenty-four pairs) of variants.

A similar concept can be applied to Miller indices. The six faces of a cube (with the origin at the centre) are  $(100)$ ,  $(\bar{1}00)$ ,  $(010)$ ,  $(0\bar{1}0)$ ,  $(001)$ ,  $(00\bar{1})$ . These are expressed collectively as planes 'of the form'  $\{100\}$ , i.e. in  $\{$ curly $\}$  brackets. Again, for the general plane  $\{hkl\}$  there are forty-eight (twenty-four pairs) of variants.

In cubic crystals, directions are perpendicular to planes with the same numerical indices; for example, the direction  $[111]$  is perpendicular to the plane  $(111)$ , or equivalently it is parallel to the normal to the plane  $(111)$ . This parallelism between directions and normals to planes with the same numerical indices does not apply to crystals of lower symmetry except in special cases. This



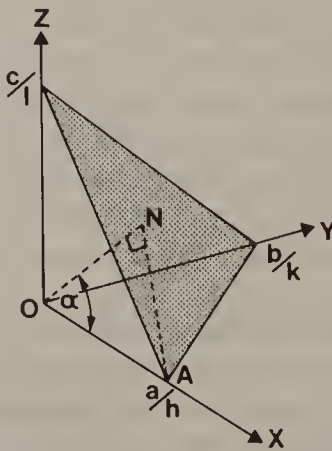
**Fig. 5.5.** Plans of (a) cubic and (b) orthorhombic unit cells perpendicular to the  $z$ -axis, showing the relationships between planes and zone axes of the same numerical indices.

will be made clear by considering Figs 5.5(a) and (b), which show plans of unit cells perpendicular to the  $z$ -axis of a cubic and an orthorhombic crystal. The traces of the  $(110)$  plane and  $[110]$  directions are shown in each case. Clearly, the  $(110)$  plane and  $[110]$  direction are only perpendicular to each other in the cubic crystal. In the orthorhombic crystal it is only in the special cases, e.g.  $(100)$  planes and  $[100]$  directions, that the directions are perpendicular to planes of the same numerical indices.

### 5.5 Lattice plane spacings, Miller indices and Laue indices

The calculation for lattice plane spacings (also called interplanar spacings or  $d$ -spacings),  $d_{hkl}$ , is simple in the case of crystals with orthogonal axes. Consider Fig. 5.6, which shows the first plane away from the origin in a family of  $(hkl)$  planes. As there is another plane in the family passing through the origin, the lattice plane spacing is simply the length of the normal  $ON$ . Angle  $AON = \alpha$  (angle between normal and  $x$ -axis) and angle  $ONA = 90^\circ$ . Hence

$$OA \cos \alpha = ON \quad \text{or} \quad (a/h) \cos \alpha = d_{hkl} \quad \text{or} \quad \cos \alpha = \left( \frac{h}{a} \right) d_{hkl}.$$



**Fig. 5.6.** Intercepts of a lattice plane  $(hkl)$  on the unit cell vectors  $a$ ,  $b$ ,  $c$ .  $ON = d_{hkl}$  = interplanar spacing.



Given that  $\beta$  and  $\gamma$  (not shown in Fig. 5.6) are the angles between ON and the  $y$ - and  $z$ -axes, respectively, then

$$\cos \beta = \left( \frac{k}{b} \right) d_{hkl} \quad \text{and} \quad \cos \gamma = \left( \frac{l}{c} \right) d_{hkl}.$$

For orthogonal axes  $\cos^2 \alpha + \cos^2 \beta + \cos^2 \gamma = 1$  (Pythagoras), hence

$$\left( \frac{h}{a} \right)^2 d_{hkl}^2 + \left( \frac{k}{b} \right)^2 d_{hkl}^2 + \left( \frac{l}{c} \right)^2 d_{hkl}^2 = 1.$$

For a cubic crystal  $a = b = c$ , hence

$$\frac{1}{d_{hkl}^2} = \frac{h^2 + k^2 + l^2}{a^2}.$$

The concept of lattice planes and interplanar spacings is the basis of the concept of the reciprocal lattice (Chapter 6) and also Bragg's law (Chapter 8)—an equation which every schoolboy (or girl) knows!

$$n\lambda = 2d_{hkl} \sin \theta$$

where  $n$  is the order of reflection,  $\lambda$  is the wavelength,  $d_{hkl}$  is the lattice plane spacing and  $\theta$  is the angle of incidence/reflection to the lattice planes. However, it is very important, when using Bragg's law, to distinguish between lattice planes and **reflecting planes**.

Except in the cases of non-primitive cells discussed above (Section 5.3), indices for lattice planes do not have common factors. However, the indices for reflecting planes frequently do have common factors. They are sometimes called **Laue indices** and are usually written without brackets. Their relationship with Miller indices for lattice planes is best illustrated by way of an example. Apply Bragg's law to the (111) lattice planes in a crystal:

$$\text{first-order reflection } (n = 1): 1\lambda = 2d_{111} \sin \theta_1$$

$$\text{second-order reflection } (n = 2): 2\lambda = 2d_{111} \sin \theta_2, \text{ etc.}$$

Now the order of reflection is written on the right-hand side, i.e. for the second-order reflection ( $n = 2$ )

$$1\lambda = 2 \left( \frac{d_{111}}{2} \right) \sin \theta_2.$$

This suggests that second-order reflections from the (111) lattice planes of  $d$ -spacing  $d_{111}$  can be regarded as first-order reflections from planes of half the spacing,  $d_{111}/2$ . Halving the intercepts implies doubling the indices, so these planes are called 222 (no brackets) of  $d$ -spacing  $d_{222} = d_{111}/2$ . These 222 planes are imaginary in the sense that only half of them pass through lattice points, but they are a useful fiction in the sense that the order of reflection,  $n$  in Bragg's law, can be omitted. Continuing the above example, third-order reflections from the (111) lattice planes can be regarded as first-order reflections from the 333

reflecting planes (only a third of which in a family pass through lattice points). As mentioned above, these unbracketed indices are sometimes called Laue indices or reflection indices.

However, it should be pointed out that, in practice, when analysing X-ray or electron diffraction patterns, crystallographers very often do not make this distinction between Miller indices and Laue indices, but simply refer, for example, to 333 reflections (no brackets) from (333) 'planes' (with brackets). This should not lead to any confusion, except perhaps in the case of centred lattices where lattice planes may have common factors. For example, the 200 reflecting planes in the cubic *F* lattice (Fig. 5.4) are also the (200) lattice planes, but the 200 reflecting planes in the cubic *P* lattice refer to second-order reflections from the (100) lattice planes.

## 5.6 Zones, zone axes and the zone law, the addition rule

The concept of a zone has been introduced in Section 5.1. In this section some useful geometrical relationships are listed, the proofs of which are given in Section 6.5, in which use is made of reciprocal lattice vectors. It is possible, of course, to prove the relationships given below without making use of the concept of the reciprocal lattice, but the proofs tend to be long, tedious and not very obvious.

### 5.6.1 The zone law (or Weiss\* zone law)

If a plane (*hkl*) lies in a zone [*uvw*] (i.e. if the direction [*uvw*] is parallel to the plane (*hkl*)), then

$$hu + kv + lw = 0.$$

### 5.6.2 Zone axis at the intersection of two planes

The line or direction of intersection of two planes in a zone (*h*<sub>1</sub>*k*<sub>1</sub>*l*<sub>1</sub>) and (*h*<sub>2</sub>*k*<sub>2</sub>*l*<sub>2</sub>) gives the zone axis, [*uvw*], where

$$u = (k_1 l_2 - k_2 l_1); \quad v = (l_1 h_2 - l_2 h_1); \quad w = (h_1 k_2 - k_2 h_1).$$

To remember these relationships, use the following 'memogram':

<i>h</i> <sub>1</sub>	<i>k</i> <sub>1</sub>	<i>l</i> <sub>1</sub>	<i>h</i> <sub>1</sub>	<i>k</i> <sub>1</sub>	<i>l</i> <sub>1</sub>
<i>h</i> <sub>2</sub>	<i>k</i> <sub>2</sub>	<i>l</i> <sub>2</sub>	<i>h</i> <sub>2</sub>	<i>k</i> <sub>2</sub>	<i>l</i> <sub>2</sub>
<i>u</i>			<i>v</i>		
<i>u</i>			<i>w</i>		

Write down the indices twice and strike out the first and last pairs. Then *u* is given by cross-multiplying, i.e.

$$u = (\text{plus } k_1 l_2 \text{ minus } k_2 l_1),$$

and similarly for *v* and *w*.

\* Denotes biographical notes available in Appendix 3.

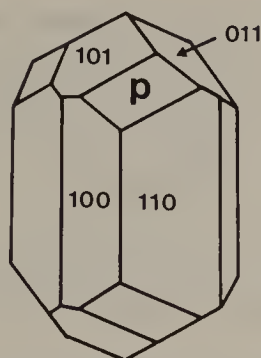


Fig. 5.7. A monoclinic crystal (class  $m$ ) in which the face  $P$  lies in two zones, one containing (101) and (110), the other containing (011) and (100).

### 5.6.3 Plane parallel to two directions

To find the plane lying parallel to two directions  $[u_1v_1w_1]$  and  $[u_2v_2w_2]$ , write down the 'memogram'

$$\begin{array}{c|cc|cc|cc|c}
 u_1 & v_1 & & w_1 & & u_1 & v_1 & w_1 \\
 u_2 & v_2 & \begin{array}{c} \times - \\ + \end{array} & w_2 & \begin{array}{c} \times - \\ + \end{array} & u_2 & v_2 & w_2 \\
 \hline
 & & h & & k & & l & 
 \end{array}$$

and proceed as above, i.e.  $h = (v_1w_2 - v_2w_1)$ , etc.

### 5.6.4 The addition rule

Consider two planes  $(h_1k_1l_1)$  and  $(h_2k_2l_2)$  lying in zone. Then the index of another plane  $(HKL)$  in the zone lying between these planes is given by  $H = (mh_1 + nh_2)$ ;  $K = (mk_1 + nk_2)$ ;  $L = (ml_1 + nl_2)$ , where  $m$  and  $n$  are small whole numbers.

The rule enables us to work out the indices of 'in-between' planes in zones. Consider, for example, the plane marked  $P$  in Fig. 5.7, which lies both in the zone containing (100) and (011) and the zone containing (101) and (110). We need a choose values of  $m$  and  $n$  such that adding the pairs of indices as above gives the same result for  $(HKL)$ . This is much more easily done than said! The plane is (211), i.e.

$$(101) + (110) = (211) \quad (m = 1, n = 1)$$

and

$$(011) + 2(100) = (211) \quad (m = 1, n = 2).$$

## 5.7 Indexing in the trigonal and hexagonal systems: Weber symbols and Miller-Bravais indices

As shown in Section 3.3, the rhombohedral and hexagonal lattices both consist of hexagonal layers of lattice points which in the rhombohedral lattice are

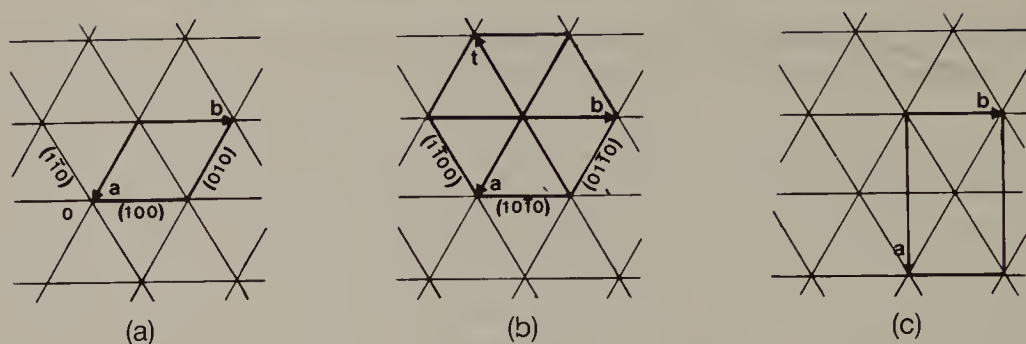


Fig. 5.8. Hexagonal net of the hexagonal  $P$  lattice showing (a) primitive hexagonal unit cell with the traces of the six prism faces indexed  $\{hkl\}$ , (b) hexagonal (four-index) unit cell with the traces of the six prism faces indexed  $\{hkil\}$ , (c) orthohexagonal (Base or  $C$ -centred) unit cell.

'stacked' in the ABCABC... sequence (Fig. 3.3(b)) and in the hexagonal lattice are 'stacked' in the AAA... sequence (Fig. 3.3(a)). In both cases, it is convenient to outline unit cells using the easily recognized hexagonal layers as the 'base' of the cells and with the  $z$ -axis (or  $c$  vector) perpendicular thereto. However, at least three choices of unit cell are commonly made and these are illustrated in the case of the hexagonal lattice in Fig. 5.8 (the corresponding unit cells of the rhombohedral lattice differ only insofar as they contain additional lattice points of the B and C layers at fractional distances of  $\frac{1}{3}$  and  $\frac{2}{3}$  of the unit edge length along the  $z$ -axis).

Figure 5.8(a) shows the primitive hexagonal unit cell, the smallest that can be chosen with the  $x$ - and  $y$ -axes at  $120^\circ$ . However, this is often inconvenient in that it does not reveal the hexagonal symmetry of the lattice. For example, all the (pencil) faces parallel to the  $z$ -axis are crystallographically equivalent or of the same form, but their indices differ in type as shown—some have indices of the type  $(1\bar{1}0)$  and some have indices of the type  $(100)$ . To overcome this problem a *fourth* axis—the  $u$ -axis—is inserted at  $120^\circ$  to both the  $x$ - and  $y$ -axes, as shown in Fig. 5.8(b). These are called Miller–Bravais axes  $x, y, u, z$  (or vectors  $\mathbf{a}, \mathbf{b}, \mathbf{t}, \mathbf{c}$ ) and the indices of the lattice planes, called Miller–Bravais indices, now consist of four numbers  $\{hkil\}$ . The indices for the pencil faces are shown in Fig. 5.8(b) and they are all of the same form  $\{10\bar{1}0\}$ . Notice that, in all cases the sum of the first three numbers is zero, i.e.  $h + k + i = 0$ . As therefore  $i = -(h + k)$ , is sometimes simply represented as a dot, i.e.  $\{hk.l\}$ . However, this unnecessary abbreviation should be discouraged, as it defeats the object of using Miller–Bravais axes in the first place.

Similarly, zone axis symbols, sometimes called **Weber\* symbols**, consist of four numbers  $\langle UVTW \rangle$ . However, determining these numbers (i.e. determining the components of a vector using four base vectors in three-dimensional space) is not straightforward. Essentially, the components of a vector are adjusted such

\* Denotes biographical notes available in Appendix 3.



that the sum of the first three numbers is zero, i.e.  $U + V + T = 0$ . In practice, the simplest procedure is to determine first the zone axis symbol  $[uvw]$  of a direction using three axes (Fig. 5.8(a)) and then transform these to  $[UVTW]$  using the following identities:

$$U = \frac{1}{3}(2u - v), \quad V = \frac{1}{3}(2v - u), \quad T = -(U + V), \quad W = w.$$

On this basis the zone axis symbols for the  $x$ -,  $y$ - and  $u$ -axes are  $[2\bar{1}\bar{1}0]$ ,  $[\bar{1}2\bar{1}0]$  and  $[\bar{1}\bar{1}20]$ , respectively. The reverse transformation from  $[UVTW]$  to  $[uvw]$  is given by the identities

$$u = (U - T), \quad v = (V - T), \quad w = W.$$

When using Miller–Bravais indices and Weber symbols, the zone law becomes

$$hU + kV + iT + lW = 0.$$

Another unit cell—the orthohexagonal cell—is shown in Fig. 5.8(c). The ratio of the lengths of the edges,  $a/b$  is  $\sqrt{3}$ . As with the primitive hexagonal cell this does not reveal the hexagonal symmetry of the lattice. This base-centred cell has the advantage that the axes are orthogonal and is particularly useful in showing the relationships between the crystals which have similar structures but where small distortions can change the symmetry from hexagonal to orthorhombic, i.e. in situations in which the ratio  $a/b$  is no longer precisely  $\sqrt{3}$ .

To summarize, great care must be taken in interpreting plane indices and zone axis symbols in the hexagonal and trigonal systems—an index such as (111) could refer to the primitive hexagonal or orthohexagonal unit cell, or it could even refer to the Miller–Bravais hexagonal unit cell and be the contracted form of  $(11\bar{2}1)$ , i.e. (11.1), in which the dot may have been omitted in printing!

## 5.8 Transforming Miller indices and zone axis symbols

As mentioned in Section 3.3, different choices of axes (i.e. different unit cells) are frequently encountered in trigonal crystals with the rhombohedral Bravais lattice and it is therefore important to know how to transform Miller indices and zone axis symbols from one axis system to the other. The appropriate matrix equations or **transformation matrices** are given in Section 5.9. However, the concept and derivation of transformation matrices are best understood by way of an easily visualized, in effect, ‘two-dimensional’ example (Fig. 5.9) in which one of the axes (out of the plane of the paper) is common to both cells.

Figure 5.9 shows a plan view of a lattice with two possible unit cells outlined by vectors  $\mathbf{a}, \mathbf{b}, \mathbf{c}$  and  $\mathbf{A}, \mathbf{B}, \mathbf{C}$ . The common vectors  $\mathbf{c} = \mathbf{C}$  lie out of the plane of the paper. The unit cell vectors  $\mathbf{A}, \mathbf{B}, \mathbf{C}$  can be expressed as components of  $\mathbf{a}, \mathbf{b}, \mathbf{c}$ :

$$\begin{aligned} \mathbf{A} &= 1\mathbf{a} + 2\mathbf{b} + 0\mathbf{c} \\ \mathbf{B} &= \bar{1}\mathbf{a} + 1\mathbf{b} + 0\mathbf{c} \\ \mathbf{C} &= 0\mathbf{a} + 0\mathbf{b} + 1\mathbf{c}. \end{aligned}$$

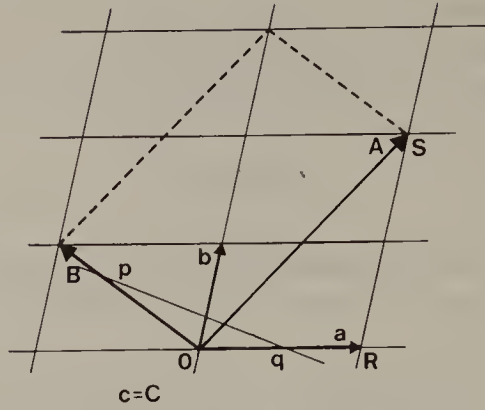


Fig. 5.9. Alternative unit cells in a lattice defined by unit cell vectors  $\mathbf{a}$ ,  $\mathbf{b}$ ,  $\mathbf{c}$  and  $\mathbf{A}$ ,  $\mathbf{B}$ ,  $\mathbf{C}$ .

Now there are two ways of writing these three equations in matrix form; the vectors may either be written as column matrices:

$$\begin{pmatrix} \mathbf{A} \\ \mathbf{B} \\ \mathbf{C} \end{pmatrix} = \begin{pmatrix} 1 & 2 & 0 \\ \bar{1} & 1 & 0 \\ 0 & 0 & 1 \end{pmatrix} \begin{pmatrix} \mathbf{a} \\ \mathbf{b} \\ \mathbf{c} \end{pmatrix}$$

or as row matrices:

$$(\mathbf{A} \quad \mathbf{B} \quad \mathbf{C}) = (\mathbf{a} \quad \mathbf{b} \quad \mathbf{c}) \begin{pmatrix} 1 & \bar{1} & 0 \\ 2 & 1 & 0 \\ 0 & 0 & 1 \end{pmatrix}.$$

Notice that the rows and columns of the  $3 \times 3$  matrix are transposed.

Let  $(hkl)$  and  $[uvw]$  be the Miller indices and zone axis symbols referred to the primitive unit cell  $\mathbf{a}, \mathbf{b}, \mathbf{c}$  and  $(HKL)$  and  $[UVW]$  be the Miller indices and zone axis symbol referred to the 'large' unit cell  $\mathbf{A}, \mathbf{B}, \mathbf{C}$  (which has three lattice points per cell).

Consider first the transformation between the indices  $(hkl)$  and  $(HKL)$ . Figure 5.9 shows the trace  $pq$  of the first plane from the origin in a family of planes in the lattice. By definition, the intercepts of this plane are  $a/h$  on the  $\mathbf{a}$  lattice vector,  $A/H$  on the  $\mathbf{A}$  lattice vector,  $b/k$  on the  $\mathbf{b}$  lattice vector and so on. Or, recall the equivalent definition that  $h$  is the number of planes intersected along the  $\mathbf{a}$  lattice vector,  $H$  is the number intersected along the  $\mathbf{A}$  lattice vector, and so on;  $h$  is the number intersected along  $\mathbf{a}$  (i.e. 0 to R) and  $2k$  is the number intersected along  $2\mathbf{b}$  (i.e. R to S). Hence,  $h + 2k$  is the total number of planes intersected along  $1\mathbf{a} + 2\mathbf{b}$  (i.e. O to S) and, as  $\mathbf{A} = 1\mathbf{a} + 2\mathbf{b}$ , then this number is the  $H$  index. Hence

$$H = 1h + 2k + 0l$$

$$K = \bar{1}h + 1k + 0l$$

$$L = 0h + 0k + 1l,$$

and the indices transform in the same way as the unit cell vectors, and again can

be written in matrix form as column matrices or row matrices. We shall choose the *row* matrix form, viz.

$$(HKL) = (hkl) \begin{pmatrix} 1 & \bar{1} & 0 \\ 2 & 1 & 0 \\ 0 & 0 & 1 \end{pmatrix}.$$

The relationship between  $[uvw]$  and  $[UVW]$  may be derived as follows. A vector  $\mathbf{r}$  in the lattice is written in terms of its components on the two sets of lattice vectors, i.e.

$$\mathbf{r} = u\mathbf{a} + v\mathbf{b} + w\mathbf{c} = U\mathbf{A} + V\mathbf{B} + W\mathbf{C}.$$

Substituting for  $\mathbf{A}$ ,  $\mathbf{B}$  and  $\mathbf{C}$ :

$$u\mathbf{a} + v\mathbf{b} + w\mathbf{c} = U(1\mathbf{a} + 2\mathbf{b} + 0\mathbf{c}) + V(\bar{1}\mathbf{a} + 1\mathbf{b} + 0\mathbf{c}) + W(0\mathbf{a} + 0\mathbf{b} + 1\mathbf{c}).$$

Collecting terms together for  $u$ ,  $v$  and  $w$  gives

$$\begin{aligned} u &= 1U + \bar{1}V + 0W \\ v &= 2U + 1V + 0W \\ w &= 0U + 0V + 1W. \end{aligned}$$

Writing the zone axis symbols as *column* matrices gives

$$\begin{pmatrix} u \\ v \\ w \end{pmatrix} = \begin{pmatrix} 1 & \bar{1} & 0 \\ 2 & 1 & 0 \\ 0 & 0 & 1 \end{pmatrix} \begin{pmatrix} U \\ V \\ W \end{pmatrix}.$$

Hence the *same*  $3 \times 3$  matrix relates plane indices written as *row* matrices from the primitive to 'large' unit cell and zone axis symbols written as column matrices from the 'large' to the primitive unit cell.

The reverse relationships are found from the inverse of the matrix. The procedures for inverting a matrix and for finding its determinant may be found in many A-level mathematics textbooks. For this example the inverse matrix is given by

$$\begin{pmatrix} 1 & \bar{1} & 0 \\ 2 & 1 & 0 \\ 0 & 0 & 1 \end{pmatrix}^{-1} = \frac{1}{3} \begin{pmatrix} 1 & 1 & 0 \\ \bar{2} & 1 & 0 \\ 0 & 0 & 3 \end{pmatrix};$$

hence

$$(hkl) = (HKL) \frac{1}{3} \begin{pmatrix} 1 & 1 & 0 \\ \bar{2} & 1 & 0 \\ 0 & 0 & 3 \end{pmatrix}$$

and

$$\begin{pmatrix} U \\ V \\ W \end{pmatrix} = \frac{1}{3} \begin{pmatrix} 1 & 1 & 0 \\ \bar{2} & 1 & 0 \\ 0 & 0 & 3 \end{pmatrix} \begin{pmatrix} u \\ v \\ w \end{pmatrix}.$$

Finally, note that the determinant of the matrix equals 3 (and its inverse equals  $\frac{1}{3}$ ), the ratio of the volumes, or number of lattice points, in the unit cells.

In transforming indices and zone axis symbols from one set of crystal axes to another it is usually best to work from first principles as above because it is very easy to fall into error by using a transformation matrix without knowing which conventions for writing lattice planes and directions are being used.

### 5.9 Transformation matrices for trigonal crystals with rhombohedral lattices

Figure 5.10 shows a plan view of hexagonal layers of lattice points stacked in the rhombohedral ABC... sequence. (See also Fig. 3.3(b).) (To avoid confusion only the A hexagonal layers are outlined.) The (primitive) rhombohedral unit cell with equi-inclined lattice vectors **a**, **b**, **c** is outlined, as is a unit cell of a non-primitive hexagonal unit cell with lattice vectors **A** and **B** at 120° to each other and **C** perpendicular to the plan view. Proceeding as described in Section 5.8,

$$(HKL) = (hkl) \begin{pmatrix} 1 & 0 & 1 \\ \bar{1} & 1 & 0 \\ 0 & \bar{1} & 1 \end{pmatrix}; \quad \begin{pmatrix} u \\ v \\ w \end{pmatrix} = \begin{pmatrix} 1 & 0 & 1 \\ \bar{1} & 1 & 0 \\ 0 & \bar{1} & 1 \end{pmatrix} \begin{pmatrix} U \\ V \\ W \end{pmatrix}$$

$$(hkl) = (HKL) \begin{pmatrix} \frac{2}{3} & \frac{1}{3} & \frac{1}{3} \\ \frac{1}{3} & \frac{1}{3} & \frac{2}{3} \\ \frac{1}{3} & \frac{1}{3} & \frac{1}{3} \end{pmatrix}; \quad \begin{pmatrix} U \\ V \\ W \end{pmatrix} = \begin{pmatrix} \frac{2}{3} & \frac{1}{3} & \frac{1}{3} \\ \frac{1}{3} & \frac{1}{3} & \frac{2}{3} \\ \frac{1}{3} & \frac{1}{3} & \frac{1}{3} \end{pmatrix} \begin{pmatrix} u \\ v \\ w \end{pmatrix},$$

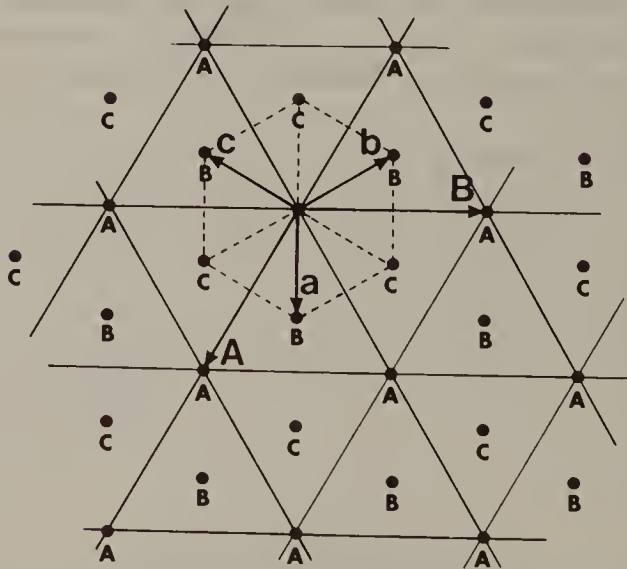


Fig. 5.10. A plan view of the hexagonal layers of lattice points, A, B and C, in the rhombohedral lattice. The rhombohedral unit cell and the triple hexagonal unit cell are outlined.



where  $(HKL)$ ,  $[UVW]$  and  $(hkl)$ ,  $[uvw]$  refer to the Miller indices and zone axis symbols for the hexagonal and rhombohedral unit cells, respectively. Note that the determinants of these two matrices are 3 and  $\frac{1}{3}$  respectively, i.e. equal to the ratios of the number of lattice points in the two cells. Hence the hexagonal unit cell is known as a triple hexagonal cell because it contains three lattice points per cell. Note also that it is possible to choose the hexagonal **A** and **B** axes differently (e.g. rotated  $60^\circ$  to those shown in Fig. 5.10); this will give rhombohedral unit cells that are mirror-related, sometimes known as 'obverse' and 'reverse' unit cells.

## Exercises

- 5.1 Write down the Miller indices and zone axis symbols for the slip planes and slip directions in fcc and bcc crystals. (See also Exercise 1.4.)
- 5.2 Which of the directions  $[010]$ ,  $[432]$ ,  $[\bar{2}10]$ ,  $[23\bar{1}]$ , if any, lie parallel to the plane  $(115)$ ? Which of the planes  $(112)$ ,  $(321)$ ,  $(911\bar{2})$ ,  $(\bar{1}\bar{1}1)$ , if any, lie parallel to the direction  $[1\bar{1}\bar{1}]$ ?
- 5.3 Write down the planes whose normals are parallel to directions with the same numerical indices in the triclinic, monoclinic and tetragonal systems.
- 5.4 Find the plane which lies parallel to the directions  $[131]$  and  $[0\bar{1}1]$ . Find the plane which lies parallel to the directions  $[102]$  and  $[\bar{1}11]$ . Find the direction which lies parallel to the intersection of the planes  $(342)$  and  $(10\bar{3})$ . Find the direction which lies parallel to the intersection of the planes  $(21\bar{3})$  and  $(110)$ .
- 5.5 An orthorhombic crystal (cementite,  $\text{Fe}_3\text{C}$ ) has unit cell vectors (or lattice parameters) of lengths  $a = 452$  pm,  $b = 508$  pm,  $c = 674$  pm.
  - (a) Find the  $d$ -spacings of the following families of planes:  $(101)$ ,  $(100)$ ,  $(111)$  and  $(202)$ .
  - (b) Find the angles  $\alpha$ ,  $\beta$ ,  $\gamma$  (Fig. 5.6) between the normal to the plane  $(111)$  and the three crystal axes.
  - (c) Find the angles  $p$ ,  $q$ ,  $r$  between the  $[111]$  direction and the three crystal axes. Briefly explain why these angles are not the same as those in (b).
- 5.6 Draw the directions (zone axes)  $[001]$ ,  $[010]$ ,  $[210]$ ,  $[110]$  in a hexagonal unit cell, and determine their Weber zone axis symbols,  $\langle UVTW \rangle$ .
- 5.7 Figure 3.2 shows the cubic *I* and cubic *F* lattices and the corresponding primitive rhombohedral unit cells. Study these figures carefully, then close the book and redraw them for yourself—to ensure that you understand the geometries of the cells in each case. Assign unit cell vectors **A**, **B**, **C** to the primitive rhombohedral cells and unit cell vectors **a**, **b**, **c** to the cubic *I* and cubic *F* cells and derive the transformation matrices for indices  $(hkl) \rightleftharpoons (HKL)$  and direction symbols  $[UVW] \rightleftharpoons [uvw]$  in each case.

---

# The reciprocal lattice

## 6.1 Introduction

The **reciprocal lattice** is often regarded by students of physics as a geometrical abstraction, comprehensible only in terms of vector algebra and difficult diffraction theory. It is, in fact, a very simple concept and therefore a very important one. It provides a simple geometrical basis for understanding not only the geometry of X-ray and electron diffraction patterns but also the behaviour of electrons in crystals—reciprocal space being essentially identical to ' $k$ -space'.

The concept of the reciprocal lattice may be approached in two ways. First, reciprocal lattice unit cell vectors may be defined in terms of the (direct) lattice unit cell vectors  $\mathbf{a}, \mathbf{b}, \mathbf{c}$ , and the geometrical properties of the reciprocal lattice developed therefrom. This is certainly an elegant approach, but it very often fails to provide the student with an immediate understanding of the relationships, for example, between the reciprocal lattice of a crystal and the diffraction pattern. The second approach, which is the one adopted in this chapter, is much less elegant. It develops the notion that families of planes in crystals can be represented simply by their normals, which are then specified as (reciprocal lattice) vectors and which can then be used to define a pattern of (reciprocal lattice) points, each (reciprocal lattice) point representing a family of planes. The advantage of this approach is that it accentuates the connections between families of planes in the crystals, Bragg's law and the directions of the diffracted or reflected beams.

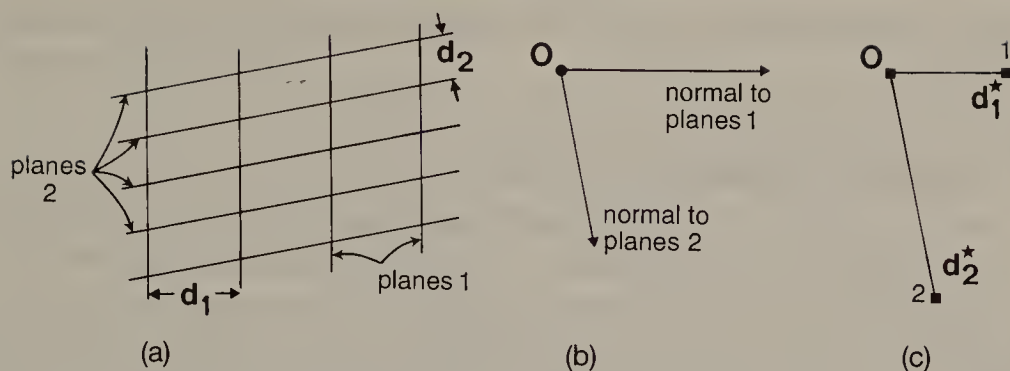
The notion that crystal axes can be defined in terms of the *normals* to crystal faces belongs to Bravais\* (1850) who called them 'polar axes' (not to be confused with current usage of the term which means axes or directions whose ends are not related by symmetry). However, the credit for the development of this idea to the concept of the reciprocal lattice, and the application of this concept to the analysis of X-ray diffraction patterns, belongs to P. P. Ewald\*, whose story is told in Section 8.1.

A study of the reciprocal lattice does require an elementary knowledge of vectors, their symbolism and some simple rules governing their manipulation (vector algebra). If you are unfamiliar with these topics, or wish to refresh your memory, Appendix 5 provides all the information you will require in order to follow the rest of this chapter.

## 6.2 Reciprocal lattice vectors

Consider a family of planes in a crystal (for example, those in Figs 5.2 or 5.3). Geometrically, the planes can be specified by two quantities: (1) their orienta-

\* Denotes biographical notes available in Appendix 3.



**Fig. 6.1.** (a) Traces of two families of planes 1 and 2 (perpendicular to the plane of the paper), (b) the normals to these families of planes drawn from a common origin and (c) definition of these planes in terms of the reciprocal (lattice) vectors  $\mathbf{d}_1^*$  and  $\mathbf{d}_2^*$ , where  $\mathbf{d}_1^* = K/d_1$ ,  $\mathbf{d}_2^* = K/d_2$ ,  $K$  being a constant.

tion in the crystal and (2) their  $d$ -spacing. Now, the orientation of the planes is defined by the direction of their normal. In Fig. 6.1(a) two families of planes, labelled 1 and 2, are sketched 'edge on'. It is immaterial where the crystal axes are in relation to these planes, so they are omitted. In Fig. 6.1(b), the normals to these planes are drawn from a common origin and these specify the orientation of the planes. Now the  $d$ -spacings,  $d_1$  and  $d_2$ , need to be specified. An 'obvious' way of doing this might be to make the lengths of the normals directly proportional to the  $d$ -spacings, i.e. by expressing them as vectors with moduli equal to  $K \times (d\text{-spacing})$  where  $K$  is a proportionality constant. However, this is *not* the way; instead, we make the lengths or the moduli of the vectors *inversely* proportional to the  $d$ -spacings, i.e. equal to  $K/d\text{-spacing}$  (where  $K$  is a proportionality constant, taken as unity or, in X-ray diffraction, as  $\lambda$ , the X-ray wavelength), i.e. a *longer* vector, indicating a *smaller*  $d$ -spacing. The reason for making the moduli of the vectors inversely proportional to the  $d$ -spacings will be apparent shortly (recall also the inversion of the intercepts in the definition of Miller indices). These vectors are called **reciprocal (lattice) vectors**, symbols  $\mathbf{d}_1^*$  and  $\mathbf{d}_2^*$ , and are shown in Fig. 6.1(c). The 'end points' of the vectors (called reciprocal lattice points) are labelled 1 and 2, corresponding to the planes which they represent. Reciprocal lattice vectors have dimensions of  $1/\text{length}$  (for  $K = 1$ ), e.g. reciprocal ångströms,  $\text{\AA}^{-1}$ , or reciprocal picometres,  $\text{pm}^{-1}$ . For example, if  $d_1 = 0.5 \text{ \AA}$ , the length or modulus of  $\mathbf{d}_1^*$  (for  $K = 1$ ) is

$$|\mathbf{d}_1^*| = \frac{1}{0.5 \text{ \AA}} = 2 \text{ \AA}^{-1}.$$

This completes the simple definition of reciprocal lattice vectors. But, like all simple concepts, it is capable of great development, which will be done for particular examples in the sections below. First a practical note. In drawing crystals and in sketching crystal planes we have to use a 'map scale' in 'direct space', choosing a scale to fit our piece of paper, e.g.  $1 \text{ \AA}$  equals  $1 \text{ cm}$ . So also when drawing reciprocal lattice vectors we have to use a quite separate 'map

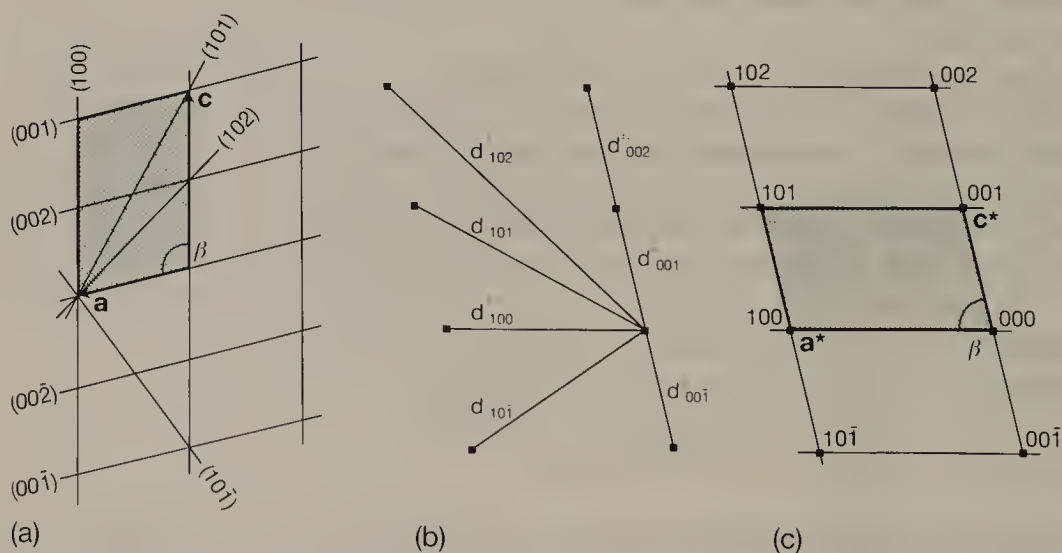
scale' in 'reciprocal space,' e.g.  $1 \text{ \AA}^{-1}$  equals 1 cm or 10 cm or 1 inch, as convenient.

### 6.3 Reciprocal lattice unit cells

To avoid the pitfalls of making hasty assumptions about the relationships between reciprocal and (direct) lattice vectors, a monoclinic crystal will be used as an example. First, we shall draw the reciprocal lattice vectors in a section perpendicular to the  $y$ -axis (i.e. containing the  $\mathbf{a}$  and  $\mathbf{c}$  lattice vectors) from which we will find the reciprocal lattice unit cell vectors  $\mathbf{a}^*$  and  $\mathbf{c}^*$ . This then enables us to express reciprocal lattice vectors in this section in terms of their components on these vectors. It is then a simple step to extend these ideas to three dimensions.

Figure 6.2(a) shows a section of a monoclinic  $P$  lattice through the origin and perpendicular to the  $y$ -axis or  $\mathbf{b}$  unit cell vector. The section of the unit cell is outlined by the lattice vectors  $\mathbf{a}$  and  $\mathbf{c}$  at the obtuse angle  $\beta$  and also the traces of some planes of the type  $\{h0l\}$  (i.e. those planes parallel to the  $y$ -axis). In Fig. 6.2(a) (and Fig. 6.4(a)) no distinction is made between Miller indices and Laue indices—the indices of the planes are all put in brackets whether or not they all pass through lattice points.

Figures 6.2(b) and (c) show the reciprocal lattice vectors for these planes, with the reciprocal lattice points labelled with the index of the planes they represent. Note again the reciprocal relationships between the lengths of the vectors and the  $d_{hkl}$ -spacings, e.g. the  $(002)$  planes with half the  $d$ -spacing of the  $(001)$  planes are represented by a reciprocal lattice point  $002$ , twice the distance from



**Fig. 6.2.** (a) Plan of a monoclinic  $P$  unit cell perpendicular to the  $y$ -axis with the unit cell shaded. The traces of some planes of type  $\{h0l\}$  (i.e. parallel to the  $y$ -axis) are indicated, (b) the reciprocal (lattice) vectors,  $\mathbf{d}_{hkl}^*$  for these planes and (c) the reciprocal lattice defined by these vectors. Each reciprocal lattice point is labelled with the indices of the plane it represents and the unit cell is shaded. The angle  $\beta^*$  is the complement of  $\beta$ .



the origin as the reciprocal lattice point 001. Obviously, 003 will be three times the distance, and so on.

It can be seen that the reciprocal lattice points (the 'end points' of the reciprocal lattice vectors) do indeed form a grid or lattice—hence the name. This is emphasized in Fig. 6.2(c), which also shows the **reciprocal lattice unit cell** for this section outlined by reciprocal lattice cell vectors  $\mathbf{a}^*$  and  $\mathbf{c}^*$ , where

$$\mathbf{a}^* = \mathbf{d}_{100}^* \quad \text{and} \quad |\mathbf{a}^*| = 1/d_{100}; \quad \mathbf{c}^* = \mathbf{d}_{001}^* \quad \text{and} \quad |\mathbf{c}^*| = 1/d_{001}.$$

Note that  $\mathbf{a}^*$  and  $\mathbf{c}^*$  are *not* parallel to  $\mathbf{a}$  and  $\mathbf{c}$ , respectively, because the normals to the (100) and (001) planes in the monoclinic lattice are not parallel to  $\mathbf{a}$  and  $\mathbf{c}$ , respectively. Also the angle  $\beta^*$  between  $\mathbf{a}^*$  and  $\mathbf{c}^*$  is the complement of the angle  $\beta$ .

These ideas are readily extended to the third dimension; the  $\mathbf{b}^*$  vector is perpendicular to the plane of the paper, normal to the (010) planes which are parallel to the plane of the paper, i.e. in the monoclinic system  $\mathbf{b}$  is parallel to  $\mathbf{b}^*$ .

The reciprocal lattice vectors can now be expressed in terms of their components of the reciprocal unit cell vectors  $\mathbf{a}^*$ ,  $\mathbf{b}^*$ ,  $\mathbf{c}^*$ . For example, for the (102) family of planes [Figs 6.2(b) and (c)]  $\mathbf{d}_{102}^* = 1\mathbf{a}^* + 0\mathbf{b}^* + 2\mathbf{c}^*$ , or, in general,

$$\mathbf{d}_{hkl}^* = h\mathbf{a}^* + k\mathbf{b}^* + l\mathbf{c}^*.$$

Hence, just as direction symbols  $[uvw]$  are the components of a vector  $\mathbf{r}_{uvw}$  in direct space (Section 5.2), so also plane indices are the components of a vector  $\mathbf{d}_{hkl}^*$  in reciprocal space.

It is worth while rewriting these two equations once again to emphasize their importance and what might be called their symmetry:

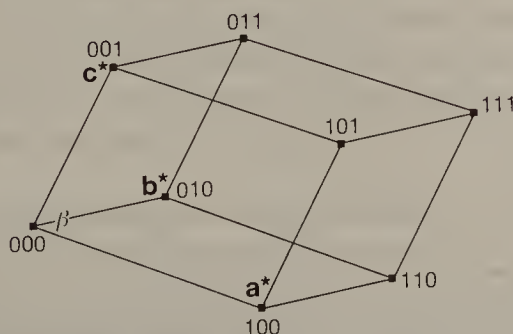
$$\mathbf{r}_{uvw} = u\mathbf{a} + v\mathbf{b} + w\mathbf{c}$$

(direction symbols are simply the components of a direct lattice vector)

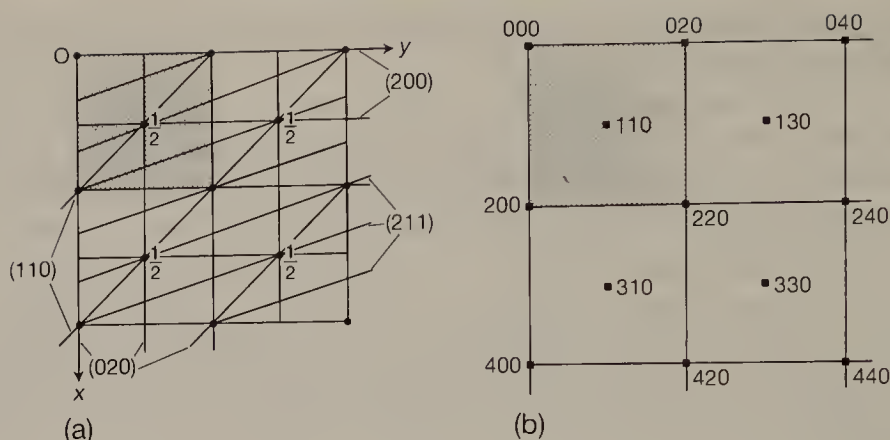
$$\mathbf{d}_{hkl}^* = h\mathbf{a}^* + k\mathbf{b}^* + l\mathbf{c}^*$$

(Miller indices are simply the components of a reciprocal lattice vector).

The reciprocal unit cell of the monoclinic crystal is sketched in Fig. 6.3. Note that each corner represents a family of planes and is labelled with the appropriate plane index and that the origin is labelled 000.



**Fig. 6.3.** The reciprocal lattice unit cell of a monoclinic  $P$  crystal defined by reciprocal lattice vectors  $\mathbf{a}^*$ ,  $\mathbf{b}^*$  and  $\mathbf{c}^*$ .  $\beta^*$  is the angle between  $\mathbf{a}^*$  and  $\mathbf{c}^*$ .



**Fig. 6.4.** (a) Plan of a cubic *I* crystal perpendicular to the *z*-axis and (b) pattern of reciprocal lattice points perpendicular to the *z*-axis. Note the cubic *F* arrangement of reciprocal lattice points in this plane.

## 6.4 Reciprocal lattice cells for cubic crystals

In crystals with orthogonal axes (cubic, tetragonal, orthorhombic) the reciprocal lattice vectors  $\mathbf{a}^*$ ,  $\mathbf{b}^*$ ,  $\mathbf{c}^*$  are parallel to  $\mathbf{a}$ ,  $\mathbf{b}$ ,  $\mathbf{c}$ , respectively. Hence we have the further identities that  $\mathbf{a} \cdot \mathbf{b} = 0$ ,  $\mathbf{a}^* \cdot \mathbf{b} = 0$ , etc. The reciprocal lattice unit cell of a simple cubic crystal (cubic *P* lattice) is obviously a cube with reciprocal lattice points only at the corners. The reciprocal unit cells of the cubic *I* and cubic *F* lattices also have additional lattice points within the unit cells, i.e. they are also not primitive. This is illustrated for the case of the cubic *I* lattice in Fig. 6.4, which shows four unit cells with the *z*-axis perpendicular to the plane of the paper and the traces of several *hk*0 planes (parallel to the *z*-axis) sketched in. Notice (for example) that in the direction of the *x*-axis the first set of lattice planes encountered is not (100) but (200) because of the presence of the additional lattice points in the centres of the cells (see also Fig. 5.4). Hence the reciprocal lattice vector in this direction is equal to  $\mathbf{d}_{200}^*$  not  $\mathbf{d}_{100}^*$ ; similarly, in the direction of the *y*-axis it is  $\mathbf{d}_{020}^*$ . In the [110] direction, however, the first set of lattice planes encountered is (110), which gives a reciprocal lattice point in the centre of the face of the cell and the second-order 220 reciprocal lattice point at the corner. Proceeding in this way we find that this section of the reciprocal lattice is *face-centred*. Repeating this procedure in the other sections gives a **face-centred cubic reciprocal lattice (cubic *F*)** (Fig. 6.5) for the **body-centred cubic (direct) lattice (cubic *I*)**—the two are reciprocally related. In the same way, we find that the reciprocal lattice of the face-centred cubic lattice is body-centred (Fig. 6.6).

There is another way of looking at these reciprocal relationships. Recall that the cubic lattices may all be referred to rhombohedral axes (primitive cells) with axial angles at  $60^\circ$  (cubic *F*),  $90^\circ$  (cubic *P*), and  $109.47^\circ$  (cubic *I*) (Section 3.2, Fig. 3.2). The reciprocals of these cells are again rhombohedral cells with axial angles  $109.47^\circ$  (i.e. cubic *I*),  $90^\circ$  (i.e. cubic *P*) and  $60^\circ$  (i.e. cubic *F*), respectively.

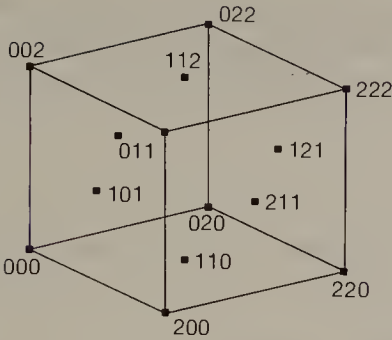


Fig. 6.5. The cubic *F* reciprocal lattice unit cell of the cubic *I* (direct) lattice.

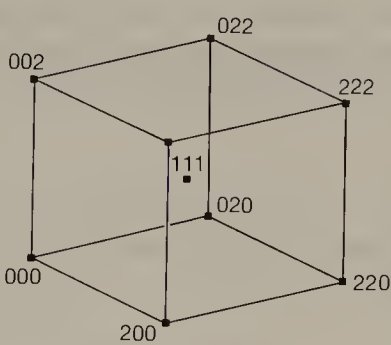


Fig. 6.6. The cubic *I* reciprocal lattice cell of the cubic *F* (direct) lattice.

### 6.5 Proofs of some geometrical relationships using reciprocal lattice vectors

Some useful geometrical relationships stated without proof in Chapter 5 can be proved very simply using the concept of the reciprocal lattice and an elementary knowledge of vector algebra (see Appendix 5). The results are summarized in Appendix 4.

#### 6.5.1 Relationships between $\mathbf{a}$ , $\mathbf{b}$ , $\mathbf{c}$ and $\mathbf{a}^*$ , $\mathbf{b}^*$ , $\mathbf{c}^*$

Consider, for example,  $\mathbf{c}^*$  (Fig. 6.2) and its relationships with  $\mathbf{a}$ ,  $\mathbf{b}$  and  $\mathbf{c}$ , which are redrawn for clarity in Fig. 6.7. showing in addition the angle  $\phi$  between  $\mathbf{c}$  and  $\mathbf{c}^*$ .

Since  $\mathbf{c}^*$  is perpendicular to both  $\mathbf{a}$  and  $\mathbf{b}$ , the scalar (or dot) products are zero, i.e.  $\mathbf{c}^* \cdot \mathbf{a} = 0$ ,  $\mathbf{c}^* \cdot \mathbf{b} = 0$  and similarly for  $\mathbf{a}^*$  and  $\mathbf{b}^*$ , i.e.  $\mathbf{a}^* \cdot \mathbf{b} = 0$ ,  $\mathbf{a}^* \cdot \mathbf{c} = 0$ ,  $\mathbf{b}^* \cdot \mathbf{a} = 0$ ,  $\mathbf{b}^* \cdot \mathbf{c} = 0$ .

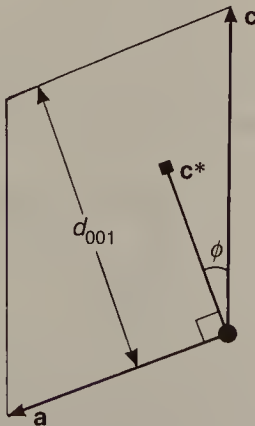


Fig. 6.7. Plan of a monoclinic unit cell perpendicular to the *y*-axis emphasizing the geometrical relationships between  $\mathbf{a}$ ,  $\mathbf{c}$  and  $\mathbf{c}^*$  (see Fig. 6.2 and Section 6.5.1).

Now consider the scalar product  $\mathbf{c} \cdot \mathbf{c}^* = c |\mathbf{c}^*| \cos \phi$ . However, since  $|\mathbf{c}^*| = 1/d_{001}$  by definition and  $c \cos \phi = d_{001}$ , then  $\mathbf{c} \cdot \mathbf{c}^* = d_{001}/d_{001} = 1$  and similarly for  $\mathbf{a} \cdot \mathbf{a}^* = 1$  and  $\mathbf{b} \cdot \mathbf{b}^* = 1$ .

### 6.5.2 The addition rule

This rule is simply based on the addition of reciprocal lattice vectors. For example (Fig. 6.2(b)),  $\mathbf{d}_{102}^* = \mathbf{d}_{101}^* + \mathbf{d}_{001}^*$  or, in general,

$$\mathbf{d}_{(mh_1 + nh_2)(mk_1 + nk_2)(ml_1 + nl_2)}^* = \mathbf{d}_{m(h_1 k_1 l_1)}^* + \mathbf{d}_{n(h_2 k_2 l_2)}^*.$$

### 6.5.3 The (Weiss) zone law

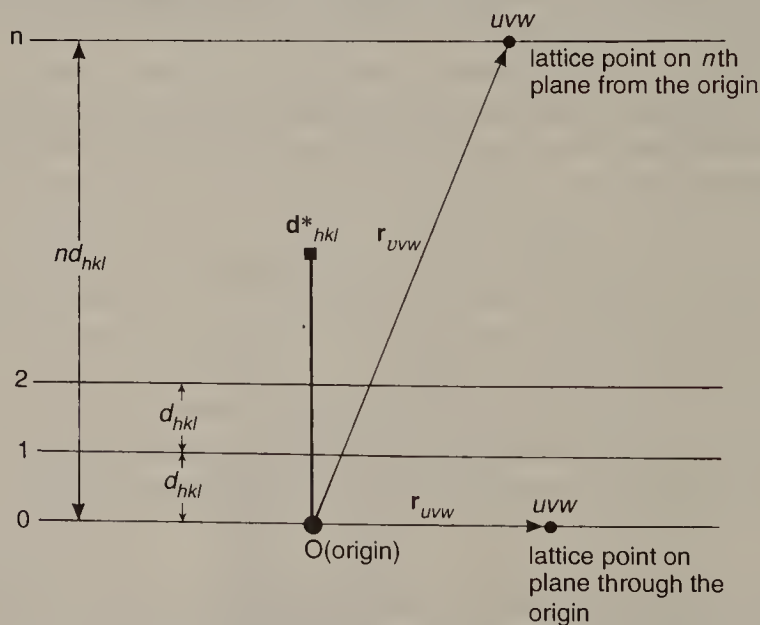
If a plane  $(hkl)$  lies in a zone  $[uvw]$ , then  $\mathbf{d}_{hkl}^*$  is perpendicular to  $\mathbf{r}_{uvw}$ , i.e.  $\mathbf{d}_{hkl}^* \cdot \mathbf{r}_{uvw} = 0$ . Writing  $\mathbf{d}_{hkl}^*$  and  $\mathbf{r}_{uvw}$  in terms of their components,

$$(h\mathbf{a}^* + k\mathbf{b}^* + l\mathbf{c}^*) \cdot (u\mathbf{a} + v\mathbf{b} + w\mathbf{c}) = 0.$$

Hence

$$hu + kv + lw = 0 \quad \text{because } \mathbf{a}^* \cdot \mathbf{a} = 1, \mathbf{a}^* \cdot \mathbf{b} = 0, \text{ etc.}$$

The zone law can be generalized as follows. Consider the condition for a lattice point with coordinates  $uvw$  (or with position vector  $\mathbf{r}_{uvw}$ ) to lie in a lattice plane  $(hkl)$  (Fig. 6.8). For the lattice plane passing through the origin,  $\mathbf{r}_{uvw}$  is perpendicular to  $\mathbf{d}_{hkl}^*$  and hence  $hu + kv + lw = 0$  as before. Now consider the  $n$ th lattice plane which lies at a perpendicular distance  $nd_{hkl}$  from the origin.



**Fig. 6.8.** Diagram representing the geometry of the (generalized) zone law. A set of  $hkl$  planes are drawn 'edge on'. When a lattice point  $uvw$  lies on a plane through the origin then  $hu + kv + lw = 0$ ; when a lattice point lies on the  $n$ th plane from the origin then  $hu + kv + lw = n$ .



The condition for a lattice point to be in this plane is that the component of  $\mathbf{r}_{uvw}$  perpendicular to the planes should equal this distance; i.e.  $\mathbf{r}_{uvw} \cdot \mathbf{i} = nd_{hkl}$  where  $\mathbf{i}$  is a unit vector perpendicular to the planes. Now, since by definition

$$\mathbf{i} = \frac{\mathbf{d}_{hkl}^*}{|\mathbf{d}_{hkl}^*|} = \mathbf{d}_{hkl}^* d_{hkl}$$

then

$$\mathbf{r}_{uvw} \cdot \mathbf{d}_{hkl}^* d_{hkl} = nd_{hkl};$$

hence

$$\mathbf{r}_{uvw} \cdot \mathbf{d}_{hkl}^* = n$$

and, substituting for  $\mathbf{r}_{uvw}$  and  $\mathbf{d}_{hkl}^*$  as before,

$$hu + kv + lw = n.$$

#### 6.5.4 *d-spacing of lattice planes (hkl)*

Recalling (Appendix 5) that the scalar product of a vector multiplied by itself is the modulus squared:

$$\mathbf{d}_{hkl}^* \cdot \mathbf{d}_{hkl}^* = \frac{1}{d_{hkl}^2} = (h\mathbf{a}^* + k\mathbf{b}^* + l\mathbf{c}^*) \cdot (h\mathbf{a}^* + k\mathbf{b}^* + l\mathbf{c}^*).$$

Simple expressions are only obtained for crystals with orthogonal axes (orthorhombic, tetragonal, cubic) where  $\mathbf{a}^* \cdot \mathbf{b}^* = 0$  etc., i.e. for orthorhombic crystals;

$$\frac{1}{d_{hkl}^2} = h\mathbf{a}^* \cdot h\mathbf{a}^* + k\mathbf{b}^* \cdot k\mathbf{b}^* + l\mathbf{c}^* \cdot l\mathbf{c}^* = \frac{h^2}{a^2} + \frac{k^2}{b^2} + \frac{l^2}{c^2}$$

$$\text{since } \mathbf{a}^* \cdot \mathbf{a}^* = \frac{1}{a^2} \text{ etc.}$$

#### 6.5.5 *Angle $\rho$ between plane normals $(h_1 k_1 l_1)$ and $(h_2 k_2 l_2)$*

The angle  $\rho$  between two vectors  $\mathbf{a}$  and  $\mathbf{b}$  is given by (Appendix 5):

$$\cos \rho = \frac{\mathbf{a} \cdot \mathbf{b}}{ab}.$$

Hence:

$$\cos \rho = \frac{\mathbf{d}_{h_1 k_1 l_1}^* \cdot \mathbf{d}_{h_2 k_2 l_2}^*}{|\mathbf{d}_{h_1 k_1 l_1}^*| |\mathbf{d}_{h_2 k_2 l_2}^*|}.$$

Again, substituting in terms of components gives a simple expression only for cubic crystals.

### 6.5.6 Definition of $\mathbf{a}^*$ , $\mathbf{b}^*$ , $\mathbf{c}^*$ in terms of $\mathbf{a}$ , $\mathbf{b}$ , $\mathbf{c}$

The volume of the unit cell  $V$  is given by  $\mathbf{a} \cdot (\mathbf{b} \times \mathbf{c})$  (see Appendix 5). Now, as  $(\mathbf{b} \times \mathbf{c})$  is a vector parallel to  $\mathbf{a}^*$  and of modulus equal to the area of the face of the unit cell defined by  $\mathbf{b}$  and  $\mathbf{c}$ , then  $\mathbf{a}^* = (\mathbf{b} \times \mathbf{c})/V = (\mathbf{b} \times \mathbf{c})/\mathbf{a} \cdot (\mathbf{b} \times \mathbf{c})$ , and similarly for  $\mathbf{b}^*$  and  $\mathbf{c}^*$ .  $\mathbf{a}$ ,  $\mathbf{b}$  and  $\mathbf{c}$  can be defined in the same way, i.e.  $\mathbf{a} = (\mathbf{b}^* \times \mathbf{c}^*)/V^*$ , and similarly for  $\mathbf{b}$  and  $\mathbf{c}$ , where  $V^*$  is the volume of the reciprocal unit cell.

Hence to summarize:

$$\begin{aligned} \mathbf{a}^* &= \frac{\mathbf{b} \times \mathbf{c}}{V}, & \mathbf{b}^* &= \frac{\mathbf{c} \times \mathbf{a}}{V}, & \mathbf{c}^* &= \frac{\mathbf{a} \times \mathbf{b}}{V}, \\ \mathbf{a} &= \frac{\mathbf{b}^* \times \mathbf{c}^*}{V^*}, & \mathbf{b} &= \frac{\mathbf{c}^* \times \mathbf{a}^*}{V^*}, & \mathbf{c} &= \frac{\mathbf{a}^* \times \mathbf{b}^*}{V^*}. \end{aligned}$$

### 6.5.7 Zone axis at intersection of planes $(h_1 k_1 l_1)$ and $(h_2 k_2 l_2)$

The zone axis is defined by  $\mathbf{r}_{uvw}$ , the vector product of

$$\mathbf{d}_{h_1 k_1 l_1}^* \quad \text{and} \quad \mathbf{d}_{h_2 k_2 l_2}^*.$$

Substituting in terms of their components and remembering the identities  $\mathbf{a} = (\mathbf{b}^* \times \mathbf{c}^*)/V^*$  etc., gives

$$u\mathbf{a} + v\mathbf{b} + w\mathbf{c} = \mathbf{a}(k_1 l_2 - k_2 l_1) + \mathbf{b}(l_1 h_2 - l_2 h_1) + \mathbf{c}(h_1 k_2 - h_2 k_1)$$

therefore

$$u = (k_1 l_2 - k_2 l_1); \quad v = (l_1 h_2 - l_2 h_1); \quad w = (h_1 k_2 - h_2 k_1).$$

### 6.5.8 A plane containing two directions $[u_1 v_1 w_1]$ and $[u_2 v_2 w_2]$

The plane is defined by  $\mathbf{d}_{hkl}^*$ , the vector product of  $\mathbf{r}_{u_1 v_1 w_1}$  and  $\mathbf{r}_{u_2 v_2 w_2}$ . Proceeding as above gives

$$h = (v_1 w_2 - v_2 w_1); \quad k = (w_1 u_2 - w_2 u_1); \quad l = (u_1 v_2 - u_2 v_1)$$

## Exercises

- 6.1 Derive the  $[0001]$  reciprocal lattice section for the hexagonal  $P$  lattice and  $[111]$  reciprocal lattice sections for the cubic  $I$  and cubic  $F$  lattices.
- 6.2 Derive expressions for  $1/d_{hkl}$  and  $\cos \rho$  for orthorhombic crystals.
- 6.3 Do the relationships derived in Section 6.4 apply also to non-cubic centred Bravais lattices and their reciprocal unit cells?

---

# The diffraction of light

## 7.1 Introduction

As introduced in Chapter 6, the reciprocal lattice is the basis upon which the geometry of X-ray and electron diffraction patterns can be most easily understood and, as we shall see in Chapters 8 and 9, the electron diffraction patterns observed in the electron microscope, or the X-ray diffraction patterns recorded with a precession camera, are simply sections through the reciprocal lattice of a crystal—the pattern of spots on the screen or photographic film and the pattern of reciprocal lattice points in the corresponding plane or section through the crystal are identical.

This also applies to the diffraction of light from ‘two-dimensional crystals’ such as umbrella cloths, net window curtains and the like and in which the warp and weft of the cloth correspond in effect to intersecting lattice planes. The diffraction patterns which we see through umbrellas and curtains are, in effect, the two-dimensional reciprocal lattices of these two-dimensional lattices.

The important point to realize at the outset is that the reciprocal lattice is not merely an elegant geometrical abstraction, or a crystallographer’s way of formally representing lattice planes in crystals or two-dimensional nets, but that it is something we can ‘see for ourselves’. Indeed, in the case of light it is a familiar part of our everyday visual sensations. Furthermore, as explained in Section 7.2 below, when our eyes are relaxed and focused on infinity we see the patterns of spots and streaks around the lights from distant street lamps when viewed through umbrellas and net curtains, or the circles of haze around them on foggy nights quite clearly. Hence, it might be suggested that diffraction patterns constitute our first visual sensations, before we have learned to near-focus upon the world!

The familiarity and ease of demonstration is the main justification or reason for considering the diffraction of light, but there are three others. First, there is a geometrical analogy between light and electron diffraction: in both cases the wavelengths (of light and electrons) are small in comparison with the spacings of the diffracting objects (the fibre separations in woven fabrics or the lattice spacings in crystals). For example, the wavelength of green light ( $\sim 0.5 \mu\text{m}$ ) is about  $500\times$  smaller than the fibre spacings in nets and fabrics ( $\sim 0.25 \text{ mm}$ ); similarly, the wavelength of electrons in a 100 kV electron microscope ( $\sim 4.0 \text{ pm}$ ) is about  $100\times$  smaller than the lattice spacings in crystals ( $\sim 0.4 \text{ nm}$ ). In both cases therefore (as explained in Sections 7.4 and 9.5) the diffraction angles are also small and electron diffraction patterns can, at least initially, be interpreted as sections through the reciprocal lattice of the crystal.

The geometry of X-ray diffraction patterns is rather more complicated because the wavelengths of X-rays ( $\sim 0.2$  nm) are roughly comparable with the lattice spacings in crystals. Hence the diffraction angles are large (Sections 8.2, 8.3, 8.4 and 9.3) and X-ray diffraction patterns are in a sense 'distorted' representations of the patterns of reciprocal lattice points from crystals, the nature of the 'distortion' depending upon the particular X-ray technique used.

The second reason for considering the diffraction of light is that it provides a simple basis or analogy for an understanding of how and why the **intensities** of X-ray diffraction beams vary (Section 9.1), **line broadening** and the occurrence of **satellite** reflections (Section 9.2). The analogy is provided by a consideration of the diffraction grating, which is, in effect, a one-dimensional crystal. There are three variables to consider in the diffraction of light from a diffraction grating—the line or slit spacing, the width of each slit and the total number of slits. The slit spacing corresponds to the lattice spacings in crystals and determines the directions of the diffracted beams, or, in short, the geometry of the diffraction patterns. The width of the slits determines, for each diffracted beam direction, the sum total of the interference of all the little Huygens' wavelets which contribute to the total intensity of the light from each slit (Section 7.4), which is analogous to the sum total of the interference between all the diffracted beams from all the atoms in the motif. In short it is the lattice which determines the *geometry* of the pattern and the motif which determines the *intensities* of the X-ray diffracted beams. The analogy, however, must not be pressed too far because it takes no account of the dynamical interactions between diffracted beams, i.e. the interference effects arising from re-reflection (and re-re-reflection etc.) of the direct and diffracted/reflected beams as they pass through a crystal. This desideratum is particularly important in the case of electron diffraction. Finally, the total number of slits in a diffraction grating determines the numbers and intensities of the satellite or subsidiary diffraction peaks each side of a main diffraction peak—the greater the number of slits, the greater the numbers and the smaller are the intensities of the satellite peaks. In most X-ray and electron diffraction situations the total number of diffracting planes is so large that satellite peaks are unobservable and of no importance, but in the case of X-ray diffraction from thin film multilayers, consisting not of thousands but only of tens or hundreds of layers, the numbers and intensities of the satellite peaks are important and useful.

Third, it is the diffraction of light which sets a limit, 'the diffraction limit,' to the resolving power or limit of resolution of optical instruments, in particular telescopes and microscopes, and is therefore of utmost importance to an understanding of how these instruments work. The diffraction limit however is not unsurmountable and it is an important characteristic of modern microscopical techniques—for example scanning tunnelling, atom force, or near field scanning optical microscopes—that they overcome this limit by virtue of the close approach of a fine probe to a specimen surface.

Finally, to generalize the point made in the first paragraph, the reciprocal relationship between an object and its diffraction pattern is formally expressed



by what is known as a Fourier transform, which is a (mathematical) operation which transforms a function containing variables of one type (in our case distances in an object or *displacements*) into a function whose variables are reciprocals of the original type (in our case  $1/\text{displacements}$ ). The reciprocal lattices which we worked out in Chapter 6 using very simple geometry are, in fact, the Fourier transforms of the corresponding (real) lattices.

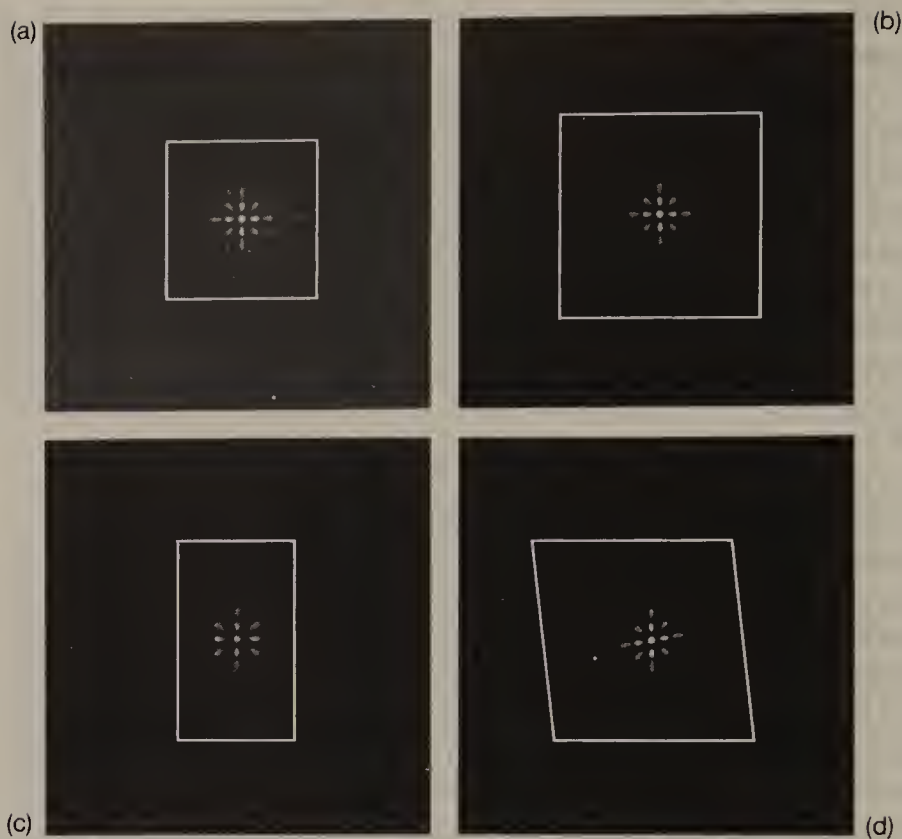
In this sense diffraction patterns may be described as ‘visual representations’ of ‘images’ of the Fourier transforms of objects—irrespective as to whether they are generated using light, X-rays or electrons. In the case of light, diffraction patterns are often described as the ‘optical transforms’ of the corresponding objects.

## 7.2 Simple observations of the diffraction of light

The diffraction of light is most easily demonstrated using a laser—the hand-held types which are designed to be used as ‘pointers’ on screens for lecturers are more than adequate and are relatively safe (but you should never look directly at the laser light). Many everyday objects may be used as ‘diffraction gratings’ either in transmission or reflection—fabrics, nets, stockings (transmission) or graduated metal rulers (reflection) and the resultant diffraction patterns may be projected on to a wall or screen. Such experiments will quickly make apparent the inverse or reciprocal relationships between the spacings of the nets, graduations etc. and the spacings between the diffracted spots. For example, when laser light is reflected from a graduated metal scale or ruler, in addition to the mirror-reflected beam, diffracted beams will be observed on each side; the spacings of these will change as the angle of the surface of the ruler to the laser beam (and hence the apparent spacings between the graduations) is changed, but, more convincingly, when the beam is shifted from the ‘ $\frac{1}{2}$  mm’ to the ‘1 mm’ graduated regions of the ruler, the spacings of the diffraction spots are halved. However, it is probably better to begin with the familiar diffraction patterns which are obtained with a simple point source of light and a piece of fabric with an open weave and which moreover serve to emphasize some important ideas about the angular relationships between the diffracted beams. A point-source of light may in practice be a distant street lamp or, in order to conduct the experiments indoors, a mini torch bulb or a domestic light bulb placed behind a screen with a pinhole (or a fine needle hole) punched into it. Nylon net curtain material is an effective fabric to use—the filaments of nylon which make up the strands are tightly twisted giving sharply defined transparent/opaque boundaries.

Observe the point source (which should be at least 5 m distant) through the net. The image of the point source will be seen to be repeated to form a grid (or reciprocal lattice) of diffraction spots (Fig. 7.1(a)). In general the spots are of greatest intensity, and are streaked, in directions perpendicular to the lines or strands of the net.

These familiar observations may be supplemented by two more. First the



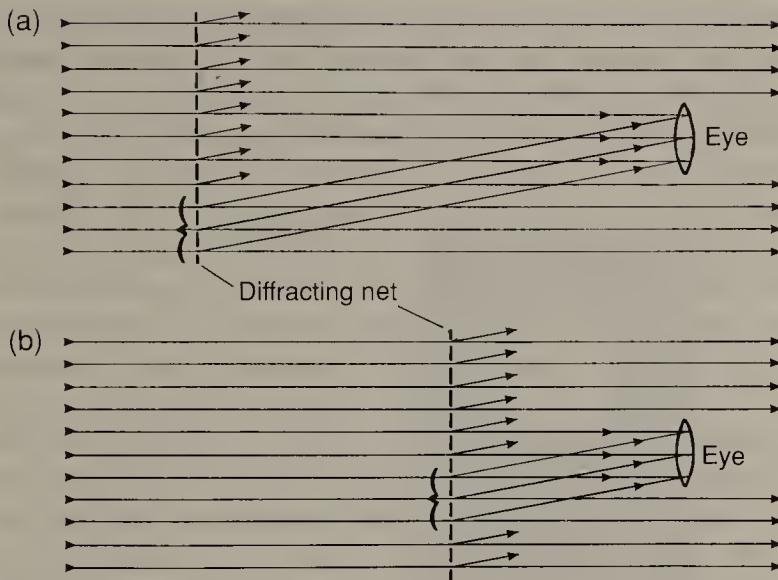
**Fig. 7.1.** (a) A diffraction pattern from a piece of net curtain with a square weave. The outline of the net is indicated by the white frame. Note that two rows of strong spots and the fainter spots forming a square grid diffraction pattern. (b) The diffraction pattern is identical in scale when the net is brought closer to the observer's eye. (c) Rotating the net about a vertical axis reduces the effective spacing of the vertical lines of the weave, resulting in diffraction spots in the horizontal direction which are further apart. (d) Shearing or distorting the net such that the strands or lines are no longer at  $90^\circ$  to each other results in a diffraction pattern 'sheared' in the opposite sense—the rows of strong diffraction spots remain perpendicular to the lines of the net.

same pattern of spots is seen whether both, or only one, eye is used. Second the size of the pattern—the apparent spacings of the spots—is *independent* of the position of the net. The diffraction pattern appears to be unchanged, irrespective of whether the net is held away from, or close to the eyes (Fig. 7.1(b))\*.

These observations show that the diffraction spots or diffracted beams bear *fixed angular relationships* to the direct beam.

The reciprocal relationship between the net and diffraction pattern may be demonstrated in two ways. First, a net with a finer line spacing will be found to give diffraction spots more widely spaced. If a finer net is not available, the effective spacing of the lines may be decreased by rotating the net such that it is

\* If the light falling on the net is not parallel but is slightly diverging (i.e. the point source is not effectively at infinity), then the apparent spacing of the spots will change slightly as the net is held at different distances from the eyes.



**Fig. 7.2.** (a) Parallel light (from a distant point source) falls on the net and is diffracted; only one set of diffracted beams is shown. The region of the net contributing to the diffracted light entering the eye of the observer is indicated by brackets. (b) As the net is moved towards the eye, the region of the net which contributes to the diffracted light entering the eye is different. The angular relationship between the direct and diffracted light at the eye remains unchanged.

no longer oriented perpendicular to the line of sight to the light (Fig. 7.1(c)). Secondly, the net may be twisted or sheared such that the strands—the weft and the warp—no longer lie in lines at  $90^\circ$  to each other. It will be seen that the rows of strong diffraction spots rotate in such a way that they continue to lie in directions perpendicular to the lines of the net—the grid of diffraction spots is reciprocally related to the sheared lattice (Fig. 7.1(d)).

These reciprocal relationships are analogous to those shown for a set of planes in a zone parallel to the  $y$ -axis in a monoclinic crystal (corresponding to the net, Fig. 6.2(a)) and its reciprocal lattice section (corresponding to the diffraction pattern, Fig. 6.2(c)).

The observation that the size of the pattern is independent of the position of the net, and that it is seen to be identical with both eyes, may be explained by reference to Fig. 7.2. The light from a point source radiates out in all directions, but if it is distant then that part incident upon the net is (approximately) parallel.

Figure 7.2 shows a parallel beam of light from a (distant) source with the net held away from the eye (Fig. 7.2(a)) and closer to the eye (Fig. 7.2(b)). One set of diffracted beams from the net is shown. Of all the direct light and diffracted light from the net, only a portion will enter the eye. The portion of the net from which the diffracted light entering the eye originates changes as the net is moved: the further the net is moved away from the eye the greater the contribution from its outer regions (compare Fig. 7.2(a) with Fig. 7.2(b)). However, for incident parallel light, irrespective of the position of the net, the



angular relationship at the eye between the direct and diffracted beams, and hence the apparent size of the diffraction pattern, remains unchanged. And what is true for one eye is true for both eyes; you do not need to squint, or keep your head still: the diffraction pattern remains unchanged.

When using lasers to observe diffraction, a narrow, parallel beam of monochromatic light is available, as it were, ready made. Hence, unlike the previous situation, the diffraction pattern can be recorded on a screen because the diffracted beams all originate from the same small area of the net which is illuminated by the laser. (In the previous case, Fig. 7.2, because the diffracted beams originate from a large area of the net, they will correspondingly be 'blurred out' when they fall on a screen.) Only if most of the incident light is 'blocked off' such that only a small area of the net is exposed (or illuminated in the case of a laser) will a (faint) diffraction pattern be recorded. These points are best appreciated by 'self modifying' Fig. 7.2. Remove the 'eye' and extend all the arrows showing the diffracted beams: notice how broad is the width of the total beam. Now 'block off' all the beams except those passing through a small (bracketed) area of the net and add a screen, in place of the eye, on the right. The direct and diffracted spots will be about equal to the area of the diffracting net (or the diameter of the laser beam), and their separation will increase the more distant is the screen.

The reciprocal relationship between the diffracting object and its diffraction pattern also extends to the shapes and sizes of the diffracting apertures (the 'holes' in the net) as well as their spacings. However, this is not easy to demonstrate simply without a laser carefully set up on an optical bench, with diffracting apertures of various shapes and sizes and appropriate lenses to focus the diffraction patterns (see Section 7.4 below).

Figure 7.3 shows a sequence of pinholes or apertures and the corresponding diffraction patterns using a laser as a coherent source of light (see Section 7.3). Figures 7.3(a)–(c) show the diffraction patterns (right) from the simplest apertures (left)—single pinholes of various sizes (which may be simply made by punching holes in thin aluminium foil and observing the diffraction pattern on a screen in a darkened room). The diffraction patterns consist of a central disc (of diameter greater than the geometrical shadow of the pinhole) surrounded by

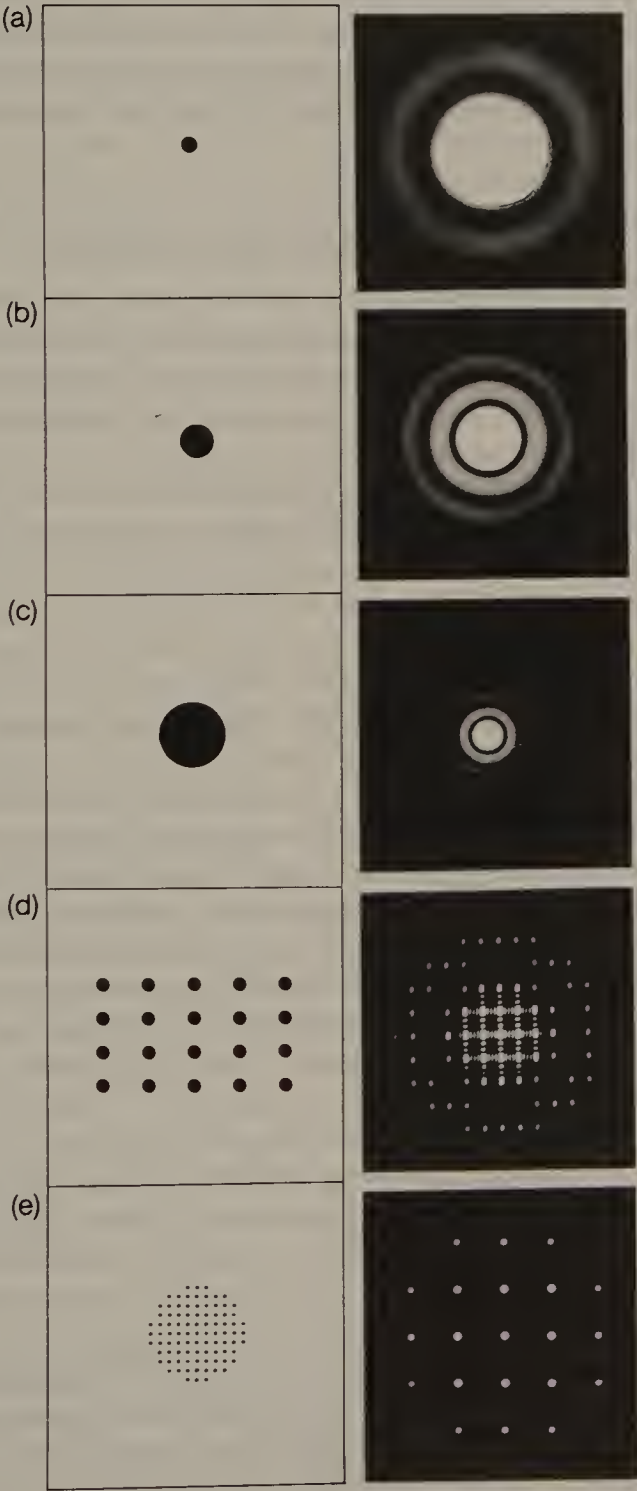
---

▷

**Fig. 7.3.** Diffracting apertures (reproduced as black dots on a white background) (left) and their corresponding diffraction patterns (or optical transforms) (right) taken using a laser. (a), (b) and (c) show the diffraction patterns (Airy discs and surrounding haloes or rings) from circular apertures of increasing diameters. (d) shows the diffraction pattern from a  $4 \times 5$  net of small apertures (as in (a)). Note the reciprocal relationship between the net and the diffraction pattern, the  $2 \times 3$  number of subsidiary peaks in each direction and the overall variation in intensity of the diffraction pattern in accordance with that for a single aperture (a). (e) shows that for a net of many apertures the subsidiary maxima are not discernible. (From *Atlas of Optical Transforms* by G. Harburn, C. A. Taylor and T. R. Welberry, Bell and Hyman, 1983, an imprint of HarperCollins Publishers Ltd.)



much fainter (and sometimes difficult to see) annuli or rings; notice that the diameters of the disc and rings decrease as the diameter of the aperture increases. Figure 7.3(d) shows the diffraction pattern (right) from a rectangular net or lattice (left) of 20 (4 by 5) of the smallest apertures. There are three



things to notice about this net and its associated diffraction pattern. First, the reciprocal relationship between the unit cell of the net and that of the diffraction pattern (see also Fig. 7.1(c); second the intensities of the diffraction spots which vary in the same way as the intensities of the central disc and rings from a single aperture (Fig. 7.3(a)), and third that there are faint spots, or subsidiary maxima, between the main diffraction spots. Finally, Fig. 7.3(e) shows the diffraction pattern (right) from a square net of many small apertures (left). The diffraction spots all lie within the region of the large central disc from a single small aperture and the subsidiary maxima between the main diffraction spots are no longer evident.

### 7.3 The nature of light: coherence, scattering and interference

In the previous section we surveyed the phenomenon of diffraction: the pattern of beams which occur when light passes through pinholes and nets or is reflected from graduated rulers. We examined the conditions under which diffraction patterns can be observed either by looking at a point source of light through a net, or when using a laser, by projection onto a screen. Finally we observed the inverse or reciprocal relationship between the diffracting object and the diffraction pattern. All these observations need to be explained and given a quantitative basis (Section 7.4), but before doing so we need to know something of the nature of light itself and the notions of coherence, scattering and interference.

The nature of light is expressed through the ‘working models’ which seek to describe it. Physics provides us with two such models—light as ‘particles’ (photons or quanta) and light as waves. These working models are not contradictory or opposed; rather they express different aspects of the quantum-mechanical interpretation of light and matter. Visible light occupies a very small part of the whole spectrum of electromagnetic radiation, with a wavelength range from about 400 nm (violet-blue) to about 700 nm (red). In the range below we have ultraviolet ( $\sim 400\text{ nm}$ – $1\text{ nm}$ ), X-rays ( $\sim 10\text{ nm}$ – $10\text{ pm}$ ), and the very shortest,  $\gamma$ -rays ( $\sim 10\text{ pm}$ – $10\text{ fm}$ ). In the range above we have infrared ( $\sim 700\text{ nm}$ – $1\text{ mm}$ ), microwaves ( $\sim 1\text{ mm}$ – $500\text{ mm}$ ) and, the very longest, radio waves ( $\sim 500\text{ mm}$ – $100\text{ km}$ ).

Light (in common with all other electromagnetic radiation) has both wave-like and particle-like character which are linked by an equation of great simplicity—Planck’s equation:  $E = hc/\lambda$ , where  $E$  is the energy of the photon (a particle-like quantity),  $c$  is the velocity of light ( $\sim 3 \times 10^8\text{ ms}^{-1}$ ),  $\lambda$  is the wavelength (a wave-like quantity) and  $h$  is the Planck constant ( $6.6256 \times 10^{-34}\text{ Js}$ ). Notice that the smaller is the wavelength, the higher is the energy of the photon—a matter of great physiological and practical importance: we are all continuously bathed in radio waves with no ill effects, but a short exposure to X-rays or  $\gamma$ -rays results in severe damage to our body tissues. Light obviously occupies an important niche in between.

Matter—electrons, protons, particles of any sort—also has wave-like as well as particle-like character, which are similarly linked by de Broglie's equation,  $\lambda = h/mv$ , where  $m$  and  $v$  are the mass and velocity of the particle respectively and  $\lambda$  is the wavelength. As before, the 'linking constant' between the particle-like and wave-like character is  $h$ , the Planck constant\*.

The notion that light has both particle-like and wave-like character reaches back to the seventeenth century and the work of Isaac Newton<sup>†</sup> and Christiaan Huygens<sup>†</sup>. Newton has been represented as the advocate of the particle or 'corpuscular' theory of light and Huygens the advocate of the wave theory of light. Certainly Huygens' simple and elegant interpretation of reflection and refraction in terms of wavefronts made up of the envelopes of secondary waves or wavelets, which was taken up and extended by Thomas Young<sup>†</sup> and Augustin Jean Fresnel<sup>†</sup> early in the nineteenth century, has been far more fruitful than Newton's corpuscular theory. However, it is clear from his own writings that Newton himself was undecided. In his great work *Opticks* there are a number of *Queries* which represent his reflections on his life's work on the properties of light. In Query 13 he asks:-

Do not several sorts of Rays make Vibrations of several bignesses, which according to their bignesses excite Sensations of several Colours?

and in Query 17:

considering the lastingness of Motions excited in the bottom of the Eye by Light, are they not of a vibrating nature?

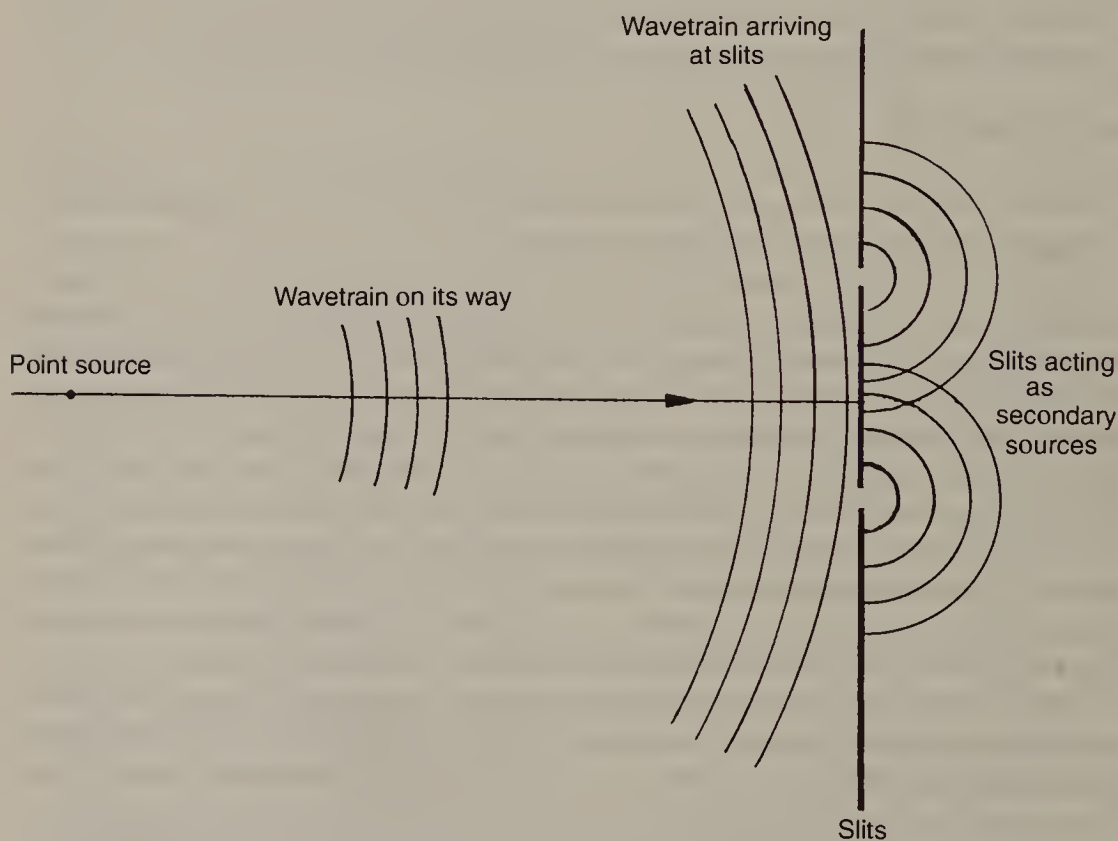
Light originates from the transitions of electrons which occur within excited atoms, excited by virtue of being at a high temperature, as in lamp filaments and the Sun, or by simulated emission, as in a laser. The physics of the processes in either case does not concern us; the important point is that each atom emits a wavetrain for a period of time (about  $10^{-8}$  s for lamp filaments; or from about  $10^{-12}$  s for pulsed lasers to indefinite times for continuous lasers). In the former cases the wave is therefore not infinite in extent, but begins and ends, like a group of ripples moving outward from a point where a stone has been thrown into a pond. It is called a *wavetrain* or a *photon*, so leading back, in a sense, to the corpuscles of Newton. The length of each wavetrain depends on the velocity of light,  $3 \times 10^8 \text{ ms}^{-1}$  in air, and the period of emission; for lamp filaments a wavetrain is typically about 3 m long ( $3 \times 10^8 \text{ ms}^{-1} \times 10^{-8} \text{ s}$ ) and for lasers from about 0.3 mm long ( $3 \times 10^8 \text{ ms}^{-1} \times 10^{-12} \text{ s}$ ) to much longer lengths (for 'continuous' lasers).

\* De Broglie's equation provides the basis for the determination of the wavelength  $\lambda$  of electrons in the electron microscope. The momentum  $mv$  of the electrons ( $m$  being relativistically corrected and  $v$  the velocity) depends on the accelerating voltage  $V$  and is determined by equating the potential energy  $eV$  (lost) where  $e$  is the charge on the electron, with the kinetic energy  $\frac{1}{2}mv^2$  (gained). But de Broglie's equation applies to all moving particles—including pieces of chalk flung at dozing students—but, as a simple calculation shows, the associated wavelengths are very small.

<sup>†</sup> Denotes biographical notes available in Appendix 3.

For lamp filaments there are, in general, no phase relationships between the individual wavetrains; they overlap and follow on each other's heels without any registration between the individual 'peaks' and 'troughs'. Furthermore, the vibration directions of each wavetrain will be more or less random—and the light is said to be **natural** or **unpolarized**.

Light from an extended source is said to be **incoherent**. Interference will occur spasmodically as it were, between the peaks and troughs of adjacent similarly polarized wavetrains, but the net effect is zero. Coherence, the condition which gives rise to clearly defined diffraction beams, is only achieved by a point source, a small part of an extended source (which condition is fulfilled by the distant street lamp) or by a laser. The condition for coherence may be illustrated by an example. Consider a distant light source shining on two slits (or pinholes). Figure 7.4 shows the arrangement with a point source, a wavetrain 'on its way' and at its arrival *at the same time* at the slits. The slits, in turn, will act as secondary waves or sources of light according to Huygens' construction—the peaks and troughs of the waves being 'in step' with each other. As the waves spread out they meet and interfere—where peak meets peak or trough meets



**Fig. 7.4.** A diagram of a distant light source emitting coherent wavetrains. When one of these strikes a screen which has adjacent slits, the slits act as secondary sources of light according to Huygens' construction, which then meet and interfere (from *Qualitative Polarized Light Microscopy* by P. C. Robinson and S. Bradbury, Oxford University Press/Royal Microscopical Society, 1992).



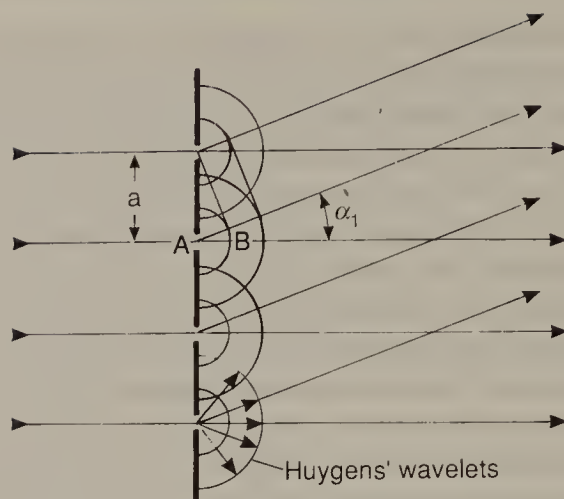
trough we have reinforcement or constructive interference, and where peak meets trough we have cancellation or destructive interference. In Section 7.4 we shall determine the particular angles or directions in which constructive and destructive interference occur. The important point to note now is that the geometrical conditions for interference which apply to just *one* wavetrain apply to *all* the wavetrains, and the resultant pattern of light and dark on the screen is the diffraction pattern. The words ‘diffraction pattern’ are a very inadequate description of the physical processes which are involved and the words or phrase ‘diffraction (or scattering)-followed-by-interference-between-the-diffracted (or scattered)-beams-pattern’ would be more accurate, albeit rather long-winded!

Now consider the situation when the slits are illuminated by separate light sources, or by an extended source. *Separate* sets of wavetrains from different parts of the source will arrive independently at the slits and thus the secondary waves emanating from each slit will bear no relationship with each other. To be sure, when ‘peak meets peak’ constructive interference will occur and where ‘peak meets trough’ destructive interference will occur—but these effects will be quite random in space and will cancel out: the light in this situation is said to be *incoherent*. Laser light, by contrast, is highly coherent.

## 7.4 Analysis of the geometry of diffraction patterns from gratings and nets

We will now analyse the diffraction phenomena described in Section 7.1 by considering the constructive and destructive interference conditions for all the scattered waves which emerge from nets and apertures of different sizes, shapes and spacings. We will do this step-by-step by first considering diffraction from a grating, which consists of a set of parallel lines engraved or photographed on to a glass or a polished metal plate. Diffraction occurs when light passes through the transparent ‘slits’ between the lines, or when it is reflected from the metal ‘strips’. The constructive and destructive interference conditions in each case are identical, but it is much easier to draw the transmission case because the incident and diffracted beams do not overlap. This situation is analogous to the ray diagrams used in light microscopy; it is simpler to demonstrate image formation in transmitted light microscopy by showing light passing from the condenser and through the specimen and objective lens to the eyepiece rather than light passing in two directions through the condenser/objective lens as it is reflected from the specimen as in reflected light microscopy.

The conditions for constructive/destructive interference from a set of parallel slits will, fairly obviously (ignoring end effects), be the same all along their length and the diffraction pattern will be a series of light/dark bands (corresponding to constructive and destructive interference conditions, respectively) running parallel to the slits. A net may be regarded as a two-dimensional grating, with a criss-cross pattern of slits, or two gratings superimposed upon each other with their slits running in different directions. Each grating will give rise to its own diffraction pattern of light/dark bands, but the net effect is that



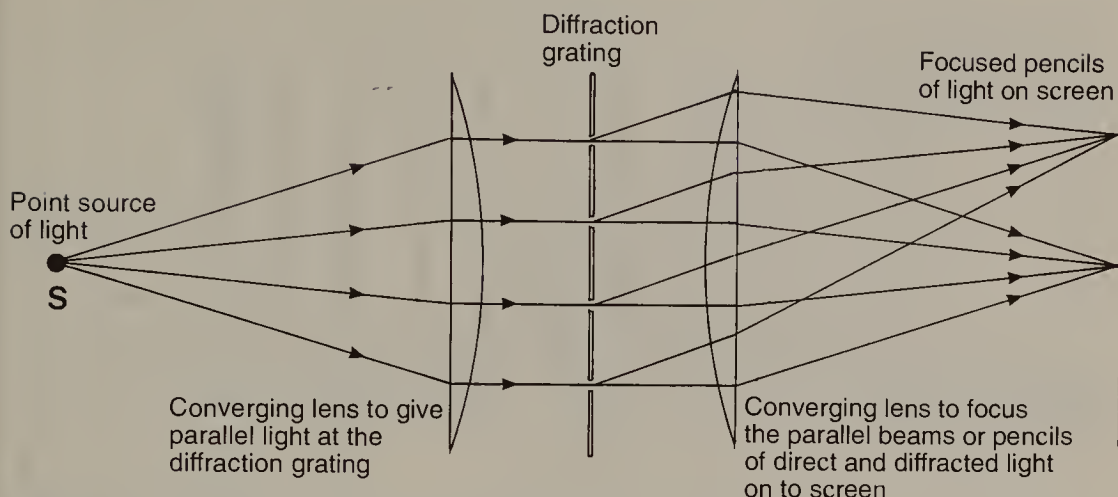
**Fig. 7.5.** A set of lines in the net acts as a diffraction grating, each slit acting as the source of a single set of Huygens' wavelets. The diffracted beam is drawn for a path difference of one wavelength.

constructive interference will only occur when the light bands intersect and reinforce—giving rise to the observed diffraction peaks or spots. Hence, consideration of the, in effect, 'one-dimensional diffraction' case of a grating will lead us to a complete analysis of the 'two-dimensional diffraction' case of a net.

First we will consider diffraction from a grating made up of very narrow or thin slits spaced distance  $a$  apart in which each slit is the source of just one Huygens' wavelet across its width; from this we will determine the conditions for constructive interference and therefore the directions of the diffracted beams. By simply extending the analysis to two dimensions we will demonstrate the reciprocal relationship between the diffracting net and the positions of the spots in the diffraction pattern. Then we shall consider diffraction from a wide aperture—a circular hole or wide slit which is the source of not one but many Huygens' wavelets and we shall see that this modifies the intensities, but does not change the positions, of the diffracted spots. Finally we shall consider gratings or nets of limited extent and will show how this leads to the occurrence of subsidiary peaks or spots.

Figure 7.5 shows just part of a diffraction grating—a one-dimensional net—consisting of many narrow slits distance  $a$  apart. The incident light is shown as parallel beams from a distant source (i.e. a plane wavefront). This special case is sometimes called the case of Fraunhofer\* diffraction as opposed to the case of Fresnel\* diffraction in which the source is not distant and the wavefront is an arc, as shown in Fig. 7.4. Of course they are not different 'types' of diffraction, it is simply that Fraunhofer diffraction is simpler to treat mathematically. However, Fresnel diffraction may in practice be 'converted' to Fraunhofer diffraction by inserting a converging (positive) lens into the light beam with the point source at its focus and from which of course emerges parallel light (Fig. 7.6).

\* Denotes biographical notes available in Appendix 3.



**Fig. 7.6.** A plane wavefront (parallel light) incident upon a grating may be achieved by inserting a lens (left) with the point source at its focus. Conversely, the parallel ‘pencils’ of the direct and diffracted light may be sharply focused onto a screen or photographic plate by inserting another lens (right). (Compare with Fig. 7.5.)

Each narrow slit (Fig. 7.5) acts as a *single* source of Huygens’ wavelets spreading out in all directions. Constructive interference occurs in those directions where the path difference (AB) between adjacent slits equals a whole number of wavelengths, i.e.

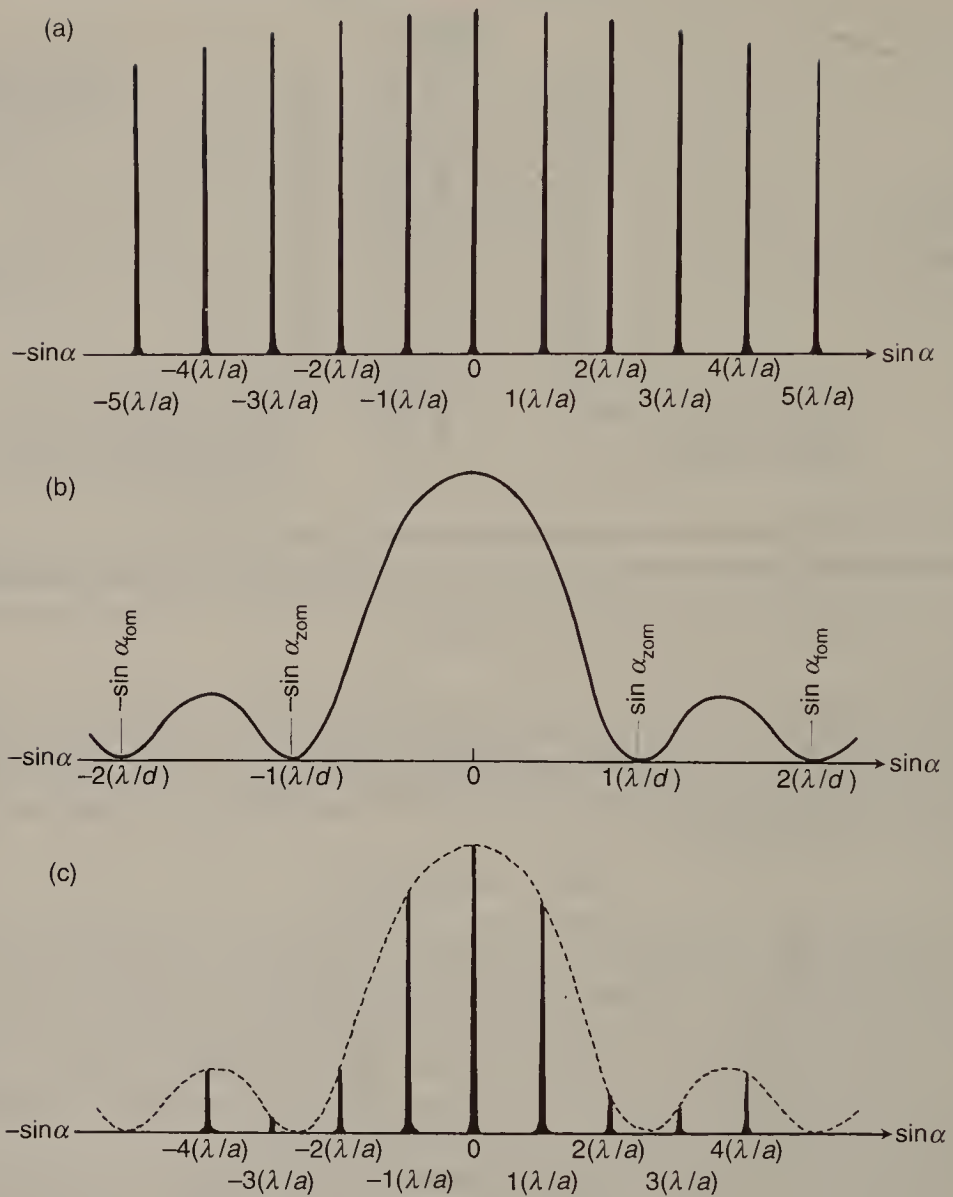
$$AB = n\lambda = a \sin \alpha_n$$

where  $a$  = the line (or lattice) spacing and  $\alpha_n$  = the diffracted angle for the  $n$ th order diffracted beam. Since  $\lambda \approx 0.5 \mu\text{m}$  and typically  $a \approx 0.5\text{--}2 \text{ mm}$ , then, as pointed out in Section 7.1, the diffraction angles are small (because  $a \gg \lambda$ ) and  $\sin \alpha_n \approx \alpha_n$ . Hence, for the first few visible diffraction orders  $AB = n\lambda = a\alpha_n$ , from which the angle  $\alpha_n = n\lambda/a$ : here we have the reciprocal relationship between the diffraction angles,  $\alpha_n$ , and lattice spacing,  $a$ .

The screen on which the diffracted beams fall (not shown in Fig. 7.5) should be a long distance from the grating compared with its width—and of course the further it is away the greater is the separation between the beams. This may, in practice, be rather inconvenient, but the inconvenience may be overcome by placing a converging (positive) lens after the grating and placing the screen at its focal point such that the ‘pencils’ or parallel light of the direct and diffracted beams are sharply focused there (Fig. 7.6). The presence of such a lens does not modify in any way our understanding of the diffraction and interference phenomena at the grating and is best ‘left out’ of diagrams because it may appear to complicate the ray paths unnecessarily.

Figure 7.7(a) shows diagrammatically the diffraction pattern from such a grating—a central maximum or peak with the first, second, third, order etc. diffracted beams each side. Their intensity decreases because as the angle  $\alpha_n$  increases the screen is further away from the diffraction grating.

This analysis of diffraction from a grating—a one-dimensional net—may readily be extended to the other set of lines in the net spaced, say, distance  $b$

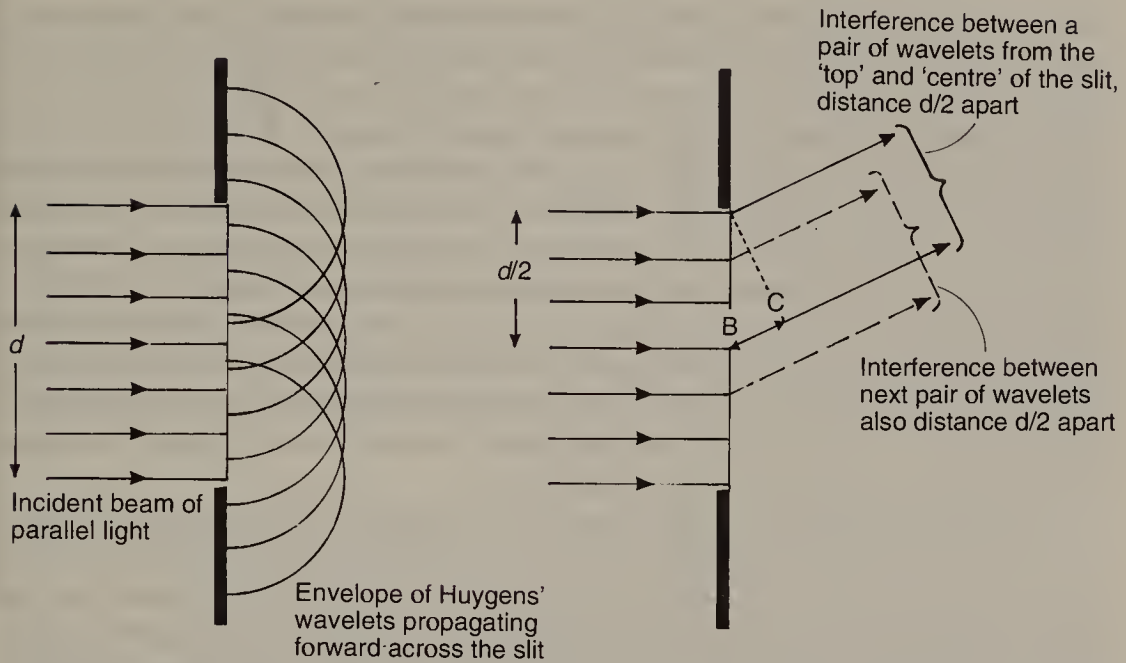


**Fig. 7.7.** Diagrams of the diffraction patterns from gratings and a single slit as a function of angle  $\alpha$ ; the intensities of the peaks are represented only qualitatively. (a) The diffracted beams for a narrow-slit grating. Constructive interference occurs at  $\sin \alpha_n$  angles of  $\pm n(\lambda/a)$  where  $n$  = the order of the diffracted beams ( $n = 0$  represents the direct beam). (b) The diffraction profile for a single slit. Destructive interference occurs at  $\sin \alpha$  angles  $1(\lambda/d)$  (zero order minimum),  $2(\lambda/d)$  (first order minimum) etc. (c) For a wide-slit grating (slit-width  $d$ , slit spacing  $a$ ) the intensities of the diffracted beams Fig. 7.7(a) are modulated by the intensity profile for a single slit Fig. 7.7(b).

apart, giving a second set of diffracted beams whose diffraction angles are again reciprocally related to  $b$ , the observed diffraction spots forming, as stressed before, the two-dimensional reciprocal lattice of the two-dimensional net (Figs 7.1(c) and 7.3(d) and (e)).

Now, the practical requirements for narrow slits which are the source of just one Huygens' wavelet are difficult if not impossible to achieve. Not only must





**Fig. 7.8.** Showing (a) a wide slit as the source of many Huygens' wavelets (shown propagating in the forward direction) and (b) the condition for destructive interference for the zero order peak. For the pair of wavelets separated by distance  $d/2$ —one at the 'top' edge and one at the centre of the slit (shown bracketed)—destructive interference occurs when the path difference  $BC = \lambda/2$ . Similarly for the next pair down (indicated by dashed lines and brackets), and so on for pairs of wavelets across the whole slit.

the slit width be a small fraction of the wavelength of light, but it must also be equally thin—otherwise it will be, in effect, not a slit but a little rectangular tunnel—rather like the narrow openings in castle walls! Furthermore, the narrower (and thinner) are the slits, the smaller is the intensity of light.

In practice, therefore, slits are wide, which means that they are the source of many Huygens' wavelets, as shown in Fig. 7.8(a). The problem now is to sum all the contributions of all the wavelets. This may be carried out analytically or graphically by means of amplitude—phase diagrams, which are described in optics textbooks. However, we shall use a simplified approach, which is quite adequate and emphasizes the principles involved.

In the forward (direct beam) direction, all the wavelets are in phase and interfere constructively. At increasing angles to the direct beam the wavelets become progressively more out of step; they begin to interfere destructively and the intensity falls: we need to work out the angle at which it falls to zero. Now consider a pair of wavelets; one wavelet at the 'top edge' of the slit and the other at the centre of the slit (Fig. 7.8(b)); when the path difference between them is  $\lambda/2$  'trough meets peak' and total destructive interference occurs. Hence from Fig. 7.8(b),

$$BC = \lambda/2 = d/2 \sin \alpha_{\text{zom}}$$

i.e.

$$\lambda = d \sin \alpha_{\text{zom}}$$

where  $d$  is the slit width and  $\alpha_{\text{zom}}$  is the angle at which total destructive interference of the direct (zero order) peak occurs, i.e. zero order *minimum*,  $\alpha_{\text{zom}}$ ).

Now consider the next pair of wavelets again distance  $d/2$  apart, one just below that at the top edge and one just below that at the centre, as shown by dashed lines in Fig. 7.8(b). The condition for destructive interference between this pair of wavelets will be the same—and so on for all the pairs of wavelets across the whole slit. Hence the above condition for total destructive interference applies to the *whole* slit and gives the angle at which the intensity of the direct or zero order beam or the ‘central maximum’ falls to zero. Notice that the equation ‘looks’ the same as that for constructive interference *between* the slits; the difference is of course that in the former case only two Huygens’ wavelets needed to be considered, one from each slit.

As the angle increases further there will be some net constructive interference, giving a first order diffracted beam but of much smaller intensity than the zero order beam. The next condition for total destructive interference may be found by again considering the condition for destructive interference between a pair of wavelets, one wavelet at the ‘top edge’ of the slit as before and the other a *quarter* of the slit width from the top. Again, when the path difference between them is  $\lambda/2$ , destructive interference occurs. Continuing as before, i.e. considering pairs of such wavelets across the whole slit width, it is seen that this is again the condition for total destructive interference of all the wavelets across the slit, i.e. for the first order zero or minimum

$$\lambda/2 = (d/4)\sin \alpha_{\text{fom}}, \quad \text{i.e. } 2\lambda = d \sin \alpha_{\text{fom}}$$

where  $\alpha_{\text{fom}}$  is the angle for first order destructive interference (first order *minimum*  $\alpha_{\text{fom}}$ ). Note that  $\sin \alpha_{\text{fom}} = 2(\lambda/d) = 2\sin \alpha_{\text{zom}}$ , i.e. for small angles where  $\sin \alpha \approx \alpha$ , the first order minimum occurs at twice the angle of the zero order minimum\*.

The diffraction pattern from a single slit is therefore a central maximum with much fainter bands of half the width of the central maximum on each side. It is represented diagrammatically in Fig. 7.7(b). The diffraction pattern from a circular hole or aperture is, correspondingly, a central disc surrounded by much fainter rings or haloes, as shown in Figs 7.3(a)–(c). The disc is called the Airy disc because its diameter was worked out precisely by Sir George Airy†. His calculation for the angle  $\alpha_{\text{zom}}$  of the zero order minimum, which takes into account the circular symmetry of a round hole or aperture, only differs from our simple calculation by a factor of 1.22, i.e.  $1.22\lambda = d \sin \alpha_{\text{zom}}$ . The Airy disc is of immense importance in optics since it determines the limit of resolution of telescopes and microscopes, as explained in Section 7.5.

\*The angle for maximum *constructive* interference for the first order diffracted beam cannot be determined precisely by such a simple approach as we have used. It turns out that the peak is slightly asymmetrical—the peak does not lie at an angle half way between  $\alpha_{\text{zom}}$  and  $\alpha_{\text{fom}}$  but is displaced slightly to a lower angle. The analysis is given in the optics textbooks listed in Further Reading.

† Denotes biographical notes available in Appendix 3.

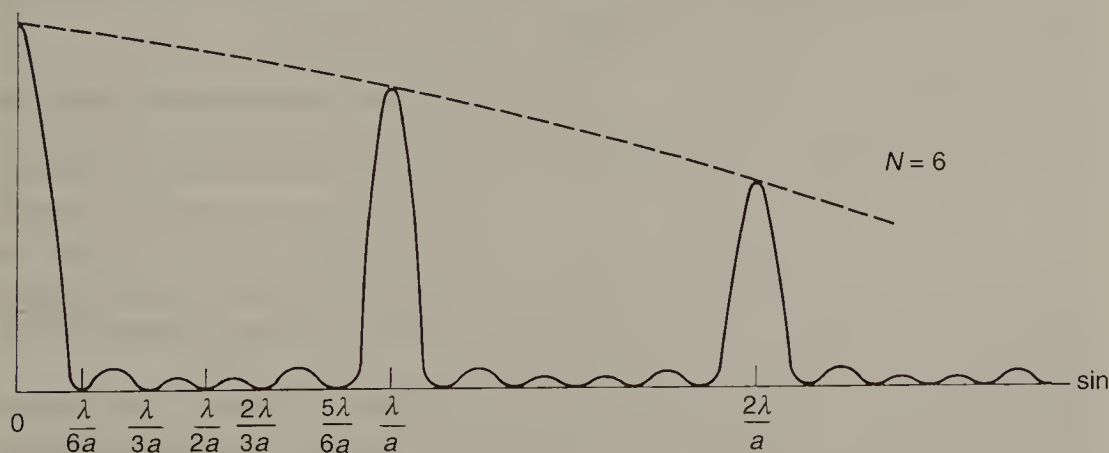
Now we have to consider the diffraction patterns from a grating with wide slits (width  $d$ ) separated a distance  $a$  apart. The result is simply the combination of the narrow-slit diffraction pattern (Fig. 7.7(a)) and the single wide-slit diffraction pattern (Fig. 7.7(b)). The resultant is shown in Fig. 7.7(c). Notice that the angles at which the diffraction peaks occur are unchanged and are determined solely by the slit spacing  $a$ , but that their intensities are modulated by the intensity profile of a single slit of width  $d$ .

Finally, we have to consider the situation where the diffraction grating is of limited extent, consisting of a limited number of slits. If  $W$  is the width of the grating and  $N$  is the number of slits, then  $W = Na$ . We simply consider the whole grating as a very wide slit, then work out the conditions for destructive interference as before. The sines of the angles are simply

$$1(\lambda/W), 2(\lambda/W), 3(\lambda/W), \dots \quad \text{or} \quad \frac{1}{N}(\lambda/a), \frac{2}{N}(\lambda/a), \frac{3}{N}(\lambda/a) \dots$$

Each of the diffracted peaks or 'principal maxima' will no longer be 'sharp', as indicated in Figs 7.7(a) and (c), but will be broadened and surrounded by fringes or 'subsidiary maxima'. The number of fringes increases with  $N$  and their intensities decrease with  $N$ , such that they are generally not detectable for large  $N$  values.

Figure 7.9 shows the zero, first and second order principal maxima and the subsidiary maxima from a grating with  $N$  slits. Note that the (half) angular widths of the principal maxima, and the angular widths of the subsidiary maxima, are simply equal to  $1/N$  of the angular separation of the principal maxima. This leads to the simple result that there are  $(N - 2)$  subsidiary maxima between the principal maxima, as shown in Fig. 7.9. The proof is as follows. The first minimum of the zero order principal maximum (the direct



**Fig. 7.9.** Diagram of the diffraction pattern from a grating (drawn on one side of the direct beam) consisting of  $N$  narrow slits of spacing  $a$ . Between the principal maxima there are  $(N - 2)$  subsidiary maxima or fringes. The diagram is drawn for  $N = 6$  (modified from *Optics* by E. Hecht and A. Zajac, Addison-Wesley, 1980).



beam) occurs at angle  $1/N(\lambda/a)$ , the second minimum at  $2/N(\lambda/a)$  and so on. Altogether therefore, going from the zero to the first order principal maximum which occurs at angle  $1(\lambda/a)$ , there will be  $(N - 1)$  subsidiary minima, the  $(N - 1)$ th minimum defining, in effect, the first minimum of the first order principal maximum. Hence, between the  $(N - 1)$  minima there will be  $(N - 2)$  subsidiary maxima.

Figure 7.9 is drawn for  $N = 6$  and shows the principal maxima at  $\sin \alpha$  angles  $1(\lambda/a)$ ,  $2(\lambda/a)$  and the subsidiary minima at  $\sin \alpha$  angles  $1/6(\lambda/a)$ ,  $2/6(\lambda/a)$ ,  $3/6(\lambda/a)$ ,  $4/6(\lambda/a)$  and  $5/6(\lambda/a)$ .

All these considerations—the sizes and numbers of diffracting apertures—may be extended to the two-dimensional case of nets, as shown in Figs 7.3(d) and (e). The intensities of the diffraction peaks are modulated by the intensity profiles of the Airy disc and its surrounding fainter rings or haloes and the numbers of subsidiary maxima between the principal maxima are two less than the number of apertures in each direction—and clearly will become insignificant as the number of apertures becomes large. Hence, although we have not determined quantitatively the light intensity distribution in the diffraction patterns from nets, the main features that we noted in Section 7.2 are now explained.

## 7.5 The resolving power of optical instruments

One of the most important and useful applications of the study of diffraction is the determination of the resolving power of optical instruments, in particular the telescope and the microscope. By resolving power we mean the ability to distinguish points with small angular separations, such as stars in the telescope, or points which are small distances apart as in the microscope. In both cases the customary term *resolving power* is better expressed by the more precise term *limit of resolution*; either an angular limit of resolution as in the telescope or a distance limit of resolution as in the microscope. In either case the resolving power is a term reciprocally related to the limit of resolution.

There are several other factors which determine the limit of resolution of optical instruments, in particular lens defects, such as spherical and chromatic aberration, and coma. To a large extent these can be eliminated by appropriate lens design or the use of reflecting elements: mirrors have almost wholly replaced lenses as the principal element in astronomical telescopes and, except for the difficulties in manufacture, could partially replace objective lenses in microscopes. But the limit of resolution is ultimately limited by diffraction—either at the aperture of the telescope or at closely spaced features in the microscope.

Consider first the limit of resolution of a telescope. Parallel rays from a distant point source—a star—enter the aperture, diameter  $d$ , and are focused by the objective lens on to a screen, photographic plate or the focal plane of the eyepiece. As explained in Section 7.4, the image of the distant point source is not a point, but an Airy disc (surrounded by haloes of decreasing intensity), as shown in Figs 7.3(a)–(c) and Fig. 7.10. Now consider light from another star;



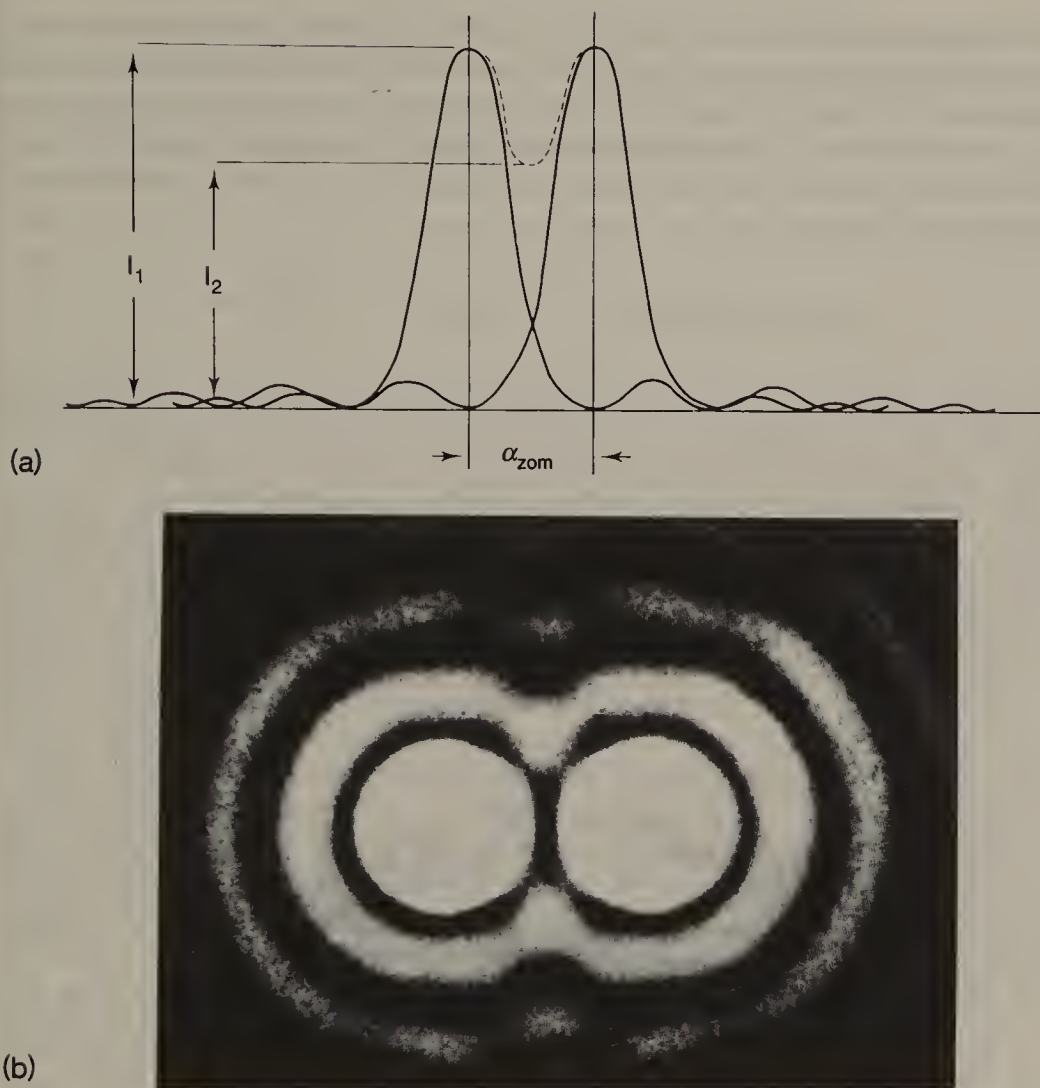


Fig. 7.10. (a) The intensity profile of an Airy disc pattern of two points separated by an angle which just satisfies the Rayleigh criterion for resolution. (Note that the centre of one disc falls on the zero order minimum of the other.) The overall intensity profile is indicated by the dotted line and the minimum,  $I_2$ , is about 85% of the maximum,  $I_1$ . (b) Corresponding photograph of two point sources which are just resolved (from *An Introduction to the Optical Microscope*, 2nd edn, by S. Bradbury, Oxford University Press/Royal Microscopical Society, 1989).

again its image is an Airy disc, as also shown in Fig. 7.10. The net intensity in the image plane is the sum of the intensities of the two discs (and their haloes). As the angular separation between the stars decreases their Airy discs overlap and the limit of resolution is the point at which the net intensity does not show a discernible decrease between the central maxima of the Airy discs. Determining this point is a matter of some difficulty, but the criterion proposed by Lord Rayleigh\* is most generally adopted. The Rayleigh criterion is that the centre of

\* Denotes biographical notes available in Appendix 3.

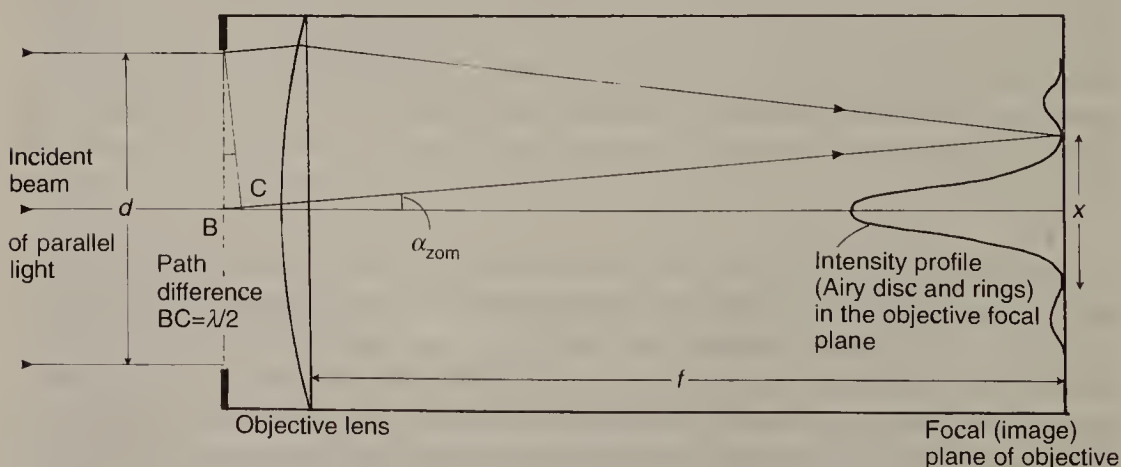
one Airy disc should coincide with the zero order minimum of the adjacent Airy disc. This criterion is shown in Fig. 7.10. The net intensity profile shows a small dip of about 85% of the maxima each side—which is easily discernible by the eye or detectable by a photographic plate. Hence the angular resolution of a telescope is  $\alpha_{\text{zom}}$ , the zero order minimum angle for destructive interference, i.e. referring to Section 7.4:

$$\text{Limit of resolution} = \alpha_{\text{zom}} \approx \sin \alpha_{\text{zom}} = \frac{1.22 \lambda}{d}.$$

Clearly, the greater is the aperture of a telescope, the smaller is the limit of resolution and this explains why astronomical telescopes in particular are constructed with objective mirrors with as large a diameter as possible.

These considerations are also relevant to an estimation of the limit of resolution of cameras in which the dimension  $x$  of the Airy disc depends, additionally, on the focal length of the telescope or camera objective,  $f$ , the radius or half-diameter  $x/2$  being given approximately by  $x/2 = f \sin \alpha_{\text{zom}}$  (Fig. 7.11). Substituting from above gives  $x = 2.44 \lambda (f/d)$ . The ratio  $(f/d)$  is called the  $f$ -number and is the important number engraved on camera lenses and the like. For blue-green light  $\lambda \approx 0.5 \mu\text{m}$  and therefore  $x$  is *roughly* equal to the  $f$ -number expressed as micrometres. ‘Stopping down’ a camera lens (i.e. increasing the  $f$ -number) means increasing the size of the Airy disc. How important this is (in comparison with other factors such as the depth of field) depends upon the relation between the size of the Airy disc and the ‘grain size’ of the photographic film. Clearly, deterioration in image sharpness will only begin to occur when the Airy disc becomes (roughly) equal to the grain size.

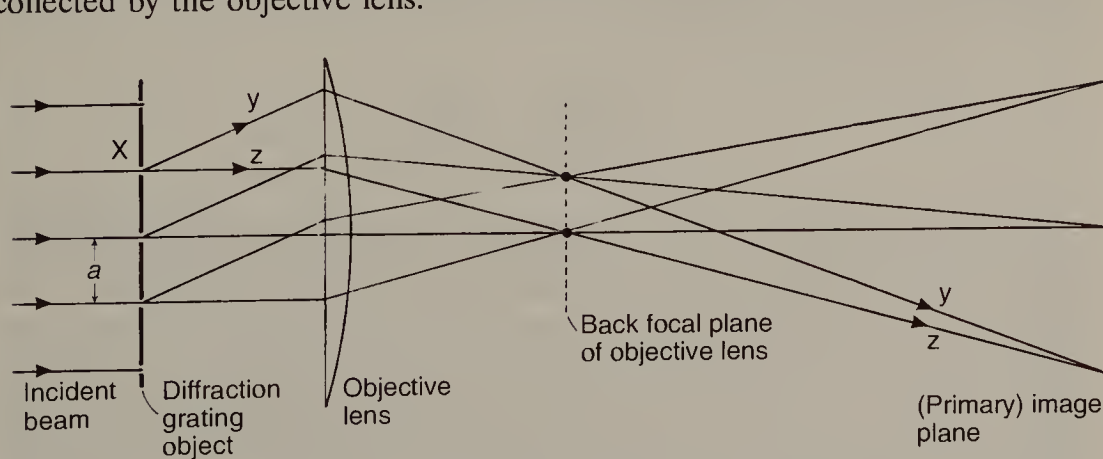
The diffraction-limited resolution of the microscope can be treated in the same way as for a telescope—by considering the separation between the Airy discs of two closely separated point sources of light in the object plane and



**Fig. 7.11.** The formation of the Airy disc in the focal plane of a telescope or camera. The half-diameter  $x/2$  (shown much exaggerated) is given by  $f \sin \alpha_{\text{zom}}$ . Only two incident rays are shown for which the path difference is  $\lambda/2$  (compare with Fig. 7.8(b)).

situated of course close to the front focal plane of the objective rather than (as in the telescope) a long distance away. In doing so a simplifying assumption may be made that the two point sources are entirely independent, or rather that they are incoherent with one another and hence that there is no interference between them. This assumption is obviously invalid—microscopical specimens do not consist of independent points of light of different intensities across their surfaces. It is more reasonable to assume that the specimen is illuminated with coherent light and that interference occurs between the light waves diffracted at the light/dark regions across the specimen surface. In this case the simplest type of specimen to consider is a narrow-slit diffraction grating consisting of slits spaced  $a$  apart and the limit of resolution is simply the limit at which the microscope objective can resolve the slits, i.e. the limit at which it can form an image of the grating. This, essentially, was the approach of Ernst Abbe\*, the optical designer for Carl Zeiss. It turns out (from a much more rigorous analysis) that the expressions for the limit of resolution of the microscope are formally identical irrespective of the assumptions made about the nature of the illumination or self-illumination of the specimen, but the Abbe approach serves to emphasize the physical principles involved in image formation in a more direct and comprehensible way.

The Abbe criterion is as follows: in order for the microscope to form an image of the specimen (i.e. in order to resolve the slits or lines of a grating), at least two beams (usually the direct beam and the first order diffracted beam) should enter the objective lens. This situation is shown in Fig. 7.12. The specimen/grating is illuminated with a parallel beam of light (from a distant source or a sub-stage condenser in which the aperture diaphragm is almost fully closed) and the first order diffracted beams (on either side of the direct beam) are just collected by the objective lens.



**Fig. 7.12.** Image formation in the light microscope. The direct and diffracted beams enter the objective lens and are focused to form a diffraction pattern in its (back) focal plane (compare with Fig. 7.6). The rays 'continue on their way' to form an image by the recombination of the diffracted light, e.g. incident ray X is separated into z (direct) and y (diffracted) light; these two rays recombine in the image plane.

\* Denotes biographical notes available in Appendix 3.

These parallel beams are then focused by the objective lens to give diffraction spots which are situated, as shown, in its back focal plane (a screen placed here would record this diffraction pattern, just as shown in Fig. 7.6). However, the beams or rays continue on their way and intersect, as shown, to form the (primary) image, (which is then magnified by the eyepiece or photographic projection lens). The important point is that the image is formed by the *recombination* of light which was *separated* at the specimen by diffraction. Consider, for example, the incident beam marked X (Fig. 7.12); this is separated by diffraction into z (direct beam) and y (diffracted beam). These two beams then contribute to the separate (zero and first order) diffraction spots, but then continue on their way to be reunited or recombined and, as Abbe pointed out, it is this recombination that constitutes an image. The greater the number of diffracted beams which are collected by the objective lens and thence recombined, the closer the image approximates to the object, but the limit of resolution is determined by the criterion that at least two beams should enter the objective.

Hence, for the case of normal incidence, in which the direct and two first order beams enter the objective lens (Fig. 7.13(a)), the limit of resolution is simply obtained from the equation derived in Section 7.4, i.e.  $1\lambda = a \sin \alpha_1 = a \sin i$ , i.e. the limit of resolution  $a = \lambda / \sin i$ , where  $i$  is the semi-angle of the objective lens subtended at the specimen which is set equal to  $\alpha_1$ , the angle between the direct and first order diffracted beams.

This equation can be modified in several ways. First the Airy correction factor 1.22 may be included to account for the circular symmetry of the objective lens. Second, the space between the specimen and objective lens may be filled with immersion oil of refractive index  $n$ , which is simply the ratio of the wavelength  $\lambda$  of light in air (or vacuum) and the wavelength  $\lambda'$  in the oil, i.e. by definition  $n = \lambda / \lambda'$ . Including these factors gives

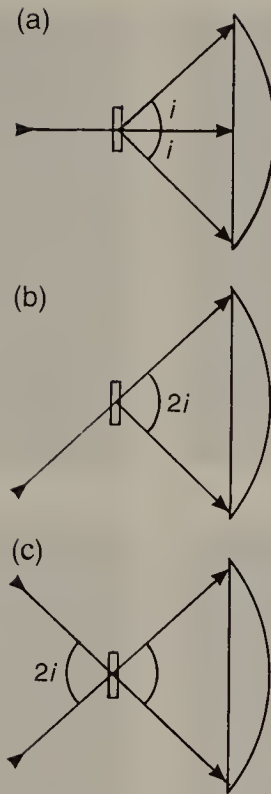
$$a = \frac{1.22 \lambda'}{\sin i} = \frac{1.22 \lambda}{n \sin i}.$$

The important quantity  $n \sin i$  in this equation is called the **numerical aperture** (NA) and fulfils, in effect, the same role with respect to the microscope as the diameter  $d$  of the objective lens/mirror with respect to the telescope.

Finally, Fig. 7.13(a) shows an over-fulfilled case in which, because the incident beam is normal to the specimen and axial with the microscope, two diffracted beams, as well as the direct or zero order beam, enter the objective. Fig. 7.13(b) shows the situation in which the incident beam is inclined such that the zero order beam passes through one edge of the objective lens and one diffracted beam passes through the opposite edge. The angle between them is now double that previously so that the limit of resolution is halved, i.e.

$$a = \frac{0.61 \lambda}{n \sin i} = \frac{0.61 \lambda}{\text{NA}}.$$





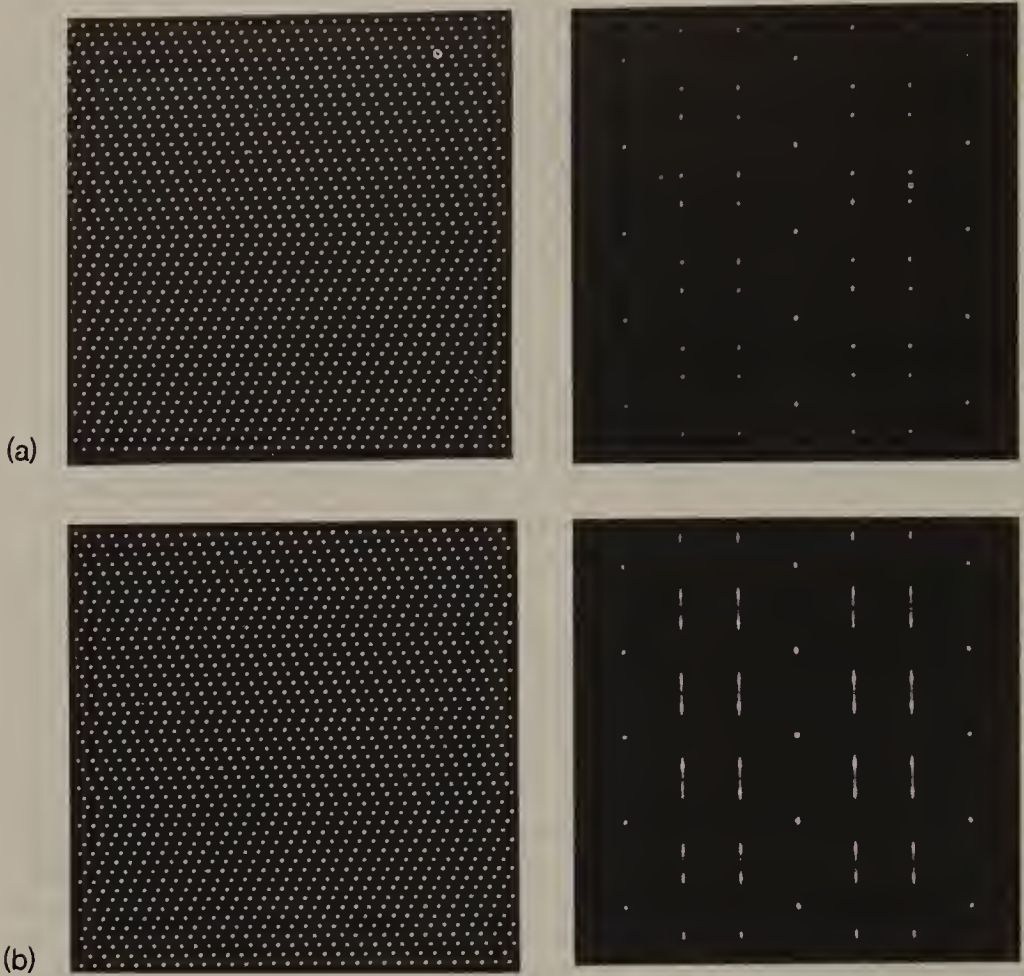
**Fig. 7.13.** The Abbe criterion for the limit of resolution of an objective lens of semi-angular aperture  $i$ . (a) Normal incidence, parallel light (condenser diaphragm closed down); the direct and two first-order beams enter the objective and contribute to the image; (b) as (a) but inclined incidence; the direct beam and just one first-order beam at angle  $2i$  enter the objective and contribute to the image; (c) the practical arrangement for maximum resolving power; the condenser diaphragm is opened to pass a cone of light of semi-angle  $i$  to fulfil, at all angles, the geometrical requirements for the limit of resolution as in (b).

This situation is effectively brought about when the aperture diaphragm in the condenser lens is opened out to give a highly convergent beam of light on the specimen of semi-angle  $i$  equal to the semi-angle or aperture of the objective lens (Fig. 7.13(c)).

The Abbe criterion applies equally to light microscopes and electron microscopes. The enormous decrease in the limit of resolution obtainable in the transmission electron microscope arises because of the much smaller values of  $\lambda$  for electrons (typically 4 pm for 100 kV instruments compared with light (typically 500 nm)). This (approximate) 100 000 decrease is however offset because of the high inherent spherical aberrations in electron lenses which limit NA values to the order of 0.01 compared with NA values up to 1.4 for oil immersion light objectives.

## Exercises

7.1 Figure 7.14(a) shows a net with a single twin and the corresponding diffraction pattern (optical transform) and Fig. 7.14(b) shows a net with several twins and the



**Fig. 7.14.** (a) A net with a single twin, and (b) a net with several twins and their corresponding diffraction patterns (from *Atlas of Optical Transforms* by G. Harburn, C. A. Taylor and T. R. Welberry, Bell & Hyman, 1983, an imprint of HarperCollins Publishers Ltd.)

corresponding diffraction pattern (see Figs. 1.18, 1.20 and 4.4(b)). Using a tracing paper overlay on the diffraction pattern in Fig. 7.14(a), outline the reciprocal lattice unit cells of the two twin orientations and note those reciprocal lattice points which are common to both twin orientations.

The diffraction pattern in Fig. 7.14(b) is similar to that in Fig. 7.14(a) except that some of the spots are streaked in a direction perpendicular to the twin plane. Explain this streaking qualitatively after you have read Section 9.3.

- 7.2 With reference to Fig. 7.7(c), describe the diffraction pattern which you would obtain with a diffraction grating in which the slit width  $d$  is equal to half the slit spacing  $a$ .
- 7.3 Using de Broglie's equation, derive a simple equation for the (non-relativistically corrected) wavelength  $\lambda$  of electrons in the electron microscope in terms of  $m$ ,  $e$  (electron mass and charge) and  $V$  the microscope accelerating voltage. Given the following values of  $m$  (rest mass)  $= 9.11 \times 10^{-31}$  kg,  $e$  (electron charge)  $= 1.6 \times 10^{-19}$  C, and  $h$  (Planck constant)  $= 6.63 \times 10^{-34}$  Js, determine  $\lambda$  for  $V = 10$  kV, 100 kV and 1 MV.

# X-ray diffraction: the contributions of Max von Laue, W. H. and W. L. Bragg and P. P. Ewald

## 8.1 Introduction

The experimental technique which has been of the greatest importance in revealing the structure of crystals is undoubtedly X-ray diffraction.

The story of the discovery of X-ray diffraction in crystals by Laue\*, Friedrich and Knipping in Munich in 1912 and the development of the technique by W. H. Bragg\* and W. L. Bragg\* in Leeds and Cambridge in the years preceding the First World War is well known. But why did the Braggs make such rapid advances in the analysis of X-ray diffraction photographs in comparison with Laue and his co-workers? An important factor in the answer seems to be that Laue envisaged crystals in terms of a three-dimensional network of rows of atoms and based his analysis on the notion that the crystal behaved, in effect, as a three-dimensional diffraction grating. This approach is not wrong, but it is in practice rather clumsy or protracted. On the other hand, the Braggs (and here the credit must go to W. L. Bragg, the son) envisaged crystals in terms of layers or planes of atoms which behaved in effect as reflecting planes (for which the angle of incidence equals the angle of reflection), strong 'reflected' beams being produced when the path differences between reflections from successive planes in a family is equal to whole number of wavelengths. This approach is not correct in a physical sense—planes of atoms do not reflect X-rays as such—but it is correct in a geometrical sense and provides us with the beautifully simple expression for the analysis of crystal structure:

$$n\lambda = 2d_{hkl} \sin \theta,$$

where  $\lambda$  is the wavelength,  $n$  is the order of reflection,  $d_{hkl}$  is the lattice plane spacing and  $\theta$  is the angle of incidence/reflection to the planes.

What led W. L. Bragg to this novel perception of the diffraction? Simply his observation of the elliptical shapes of the diffraction spots, which he noticed were also characteristic of the reflections from mirrors of a pencil-beam of light (see the Laue photograph on p. xii). Only connect!

Finally, we come to the contribution of P. P. Ewald\*, a physicist who never

\* Denotes biographical notes available in Appendix 3.

achieved the recognition that was his due. The story is briefly recorded in his autobiographical sketch in *50 Years of X-ray Diffraction*. Ewald was a 'doctorand'—a research student working in the Institute of Theoretical Physics in the University of Munich under Professor A. Sommerfeld. The subject of his thesis was 'To find the optical properties of an anisotropic arrangement of isotropic oscillators'. In January 1912, while he was in the final stages of writing up his thesis, he visited Max von Laue, a staff member of the Institute, to discuss some of the conclusions of his work. Ewald records that Laue listened to him in a slightly distracted way and insisted first on knowing what was the distance between the oscillators in Ewald's model; perhaps  $1/500$  or  $1/1000$  of the wavelength of light, Ewald suggested. Then Laue asked 'what would happen if you assumed very much shorter waves to travel through the crystal?'. Ewald turned to Paragraph 6, Formula 7, of his thesis manuscript, saying 'this formula shows the results of the superposition of all wavelets issuing from the resonators. It has been derived without any neglect or approximation and is therefore valid also for short wavelengths.' Ewald copied the formula down for Laue shortly before taking his leave, saying that he, Laue, was welcome to discuss it. Laue's question, of course, arose from his intuitive insight that if X-rays were waves and not particles, with wavelengths very much smaller than light, then they might be diffracted by such an array of regularly spaced oscillators.

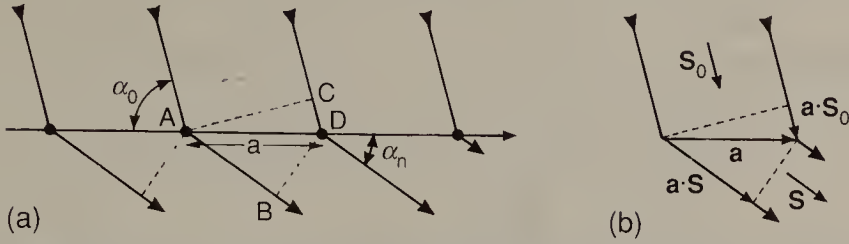
The next Ewald heard of Laue's interest was through a report which Sommerfeld gave in June 1912 on the successful Laue-Friedrich-Knipping experiments. He realized that the formula which he had copied down for Laue, and which Laue had made no use of, provided the obvious way of interpreting the geometry of the diffraction patterns—by means of a construction which he called the reciprocal lattice and a sphere determined by the mode of incidence of the X-rays on the crystal (the Ewald or reflecting sphere). Ewald's interpretation of the geometry of X-ray diffraction was not published until 1913, by which time rapid progress in crystal structure analysis had already been made by W. H. and W. L. Bragg in Leeds and Cambridge.

## 8.2 Laue's analysis of X-ray diffraction: the three Laue equations

Laue's analysis of the geometry of X-ray diffraction patterns has been referred to in Section 8.1. What follows is a much simplified treatment which does not take into consideration Laue's interpretation of the origin of the diffracted waves from irradiated crystals.

Consider a simple crystal in which the motif is one atom and the atoms are simply to be regarded as scattering centres situated at lattice points. The more general situation in which the motif consists of more than one atom and in which the different scattering amplitudes of the atoms and the path differences between the atoms have to be taken into account is discussed in Section 9.2. The crystal may be considered to be built up of rows of atoms in three dimensions:





**Fig. 8.1.** (a) Diffraction from a lattice row along the  $x$ -axis. The incident and diffracted beams are at angles  $\alpha_0$  and  $\alpha_n$  to the row. The path difference between the diffracted beams =  $(AB - CD)$ . (b) The incident and diffracted beam directions and the path difference between the diffracted beams as expressed in vector notation.

rows of atoms of spacing  $a$  along the  $x$ -axis, of spacing  $b$  along the  $y$ -axis and of spacing  $c$  along the  $z$ -axis. Consider first of all the condition for constructive interference for the waves scattered from the row of atoms along the  $x$ -axis—which may simply be reduced to a consideration of the path differences between waves scattered from adjacent atoms in the row (Fig. 8.1(a)).

For constructive interference the path difference  $(AB - CD)$  must be a whole number of wavelengths, i.e.

$$(AB - CD) = a(\cos \alpha_n - \cos \alpha_0) = n_x \lambda$$

where  $\alpha_n, \alpha_0$  are the angles between the diffracted and incident beams to the  $x$ -axis, respectively, and  $n_x$  is an integer (the order of diffraction).

This equation, known as the first Laue equation, may be expressed more elegantly in vector notation. Let  $s, s_0$  be unit vectors along the directions of the diffracted and incident beams, respectively, and let  $a$  be the translation vector from one lattice point (or atom position) to the next [Fig. 8.1(b)]. The path difference  $a(\cos \alpha_n - \cos \alpha_0)$  may be represented by the scalar product  $a \cdot s - a \cdot s_0 = a \cdot (s - s_0)$ . Hence the first Laue equation may be written

$$a(\cos \alpha_n - \cos \alpha_0) = a \cdot (s - s_0) = n_x \lambda.$$

Now Fig. 8.1 is misleading in that it only shows the diffracted beam at angle  $\alpha_n$  below the atom row—but the same path difference obtains if the diffracted beam lies in the plane of the paper at angle  $\alpha_n$  above the atom row—or indeed out of the plane of the paper at angle  $\alpha_n$  to the atom row. Hence all the diffracted beams with the same path difference occur at the same angle to the atom row, i.e. the diffracted beams of the same order all lie on the surface of a cone—called a Laue cone—centred on the atom row with semi-apex angle  $\alpha_n$ . This situation is illustrated in Fig. 8.2 which shows just three Laue cones with semi-apex angle  $\alpha_0$  (zero order,  $n_x = 0$ ), semi-apex angle  $\alpha_1$  (first order,  $n_x = 1$ ) and semi-apex angle  $\alpha_2$  (second order,  $n_x = 2$ ). Clearly there will be a whole set of such cones with semi-apex angles  $\alpha_n$  varying between  $0^\circ$  and  $180^\circ$ .

The analysis is now repeated for the atom row along the  $y$ -axis, giving the second Laue equation:

$$b(\cos \beta_n - \cos \beta_0) = b \cdot (s - s_0) = n_y \lambda,$$

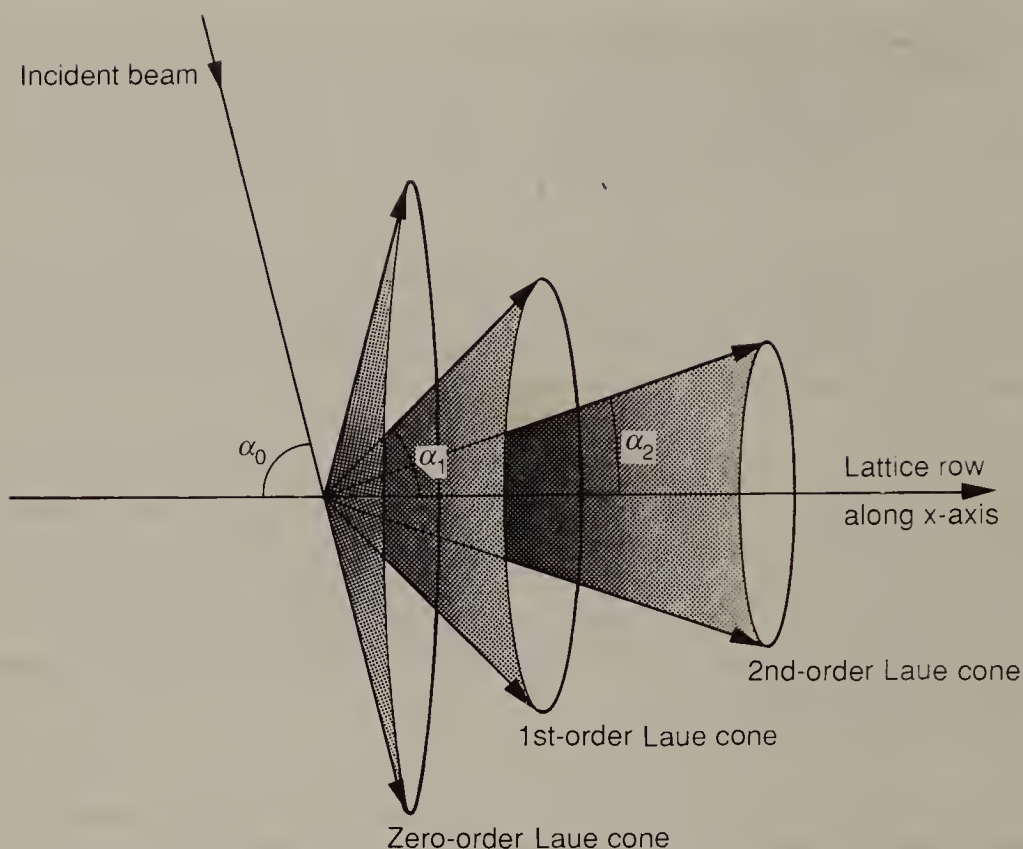


Fig. 8.2. Three Laue cones representing the directions of the diffracted beams from a lattice row along the  $x$ -axis with  $0\lambda$  ( $n_x = 0$ ),  $1\lambda$  ( $n_x = 1$ ) and  $2\lambda$  ( $n_x = 2$ ) path differences.

and for the atom row along the  $z$ -axis giving the third Laue equation:

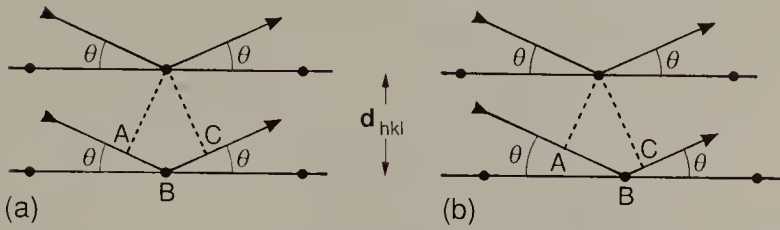
$$c(\cos \gamma_n - \cos \gamma_0) = \mathbf{c} \cdot (\mathbf{s} - \mathbf{s}_0) = n_z \lambda,$$

where the angles  $\beta_n, \beta_0, \gamma_n, \gamma_0$  and the integers  $n_y$  and  $n_z$  are defined in the same way as for  $\alpha_n, \alpha_0$  and  $n_x$ .

Now, for constructive interference to occur simultaneously from all three atom rows, all three Laue equations must be satisfied simultaneously. This is equivalent to the geometrical condition that diffracted beams only occur in those directions along which three Laue cones, centred along the  $x$ -,  $y$ - and  $z$ -axes, intersect. Each diffracted beam may be identified by three integers  $n_x, n_y$  and  $n_z$  which, as pointed out above, represent the order of diffraction from each of the atom rows. We shall find in Section 8.3 that these integers are simply  $h, k$  and  $l$  Laue indices (see Section 5.5) of the reflecting planes in the crystal.

### 8.3 Bragg's analysis of X-ray diffraction: Bragg's law

Laue's analysis is in effect an extension of the idea of a diffraction grating to three dimensions. It suffers from the severe practical disadvantage that in order to calculate the directions of the diffracted beams, a total of six angles  $\alpha_n, \alpha_0,$



**Fig. 8.3.** (a) Bragg's law for the case of a rectangular grid, i.e.  $AB = BC = d_{hkl} \sin \theta$ ; the path difference  $(AB + BC) = 2d_{hkl} \sin \theta$ . (b) Bragg's law for the general case in which  $AB \neq BC$ . Again, the path difference  $(AB + BC) = 2d_{hkl} \sin \theta$ .

$\beta_n$ ,  $\beta_0$  and  $\gamma_n$ ,  $\gamma_0$ ; three lattice spacings  $a$ ,  $b$  and  $c$ , and three integers  $n_x$ ,  $n_y$  and  $n_z$  need to be determined. As discussed in Section 5.5, W. L. Bragg envisaged diffraction in terms of reflections from crystal planes giving rise to the simple relationship (Bragg's law, derived below):

$$n\lambda = 2d_{hkl} \sin \theta.$$

It can be seen immediately, by comparing the Laue equations with Bragg's law, that the number of variables needed to calculate the directions of the diffracted beams are much reduced.

Bragg's law may be derived with reference to Fig. 8.3(a) which shows (as for the derivation of the Laue equations) a simple crystal with one atom at each lattice point. The path difference between the waves scattered by atoms from adjacent  $(hkl)$  lattice planes of spacings  $d_{hkl}$  is given by

$$(AB + BC) = (d_{hkl} \sin \theta + d_{hkl} \sin \theta) = 2d_{hkl} \sin \theta.$$

Hence for constructive interference:

$$n\lambda = 2d_{hkl} \sin \theta,$$

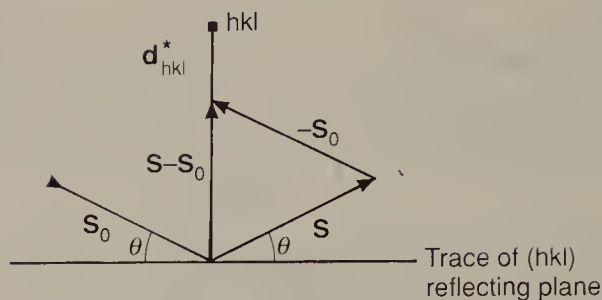
where  $n$  is an integer (the order of reflection or diffraction).

As explained in Section 5.5,  $n$  is normally incorporated into the lattice plane symbol, i.e.

$$\lambda = 2 \left( \frac{d_{hkl}}{n} \right) \sin \theta = 2d_{nh\ nk\ nl} \sin \theta$$

where  $nh\ nk\ nl$  are the Laue indices for the reflecting planes of spacing  $d_{hkl}/n$ .

Figure 8.3(a) represents a particularly simple geometrical situation in which the lattice is shown as a rectangular grid and the atoms are symmetrically disposed with respect to the incident and diffracted beam, i.e.  $AB = BC$ . Figure 8.3(b) shows a more general situation in which the lattice is not rectangular and the distance  $AB$  does not equal  $BC$ . However, the sum  $(AB + BC)$  is unchanged and is again equal to  $2d_{hkl} \sin \theta$ . The important point is that Bragg's law applies irrespective of the positions of the atoms in the planes; it is solely the spacing between the planes which needs to be considered. It follows as a corollary that the path difference between the waves scattered by the atoms in the same plane



**Fig. 8.4.** Bragg's law expressed in vector notation. Vectors  $(s - s_0)$  and  $\mathbf{d}_{hkl}^*$  are parallel and the ratio of the moduli is  $\lambda$ . Hence Bragg's law is expressed as  $(s - s_0)/\lambda = \mathbf{d}_{hkl}^*$ .

is zero—i.e. all the waves scattered from the same place interfere constructively. Finally, note that (unlike the Laue equations), Bragg's law is wholly represented in two dimensions: the incident and diffracted beams and the normal to the reflecting planes (Fig. 8.3) all lie in a plane—i.e. the plane of the paper.

Bragg's law may also be expressed in vector notation. Again, let  $s, s_0$  be unit vectors along the directions of the diffracted and incident beams, then (with reference to Fig. 8.4) the vector  $(s - s_0)$  is parallel to  $\mathbf{d}_{hkl}^*$ , the reciprocal lattice vector of the reflecting planes. Comparing the moduli of these vectors  $|s - s_0| = 2\sin \theta$  and  $|\mathbf{d}_{hkl}^*| = 1/d_{hkl}$ , it is seen from Bragg's law that their ratio is simply  $\lambda$ . Hence Bragg's law may be written:

$$\frac{(s - s_0)}{\lambda} = \mathbf{d}_{hkl}^* = h\mathbf{a}^* + k\mathbf{b}^* + l\mathbf{c}^*.$$

Hence constructive interference occurs, or Bragg's law is satisfied when the vector  $(s - s_0)/\lambda$  coincides with the reciprocal lattice vector  $\mathbf{d}_{hkl}^*$  of the reflecting planes.

The vector form of Bragg's law may be combined with each of the three Laue equations: i.e. for the first Laue equation:

$$\mathbf{a} \cdot (s - s_0) = n_x \lambda = \mathbf{a} \cdot \mathbf{d}_{hkl}^* \cdot \lambda = \mathbf{a} \cdot (h\mathbf{a}^* + k\mathbf{b}^* + l\mathbf{c}^*) \lambda.$$

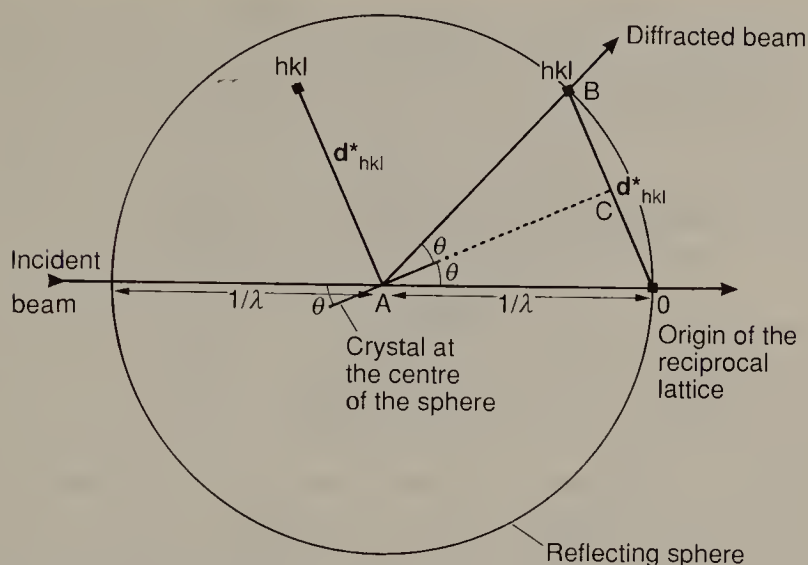
Hence  $n_x = h$  (since  $\mathbf{a} \cdot \mathbf{a}^* = 1$ ,  $\mathbf{a} \cdot \mathbf{b}^* = 0$ , etc), and similarly  $n_y = k$  and  $n_z = l$  for the other Laue equations. The integers  $n_x$ ,  $n_y$  and  $n_z$  of the Laue equations are simply the Laue indices  $h, k, l$  of the reflecting planes.

Bragg's law, like Newton's laws, and all such uncomplicated expressions in physics, is deceptively simple. Its applicability and relevance to problems in X-ray and electron diffraction only unfold themselves gradually (to teachers and students alike!). Newton was once asked how he made his great discoveries: he replied 'by always thinking unto them'. The student of crystallography could do no better with respect to Bragg's law!

## 8.4 Ewald's synthesis: the reflecting sphere construction

Ewald's synthesis is a geometrical formulation or expression of Bragg's law which involves the reciprocal lattice and a 'sphere of reflection'. It is best illustrated and understood by way of an example. Consider a crystal with the  $(hkl)$  reflecting planes (Laue indices) at the correct Bragg angle (Fig. 8.5). The

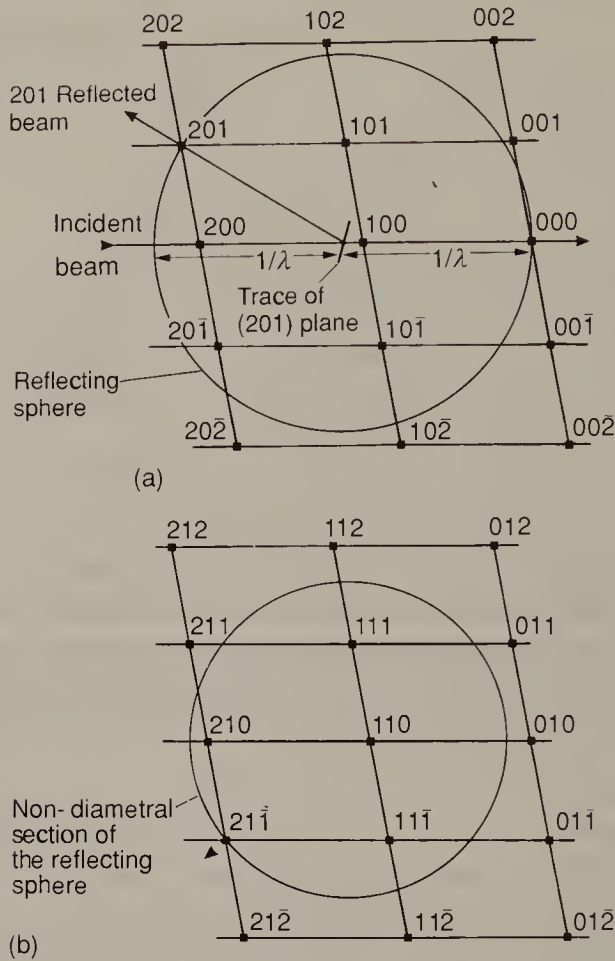




**Fig. 8.5.** The Ewald reflecting sphere construction for a set of planes at the correct Bragg angle. A sphere (the Ewald or reflecting sphere) is drawn, of radius  $1/\lambda$  with the crystal at the centre. The vector  $\mathbf{OB}$  is identical to  $\mathbf{d}_{hkl}^*$ . The origin of the reciprocal lattice is fixed at  $O$  and the reciprocal lattice point  $hkl$  intersects the sphere at the exit point of the diffracted beam.

reciprocal lattice vector  $\mathbf{d}_{hkl}^*$  is also shown. Now draw a sphere (the reflecting or Ewald sphere) of radius  $1/\lambda$  (where  $\lambda$  is the X-ray wavelength) with the crystal at the centre. Since Bragg's law is satisfied it may be shown that the vector  $\mathbf{OB}$  (from the point where the direct beam exits from the sphere to the point where the diffracted beam exits from the sphere) is identical to  $\mathbf{d}_{hkl}^*$ : i.e. from the triangle  $AOC$ ,  $|\mathbf{OC}| = (1/\lambda) \sin \theta = (1/2) |\mathbf{d}_{hkl}^*| = 1/2 d_{hkl}$ , i.e.  $\lambda = 2d_{hkl} \sin \theta$ . Hence, if the origin of the reciprocal lattice is shifted from the centre of the sphere ( $A$ ) to the point where the direct beam exits from the sphere ( $O$ ), then  $\mathbf{OB} = \mathbf{d}_{hkl}^*$  and Bragg's law is equivalent to the statement that the reciprocal lattice point for the reflecting planes ( $hkl$ ) should intersect the sphere; the diffracted beam direction being given by the vector  $\mathbf{AB}$ —i.e. the line from the centre of the sphere to the point where the reciprocal lattice point  $\mathbf{d}_{hkl}^*$  intersects the sphere. Conversely, if the reciprocal lattice point does *not* intersect the sphere then Bragg's law is not satisfied and no diffracted beams occur.

Figure 8.5 shows the construction of just one reflecting plane and one reciprocal lattice point. It is a simple matter to extend it to all the reciprocal lattice points in a crystal. Fig. 8.6(a) shows a section of the reciprocal lattice of a monoclinic crystal perpendicular to the  $\mathbf{b}^*$  reciprocal lattice vector (i.e. the  $y$ -axis—see Fig. 6.2(b)). All the reciprocal lattice points in this section have indices of the form  $h0l$ . An incident X-ray beam is directed along the  $\mathbf{a}^*$  reciprocal lattice vector (i.e. along a direction in the crystal perpendicular to the  $y$ - and  $z$ -axes—see Fig. 6.2(a)). The centre of the reflecting sphere is at a distance  $1/\lambda$  from the origin of the reciprocal lattice along the line of the incident beam: note again that the origin of the reciprocal lattice is *not* at the centre of the sphere but is at the point where the direct beam exits from the sphere.



**Fig. 8.6.** The Ewald reflecting sphere construction for a monoclinic crystal in which the incident X-ray beam is directed along the  $a^*$  reciprocal lattice vector. (a) Shows the  $h0l$  reciprocal lattice section (through the origin and perpendicular to the  $b^*$  reciprocal lattice vector or  $y$ -axis—see Fig. 6.2(c) and Fig. 6.3) and a diametral section of the reflecting sphere radius  $1/\lambda$ . The  $201$  reciprocal lattice point intersects the sphere and the direction of the  $201$  reflected beam is indicated. (b) Shows the  $h1l$  reciprocal lattice section (i.e. the layer 'above' the  $h0l$  section) and the smaller, non-diametral section of the reflecting sphere. The  $21\bar{1}$  reciprocal lattice point intersects the sphere, the direction of the  $21\bar{1}$  reflected beam is 'upwards' from the centre of the sphere (in the  $h0l$  section below) through the  $21\bar{1}$  reciprocal lattice point as indicated by the arrow-head.

In the section shown, Fig. 8.6(a), the reflecting sphere intersects the  $201$  reciprocal lattice point: hence the only plane for which Bragg's law is satisfied is the  $(201)$  plane and the direction of the  $201$  reflected beam is as indicated.

Figure 8.6(a) only shows one layer or section of the reciprocal lattice (through the origin) and a (diametral) section of the reflecting sphere. But the reciprocal lattice sections above and below the plane of the page need to be taken into account and also the smaller non-diametral sections of the reflecting sphere which intersects them. Fig. 8.6(b) shows the 'next layer above' or  $h1l$  section of the reciprocal lattice (see Fig. 6.3) and the smaller, non-diametral section of the reflecting sphere which it intersects. Notice that this section of the sphere does

not pass through 010 (the reciprocal lattice point immediately 'above' the origin 000). The sphere intersects the  $21\bar{1}$  reciprocal lattice point, hence the  $(21\bar{1})$  plane also satisfies Bragg's law and the direction of the  $21\bar{1}$  reflected beam is from the centre of the sphere (which is *not* the point in the centre of this smaller circle but the point in the centre of the sphere in the reciprocal lattice section below—Fig. 8.6(a)) and the  $21\bar{1}$  reciprocal lattice point. The reflected beam direction therefore cannot be drawn in Fig. 8.6(b) because it is directed upwards, out of the plane of the page.

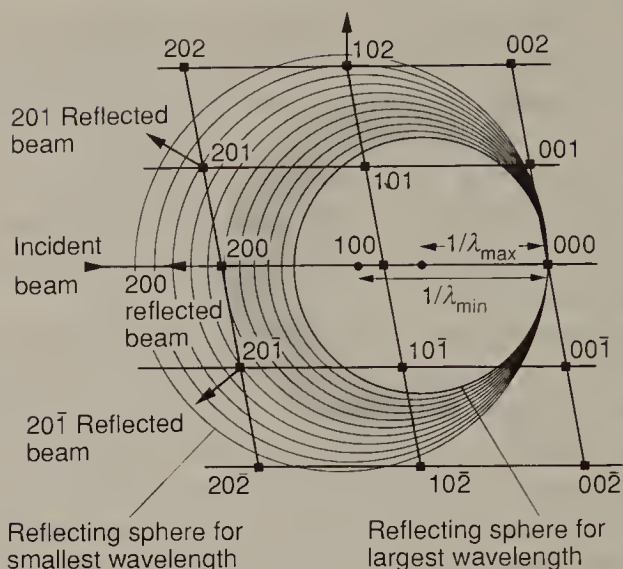
Clearly, the construction can be extended to other reciprocal lattice sections, i.e. through the  $h2l, h3l$ , etc. sections (above); the  $h\bar{1}l, h\bar{2}l, h\bar{3}l$ , etc. sections (below) and so on. The further the reciprocal lattice section is from the origin, the smaller is the section of the reflecting sphere which it intersects. In the example above, the sphere only intersects the  $h0l$  section (Fig. 8.6(a)), the  $h1l$  section (Fig. 8.6(b)) and the  $h\bar{1}l$  section (below), but no more. Hence only these sections, and the reciprocal lattice points within them, need to be considered.

In Fig. 8.6 the relative sizes of the reciprocal lattice and the sphere happen to be such that just one reciprocal lattice point in each section intersects the sphere. Clearly if the diameter of the sphere were made a little larger (i.e. the X-ray wavelength was made a little smaller) then no reciprocal lattice points would intersect the sphere and no planes in the crystal would be at the correct Bragg angle for reflection; if the diameter of the sphere were continuously made larger (or smaller) than that shown in Fig. 8.6 then other planes would reflect as their reciprocal lattice points successively intersected the sphere. This is the basis of Laue's original X-ray experiment; 'white' X-radiation was used which contains a range of wavelengths, which correspond to a range or 'nest' of spheres of different diameters. Any plane whose reciprocal lattice point falls within this range will therefore satisfy Bragg's law for one particular wavelength.

The situation is illustrated in Fig. 8.7, again for the  $h0l$  reciprocal lattice section of the monoclinic crystal shown in Fig. 8.6(a). The shaded region indicates a 'nest' of spheres with diameters in the wavelength range from largest wavelength (smallest sphere diameter) to smallest wavelength (largest sphere diameter). All the planes whose reciprocal lattice points lie within this region satisfy Bragg's law for the particular sphere on which they lie.

The Laue technique is unique in that it utilizes white X-radiation. All the others utilize monochromatic or near-monochromatic ( $K_\alpha$ ) X-radiation. In order to obtain diffraction, therefore, the crystal and the sphere (of a fixed diameter) must be moved relative to one another; whenever a reciprocal lattice point touches the sphere then 'out shoots' a diffracted (or reflected) beam from the centre of the sphere in a direction through the reciprocal lattice point. As described in Chapter 9 there are several ways in which these relative movements may be achieved in practice and several ways in which the diffracted beams may be recorded. The crystal may be oscillated (oscillation method), precessed (precession method), the film may be arranged cylindrically round the crystal or flat, it may be stationary or it may be moved in some way as in the Weissenberg method (in which the cylindrical film movement is linked to the oscillation of the crystal) or, as in the precession method, precessed with the crystal. The





**Fig. 8.7.** The Ewald reflecting sphere construction for the  $h0l$  reciprocal lattice section of the monoclinic crystal shown in Fig. 8.6(a) for the 'white' X-radiation, i.e. for a range of wavelengths from the smallest (largest sphere) to the largest (smallest sphere) giving rise to a 'nest' of spheres (shaded region) all passing through the origin. The 102, 201, 200 and  $20\bar{1}$  reciprocal lattice points lying within this region satisfy Bragg's law, each for the particular wavelength or sphere which they intersect. The directions of the reflected beams from these planes are indicated by the arrows.

geometry of these X-ray diffraction methods may *appear* to be complicated, but the basis of them all—the Ewald reflecting sphere construction—is the same.

## Exercises

- 8.1 Compare Figs 7.5 and 8.3; both show conditions for constructive interference, one for light at a diffraction grating with line spacing  $a$  (Fig. 7.5) and one for X-rays reflected from planes of spacing  $d_{hkl}$ . Show that the equations describing the conditions for constructive interference in each case ( $n\lambda = a \sin \alpha_n$  and  $n\lambda = 2d_{hkl} \sin \theta$ ) are equivalent.
- 8.2 Iron (bcc,  $a = 0.2866$  nm ( $2.866$  Å)) is irradiated with CrK $\alpha$  X-radiation ( $\lambda = 0.2291$  nm ( $2.291$  Å)). Find the indices  $\{hkl\}$  and  $d$ -spacings of the planes which give rise to X-ray reflections.  
(Note: In body-centred lattices, reflection from planes for which  $(h + k + l)$  does not equal an even integer are forbidden (see Appendix 6).)  
(Hint: Prepare a table listing the indices and  $d$ -spacings of the allowed reflecting planes in order of decreasing  $d$ -spacings and determine the  $\theta$  angles for reflection using Bragg's law.)
- 8.3 It is stated without proof with respect to Bragg's law that when the atoms are not symmetrically disposed to the incident and reflected beams (Fig. 8.3(b)), the path difference  $(AB + BC) = 2d_{hkl} \sin \theta$ . Prove, using very simple geometry, that this is indeed the case.



---

# The diffraction of X-rays and electrons

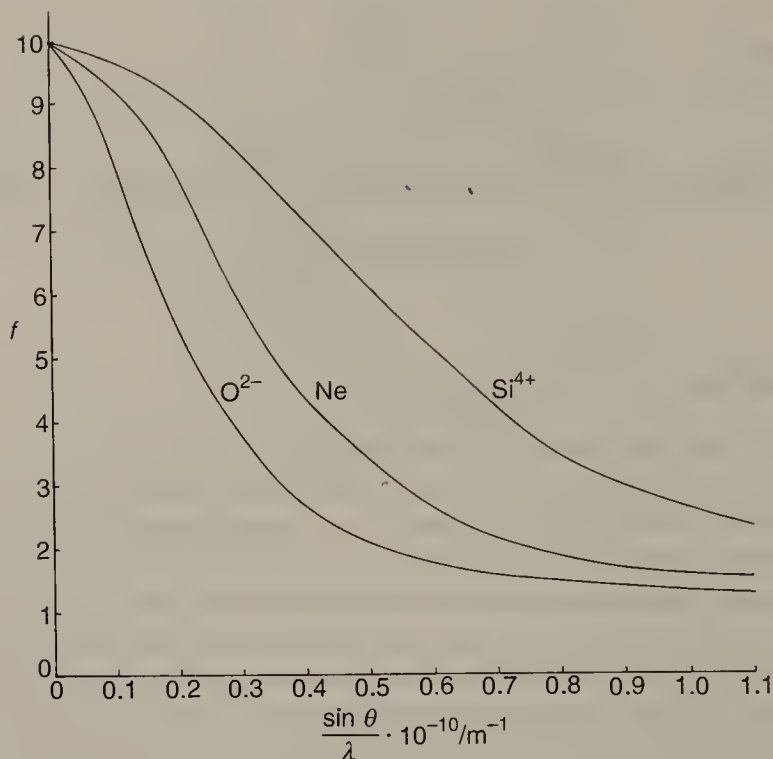
## 9.1 Introduction

In Chapter 8, the Laue equations and Bragg's law were derived on the basis that single atoms, of unspecified scattering power, were situated at each lattice point. Now we need to consider the physics of the scattering process. Since it is almost exclusively the electrons in atoms which contribute to the scattering of X-rays we have to sum the contributions to the scattered amplitude of all the electrons in all the atoms in the crystal, a problem which may be approached step-by-step. First the scattering amplitude of a single electron and the variation in scattering amplitude with angle is determined. Then the scattering amplitude of an atom is determined by summing the contributions from all  $Z$  electrons (where  $Z$  = the atomic number of the atom)—the summation taking into account the path or phase differences between all the  $Z$  scattered waves. The result of this analysis is expressed by a simple number,  $f$ , the **atomic scattering factor**, which is the ratio of the scattering amplitude of the atom divided by that of a single (classical) electron, i.e.

$$\text{atomic scattering factor } f = \frac{\text{amplitude scattered by atom}}{\text{amplitude scattered by a single electron}}.$$

At zero scattering angle, all the scattered waves are in phase and the scattered amplitude is the simple sum of the contribution from all  $Z$  electrons, i.e.  $f = Z$ . As the scattering angle increases,  $f$  falls below  $Z$  because of the increasingly destructive interference effects between the  $Z$  scattered waves. Atomic scattering factors  $f$  are plotted as a function of angle (usually expressed as  $\sin \theta / \lambda$ ). Figure 9.1 shows such a plot for the oxygen anion  $\text{O}^{2-}$ , the neon atom  $\text{Ne}$ , and the silicon cation  $\text{Si}^{4+}$ —all of which contain 10 electrons. When  $\sin \theta / \lambda = 0$ ,  $f = 10$  but with increasing angle  $f$  falls below 10. The extent to which it does depends upon the relative sizes of the atoms or ions; the silicon cation is small, hence the phase differences are small and the destructive interference between the scattered waves is least—and conversely for the large oxygen anion.

The scattering amplitude of a unit cell is determined by summing the scattering amplitudes,  $f$ , from all the atoms in the unit cell (equivalent, in the case of a primitive unit cell), to all the atoms in the motif. Again, the summation must take into account the path or phase differences between all the scattered



**Fig. 9.1.** The variation in atomic scattering factor  $f$  with scattering angle (expressed as  $\sin \theta / \lambda$ ) for atoms and ions with ten electrons. Note that the decrease in  $f$  is greatest for the (large)  $\text{O}^{2-}$  anion and least for the (small)  $\text{Si}^{4+}$  cation.

waves and is again expressed by a dimensionless number,  $F_{hkl}$ , the **structure factor**, i.e.

$$\text{structure factor } F_{hkl} = \frac{\text{amplitude scattered by the atoms in the unit cell}}{\text{amplitude scattered by a single electron}}$$

$F_{hkl}$  must not only express the amplitude of scattering from a reflecting plane with Laue indices  $hkl$  but must also express the phase angle of the scattered wave.  $F_{hkl}$  is therefore not a simple number, like  $f$ , but is represented as a vector or mathematically as a complex number (see Appendix 5).

Crystal structure determination is a two-part process: (a) the determination of the size and shape of the unit cell (i.e. the lattice parameters) from the geometry of the diffraction pattern and (b) the determination of the lattice type and distribution of the atoms in the structure from the (relative) intensities of the diffraction spots. Part (a) is in principle a straightforward process; part (b) is not, because films and counters record intensities which are proportional to the *squares* of the amplitudes. The square of a complex number,  $F_{hkl}$ , is always real (i.e. a simple number) and hence the information about the phase angles of the diffracted beams is lost. A major problem in crystal structure determination is, in effect, the recovery of this phase information and requires for its solution as much insight and intuition as mathematical and crystallographic knowledge. A

graphic account of the problems involved in the epoch-making determination of the structure of DNA is given by one of those most closely involved, James D. Watson, in his book *The Double Helix* (see Further Reading).

The distinction between the direction-problem and intensity-problem of diffracted beams from crystals has its corollary in the diffraction of light from diffraction gratings, which may be expressed as follows. A (primitive) crystal with one atom per lattice point (Fig. 9.2(a)) may be regarded as being analogous to a 'narrow slit' diffraction grating in which each slit can be regarded as the source of a single Huygens' wavelet which propagates uniformly in all directions (Fig. 7.5). Only the interference effects of light emanating from different slits (equivalent to single atoms at lattice points) need to be taken into account and these determine the directions of the diffracted beams (Section 7.4). The intensities of the diffracted beams are proportional to the squares of the scattered amplitudes of the Huygens' wavelets (for light) or the squares of the atomic scattering factors of the single atoms (for X-rays).

A (primitive) crystal with a motif consisting of more than one atom (Fig. 9.2(b)) may be regarded as being analogous to a 'wide slit' diffraction grating in which the interference effects from all the atoms in the motif may be regarded as being analogous to the interference effects between all the Huygens' wavelets distributed *across* each slit. Of course, the problem is rather more complicated because the atoms in the motif do not all lie in a plane or surface as do the Huygens' wavelets, but the principle—of summing the contributions with respect to phase differences—is the same.

As shown in Section 7.4 and Fig. 7.7, the diffraction pattern from a wide-slit diffraction grating may be expressed as that from a narrow-slit grating in which the intensities of the diffracted beams are modulated by the intensity distribution predicted to occur from a single wide slit. Similarly, in the case of X-ray diffraction from crystals it is the structure factor,  $F_{hkl}$ , which expresses the interference effects from all the atoms in the unit cell and which modulates, in effect, the intensities of the diffracted beams.

The final step is to sum the contributions from all the unit cells in the crystal. This is a difficult problem because we have to take into account the fact that the incident X-ray beam is attenuated as it is successively scattered by the atoms in the crystal—such that atoms 'deeper down' in the crystal encounter smaller amounts of incident radiation. Furthermore, the reflected beams also propagate through the crystal at the Bragg angle  $\theta$  (see Fig. 9.2(c)) and are hence 're-reflected' in a direction parallel to that of the incident beam. These re-reflected beams then interfere destructively\* with the incident or direct beam, attenuating it still further. This is covered in a comprehensive analysis, known as the dynamical theory of X-ray diffraction because it takes into account the dynamical interactions between the direct, reflected and re-reflected, etc., beams. It is much simpler to consider the case in which the size of the crystal is

\* When considering the interference between the direct and re-reflected beams, the  $180^\circ$  or  $\pi$  phase difference of the re-reflected beams needs to be taken into account. This complication does not arise when we are considering interference between the reflected or diffracted beams alone.



sufficiently small such that the attenuation of the direct beam is negligible and the intensities of the diffracted beams are small in comparison with the direct beam\*. This case is fairly readily achieved in X-ray diffraction and enables the observed relative intensities of the diffracted spots to be assumed to be equal to the relative intensities of the squares of the  $F_{hkl}$  values†. In electron diffraction, however, dynamical effects are always important and the above assumption cannot be made, but they are an important source of specimen contrast in the electron microscope.

Finally, we have to consider the connection between the diffraction pattern and the type of unit cell (whether it is centred or not) and the symmetry elements present. It turns out that the presence of the centring lattice points and translational symmetry elements (glide planes and screw axes—see Section 4.5) results in ‘zero intensity’ or *systematically absent* reflections from certain planes with Laue indices  $hkl$ . This topic, and that of *double diffraction*, which is of particular importance in the case of electron diffraction, are discussed in Appendix 6.

## 9.2 The intensities of X-ray diffracted beams: the structure factor equation and its applications

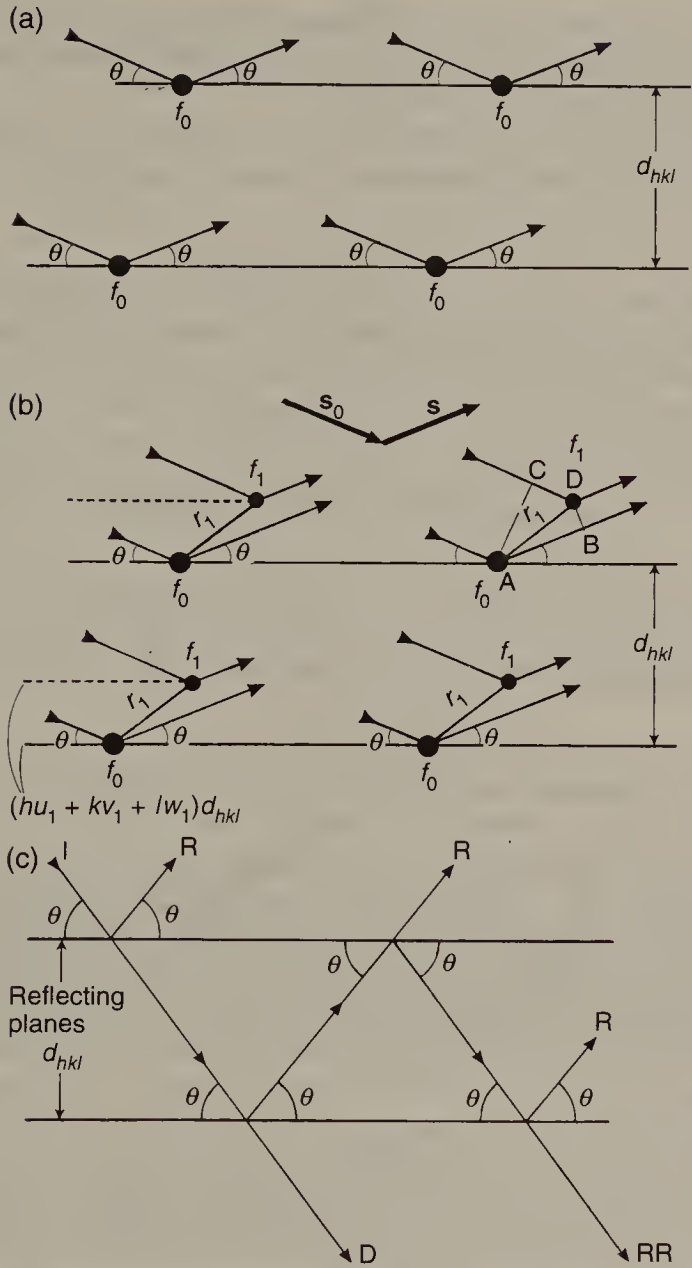
We shall begin by considering the simplest case of a primitive crystal with just one atom at each lattice point. Figure 9.2(a) shows part of such a crystal with atoms with atomic scattering factor  $f_0$  at each lattice point (the subscript 0 indicating that each atom is at an origin). Consider an X-ray beam incident at the correct Bragg angle  $\theta$  in a particular set of lattice planes ( $hkl$ ) as indicated. For all the atoms lying in one plane the path differences between the reflected beams are zero, and for the atoms lying in successive planes spaced  $d_{hkl}$ ,  $2d_{hkl}$  etc. apart the path differences are  $\lambda$ ,  $2\lambda$  etc. (Fig. 8.3). In all cases constructive interference occurs and the total scattered amplitude (relative to that of a single electron—see Section 9.1) is simply the sum of the atomic scattering factors. Hence, since we have a primitive crystal with one lattice point and therefore one atom per unit cell, the scattered amplitude from one cell,  $F_{hkl}$ , is simply equal to the atomic scattering factor,  $f_0$ .

Now consider a crystal with a motif consisting of two atoms, one at the origin with atomic scattering factor  $f_0$  as before and another with atomic scattering factor  $f_1$  at a distance from the origin defined by vector  $\mathbf{r}_1$  (Fig. 9.2(b));  $\mathbf{r}_1$  is called a **position vector** because it specifies the position of an atom within the unit cell. It may be expressed in terms of its components or fractional coordinates along the unit cell vectors  $\mathbf{a}$ ,  $\mathbf{b}$ ,  $\mathbf{c}$  in the same way as for a lattice vector

\*The crystal size in this context is better expressed by the notion of coherence length—the dimensions over which the scattering amplitudes from the unit cells can be summed. Crystal imperfections—dislocations, stacking faults, subgrain boundaries—within imperfect single crystals effectively limit or determine the coherence length as well as grain boundaries in perfect crystals.

†A number of physical and geometrical factors also need to be taken into account—temperature factor, Lorentz-polarization factor, multiplicity factor, absorption factor, etc. These are described in standard textbooks such as *Elements of X-ray Diffraction* by B. D. Cullity, Addison-Wesley, 1978.





**Fig. 9.2.** (a) Part of a crystal lattice with atoms with atomic scattering factor  $f_0$ , situated at each lattice point, and a particular set of  $(hkl)$  planes through the lattice points. Incident/reflected beams at the Bragg angle  $\theta$  to these planes are indicated by the arrows. (b) As for (a), but with another atom with atomic scattering factor  $f_1$  defined by position vector  $\mathbf{r}_1$ . The path difference (shown for simplicity for one motif) is given by  $(AB - CD)$ .  $\mathbf{s}$  and  $\mathbf{s}_0$  are unit vectors along the reflected and incident beam directions and the component of  $\mathbf{r}_1$  perpendicular to the  $(hkl)$  planes is also indicated. (c) The process of reflection and re-reflection for a single incident beam  $I$ ; as it passes through the crystal at the Bragg angle  $\theta$  it is (partially) reflected by each successive plane. The reflected beams  $R$  are then re-reflected from the 'undersides' of the planes giving rise to beams  $RR$  which interfere *destructively* with the direct beam  $D$ . Clearly, the process is repeated for all the beams throughout the crystal.

$\mathbf{r}_{uvw}$ , i.e.  $\mathbf{r}_1 = u_1\mathbf{a} + v_1\mathbf{b} + w_1\mathbf{c}$ ; the important difference being that the components  $u_1, v_1, w_1$  are *fractions* of the cell edge lengths, whereas the components  $uvw$  of a lattice vector  $\mathbf{r}_{uvw}$  are *integers*.

The path difference (P.D.) between the waves scattered by these two atoms is  $AB - CD$  (Fig. 9.2(b)), which, expressed in vector notation, is:

$$\text{P.D.} = AB - CD = \mathbf{r}_1 \cdot \mathbf{s} - \mathbf{r}_1 \cdot \mathbf{s}_0 = \mathbf{r}_1 \cdot (\mathbf{s} - \mathbf{s}_0)$$

where  $\mathbf{s}, \mathbf{s}_0$  are unit vectors along the direction of the reflected and incident beams, respectively. Two substitutions can be made in this equation. First,  $\mathbf{r}_1$  may be expressed in terms of its components and second (since Bragg's law is satisfied) the vector  $(\mathbf{s} - \mathbf{s}_0)$  may be expressed in terms of  $\lambda$  and  $\mathbf{d}_{hkl}$  (see Section 8.3), i.e.

$$(\mathbf{s} - \mathbf{s}_0) = \lambda \mathbf{d}_{hkl}^* = \lambda(h\mathbf{a}^* + k\mathbf{b}^* + l\mathbf{c}^*).$$

Hence

$$\text{P.D.} = \lambda(u_1\mathbf{a} + v_1\mathbf{b} + w_1\mathbf{c}) \cdot (h\mathbf{a}^* + k\mathbf{b}^* + l\mathbf{c}^*)$$

multiplying out, and remembering the identities  $\mathbf{a} \cdot \mathbf{a}^* = 1$  etc.,  $\mathbf{a} \cdot \mathbf{b}^* = 0$  etc.:

$$\text{P.D.} = \lambda(hu_1 + kv_1 + lw_1).$$

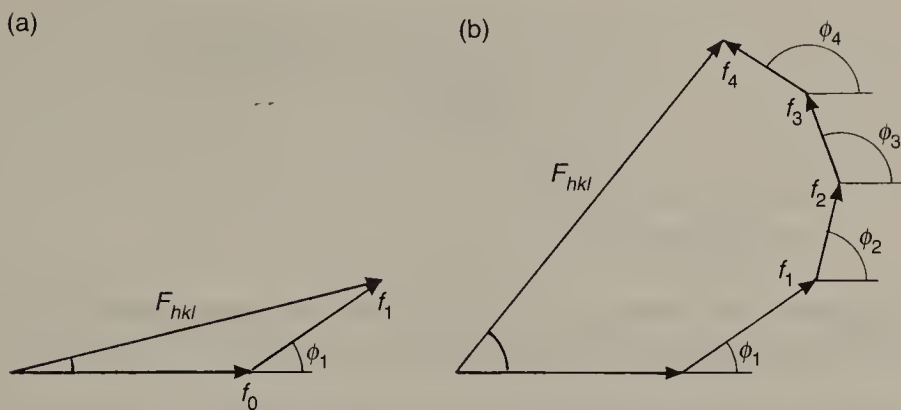
This equation is another manifestation of the Weiss zone law (Section 6.5.3); in this case the *number* within the brackets  $(hu_1 + kv_1 + lw_1)$  represents the component of  $\mathbf{r}_1$  perpendicular to the lattice planes as a fraction of the interplanar spacing,  $d_{hkl}$  (Fig. 9.2(b)). It is clearly the important number with respect to constructive/destructive interference conditions; when for example  $(hu_1 + kv_1 + lw_1) = 0$  (the two atoms lying within the  $(hkl)$  planes), complete constructive interference occurs and when  $(hu_1 + kv_1 + lw_1) = 0.5$  (the second atom lying halfway between the  $(hkl)$  planes), destructive interference occurs, which is complete when the atomic scattering factors of the two atoms in the motif are equal.

In general, in adding the contributions of the two atoms, we need to use a vector-phase diagram in which the lengths or moduli of the vectors are proportional to the atomic scattering factors of the atoms, and the phase angle between them,  $\phi_1$ , is equal to  $2\pi/\lambda(\text{P.D.})$ , i.e. in the above case

$$\phi_1 = 2\pi(hu_1 + kv_1 + lw_1).$$

This is shown in Fig. 9.3(a). The resultant is the structure factor,  $F_{hkl}$ .

The analysis may be simply extended to any number of atoms in the motif with position vectors  $\mathbf{r}_1, \mathbf{r}_2, \mathbf{r}_3$  etc. and phase angles (referred to the origin)  $\phi_1, \phi_2, \phi_3$  etc. The resultant,  $F_{hkl}$ , is found by adding all the vectors, representing the atomic scattering factors of all the atoms, as shown in Fig. 9.3(b). Note that the phase angles,  $\phi$ , are all measured with respect to the origin (horizontal line in Fig. 9.3); they are *not* the angles *between* the vectors. Note also that, although for simplicity we began with an atom at the origin, there need not be one there.



**Fig. 9.3.** Vector-phase diagrams for obtaining  $F_{hkl}$ . The atomic scattering factors  $f_1, f_2, \dots$  are represented as vectors with phase angles  $\phi_1, \phi_2, \dots$  with respect to a wave scattered from the origin: (a) result for two atoms and (b) result for several atoms.

Adding vectors graphically in this way is obviously not very convenient; in practice vector-phase diagrams, such as Fig. 9.3, are substituted by Argand diagrams in which  $F_{hkl}$  is represented as a complex number (see Appendix 5), i.e.

$$F_{hkl} = \sum_{n=0}^{n=N} f_n \exp 2\pi i(hu_n + kv_n + lw_n)$$

where  $f_n$  is the atomic scattering factor and  $2\pi(hu_n + kv_n + lw_n)$  is the phase angle  $\phi_n$  of the  $n$ th atom in the motif with fractional coordinates  $(u_n, v_n, w_n)$ .

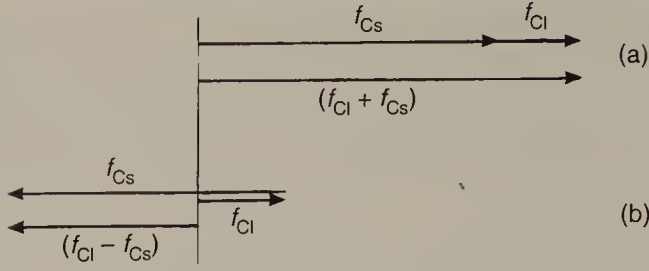
Many students are deterred at first sight of equations such as this. It is important to realize that it *merely* represents an analytical way of adding vectors 'top to tail', the convenience and ease of which is soon appreciated by way of a few examples.

**Example 1:** CsCl structure (Fig. 1.12). The  $(u_n, v_n, w_n)$  values are (000) for Cl, atomic scattering factor  $f_{\text{Cl}}$  and  $(\frac{1}{2}, \frac{1}{2}, \frac{1}{2})$  for Cs, atomic scattering factor  $f_{\text{Cs}}$ . Substituting these two terms in the equation:

$$\begin{aligned} F_{hkl} &= f_{\text{Cl}} \exp 2\pi i(h0 + k0 + l0) + f_{\text{Cs}} \exp 2\pi i(h\frac{1}{2} + k\frac{1}{2} + l\frac{1}{2}) \\ &= f_{\text{Cl}} + f_{\text{Cs}} \exp \pi i(h + k + l). \end{aligned}$$

Two situations may be identified: when  $(h + k + l) = \text{even integer}$ ,  $\exp \pi i(\text{even integer}) = 1$ , hence  $F_{hkl} = f_{\text{Cl}} + f_{\text{Cs}}$  and when  $(h + k + l) = \text{odd integer}$ ,  $\exp \pi i(\text{odd integer}) = -1$ , hence  $F_{hkl} = f_{\text{Cl}} - f_{\text{Cs}}$ . These two situations may be simply represented on the Argand diagram as shown in Fig. 9.4. Note that in both cases  $F_{hkl}$  is a real number; the imaginary component is zero. This arises because CsCl has a centre of symmetry at the origin, as explained below.

**Example 2:** hcp metal structure. We have a choice of unit cells (Fig. 5.8); it is best to refer to the primitive hexagonal cell, Fig. 5.8(a), which contains two



**Fig. 9.4.** Argand diagrams for  $F_{hkl}$  for CsCl (a)  $(h + k + l) = \text{even integer}$ ,  $F_{hkl} = f_{Cl} + f_{Cs}$ ; (b)  $(h + k + l) = \text{odd integer}$ ,  $F_{hkl} = f_{Cl} - f_{Cs}$ .

identical atoms, atomic scattering factor  $f$ , with fractional coordinates (000) (the A layer atoms) and  $(\frac{1}{3} \frac{2}{3} \frac{1}{2})$  (the B layer atoms). Substituting these two terms in the equation:

$$F_{hkl} = f \exp 2\pi i(h0 + k0 + l0) + f \exp 2\pi i(h\frac{1}{3} + k\frac{2}{3} + l\frac{1}{2})$$

$$= f(1 + \exp 2\pi i(h\frac{1}{3} + k\frac{2}{3} + l\frac{1}{2})).$$

Now let us apply this to some particular  $(hkl)$  planes, e.g. (002)  $\equiv$  (0002); (100)  $\equiv$  (10 $\bar{1}$ 0) and (101)  $\equiv$  (10 $\bar{1}$ 1).

$$F_{002} = f(1 + \exp 2\pi i) = 2f$$

$$F_{100} = f(1 + \exp \frac{2}{3}\pi i) = f(1 + \cos \frac{2}{3}\pi + i \sin \frac{2}{3}\pi) = f(0.5 + i0.866)$$

$$F_{101} = f(1 + \exp 2\pi i(\frac{1}{3} + \frac{1}{2})) = f(1 + \cos \frac{5}{3}\pi + i \sin \frac{5}{3}\pi) = f(1.5 - i0.866).$$

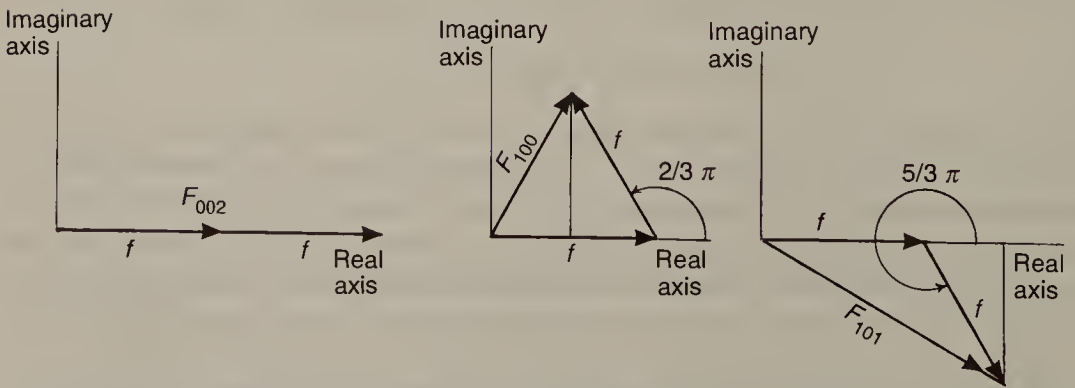
These results are shown graphically in Fig. 9.5. Note that  $F_{100}$  and  $F_{101}$  are complex numbers.

The intensities  $I_{hkl}$  of X-ray beams are proportional to their amplitudes squared, or  $F_{hkl}$  multiplied by its complex conjugate  $F_{hkl}^*$  (see Appendix 5). For the hcp metal examples above:

$$I_{002} = 2f \cdot 2f = 4f^2$$

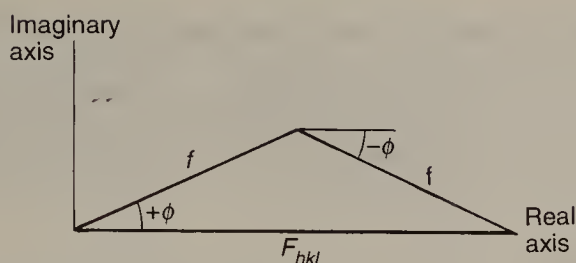
$$I_{100} = f(0.5 + i0.866)f(0.5 - i0.866) = f^2$$

$$I_{101} = f(1.5 - i0.866)f(1.5 + i0.866) = 3f^2.$$



**Fig. 9.5.** Argand diagrams for an hcp metal for (left to right)  $F_{002}$ ,  $F_{100}$  and  $F_{101}$  showing also how these structure factors are obtained graphically by vector addition.





**Fig. 9.6.** The Argand diagram for a centrosymmetric crystal. The phase angle  $+\phi$  for the atom at  $(uvw)$  is equal and opposite to the phase angle  $-\phi$  for the atom at  $(\bar{u}\bar{v}\bar{w})$ , hence  $F_{hkl}$  is real.

Again, it should be stressed that  $I_{hkl}$  is a real number, the phase information expressed in  $F_{hkl}$  is lost.

**Example 3:** A crystal with a centre of symmetry at the origin. This is an important case because the structure factor for all reflections is real. For every atom with fractional coordinates  $(uvw)$  and phase angle  $+\phi$  there will be an identical one on the *opposite* side of the origin with fractional coordinates  $(\bar{u}\bar{v}\bar{w})$  and phase angle  $-\phi$ . For these two atoms:

$$\begin{aligned} F_{hkl} &= f \exp 2\pi i(hu + kv + lw) + f \exp 2\pi i(h\bar{u} + k\bar{v} + l\bar{w}) \\ &= f \exp 2\pi i(hu + kv + lw) + f \exp -2\pi i(hu + kv + lw). \end{aligned}$$

The second term is the complex conjugate of the first, hence the sine terms cancel and

$$F_{hkl} = 2f \cos 2\pi(hu + kv + lw)$$

as shown graphically in Fig. 9.6.

**Example 4:** It follows from example 3 that the diffraction pattern from a centrosymmetric crystal is also centrosymmetric. However, even if a crystal does not possess a centre of symmetry, the diffraction pattern will be centrosymmetric. This is known as Friedel's law\*. We have to show that the intensity of the reflection  $I_{hkl}$  from the  $hkl$  planes is equal to the intensity of the reflection on the opposite side of the direct beam from the  $\bar{h}\bar{k}\bar{l}$  planes, i.e.  $I_{\bar{h}\bar{k}\bar{l}}$ . Now, applying the structure factor equation to the simplest case of a crystal with one atom at  $(uvw)$ :

$$\begin{aligned} I_{hkl} &= F_{hkl} \cdot F_{hkl}^* = f \exp 2\pi i(hu + kv + lw) f \exp -2\pi i(hu + kv + lw) \\ &= f \exp 2\pi i(hu + kv + lw) f \exp 2\pi i(\bar{h}\bar{u} + \bar{k}\bar{v} + \bar{l}\bar{w}) \end{aligned}$$

$$\begin{aligned} I_{\bar{h}\bar{k}\bar{l}} &= F_{\bar{h}\bar{k}\bar{l}} \cdot F_{\bar{h}\bar{k}\bar{l}}^* = f \exp 2\pi i(\bar{h}\bar{u} + \bar{k}\bar{v} + \bar{l}\bar{w}) f \exp -2\pi i(\bar{h}\bar{u} + \bar{k}\bar{v} + \bar{l}\bar{w}) \\ &= f \exp 2\pi i(\bar{h}\bar{u} + \bar{k}\bar{v} + \bar{l}\bar{w}) f \exp 2\pi i(hu + kv + lw). \end{aligned}$$

From which it is seen that  $F_{hkl} = F_{\bar{h}\bar{k}\bar{l}}^*$  and  $F_{\bar{h}\bar{k}\bar{l}} = F_{hkl}^*$ , hence  $I_{hkl} = I_{\bar{h}\bar{k}\bar{l}}$ .

\* Friedel's law breaks down under conditions of anomalous scattering, a discussion of which can be found in, for example, *Essentials of Crystallography* by D. McKie and C. McKie, Blackwell Scientific Publications, 1986.

Table 9.1 The eleven Laue point groups or crystal classes

Crystal system	Laue point group and centrosymmetric point group	Non-centrosymmetric point groups belonging to the Laue point group		
Cubic	$m\bar{3}m$	432	$\bar{4}3m$	
(two Laue point groups)	$m\bar{3}$	23		
Tetragonal	$4/mmm$	422	$4mm$	$\bar{4}2m$
(two Laue point groups)	$4/m$	4	$\bar{4}$	
Orthorhombic	$mmm$	222	$mm2$	
Trigonal	$3m$	32	$3m$	
(two Laue point groups)	3	3		
Hexagonal	$6/mmm$	622	$6mm$	$\bar{6}m2$
(two Laue point groups)	$6/m$	6	$\bar{6}$	
Monoclinic	$2/m$	2	$m$	
Triclinic	$\bar{1}$	1		

The presence of a centre of symmetry in the diffraction pattern means that non-centrosymmetric point groups cannot be distinguished from those with a centre of symmetry\*. There are eleven centrosymmetric point groups (Table 3.1, page 57) and hence eleven symmetries which diffraction patterns can possess. These are called the eleven Laue groups and are identified by the corresponding point group symbol of the centrosymmetric point group. They are listed in Table 9.1.

To summarize, these four simple examples show how the amplitude,  $F_{hkl}$ , and hence the intensity,  $I_{hkl}$ , of the reflected X-ray beam from a set of  $hkl$  planes can be calculated from the simple ‘Structure Factor’ equation on p. 141; all we need to know are the positions of the atoms in the unit cell (the  $u_n v_n w_n$  values) and their atomic scattering factors,  $f_n$ . The great importance of the equation is that it can be applied, as it were, ‘the other way round’: by measuring the intensities of the reflections from several sets of planes (the more the better), the positions of the atoms in the unit cell can be determined. This is the basis of crystal structure determination, which has developed and expanded since the pioneering work of the Braggs, so that, at the time of writing, some 50 000 different crystal structures are known. Many of these are very complex, for example protein crystals in which the motif may consist of several thousand atoms. Again, it should be emphasized that the procedures are invariably not straightforward because the phase information in going from the  $F_{hkl}$  to the (measured)  $I_{hkl}$  values is lost, e.g. as in Example 2. The equation is also expressed as it were in a ‘converse’ form (or transform of that on p. 141) in

\* It is, however, in situations when anomalous scattering is present, possible to distinguish non-centrosymmetric and centrosymmetric point groups by means of a statistical analysis of the X-ray intensities.

which atomic positions (expressed as electron X-ray scattering) density) are expressed in terms of the  $F_{hkl}$  values of the reflections. The books on X-ray diffraction and X-ray crystallography in Further Reading give further information and insight into this large and fascinating topic. In this book just the basic principles have been set out so that their nature and applications can begin to be appreciated.

### 9.3 The broadening of diffracted beams: reciprocal lattice points and nodes

In Section 7.4 we found that when the number  $N$  of lines in a grating, or the number of apertures in a net, were limited, the principal diffraction maxima were broadened and surrounded by much fainter subsidiary maxima. These phenomena are shown in Fig. 7.3(d) and diagrammatically in Fig. 7.9. Precisely the same considerations apply to X-ray and electron diffraction from 'real' crystals in which the number of reflecting planes is limited: and the broadening and occurrence of the subsidiary maxima can be derived by similar arguments. This, in turn, leads us to modify our concept of reciprocal lattice *points*, which are not geometrical points, but which have finite size and shape, reciprocally related, as we shall see, to the size and shape of the crystal. There is, as far as I know, no common term to express the fact that reciprocal lattice points do have a finite size and shape, except in special cases such as the reciprocal lattice streaks or '**rel-rods**' which occur in the case of thin plate-like crystals. Reciprocal lattice **nodes** seems to be the closest approximation to a common term.

The broadening of the reflected beams from a crystal of finite extent is derived as follows. Consider a crystal of thickness or dimension  $t$  perpendicular to the reflecting planes,  $d_{hkl}$ , of interest. If there are  $m$  planes then  $md_{hkl} = t$ . Consider an incident beam bathing the whole crystal and incident at the exact Bragg angle for first order reflection (Fig. 9.7(a)). For the first two planes labelled 0 and 1, the path difference  $\lambda = 2d_{hkl} \sin \theta$ ; for planes 0 and 2 the path difference is  $2\lambda = 4d_{hkl} \sin \theta$  and so on—constructive interference between all the planes occurs right through the crystal. Now consider the interference conditions for an incident and reflected beam deviated a small angle  $\delta\theta$  from the exact Bragg angle (Fig. 9.7(b)). For planes 0 and 1 the path difference will be very close to  $\lambda$  as before and there will be constructive interference. However, for planes 0 and 2, 0 and 3 etc. the 'extra' path difference will deviate increasingly from  $2\lambda$ ,  $3\lambda$  etc.—and when it is an additional half-wavelength *destructive* interference between the pair of planes will result.

The condition for destructive interference for the whole crystal is obtained by notionally 'pairing' reflections in the same way as we did for the diffraction grating (Section 7.4). Consider the constructive and destructive interference condition between planes 0 and  $(m/2)$  (half way down through the crystal). At the exact Bragg angle  $\theta$  (Fig. 9.7(a)), the condition for constructive interference is  $(m/2)\lambda = (m/2)2d_{hkl} \sin \theta$ . The condition for *destructive* interference at angle  $(\theta + \delta\theta)$  is given by  $(m/2)\lambda + \lambda/2 = (m/2)2d_{hkl} \sin(\theta + \delta\theta)$ . Now this is also the condition for destructive interference between the next pair of planes 1

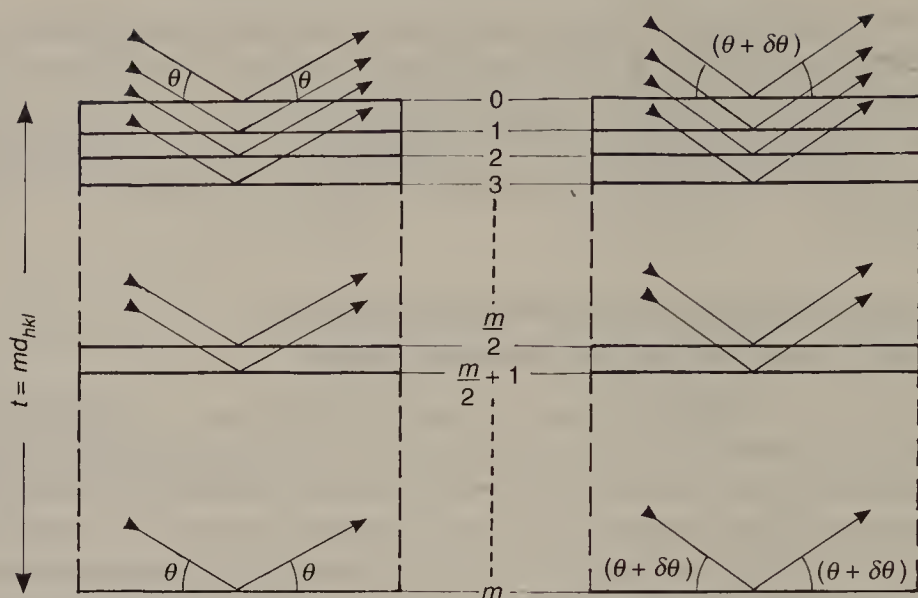


Fig. 9.7. Bragg reflection from a crystal of thickness  $t$  (measured perpendicular to the particular set of reflecting planes shown). The whole crystal is bathed in an X-ray beam (a) at the exact Bragg angle  $\theta$  and (b) at a small deviation from the exact Bragg angle, i.e. angle  $(\theta + \delta\theta)$ . The arrows represent the incident and reflected beams from successive planes  $0, 1, 2, 3 \dots (m/2)$  (half-way down) and  $\dots m$  (the lowest plane).

and  $(m/2) + 1$ —and so on through the crystal. This equation gives us, in short, the condition for destructive interference for the *whole* crystal and the angular range  $\delta\theta$  (each side of the exact Bragg angle) of the reflected beam.

Expanding the sine term and making the approximations  $\cos \delta\theta = 1$  and  $\sin \delta\theta \approx \delta\theta$  gives:

$$(m/2)\lambda + \lambda/2 = (m/2)2d_{hkl} \sin \theta + (m/2)2d_{hkl} \cos \theta \delta\theta.$$

Cancelling the terms  $(m/2)\lambda$  and  $(m/2)2d_{hkl} \sin \theta$  and substituting  $md_{hkl} = t$  gives

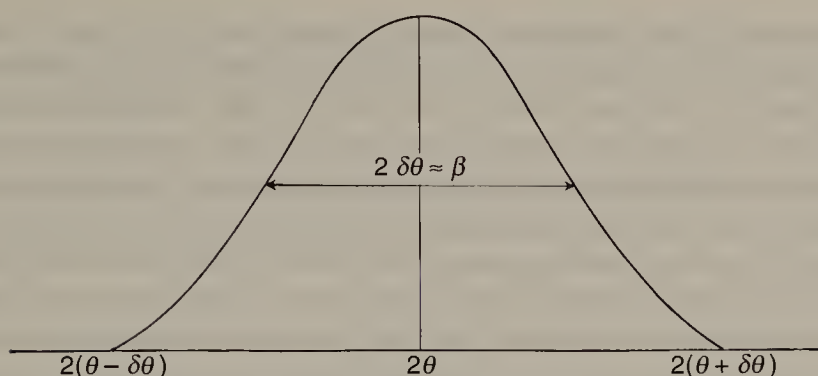
$$2\delta\theta = \frac{\lambda}{t \cos \theta}.$$

This is the basis of the Scherrer equation which relates the broadening of an X-ray beam to the crystal size  $t$ . The broadening is usually expressed as  $\beta$ , the breadth of the beam at half the maximum peak intensity and in which the angles are measured relative to the direct beam. As indicated in Fig. 9.8,  $\beta$  is approximately equal to  $2\delta\theta$ , hence

$$\beta = \frac{\lambda}{t \cos \theta} = \frac{\lambda \sec \theta}{t}.$$

The broadening can be represented in the Ewald reflecting sphere construction in terms of the extension of the reciprocal lattice point to a node of finite size. Fig. 9.9 shows a diffracted beam (angle  $2\theta$  to the direct beam) which is broadened over an angular range  $2\beta \approx 4\delta\theta$ . This is expressed by extending the





**Fig. 9.8.** A schematic diagram of a broadened Bragg peak arising from a crystal of finite thickness. The breadth at half the maximum peak intensity,  $\beta$ , is approximately equal to  $2\delta\theta$ . Note that the angular ' $2\theta$ ' scale is measured in relation to the direct and reflected beams.

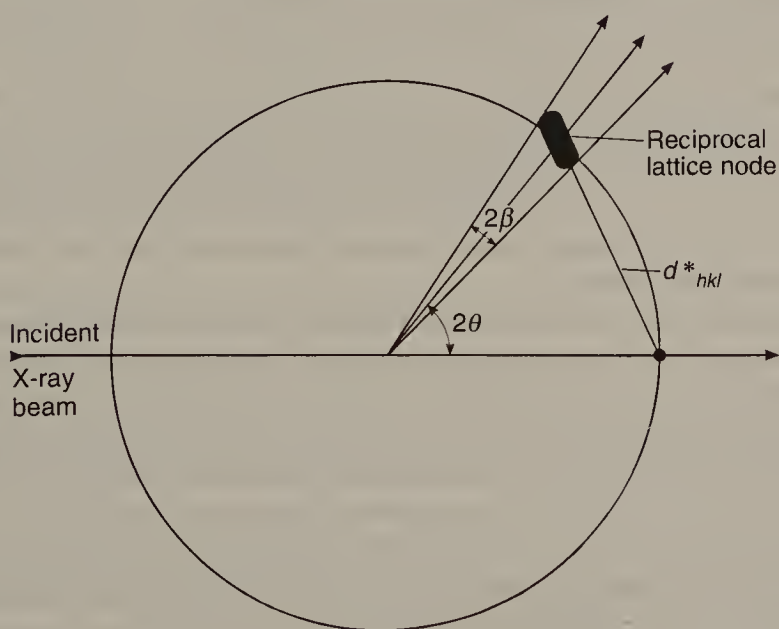
reciprocal lattice point into a node of finite length which, as the crystal rotates, intersects the reflecting sphere over this angular range. Let  $\delta(d_{hkl}^*)$  represent the extension of the reciprocal lattice point about its mean position. Now since

$$|\mathbf{d}_{hkl}^*| = d_{hkl}^* = \frac{2 \sin \theta}{\lambda};$$

$$\delta(d_{hkl}^*) = \delta\left(\frac{2 \sin \theta}{\lambda}\right) = \frac{2 \cos \theta}{\lambda} \delta\theta.$$

Substituting for  $\delta\theta$  from above gives:

$$\delta(d_{hkl}^*) = \frac{2 \cos \theta}{\lambda} \cdot \frac{\lambda}{2t \cos \theta} = \frac{1}{t}$$



**Fig. 9.9.** The Ewald reflecting sphere construction for a broadened reflected beam,  $\beta$ , which corresponds to an extension  $1/t$  of the reciprocal lattice node.

i.e. the extension of the reciprocal lattice node is simply the reciprocal of the crystal dimension perpendicular to the reflecting planes. This applies to all the other directions in a crystal with the result that the *shape* of the reciprocal lattice node is reciprocally related to the *shape* of the crystal. For example, in the case of thin, plate-like crystals (e.g. twins or stacking faults), the reciprocal lattice node is a rod or 'streak' perpendicular to the plane of the plate.

The above is a simplified treatment, both of the Scherrer equation and the extension of reciprocal lattice points into nodes. The Scherrer equation is normally applied to the broadening from polycrystalline (powder) specimens and includes a correction factor  $K$  (not significantly different from unity) to account for particle shapes\*. Hence the Scherrer equation is normally written:

$$\beta = \frac{K\lambda}{t \cos \theta} = \frac{K\lambda \sec \theta}{t}.$$

Finally, it should be noted that the reciprocal lattice nodes are also surrounded by subsidiary nodes (or satellites, maxima, or fringes) just as in the case of light diffraction from gratings with a finite number of lines (Section 7.4, Fig. 7.9). In most situations these subsidiary nodes are very weak because the number of diffracting planes contributing to the beam is large. However, in the case of X-ray diffraction from specimens consisting of a limited number of diffracting planes, superlattice repeat distances or multilayers, the subsidiary nodes (or satellites, maxima or fringes) are observable and are important in the characterization of the specimen, as described in Section 9.6.

## 9.4 Fixed $\theta$ , varying $\lambda$ X-ray techniques: the Laue method

X-ray single crystal techniques may be classified into two groups depending upon the way in which Bragg's law is satisfied experimentally. There are two variables in Bragg's law— $\theta$  and  $\lambda$ —and a series of fixed values,  $d_{hkl}$ . In order to satisfy Bragg's law for any of the  $d$ -values, either  $\lambda$  must be varied with  $\theta$  fixed, or  $\theta$  must be varied with  $\lambda$  fixed. The former case has only one significant representative—the (original) Laue method, whereas there are many methods based upon the latter case.

The geometry of the Laue method, in terms of the reflecting sphere construction, has already been explained in Section 8.4. Now we need to consider the practical applications of the technique. The important point to emphasize is that each set of reflecting planes with Laue indices  $hkl$  (see Section 8.4) gives rise to just one reflected beam. Of all the white X-radiation falling upon it, a lattice plane with Miller indices ( $hkl$ ) reflects only that wavelength (or 'colour') for which Bragg's law is satisfied, a reflecting plane of half the spacing with Laue indices  $2h\ 2k\ 2l$  reflects a wavelength of half this value, and so on. In other

\* Note that the observed breadth at half the maximum peak intensity,  $\beta_{\text{OBS}}$ , includes additional sources of broadening arising from the experimental set up and instrumentation,  $\beta_{\text{INST}}$ , which must be 'subtracted' from  $\beta_{\text{OBS}}$  in order that  $\beta$  can be determined (see Section 10.3.3).

words the reflections from planes such as, for example, (111) (Miller indices for lattice planes) 222, 333, 444, etc. (Laue indices for the parallel reflecting planes) are all superimposed.

The usual practice is to record the back-reflected beams since thick specimens which are opaque to the transmission of X-rays through them can be examined. The set-up showing just one reflected beam in the plane of the paper is shown in Fig. 9.10(a). In analysing the film it is necessary to determine the projection of the normal (or reciprocal lattice vector) of each of the reflecting planes on to the film from each reflection S and then to plot these on a stereographic projection\*. By measuring the angles between the normals, and then comparing them with lists of angles such as given for cubic crystals in Section A4.4 (Appendix 4), it is possible to identify the reflections. In practice such manual procedures (involving the use of the Greninger net†) have largely been replaced by computer programs which determine the orientation of the crystal using as input data the positions of spots on the film, film-specimen distance and (assumed) crystal structure.

Hence (back reflection) Laue photographs may be used to determine or check the orientation of single crystals and the orientation relationships between crystals. An example of a Laue photograph is shown in Fig. 9.10(b).

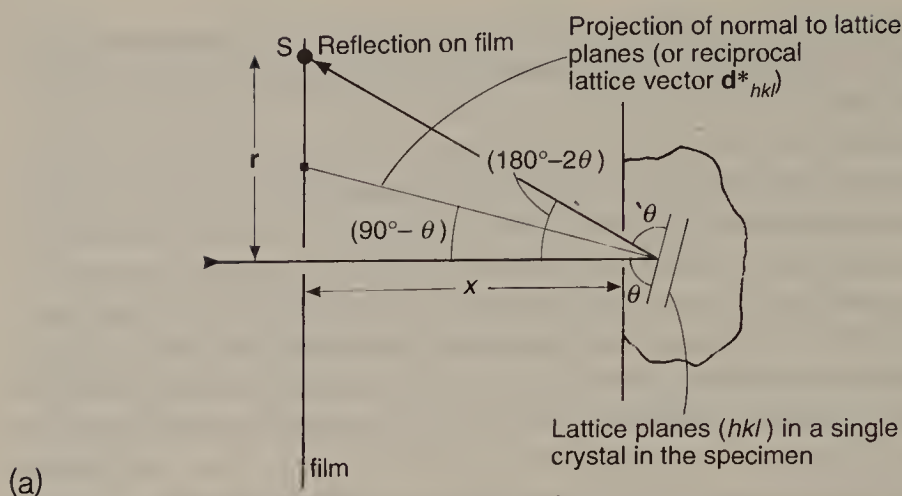
Figure 9.10(a) should be compared with Fig. 8.7. Consider for example the 201 reciprocal lattice point which is situated in the 'nest' of spheres representing the wavelength range of the incident 'white' X-radiation. Bragg's law is satisfied for the particular wavelength represented by the sphere which passes through the 201 reciprocal lattice point and the direction of the reflected beam (indicated by the arrow) is from the centre of this sphere (which can be found by construction) and the 201 reciprocal lattice point. This beam makes angle  $(180^\circ - 2\theta)$  with the incident beam and the reciprocal lattice vector  $\mathbf{d}_{201}^*$  makes angle  $(90^\circ - \theta)$  with the incident beam.

## 9.5 Fixed $\lambda$ , varying $\theta$ X-ray techniques: oscillation, rotation and precession methods

In Section 8.4, Fig. 8.6, we showed the Ewald reflecting sphere construction for the case where the incident X-ray beam was incident along the  $\mathbf{a}^*$  reciprocal lattice vector (from the left). Figure 8.6(a) shows the  $h0l$  section of the reciprocal lattice through the centre of the sphere and the origin of the

\* The stereographic projection is a major topic which is omitted from this book. It is covered in many of the books listed under Further Reading but in none of them entirely satisfactorily—perhaps the most helpful book is that by J. R. Moon *Introduction to the Stereographic Projection*, The Institute of Materials, 1972. The problem is that a book is not a very satisfactory medium from which to assimilate the geometrical procedures which are involved—and which almost always appear to a reader much more complicated than they in fact are. Models are much more useful or, lacking them, 'three-dimensional' drawings (anaglyphs) which are viewed through red-green spectacles.

† Greninger nets are prepared for a particular specimen-film distance (e.g. 30 mm), on which are drawn a series of calibrated hyperbolae (for the back reflection case). By measuring the distance between two spots along a hyperbola the angle between the normals, or the reciprocal lattice vectors of the two planes giving rise to these spots, can be obtained.



**Fig. 9.10.** (a) The geometry of the back reflection Laue method for a particular set of  $hkl$  planes in a single crystal. The wavelength of the reflected beam is that for which Bragg's law is satisfied for the particular fixed  $\theta$  and  $d_{hkl}$  value. (b) A back reflection Laue photograph of a single crystal of aluminium oriented with a  $\langle 100 \rangle$  direction nearly parallel to the incident X-ray beam showing the reflections  $S$  from many  $(hkl)$  planes. They lie on a series of intersecting hyperbolae (close to straight lines in this photograph), each hyperbola corresponding to reflections from planes in a single zone,  $[uvw]$ . Note the four-fold symmetry of the intersecting zones indicating the  $\langle 100 \rangle$  crystal orientation. (Photograph by courtesy of Prof. G. W. Lorimer.)

reciprocal lattice and Fig. 8.6(b) shows the  $h1l$  section of the reciprocal lattice and the smaller (non-diametral) section of the Ewald sphere. For the particular wavelength and particular incident beam direction drawn in Fig. 8.6, only two planes—201 and  $2\bar{1}1$  satisfy Bragg's law. Now, instead of varying  $\lambda$ , as in the



Laue case (Fig. 8.7), let us change the direction of the incident beam such that it is no longer incident along the  $\mathbf{a}^*$  reciprocal lattice vector direction. This variation in the Bragg angle is accomplished in practice by moving the crystal.

### 9.5.1 *The oscillation method*

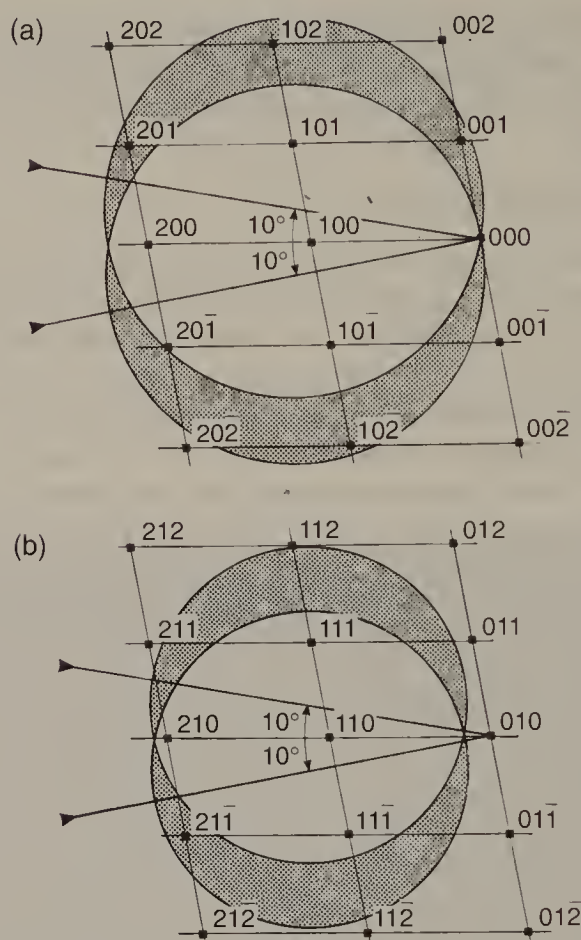
Consider the crystal, Fig. 8.6, oscillated say  $\pm 10^\circ$  about an axis parallel to the  $\mathbf{b}^*$  reciprocal lattice vector (or  $y$ -axis), i.e. perpendicular to the plane of the paper. As the crystal is (slowly) oscillated, the angles between the incident beam and  $hkl$  planes vary and whenever Bragg's law is satisfied for a particular plane 'out shoots' momentarily a reflected beam. The oscillation of the crystal can be represented by an oscillation of the reciprocal lattice about the origin: imagine a pencil fixed to the crystal perpendicular to the page with its point at the origin of Fig. 8.6(a). As you oscillate the pencil the reciprocal lattice oscillates about the origin but the Ewald sphere remains fixed, centred along the direction of the incident beam from the left: whenever a reciprocal lattice point intersects the sphere 'out shoots' a reflected beam.

The relative movement of the sphere and reciprocal lattice is most easily represented, not by drawing the whole reciprocal lattice in its different positions, but by drawing the Ewald sphere at the extreme limits of oscillation say  $10^\circ$  in one direction and  $10^\circ$  in the other. These limits are shown in Fig. 9.11 for (a) the  $h0l$  and (b) the  $h1l$  reciprocal lattice sections. The shaded regions, called 'lunes' because of their shape, represent the regions of reciprocal space through which the surface of the sphere passes as it is oscillated. Only those reciprocal lattice points which lie within these shaded regions give rise to reflected beams.

There are several ways of recording the reflected beams. The simplest is to arrange a cylindrically shaped film coaxially around the crystal (with a hole to allow the exit of the incident beam) such that reflections at all angles can be recorded. Now, all the reflected beams from the  $h0l$  reciprocal lattice section (Fig. 9.11(a)) lie in the plane of the paper and thus lie in a ring around the film. The reflected beams from the  $h1l$  reciprocal lattice section lie in a cone whose centre is the centre of the Ewald sphere and these beams also intersect the film in a ring 'higher up' than the ring from the  $h0l$  reciprocal lattice section. Figure 9.12(a) shows this geometry for the reflected beams from the  $h0l$ ,  $h1l$ ,  $h\bar{1}l$ ,  $h2l$  etc. sections of the reciprocal lattice.

When the film is 'unwrapped' and laid flat, the rings of spots appear as lines, called layer lines (Fig. 9.12(b)), the 'zero layer line' spots from the  $h0l$  reciprocal lattice section through the centre, the 'first layer line' spots from the  $h1l$  reciprocal lattice section next above—and so on for all the reciprocal lattice sections perpendicular to the axis of oscillation.

In practice it is necessary to set up a crystal such that some prominent zone axis is along the oscillation axis, such as, in our case, the  $[010]$  axis. This implies that the reciprocal lattice sections or layers perpendicular to the oscillation axis are well defined and give rise to clearly defined layer lines on the film. If, for example, we set a cubic crystal with the  $z$ -axis or  $[001]$  direction along the axis of

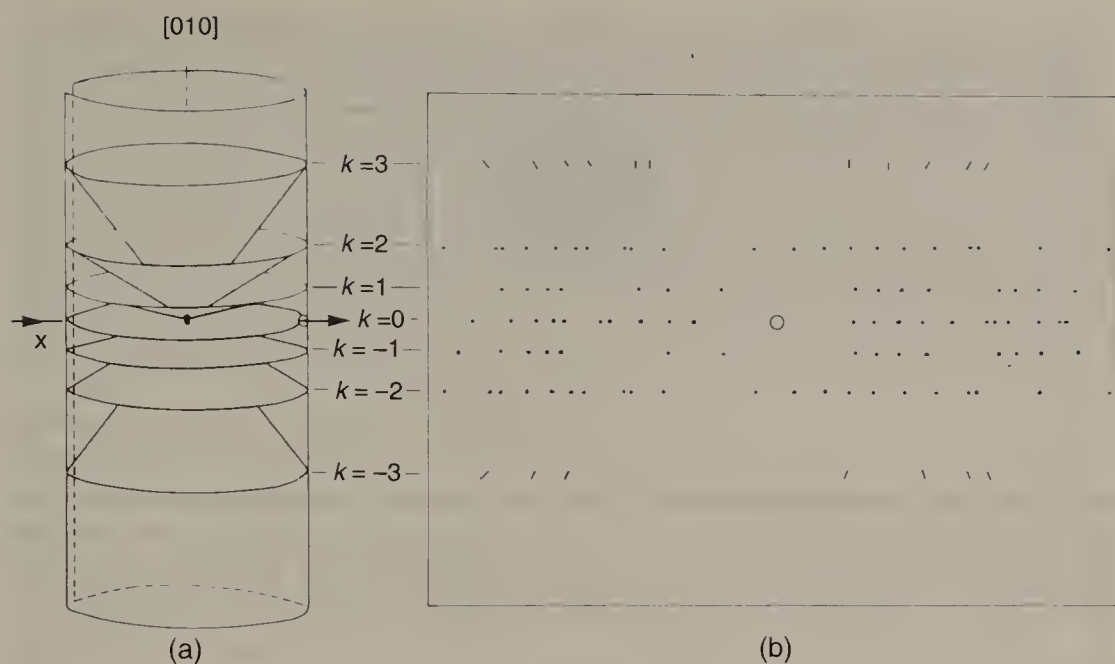


**Fig. 9.11.** The Ewald reflecting sphere construction for a monoclinic crystal in which the incident X-ray beam is oscillated  $\pm 10^\circ$  from the direction of the  $\mathbf{a}^*$  reciprocal lattice vector about the  $[010]$  direction ( $y$ -axis, perpendicular to the plane of the paper). The directions of the X-ray beams and the corresponding surface of the reflecting sphere are shown at the limits of oscillation. Any reciprocal lattice points lying in the regions of reciprocal space through which the reflecting sphere passes (the shaded regions, called 'lunes') give rise to reflections. (a) The  $h0l$  reciprocal lattice section through the origin and a diametral section of the reflecting sphere and (b) the  $h1l$  reciprocal lattice section (i.e. the layer 'above' the  $h0l$  section) and the smaller, non-diametral section of the reflecting sphere (compare with Fig. 8.6). In these two sections the planes which reflect are  $201$ ,  $102$ ,  $001$ ,  $20\bar{1}$ ,  $10\bar{2}$  (zero layer line) and  $112$ ,  $21\bar{1}$  (first layer line above).

oscillation, then the reciprocal lattice sections giving the layer lines would be  $hk0$  (zero layer line),  $hk1$  (first layer line above) and so on (see Figs 6.5 or 6.6). If on the other hand the crystal was set up in no particular orientation, i.e. no particular reciprocal lattice section perpendicular to the axis of rotation, the layer lines would, correspondingly, hardly be evident.

### 9.5.2 The rotation method

As the angle of oscillation increases, the Ewald reflecting sphere sweeps to and



**Fig. 9.12.** (a) The oscillation photograph arrangement with the crystal at the centre of the cylindrical film. The oscillation axis  $[010]$  is co-axial with the film and the reflections from each reciprocal lattice section  $h0l$ ,  $h1l$ ,  $h\bar{1}l$ ,  $h2l$  etc. lie on cones which intersect the film in circles.  $X$  indicates the incident beam direction and in (b), showing the cylindrical film 'unwrapped',  $O$  indicates the exit beam direction through a hole at the centre of the film.

from through a greater volume of reciprocal space, the lunes (Fig. 9.11) become larger and overlap and more reflections are recorded. The extreme case is to oscillate the crystal  $\pm 180^\circ$ —but this is the same as rotating it  $360^\circ$ , in which case the Ewald reflecting sphere makes a complete circuit round the origin of the reciprocal lattice. As the Ewald sphere sweeps through the reciprocal lattice, a plane will reflect twice: once when it crosses 'from outside to inside' the reflecting sphere and once when it crosses out again, the reflections being recorded on opposite sides of the direct beam. Rotation photographs are generally used to determine the orientation of small single crystals. An example is given in Fig. 9.13.

### 9.5.3 The precession method

This is an ingenious and useful technique invented by M. J. Buerger\* by means of which (unlike oscillation and rotation photographs), undistorted sections or layers of reciprocal lattice points may be recorded on a flat film. It is probably easiest to appreciate the geometrical basis of the method by using, as an example, a simple cubic crystal.

Figure 9.14(a) shows an  $(h0l)$  section of a simple cubic crystal (drawn with the  $y$ -axis or  $b^*$  reciprocal lattice unit cell vector perpendicular to the page). The

\* Denotes biographical notes available in Appendix 3.





**Fig. 9.13.** A rotation crystal photograph of topaz  $\text{Al}_2(\text{SiO}_4)(\text{OH}, \text{F})_2$ , orthorhombic. The cylindrical film is shown laid flat with the X-ray beam exit hole at the centre and the rotation axis (in this case the  $x$ -axis) vertical. Notice the large number of reflections in each layer line and the vertical and horizontal mirror lines of symmetry which arise because the reflecting sphere sweeps through a much larger region of reciprocal space during the  $360^\circ$  rotation of the crystal than for an oscillation photograph. (Photograph by courtesy of Dr. M. S. Hampar.)

X-ray beam is incident along the  $x$ -axis or  $\mathbf{a}^*$  reciprocal lattice unit cell vector and the Ewald reflecting sphere for a particular wavelength is centred about the incident beam direction. The flat film is set perpendicular to the X-ray beam. We are now going to consider the conditions by which we can obtain reflections from the reciprocal lattice points lying in the plane  $0kl$ —i.e. the plane through the origin and perpendicular to the  $x$ -axis or  $\mathbf{a}^*$  reciprocal lattice vector. Figure 9.14(a) shows only one row of these reciprocal lattice points— $001, 002, 003, 00\bar{1}, 00\bar{2}, 00\bar{3}$  etc.; the others are above and below the plane of the diagram. Now, ignoring for the time being the reciprocal lattice points not lying in this plane  $0kl$ , let us consider the movements necessary to bring  $001, 002, 003$  etc. reciprocal lattice points into reflecting positions. Clearly, we need to tilt or rotate the crystal anticlockwise such that first  $001$ , then  $002$ , then  $003$  etc. successively intersect the sphere. As we do so we tilt or rotate the film anticlockwise by the same angle (the film and crystal rotation mechanisms being coupled together). The  $001, 002, 003$  reflections then strike the film successively at equally spaced distances from the origin  $000$ . The situation in which  $003$  is in the reflecting position at a tilt or rotation angle  $\phi$  is drawn in Fig. 9.14(b). Clearly, if we rotate the crystal and film clockwise we would record the  $00\bar{1}, 00\bar{2}, 00\bar{3}$  etc. reflections on the opposite side of the film from the origin. The result (ignoring reflections from reciprocal lattice points not lying on this row) would be a row of equally spaced spots on the film corresponding to the equally spaced reciprocal lattice points in the row through the origin. These are shown on a plan view of the film (Fig. 9.14(c)), as the vertical row of spots through the centre.

Now we have to consider the reciprocal lattice points in the  $0kl$  section of the reciprocal lattice which intersect the Ewald reflecting sphere above and below the plane of Fig. 9.14(b). The sphere intersects the reciprocal lattice section  $0kl$



in a circle, Fig. 9.14(c); any reciprocal lattice point lying in this circle gives rise to a reflected beam. Now we precess the crystal and the film about the incident beam direction such that the film is always parallel to the  $0kl$  reciprocal lattice section (the precession movement means that the  $x$ -axis of the crystal rotates about the incident beam direction at the fixed angle  $\phi$ ). As we do so the circle moves through the reciprocal lattice section in an arc centred at the origin  $000$  of the reciprocal lattice, i.e. about the direction of the direct X-ray beam. Hence, in a complete revolution, all the reciprocal lattice points lying within the large circle of Fig. 9.14(c) reflect—and the pattern of spots on the film corresponds to the pattern of reciprocal lattice points in the  $0kl$  section of the reciprocal lattice, as shown in Fig. 9.14(c).

Finally, we have to eliminate the complicating effects of the reflections from reciprocal lattice points not lying in the  $0kl$  plane through the origin. This is achieved by placing a screen with an annular opening between the crystal and the film, the size of the annulus being chosen to allow reflections to pass to the screen only from reciprocal lattice points lying in the circle (Fig. 9.14(c)). The screen is indicated in cross-section in Fig. 9.14(b) for the case in which the furthest reciprocal lattice point from the origin which can be recorded is  $003$ . The screen is also linked to the crystal–film precession movements.

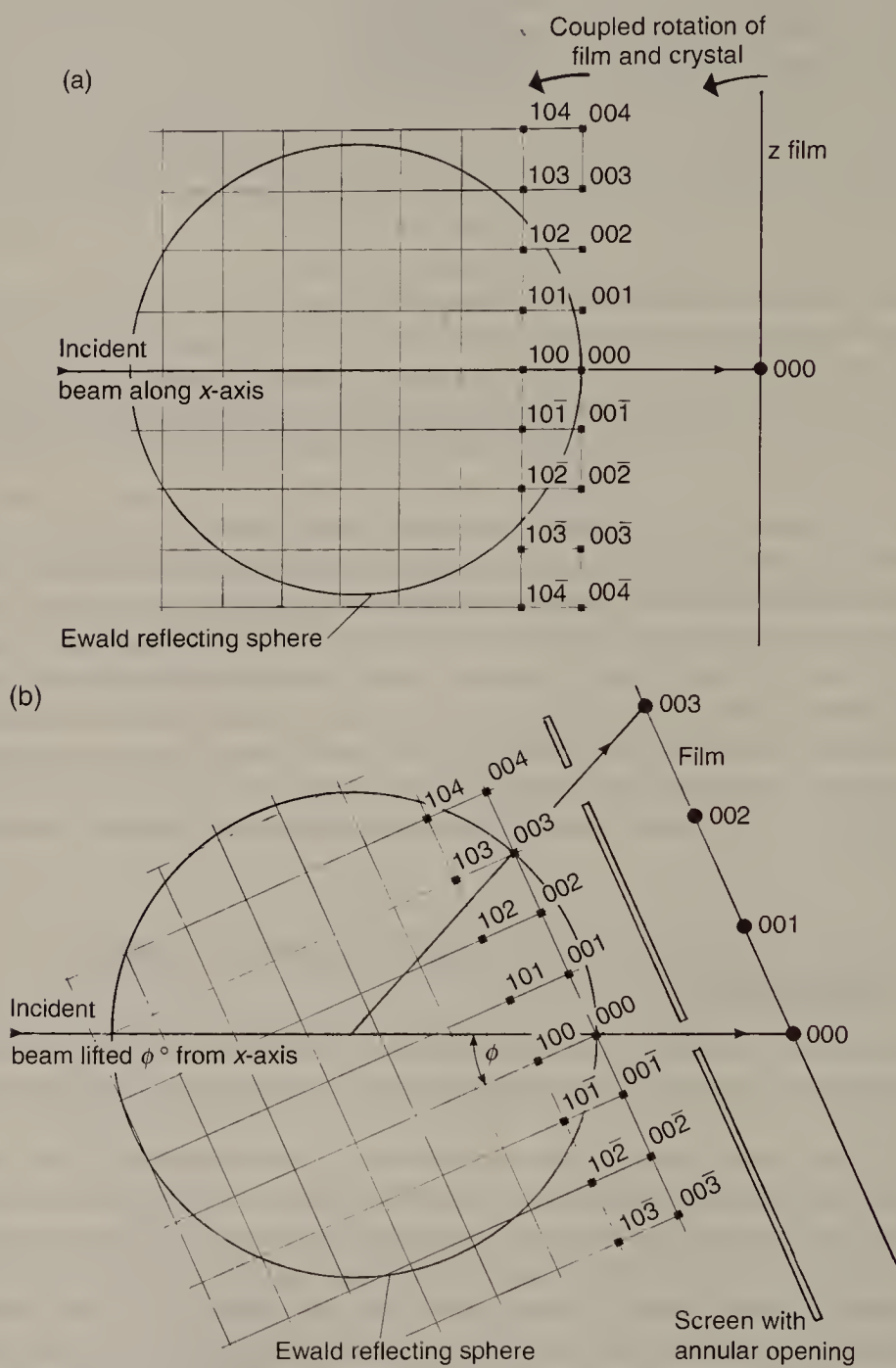
The precession method can be modified to record reciprocal lattice sections which do not pass through the origin (non-zero-level photographs), details of which can be found in the books on X-ray diffraction techniques listed in Further Reading. Its main application is in crystal structure determination by measurement of the intensities of the X-ray reflections. Figure 9.15 shows an example of a zero-level photograph (of a reciprocal lattice section passing through the origin) which shows very convincingly the pattern of reciprocal lattice points.

## 9.6 X-ray diffraction from single crystal thin films and multilayers

Thin films and multilayer specimens are invariably studied using the X-ray diffractometer, the geometrical basis of which is described in detail in Section 10.2.

The normal arrangement, as used in X-ray powder diffractometry, is the symmetrical (Bragg–Brentano) one in which only the  $d$ -spacings of those planes parallel to the specimen surface are recorded. This is achieved by arranging the X-ray source and X-ray detector and their collimating slits such that the incident and reflected beams make equal angles to the specimen surface. The arrangement is shown diagrammatically in Fig. 9.16(a). As the angle  $\theta$  is varied (either by keeping the specimen fixed and rotating the source and detector in opposite senses as indicated in Figs 10.3(a) and (b), or by keeping the source fixed and rotating the detector at twice the angular velocity of the specimen), reflections occur whenever Bragg's law is satisfied. Clearly, for a single crystal, with only

one set of planes parallel to the surface, there will only be one Bragg reflection. For multilayer specimens, which may consist of a sequence of thin crystal films (say, of copper and cobalt) mounted on a single crystal substrate, there will be



**Fig. 9.14.** The geometry of the precession method. (a) The incident beam normal to the  $0kl$  section of the reciprocal lattice (indicated by the row of reciprocal lattice points  $001, 002, 003$  etc.). In order to bring these points into reflecting positions the crystal and the film are rotated anti-clockwise as indicated. The situation in which the  $003$  reciprocal lattice point is in a reflecting position is shown in (b). (c) A plan view of the film at this angle  $\phi$  with the circle

three Bragg reflections—one from the substrate and one each from the thin films (of different crystal structure).

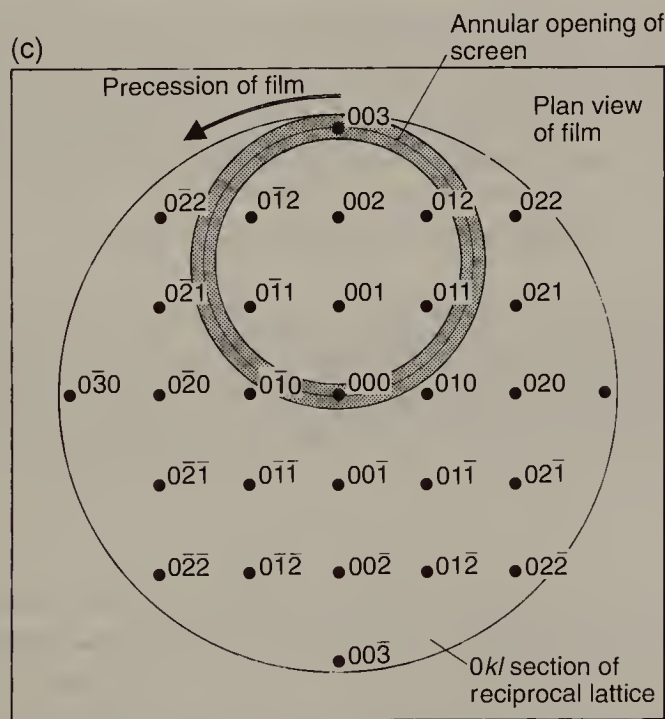
However, there are more diffraction phenomena to be recorded. First, since the layers are generally thin—of the order of 1–10 nm—the (high angle) Bragg peaks are substantially broadened and this may be used to estimate the thickness of the layers by means of the Scherrer equation (Section 9.3). Second, the repeat distance, or superlattice wavelength  $\Lambda$  of the layers can be determined from the angles of ‘satellite’ reflections which occur (given a multilayer specimen with a long range structural coherence) on either side of the (high angle) Bragg peaks. The value of  $\Lambda$  may be determined from the equation

$$\Lambda = \frac{\lambda}{2(\sin \theta_2 - \sin \theta_1)}$$

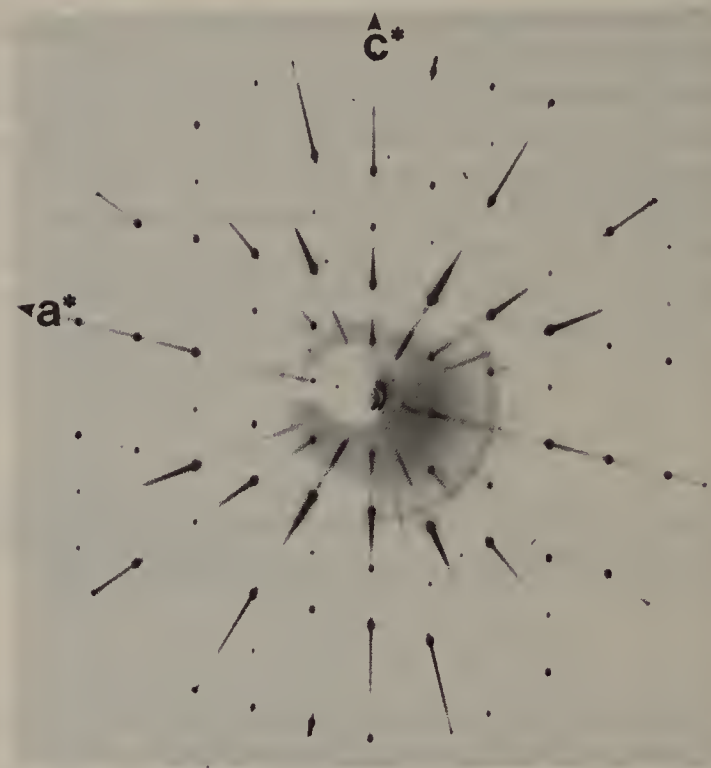
where  $\lambda$  = the X-ray wavelength and  $\sin \theta_1$ ,  $\sin \theta_2$  are the Bragg angles of adjacent satellite peaks. This equation may be rearranged to give

$$\frac{1}{\Lambda} = \frac{1}{d_2} - \frac{1}{d_1}$$

where  $d_1, d_2$  are the notional  $d$ -spacings of the satellite peaks. An example of a cobalt–gold multilayer specimen is given in Fig. 9.17(a).



representing the intersection of the  $0kl$  plane and the reflecting sphere and the projection of the annulus on to the screen. The only reflections to reach the film are those falling within the annulus (shaded region). As the crystal + screen + film are precessed about the angle  $\phi$  the annulus effectively sweeps through the  $0kl$  section of the reciprocal lattice as indicated by the arrow and all reciprocal lattice points within the large circle give rise successively to reflections.



**Fig. 9.15.** A (zero level) precession photograph of tremolite,  $\text{Ca}_2\text{Mg}_5\text{Si}_8\text{O}_{22}(\text{OH})_2$  (monoclinic  $C2/m$ ,  $a = 9.84 \text{ \AA}$ ,  $b = 18.05 \text{ \AA}$ ,  $c = 5.28 \text{ \AA}$ ,  $\beta = 104.7^\circ$ ), showing reflections from the  $h0l$  reciprocal lattice section (incident beam along the  $y$ -axis). The orientations of the reciprocal lattice vectors  $\mathbf{a}^*$  and  $\mathbf{c}^*$  are indicated. Compare this photograph with the drawing of the  $(h0l)$  reciprocal lattice section of a monoclinic crystal (Fig. 6.2(c)). The streaking arises from the presence of a spectrum of X-ray wavelengths in the incompletely filtered  $\text{MoK}\alpha$  ( $\lambda = 0.71 \text{ \AA}$ ) X-radiation. (Photograph by courtesy of Dr. J. E. Chisholm.)

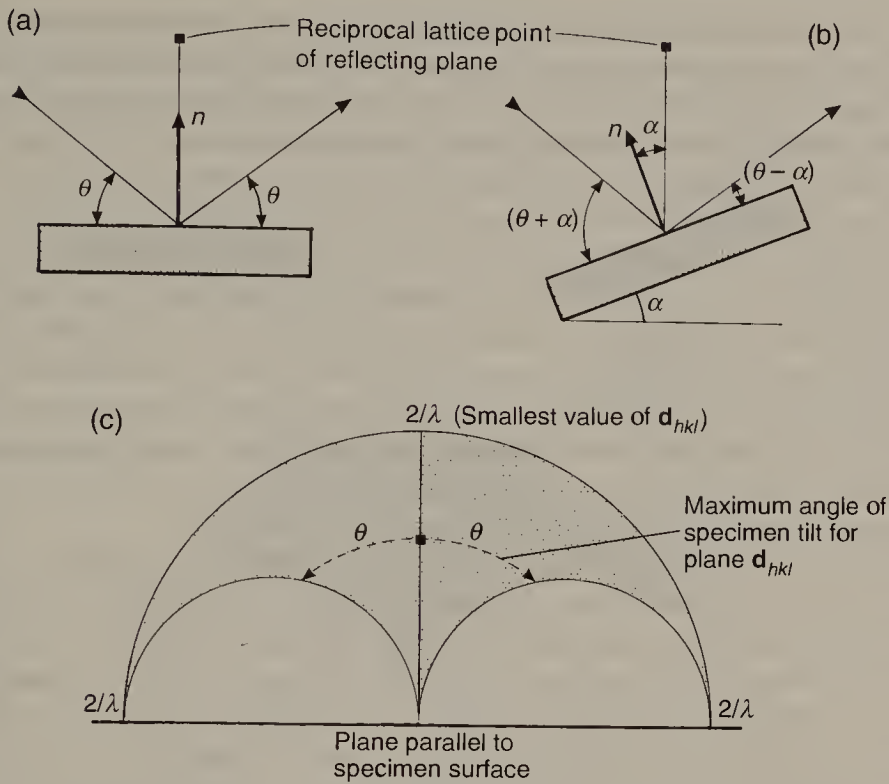
The repeat distance  $\Lambda$  of the layers also gives rise to low-angle Bragg reflections (of the order  $2\theta = 2-5^\circ$ ), between which occur a further set of satellite peaks or fringes called Keissig fringes which may be used to determine the total multilayer film thickness  $N\Lambda$  using an analogous equation to that above, viz.

$$\frac{1}{N\Lambda} = \frac{1}{d_{k2}} - \frac{1}{d_{k1}}$$

where  $d_{k1}$ ,  $d_{k2}$  are the notional  $d$ -spacings of any pair of adjacent Keissig fringes. An example of a cobalt-copper multilayer specimen is given in Fig. 9.17(b).

The occurrence of the low-angle Bragg peaks and Keissig fringes may be understood by analogy with the diffraction pattern from a limited number  $N$  of slits of width  $a$  (Section 7.4); Fig. 7.9 shows a particular case for  $N = 6$ . The principal maxima correspond to the low-angle Bragg peaks in which the slit spacing  $a$  corresponds to the repeat distance of the layers, or superlattice





**Fig. 9.16.** The X-ray diffractometer arrangements for a single crystal. (a) The symmetrical setting: the reciprocal lattice vectors of the reflecting planes are all parallel to the specimen surface normal  $n$ . (b) The asymmetrical setting, the reciprocal lattice vectors of the reflecting planes are inclined at angle  $\alpha$  to  $n$ . (c) The region of reciprocal space (shaded) within which lie the reciprocal lattice points of possible reflecting planes.

wavelength  $\Lambda$ . The subsidiary maxima, of which there are  $(N - 2)$  between principal maxima, correspond to the Keissig fringes; by counting the number of Keissig fringes (plus two) between the low-angle Bragg peaks the number of multilayers or superlattice wavelengths  $N$  can be determined and by measuring the angles between adjacent fringes the total thickness  $N\Lambda$  of the multilayers can be determined using the equation given above. Its validity can be checked by applying it, say, to the subsidiary maxima in Fig. 7.9; for the zero and first order minima the  $\sin \alpha \approx \alpha \approx 2\theta$  values are  $1(\lambda/6a)$  and  $2(\lambda/6a)$ . Substituting these values in the above equation gives  $N\Lambda = 6a$ , the total width of the grating.

In practice in X-ray diffraction the Keissig fringes are most clearly defined between the direct beam (zero order peak) and first low-angle Bragg peak (Fig. 9.17(b)).

The other arrangement used in X-ray diffractometry is the asymmetrical one in which, for any particular Bragg angle (source and detector fixed), the specimen can be rotated such that the incident and diffracted beams make different angles to the specimen surface (the angle between them remaining fixed at  $2\theta$ ). The arrangement is shown diagrammatically in Figs 9.16(b) and 10.3(c). It has the advantage in that reflections from planes which are not

parallel to the surface can be recorded (and is also a useful means of 'fine tuning' the angle of the specimen to maximize the intensity of reflections from planes which may not be exactly parallel to the specimen surface). Clearly, the maximum angle of tilt either way is  $\theta$ , otherwise the surface of the specimen will block or 'cut off' either the incident or the diffracted beam.

The Ewald reflecting sphere construction, which shows the extent to which the symmetrical and asymmetrical techniques sample a volume of reciprocal space, is shown in Fig. 9.16(c). The construction is essentially two-dimensional, since only those planes whose normals lie in the plane of the diagram (co-planar with the incident and reflected beams) can be recorded. In the symmetrical case (Fig. 9.16(a)), the reciprocal lattice points of the reflecting planes lie along a line perpendicular to the specimen surface whose maximum extent corresponds with the reciprocal lattice vector of the plane of smallest  $d_{hkl}$ -spacing that can be measured, i.e. that for which  $\theta = 90^\circ$ ; hence  $|\mathbf{d}_{hkl}^*| = 2/\lambda$ .

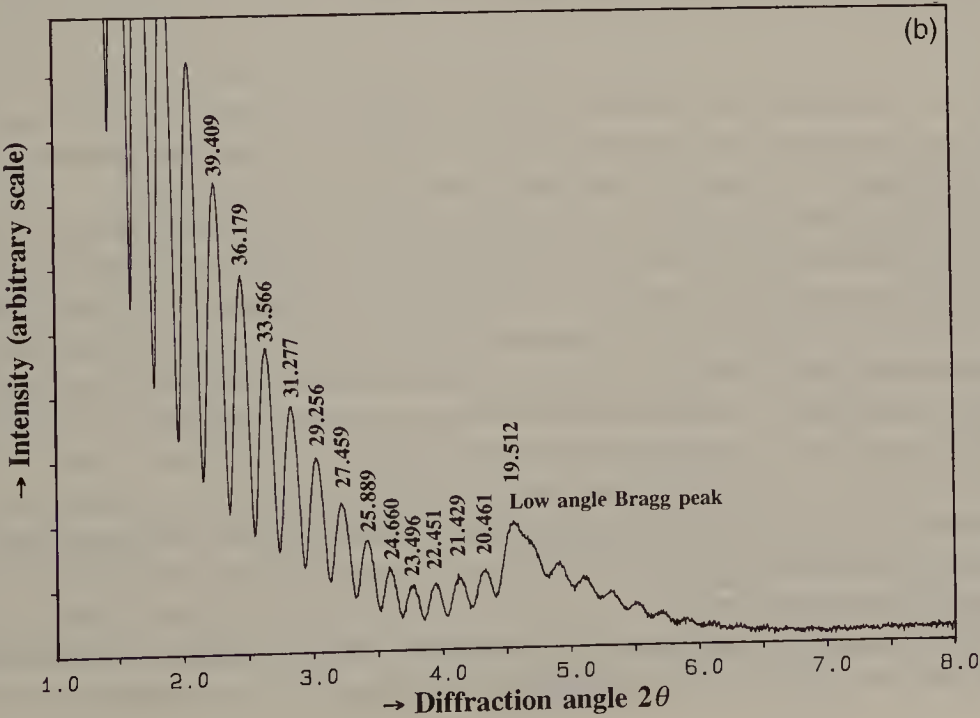
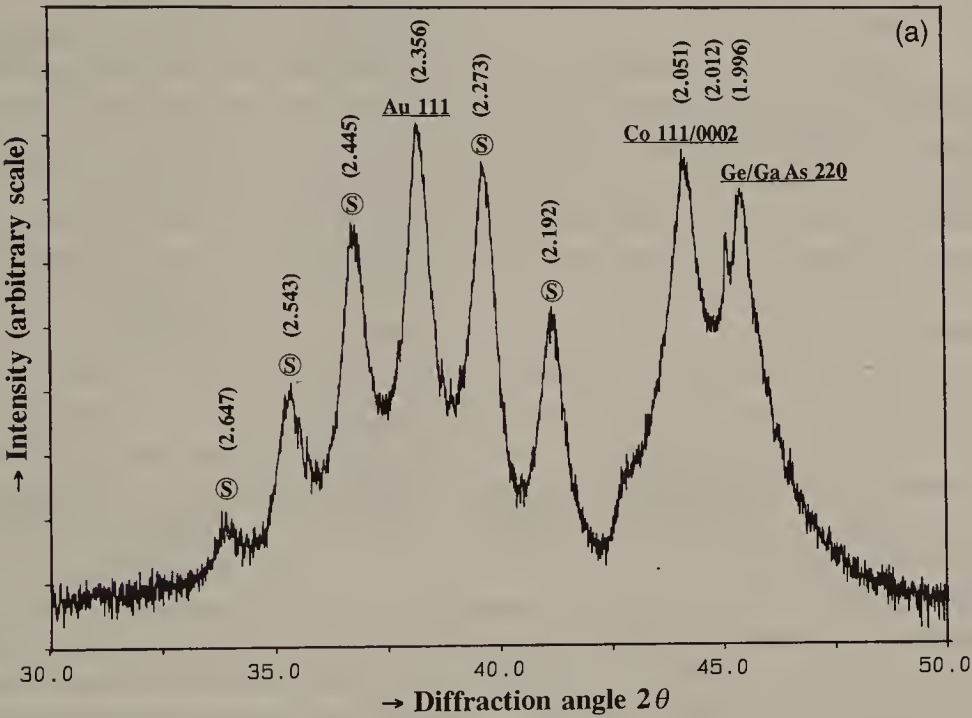
In the asymmetrical case (Fig. 9.16(b)) the crystal can be tilted or rotated clockwise or anticlockwise such that the reciprocal lattice vector of the reflecting planes is also tilted or rotated with respect to the specimen surface. The angular range,  $\pm\theta$  (limited by specimen cut-off), increases as  $|\mathbf{d}_{hkl}^*| = 2\sin\theta/\lambda$  increases, the maximum being  $\pm 90^\circ$  when  $\sin\theta = 1$ . This is shown as the shaded region in Fig. 9.16(c). Clearly, the choice of the wavelength of the X-radiation may be important, particularly in the asymmetrical case, since it determines which crystal planes in the specimen may, or may not, be recorded.

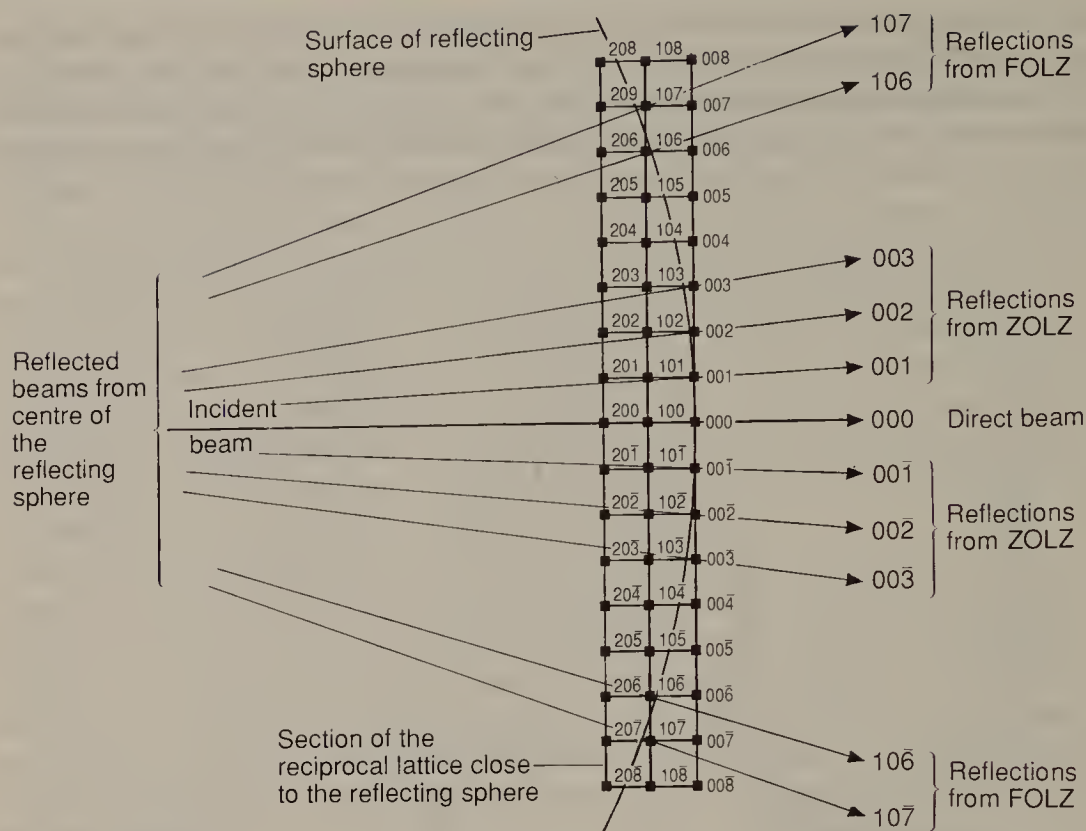
## 9.7 Electron diffraction in the transmission electron microscope

The wavelength associated with electrons depends on the accelerating voltage; for example in an electron microscope operated at 100 kV the wavelength is 3.7

▷  
**Fig. 9.17.** (a) A high angle X-ray diffraction trace ( $\text{CuK}\alpha_1$  radiation) from a cobalt-gold multilayer specimen showing the satellite peaks or fringes (S) each side of the Au 111 Bragg reflection. The repeat distance  $\Lambda$  of the layers is determined by measuring the (notional)  $d$ -spacings  $d_1$  and  $d_2$  of adjacent fringes and using the equation on page 157. The notional  $d$ -spacings ( $\text{\AA}$ ) of the fringes and the Au 111 peak are indicated (from which a value of  $\Lambda \approx 64 \text{ \AA}$  is obtained). The group of higher angle reflections are from Co 111, Co 0002, the substrate GaAs 110 and the 'buffer' layer Ge 110. (b) A low angle X-ray diffraction trace ( $\text{CuK}\alpha_1$  radiation) from a cobalt-copper multilayer specimen showing the low angle Bragg reflection at  $4.525^\circ$  and the Keissig fringes each side. The Bragg peak gives the multilayer or superlattice repeat distance  $\Lambda$  and the number  $N - 2$  of Keissig fringes between the Bragg peak and zero angle gives  $N\Lambda$ , the total thickness. In this example  $\Lambda = 19.512 \text{ \AA}$  and  $(N - 2) = 22$  (only those fringes from about  $2\theta \approx 1.5^\circ$  are shown). Hence the total thickness  $N\Lambda = 468.3 \text{ \AA}$ .  $N\Lambda$  may also be determined by measuring the (notional)  $d$ -spacings,  $d_{K1}$  and  $d_{K2}$  of adjacent Keissig fringes and using the equation on page 158. The notional  $d$ -spacings ( $\text{\AA}$ ) of fringes 11 to 22 are indicated, from which values of  $N\Lambda$ , in fair agreement with that given above (subject to experimental scatter), are obtained.

pm and at 1 MV it is 0.87 pm. These wavelengths are *very much* smaller than the lattice parameters of crystals, which are normally in the region of 0.3 nm upwards. Hence the diameter of the reflecting sphere is *very large* in comparison with the size of the unit cell of the reciprocal lattice. Referring to the reciprocal lattice sections in Figs 8.6 and 9.14(a) and (b) for example, for the case of





**Fig. 9.18.** The Ewald reflecting sphere construction for a simple cubic crystal in which the electron beam is incident along the  $\mathbf{a}^*$  reciprocal lattice vector ( $x$ -axis). The  $\mathbf{b}^*$  reciprocal lattice vector ( $y$ -axis) is perpendicular to the plane of the page. A section of the sphere (centre beyond the left-hand edge of the page) and the reflected beams passing at small angles from the centre of the sphere through the reciprocal lattice points in ZOLZ (giving spots close to the direct beam) and FOLZ (giving spots further away from the direct beam) are indicated.

electron diffraction, the centres of the reflecting spheres would be situated along the direction of the incident beam at a point far to the left of the origin of the reciprocal lattice, well beyond the left-hand edge of the paper.

The situation for a simple cubic crystal (as for Fig. 9.14(a)) is illustrated in Fig. 9.18, which shows again that part of the reciprocal lattice section perpendicular to the  $\mathbf{b}^*$  reciprocal lattice vector or  $y$ -axis (out of the plane of the paper) which lies close to the surface of the reflecting sphere, only part of which near the origin can be shown since its radius is so large. The incident electron beam is directed along the  $\mathbf{a}^*$  reciprocal lattice vector or  $x$ -axis and the centre of the reflecting sphere is far to the left of the diagram.

Close to the origin, 000, the curvature of the sphere is so small that it approximates to a plane perpendicular to the direction of the electron beam and hence passes (in this section) very close to the 001, 002, 003 and  $00\bar{1}$ ,  $00\bar{2}$ ,  $00\bar{3}$  reciprocal lattice points.

Now in order for Bragg's law to be satisfied exactly, a reciprocal lattice point must intersect the Ewald reflecting sphere. However, since reciprocal lattice



points are broadened into nodes (Section 9.3) they may be extended sufficiently to intersect the sphere and hence give rise to diffracted beams. This situation also arises in X-ray diffraction but to a lesser extent than in electron diffraction (a) because the reciprocal lattice points of the thin foil crystal sections used in electron microscopy are extended perpendicular to the foil surface and are therefore approximately parallel to the electron beam and (b) because thin foils are often slightly bent or 'buckled' such that the orientation of the electron beam varies slightly over the surface of the foil—i.e. it is never incident precisely along one crystallographic direction as indicated in Fig. 9.18.

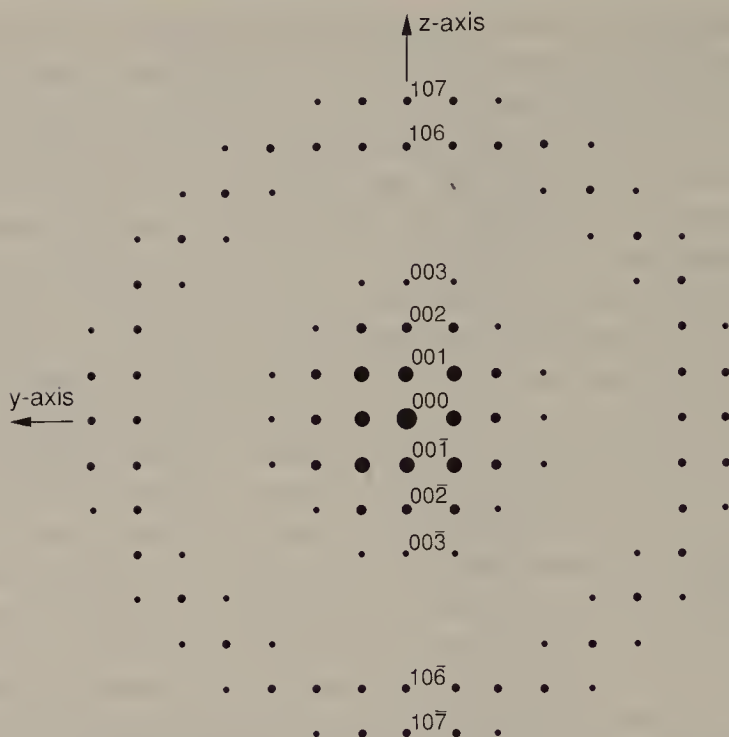
Hence (referring again to Fig. 9.18), the reciprocal lattice points  $001$ ,  $002$ ,  $003$ ,  $00\bar{1}$ ,  $00\bar{2}$ ,  $00\bar{3}$  which lie in a reciprocal lattice row perpendicular to the electron beam direction all give rise to reflected beams, which are directed from the centre of the sphere (to the far left of the page) as indicated. Similar considerations apply to the reciprocal lattice row in the 'next layer above the page', i.e. the row through  $010$  (above  $000$ ),  $011$ ,  $012$ ,  $013$  etc. and also the next layer below, i.e. through  $0\bar{1}0$  (below  $000$ ),  $0\bar{1}1$ ,  $0\bar{1}2$ ,  $0\bar{1}3$ , etc. All of these reciprocal lattice points lie in the  $(0kl)$  plane or section of the reciprocal lattice which is perpendicular to the electron beam direction. In summary, therefore, the reciprocal lattice points close to the origin, in the  $(0kl)$  reciprocal lattice section perpendicular to the electron beam direction, give rise to reflected beams.

Since the diffraction angles are small (Fig. 9.18), the pattern of spots on the screen perpendicular to the beam corresponds to the pattern of reciprocal lattice points. Figure 9.19 shows this pattern of spots from the  $(0kl)$  reciprocal lattice section grouped around the direct beam. For simplicity and clarity, only those reflected beams of type  $00l$  (in the section perpendicular to the  $y$ -axis, Fig. 9.20) are indexed.

These diffraction spots are said to belong to the zero order Laue zone (ZOLZ for short) since they all arise from reciprocal lattice points in a section through the origin or, equivalently, they all arise from planes in a zone—the zone axis being parallel (or nearly parallel) to the electron beam direction.

The pattern of electron diffraction spots (for a particular incident beam direction) in the zero order Laue zone is identical to that in the zero level X-ray precession photograph (when the crystal is precessed by the appropriate angle about the same incident beam direction). This is seen by comparing Fig. 9.14(c) with Fig. 9.19. The far simpler set-up (a stationary crystal) in electron diffraction 'works' because of the 'flatter' (large diameter) Ewald reflecting sphere, the extension of the reciprocal lattice nodes and the slight buckling of the thin foil specimens—all of which serve to provide the requisite diffraction conditions without the necessity of precessing the specimen over a very much smaller angular range.

Referring again to Fig. 9.18, as we proceed along the surface of the reflecting sphere away from the origin, we begin to intersect the next row of reciprocal lattice points which does not pass through the origin. The reciprocal lattice points in this row which lie close to the sphere, i.e.  $106$ ,  $107$ ,  $10\bar{6}$  and  $10\bar{7}$  (and in the corresponding rows above and below the plane of the diagram, all of which

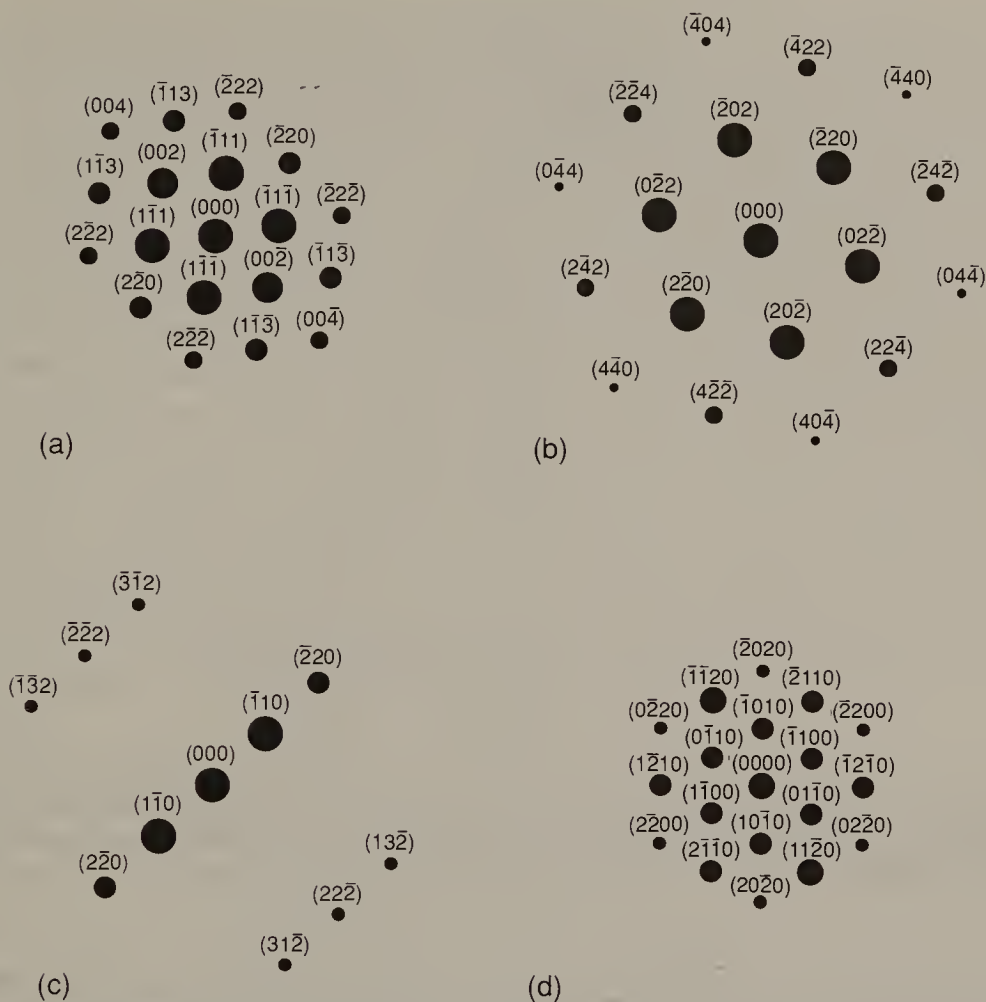


**Fig. 9.19.** The diffraction pattern on a screen perpendicular to the electron beam direction. The  $0kl$  ZOLZ spots are grouped around the direct beam (centre spot) and the  $1kl$  FOLZ spots are grouped roughly in a ring outside. Only the  $h0l$  spots in the section perpendicular to the  $y$ -axis (Fig. 9.18) are indexed (compare with Fig. 9.14(c)).

lie in the  $(1kl)$  section of the reciprocal lattice) will also give rise to diffraction spots as indicated. These spots, which lie outside those from the zero order Laue zone away from the centre of the pattern (Fig. 9.19) are said to belong to the first order Laue zone (FOLZ for short). Continuing outwards towards the edge of Fig. 9.18 we come to reciprocal lattice points in the second order Laue zone (SOLZ for short). These are just the first two in a series of higher order Laue zones (HOLZ for short).

The analysis of electron diffraction patterns is essentially a process of identifying the reciprocal lattice sections which give rise to them. Several computer programs are now available (see Appendix 2) which generate reciprocal lattice sections, given as input data the lattice parameters and type of unit cell and the electron beam (zone axis) direction. Several examples showing the ZOLZ only are given in Fig. 9.20. Care must be exercised in using such data because a number of different electron diffraction patterns from different types of high-symmetry crystals have identical symmetry and only differ in scale. For example the  $\langle 111 \rangle_{\text{fcc}}$  and  $[0001]_{\text{hcp}}$  patterns shown in Figs. 9.20(b) and (d) both consist of hexagonal patterns of points.

The first step in the analysis of electron diffraction patterns is measurement of the  $d$ -spacings. This is an easy matter. Fig. 9.21 shows a set of reflecting



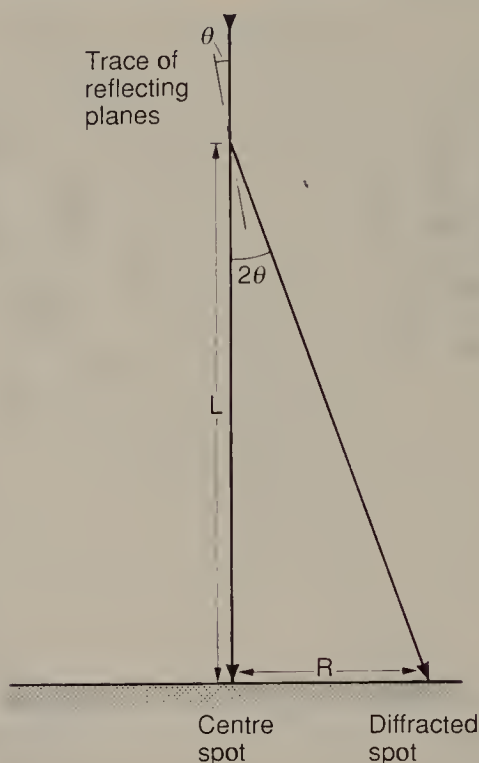
**Fig. 9.20.** Examples of the computer-generated diffraction patterns, drawn to the same scale ( $\lambda L = 16.3 \text{ \AA mm}$ ). (a) Aluminium (fcc), zone axis =  $\langle 110 \rangle$ ; (b) aluminium (fcc), zone axis =  $\langle 111 \rangle$ ; (c) iron (bcc), zone axis =  $\langle 112 \rangle$ ; (d) titanium (hcp), zone axis =  $[0001]$ .

planes at the Bragg angle  $\theta$  (much exaggerated) to the electron beam. The diffracted beam, at angle  $\theta + \theta = 2\theta$ , to the direct beam, falls on the screen at a distance  $R$  from the centre spot. Figure 9.21 does not represent the *actual* ray paths in the electron microscope, which are of course determined and controlled by the lens settings: hence  $L$ , the camera length, is not the *actual* distance between the specimen and screen, but is a ‘projected’ distance which varies with the lens settings.

From Fig. 9.21,  $\tan 2\theta = R/L$ . Since  $\theta$  is small,  $\tan 2\theta \approx 2\theta$  ( $2\theta$  of course being measured in radians). Similarly for Bragg’s law,  $\sin \theta \approx \theta$  hence  $\lambda \approx 2d_{hkl}\theta$ . Eliminating  $\theta$  from these equations we have:

$$d_{hkl} = \lambda L / R$$

where  $\lambda L$  is known as the camera constant and which, like  $L$ , varies with lens



**Fig. 9.21.** Idealized representation of the direct and diffracted ray paths in the electron microscope between the specimen and the screen.  $L$  is the camera length and  $R$  is the distance between the centre spot (direct beam) and the diffracted spot.

settings in the microscope. The units of  $\lambda L$  are best expressed in terms of the product of  $R$ , the distance measured on the screen (e.g. mm) and  $d_{hkl}$  (e.g. nm, Å or pm). Although the angstrom (Å) is not an SI (Système International) unit, it is coherent with the SI system ( $1 \text{ Å} = 10^{-10} \text{ m}$ ) and still remains in widespread use in crystallography (a) because it is roughly equal to atomic diameters and (b) because X-ray  $d_{hkl}$ -spacing data in the Powder Diffraction File (see Section 10.3) is recorded in angstroms.

The accuracy with which the  $d_{hkl}$ -spacings can be measured is very limited because of the size or 'diffuseness' of the diffraction spots. Moreover the camera constant,  $\lambda L$ , will only be known to a high degree of accuracy if a 'standard' specimen is used which gives a diffraction pattern with spots of accurately known  $d_{hkl}$ -spacings. Otherwise the small variations in lens settings from specimen to specimen and from day-to-day will limit the accuracy of  $\lambda L$  values at best to three significant figures. Hence, as pointed out above, patterns which have identical symmetry but which only differ slightly in scale with respect to the  $d_{hkl}$ -spacings of the diffraction spots are not readily distinguished.

The spots may then be indexed by reference to tables of data such as are contained in the Powder Diffraction File, which show the (Laue) indices,  $hkl$ , corresponding to the measured  $d_{hkl}$ -spacings. In doing so, a further step is required: the indexing must be such that the addition rule (Section 6.5.2) is



satisfied. A given set or family of planes  $\{hkl\}$  (which are invariably listed in data files simply as  $hkl$ —no brackets) will consist of a number of variants of identical  $d_{hkl}$ -spacings. For example, in the cubic system (see Section 5.4), there are six variants of the ‘plane of the form’  $\{100\}$ , all of which have identical  $d_{hkl}$ -spacings. The procedure consists of *choosing* the appropriate variants such that the addition rule is satisfied. Consider, for example, Fig. 9.20(a). The four spots of identical  $d_{hkl}$ -spacings closest to the centre spot are all reflections from planes of the form  $\{111\}$ . The particular indices have been chosen such that the indices of the remaining spots are determined correctly. For example,  $\mathbf{d}_{\bar{1}\bar{1}1}^* + \mathbf{d}_{1\bar{1}1}^* = \mathbf{d}_{002}^*$  and the zone axis,  $[110]$ , is found by cross-multiplication of any pair of these indices (see Section 6.5.7), the ‘choice’ only needs to be made once, and having been made, all the other spots in the pattern can be indexed consistently by repeated application of the addition rule; again, with reference to Fig. 9.20(a),  $\mathbf{d}_{\bar{1}\bar{1}1}^* + \mathbf{d}_{002}^* = \mathbf{d}_{\bar{1}\bar{1}3}^*$  and so on. The ‘choice’ is of course arbitrary: the number of different choices which can be made, all leading to a self-consistently indexed diffraction pattern, depends on the number of equivalent variants of the zone axis. In a cubic crystal there are twelve variants of the  $\langle 110 \rangle$  direction, hence there are twelve ways in which a pattern like that of Fig. 9.20(a) can be indexed.

The availability of computer-generated diffraction patterns has greatly facilitated the indexing and verification of electron diffraction pattern analysis. However, it must be said that many ‘useful’ diffraction patterns—i.e. those which may be of potential scientific interest, which have been obtained under conditions of experimental difficulty and which may consist of many spots from several crystals of varying degrees of visibility on the film—still require for their solution careful observation and measurement and an awareness of the possible occurrence of additional complicating factors such as double diffraction (see Appendix 6). Those books on electron diffraction techniques in Further Reading provide a more detailed and thorough coverage of these topics.

## Exercises

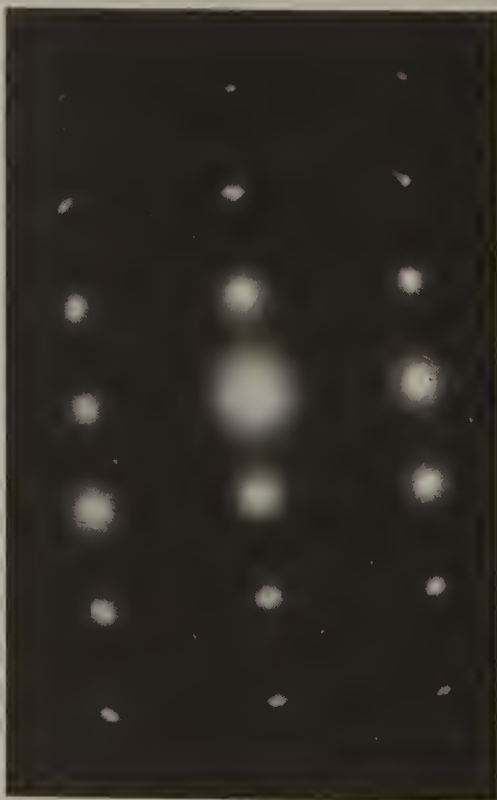
9.1 In the Laue experiment, a bcc crystal, lattice parameter  $a = 0.4$  nm ( $4 \text{ \AA}$ ) is irradiated in the  $[100]$  (or  $\mathbf{a}^*$ ) direction with an X-ray beam which contains a continuous spectrum of wavelengths in the range between  $0.167$  nm ( $1.67 \text{ \AA}$ ) and  $0.25$  nm ( $2.5 \text{ \AA}$ ). Use the reflecting sphere construction to determine the indices of the planes in the crystal for which Bragg’s law is satisfied and draw the direction of the reflected beam for *one* plane in the  $[001]$  zone.

(*Hint:* Make a scale drawing of the section of the reciprocal lattice normal to the  $[001]$  (or  $\mathbf{z}^*$ ) direction and which passes through the origin  $000$  (i.e. the section which contains the  $hk0$  reciprocal lattice points as shown in Fig. 6.4(b)). A convenient scale to use between the reciprocal lattice dimensions and A4 size drawing paper is  $1 \text{ nm}^{-1} = 0.5 \text{ cm}$  ( $1 \text{ \AA}^{-1} = 5.0 \text{ cm}$ ). Draw a line indicating the  $[100]$  direction of the incident beam and draw in the two reflecting spheres representing the limits of the wavelength range. Remember that the origin of the reciprocal lattice is located at the point where the beam *exits* from the spheres—hence the

centres of the spheres are obviously not coincident. Shade in the region of the reciprocal lattice between the two spheres; planes whose reciprocal lattice points lie in this region satisfy Bragg's law. For one reciprocal lattice point in this region, find, by construction, the sphere which it intersects. The direction of the reflected beam is from the centre of this sphere through the reciprocal lattice point, and the radius of the sphere gives the particular wavelength reflected. Draw sections of the reciprocal lattice normal to the  $[001]$  (or  $z^*$ ) direction and which pass through the  $hk1$ ,  $hk2$ ,  $hk\bar{1}$ ,  $hk\bar{2}$ , etc. reciprocal lattice points (see Fig. 6.5). In these sections of the reciprocal lattice 'above' and 'below' that through the origin, the sections of the sphere are reducing in size—simple trigonometry will show by how much. Again, planes whose reciprocal lattice points lie in the region between the spheres satisfy Bragg's law.)

- 9.2 In an oscillating crystal experiment the bcc crystal described in Exercise 9.1 is irradiated in the  $[100]$  (or  $a^*$ ) direction with a monochromatic X-ray beam of wavelength  $0.167\text{ nm}$  ( $1.67\text{ \AA}$ ). The crystal is then oscillated  $\pm 10^\circ$  about the  $[001]$  (or  $z^*$ ) direction. Find the indices  $hk0$  of the planes in the  $[001]$  zone which give rise to reflections during the oscillation of the crystal.

(*Hint:* Make a scale drawing of the section of the reciprocal lattice through the origin  $000$  and normal to the  $[001]$  (or  $z^*$ ) direction. Draw a line indicating the  $[100]$  direction of the incident beam and a single sphere corresponding to the single X-ray wavelength (see Exercise 9.1). Oscillating the crystal (at the centre of the sphere) is equivalent to oscillating the reciprocal lattice (at the origin). The simplest way to represent the relative changes in orientation between the crystal and the X-ray



**Fig. 9.22.** An electron diffraction pattern (ZOLZ) of a fcc crystal. The camera length  $L$  (adjusted for the print size) is  $715\text{ mm}$  (see Exercise 9.3).

beam is to 'oscillate' the beam. The directions of the beam at the oscillation limits are  $\pm 10^\circ$  from the  $[100]$  direction in the plane of the reciprocal lattice section. Draw in the reflecting sphere at these limits and shade in the lunes or the regions of reciprocal space through which the surface of the sphere passes. Planes whose reciprocal lattice points lie in these regions reflect the X-ray beam during oscillation.)

- 9.3 Figure 9.22 is an electron diffraction pattern of a thin crystal of aluminium (fcc,  $a = 0.4049$  nm (4.049 Å)) taken using an electron microscope operating at 100 kV, and shows diffraction spots from the ZOLZ (zero order Laue zone) only. Given the electron wavelength  $\lambda = 0.0037$  nm (0.037 Å) and the camera length  $L = 715$  mm, index the diffraction spots and determine the zone axis of the diffraction pattern. (*Note:* In face-centred lattices, reflections from the planes for which  $h$ ,  $k$  and  $l$  are not all odd or all even integers are forbidden.) (*Hint:* Refer to Table A.6.2 listing the indices  $\{hkl\}$  and  $d$ -spacings of the allowed reflecting planes. Determine the  $d_{hkl}$ -spacings of the diffraction spots in the pattern (see Section 9.7) and hence, using the table, find their indices  $\{hkl\}$ . Using the addition rule in Section 6.5.2, assign a consistent set of indices  $hkl$  to the diffraction spots and hence find their common zone axis using the equation in Section 6.5.7. Check your answer by using one of the computer programs listed in Appendix 2.)
- 9.4 In an electron diffraction experiment the bcc crystal described in Exercises 9.1 and 9.2 is irradiated in the  $[100]$  (or  $a^*$ ) direction with an electron beam of wavelength 0.002 nm (0.02 Å). Find the reciprocal lattice points which lie close to the sphere in the ZOLZ (zero order Laue zone) and FOLZ (first order Laue zone). (*Hint:* Using the same reciprocal lattice scale as in Exercises 9.1 and 9.2, it will be found that a very large sheet of paper and very large compasses are needed to draw the complete reflecting sphere! However, a sketch of the surface of the sphere near the origin will suffice. In electron diffraction, sections of the reciprocal lattice



**Fig. 9.23.** An electron diffraction pattern (ZOLZ) of a particle extracted from a nitrided chromium-containing steel. The camera constant  $\lambda L$  (adjusted for print size) is 38 Å mm (see Exercise 9.5).

perpendicular to the electron beam (i.e. normal to the [100] or  $a^*$ ) direction are most convenient. Draw the section through the origin 000 containing the  $0kl$  reciprocal lattice points (i.e. the ZOLZ), and the section containing the  $1kl$  reciprocal lattice points (i.e. the FOLZ) (see also Fig. 6.5). Estimate the regions of these reciprocal lattice sections, and hence the reciprocal lattice points, which are close to the surface of the reflecting sphere.)

9.5 Figure 9.23 is an electron diffraction pattern of a particle which has been extracted from a nitrided chromium-containing steel. It is one of three possible compounds, CrN,  $Fe_3C$  or  $(Cr,Fe)_7C_3$ . The  $d_{hkl}$ -spacings and indices of the lowest angle reflections are given below\*. Given  $\lambda L = 38 \text{ \AA mm}$ , identify the compound and index the diffraction pattern.

CrN (fcc)		$Fe_3C$ (orthorhombic)		$(Cr,Fe)_7C_3$ (hexagonal)	
$a = 4.14 \text{ \AA}$		$a = 4.524 \text{ \AA}$		$a = 13.982 \text{ \AA}$	
		$b = 5.088 \text{ \AA}$		$c = 4.506 \text{ \AA}$	
		$c = 6.741 \text{ \AA}$			
$d_{hkl}/\text{\AA}$	$hkl$	$d_{hkl}/\text{\AA}$	$hkl$	$d_{hkl}/\text{\AA}$	$hkl$
2.39	111	6.742	001	12.108	01 $\bar{1}$ 0
2.07	200	5.088	010	6.991	11 $\bar{2}$ 0
1.46	220	4.524	100	6.054	02 $\bar{2}$ 0
1.25	311	4.061	011	4.576	12 $\bar{3}$ 0
1.20	222	3.757	101	4.506	0001
1.04	400	3.381	110	4.223	01 $\bar{1}$ 1
0.950	331	3.371	002	4.036	03 $\bar{3}$ 0
0.926	420	3.022	111	3.878	11 $\bar{2}$ 1
0.845	422	2.810	012	3.615	02 $\bar{2}$ 1
0.800	511	2.703	102	3.495	22 $\bar{4}$ 0
		2.544	020	3.358	13 $\bar{4}$ 0
		2.387	112	3.211	12 $\bar{3}$ 1
		2.380	021	3.027	04 $\bar{4}$ 0
		2.262	200	3.006	03 $\bar{3}$ 1
		2.247	003	2.777	23 $\bar{5}$ 0
		2.218	120	2.767	22 $\bar{4}$ 1
		2.107	121	2.692	13 $\bar{4}$ 1
		2.067	210	2.642	14 $\bar{5}$ 1
		2.031	022	2.512	04 $\bar{4}$ 1
		2.013	103	2.421	05 $\bar{5}$ 0
		1.976	211	2.364	23 $\bar{5}$ 1
		1.872	113	2.330	23 $\bar{6}$ 0
		1.588	130	2.288	24 $\bar{6}$ 0

\* Data for CrN from the ICDD Powder Data File (11-65), for  $Fe_3C$  and  $(Cr,Fe)_7C_3$  from *Interpretation of Electron Diffraction Patterns*, 2nd edn, 1972 by K. W. Andrews, D. J. Dyson and S. R. Keown, Adam Hilger (1972).



# X-ray and electron diffraction of polycrystalline materials

## 10.1 Introduction

The preparation or synthesis of single crystals which are sufficiently large—of the order of a tenth of a millimetre or so—to be studied using the X-ray diffraction methods described in Chapter 9 is often a matter of great experimental difficulty. This is particularly the case for proteins and other complex organic crystals, the preparation of which requires considerable ingenuity and skill. However, in many situations the preparation of large single crystals is neither possible nor desirable. In materials science and petrology, for example, the crystal structures of interest are frequently those of metastable phases which occur on a very fine scale as a result of precipitation (or exsolution) from metal, ceramic or mineral matrices. As such phases grow, either as a result of natural or artificial ageing processes, their crystal structures invariably change as they evolve into more stable phases. These changes are best studied using the electron diffraction techniques outlined in Chapter 9, since electron beams can be focused down to diameters of the order of 1–10 nm, compared with beam diameters of the order of 0.1–1.0 mm for X-rays. Electron diffraction has the further advantage that crystallographic relationships between the phases and the matrices in which they occur can be investigated. Its disadvantage lies in the fact that the accuracy with which  $d_{hkl}$ -spacings can be measured is low compared to that for X-ray diffraction.

Polycrystalline or ‘powder’ X-ray diffraction techniques were developed by Debye\* and Scherrer\* and independently by Hull\* in the period 1914–1919. They may be classified as ‘fixed  $\lambda$ , varying  $\theta$ ’ techniques (see Section 9.5) in which the ‘varying  $\theta$ ’ is achieved by having a sufficiently large number of more-or-less randomly oriented crystals in the specimen such that *some* of the  $hkl$  planes in *some* of them will be orientated, by chance, at the appropriate Bragg angles for reflection. All the planes of a given  $d_{hkl}$ -spacing reflect at the same  $2\theta$  angle to the direct beam and all these reflected beams lie on a cone of semi-angle  $2\theta$  about the direct beam. The various ‘powder’ X-ray diffraction techniques may be classified as to the ways in which the cones of diffracted beams are intercepted and recorded. In situations in which the crystals are randomly oriented, the diffracted intensity in the cones will be uniform and hence only part of the cones need to be recorded. This is the case with what might be called the ‘classical’ powder camera and diffractometer techniques.

\* Denotes biographical notes available in Appendix 3.

However, in situations in which the crystals are not randomly oriented the diffracted intensity in the cones will not be uniform and, in order to determine the nature and extent of the 'non-randomness' (better described as texture or preferred orientation) the whole, or a large part, of the cones need to be recorded. This is the case with what are known as 'fibre' X-ray techniques (in which the crystals are orientated with a particular crystallographic direction (or directions) along the fibre axis) or 'sheet' techniques (in which the crystals are orientated with a particular crystal plane (or planes) parallel to the surface of the sheet).

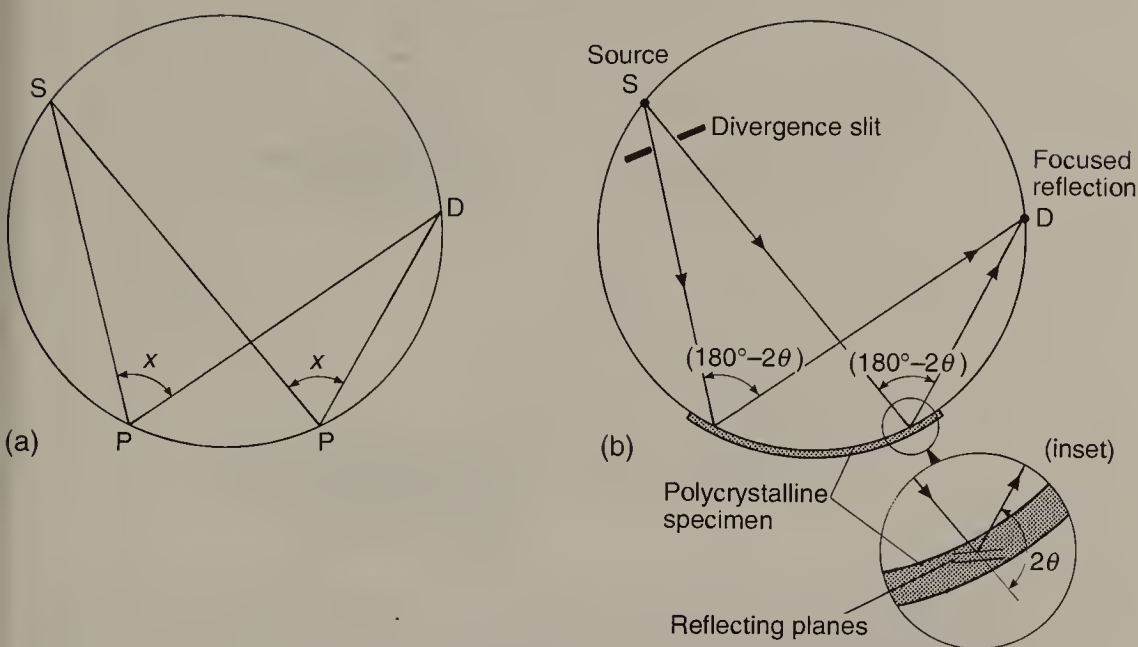
In electron diffraction the  $2\theta$  semi-angles of the cones are of course much smaller than the case with X-ray diffraction and intersect the screen of film in a series of concentric rings about the direct beam. The  $d_{hkl}$ -spacings of the rings are determined in the same way as for single crystal diffraction patterns (Section 9.7).

## 10.2 The geometrical basis of polycrystalline (powder) X-ray diffraction techniques

We begin, perhaps rather surprisingly, with a theorem which we learned off-by-heart (or should have done) in our early geometry lessons at school—never imagining that it would ever come in useful! The theorem comes from *The Elements of Euclid*, the mathematics textbook which has remained in print ever since it was first written in c. 300 B.C. The theorem, which is proved in Proposition 21, Book III of *The Elements*, states that 'the angles in the same segment of a circle are equal to one another'. It follows the other equally well known theorem (Proposition 20) that 'the angle at the centre of a circle is double that of the angle at the circumference on the same base, that is, on the same arc'.

The former theorem is illustrated (without Euclid's proof) in Fig. 10.1(a) and may be simply restated by saying that for any two points S and D on the circumference of a circle, the angle shown as  $x$  is constant irrespective of the position of point P. Now let us make use of this geometry in devising an X-ray camera (Fig. 10.1(b)). Let S be a point or slit source of monochromatic X-rays (the slit being perpendicular to the plane of the paper) and let part of the circumference P...P be 'coated' with a thin film of a polycrystalline specimen.

The X-rays diverge from the source S and in order that they should only strike the specimen we limit or collimate them with a (divergence) slit as shown. Now the angle  $x$  is, in terms of Bragg's law, the angle  $(180^\circ - 2\theta)$ —and whenever this is the correct Bragg angle for reflection for a particular set of  $hkl$  planes, reflections occur from all those crystals in the specimen which are in the right orientation and the reflected beams, as proved by Euclid, all converge to point D. In short D is a point where all the reflected beams for a particular  $d_{hkl}$  spacing are focused. Different positions of D on the circumference correspond to different  $x$ , hence different  $(180^\circ - 2\theta)$  values. Hence we will have a series of focused diffraction lines, one for each  $d_{hkl}$ -spacing in the specimen, around the circumference of the circle.



**Fig. 10.1.** (a) The geometrical basis of X-ray powder diffraction techniques; for two given points S and D on the circle, the angle  $x$  at the circumference is constant, irrespective of the position of P. (b) Application to an X-ray focusing camera. S is a source of monochromatic X-rays, the angular spread of which is collimated by a divergence slit to strike a thin layer of a powder specimen on the circumference at P...P. Angle  $x = (180^\circ - 2\theta)$ , hence any crystal planes in the right orientation for Bragg's law to be satisfied reflect to give a focused beam (as shown in the inset for a particular  $d_{hkl}$  spacing). Note that the reflecting planes are not in general tangential to the circumference of the camera, although in practice they are closely so.

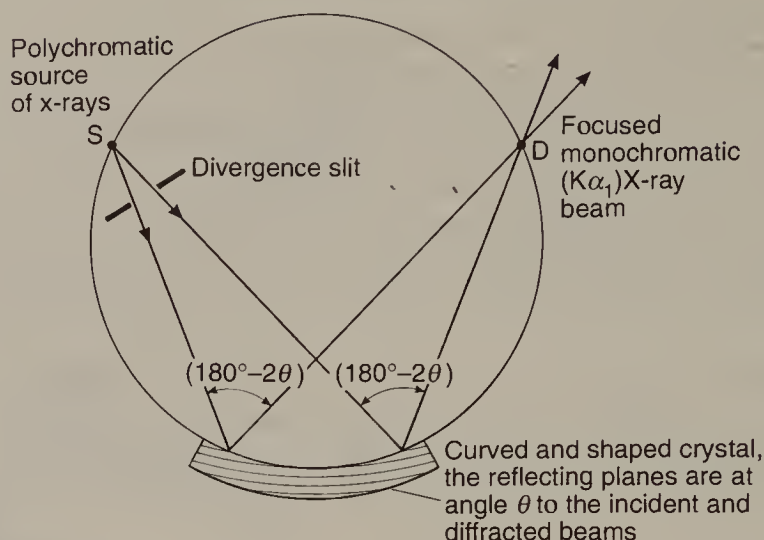
The Bragg reflecting geometry is shown in detail in the little 'inset' diagram below Fig. 10.1(b) which shows the orientation of the reflecting planes in one part of the specimen and the angle  $2\theta$  between the direct and reflected beams. Notice that the reflecting planes are not (except for some particular part of the specimen) tangential to the circumference.

A film placed around the rest of the circumference of the circle will record all the reflected beams and this arrangement is the basis of the Seeman-Bohlin camera and the variants of it devised by Guinier and Hägg. They are called **focusing X-ray methods** because they exploit the focusing geometry of Euclid's circle which is thus called the **focusing circle**.

The focusing geometry can also be used to provide a monochromatic source of X-rays (Fig. 10.2). The source S is now the line focus of an X-ray tube from which a spectrum of X-ray wavelengths (the 'white' radiation with superimposed characteristic wavelengths,  $K\alpha_1$ ,  $K\alpha_2$ ,  $K\beta$  etc.) is emitted\*. A single plate-shaped crystal is cut such that a set of strongly reflecting planes is parallel to the

\* Details of the physics of X-ray generation, X-ray spectra and the operation of X-ray tubes may be found in the appropriate books listed under 'Further Reading'. In brief, superimposed on a background of varying X-ray wavelengths (the 'white' X-radiation) there are strong components arising from specific transitions of electrons between energy levels in the atom. These are called the *characteristic* wavelengths because their wavelengths are characteristic of the atom. Monochromatization is a method by which one of these wavelengths (usually that called  $K\alpha_1$ ) is isolated from the other components and the 'white' background.





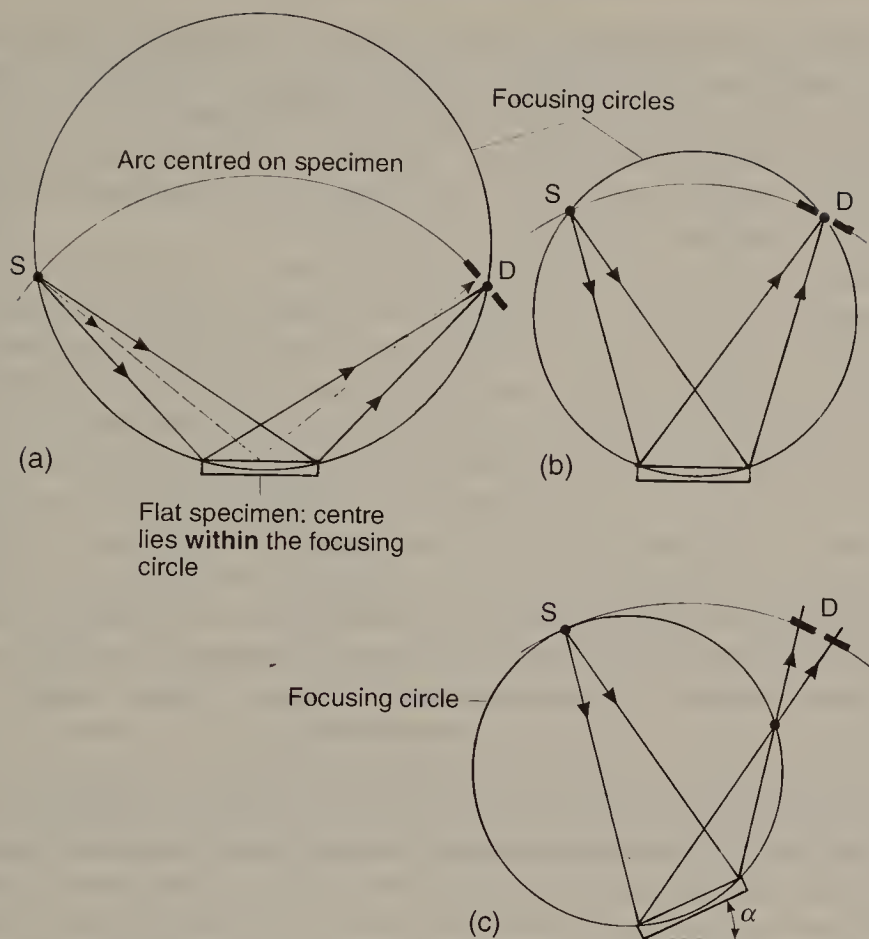
**Fig. 10.2.** The principle of the X-ray monochromator. The crystal planes are curved to a radius twice that of the focusing circle such that they make the same angle ( $\theta$ ) to the divergent incident beam. The surface of the crystal is also shaped so as to lie precisely on the focusing circle. The source and focus of the reflected beams are symmetrical (i.e. equal distances) with respect to the crystal and  $\theta$  and the  $d_{hkl}$ -spacing of the crystal planes are chosen such that only the strong  $K\alpha_1$  X-ray wavelength component is reflected.

surface. The crystal is curved or bent to a radius of curvature *twice* that of the focusing circle and then (ideally) is shaped or 'hollowed out' such that its inner surface lies along that of the focusing circle. The position of the source S, and hence the angle  $(180^\circ - 2\theta)$  is, together with the  $d_{hkl}$  spacing of the crystal planes, chosen to reflect, say, only the strong  $K\alpha_1$  component of the whole X-ray spectrum which is focused to a point or line D, symmetrical with the source S. D becomes, in effect, the line source of a beam of monochromatic X-rays, which can be used 'upstream' of the Seeman-Bohlin camera as the source S of monochromatic X-rays.

The symmetrical arrangement is also made use of in the X-ray diffractometer, which has become by far the most important classical X-ray diffraction technique. The diffractometer has become, in effect, the X-ray data acquisition end of a computer in which the data can be stored, analysed, plotted, compared with standard powder data files etc. The advantages are enormous; the disadvantage, if it can be called such, is that students may simply regard the diffractometer as a 'black box' to generate data, without understanding the principles on which the instrument works, nor the parameters underlying the data analysis procedures.

The symmetrical or Bragg-Brentano focusing geometry of the diffractometer is shown in Figs. 10.3(a) and (b). As described in Section 9.6, the source of monochromatic X-rays, S (from a monochromator upstream of the diffractometer) is at an equal distance and equal angle to the specimen surface as D, the 'receiving slit' of the detector (a proportional counter). The  $2\theta$  angle is continuously varied by the source and detector slit tracking round the arc of a circle centred on (and therefore at a fixed distance from) the specimen. Figure 10.3(a)





**Fig. 10.3.** The principle of the X-ray diffractometer. The source–specimen and specimen–detector slit distances are fixed and equal. (a) The situation for a small  $\theta$  angle and (b) for a large  $\theta$  angle, the source and detector moving round the arc of a circle centred on the specimen. Notice the change in the diameter of the focusing circle and the fact that, since the specimen is flat, complete focusing conditions are not achieved (dashed line in (a)). (c) An asymmetrical specimen arrangement for the same  $2\theta$  angle as in (b), the position and diameter of the focusing circle have changed such that the detector slit is no longer coincident with it. The reflecting planes are now those which make (approximately) angle  $\alpha$  to the specimen surface (see Fig. 9.16).

shows the situation at a low  $\theta$  angle and Fig. 10.3(b) shows the situation at a high  $\theta$  angle. In some instruments the specimen is fixed and the source and detector slit rotate in opposite senses; in others the source is fixed and the specimen and detector slit rotate in the same sense, the detector slit at twice the angular velocity of the specimen—but the result geometrically is the same.

However, the important point to note is that the polycrystalline specimen as used in a diffractometer is flat, and not curved to fit the circumference of the focusing circle. Focusing therefore is not perfect—the reflected beams from across the whole surface of the specimen do not all converge to the same point: those from the centre converge to a point a little above those from the edges, as shown in Fig. 10.3(a). The diffractometer is hence called a *semi-focusing X-ray method*. In practice the deviation from full focusing geometry is only important

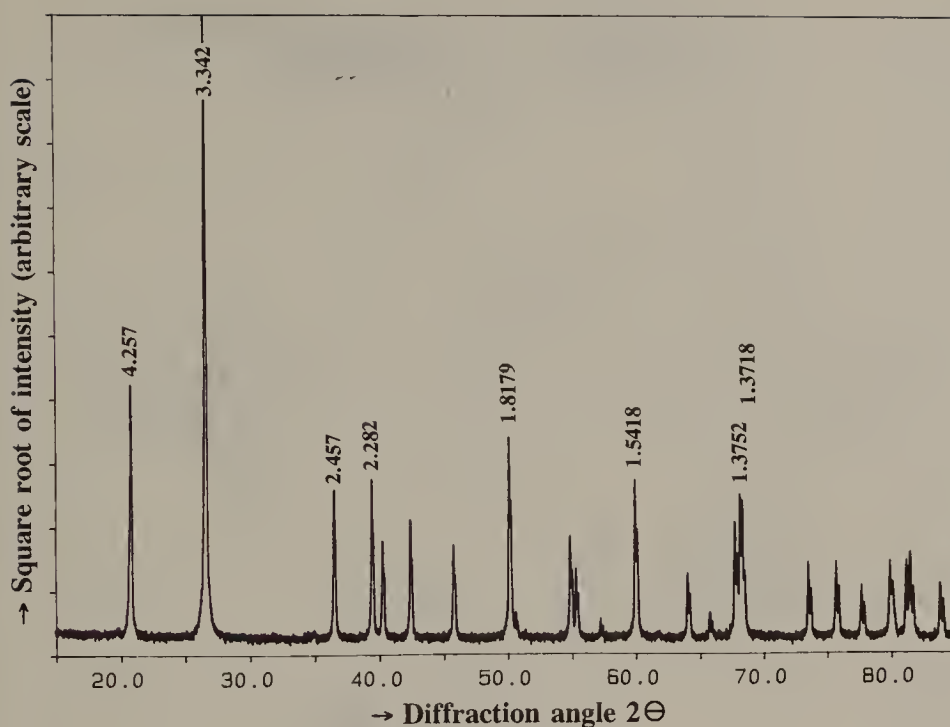
(in the symmetrical arrangement) at low  $\theta$  angles and in which a large width of specimen contributes to the reflected beam. It is not however laziness or experimental difficulty which prevents specimens being made to fit the circumference of the focusing circle, but the fact that, unlike the situation for the Seeman-Bohlin camera, the radius of the focusing circle changes with angle as is shown by a comparison with Figs 10.3(a) and (b).

As pointed out above, in the symmetrical arrangement, in which the specimen surface makes equal angles to the incident and reflected beams, the only crystal planes which contribute to the reflections are those which lie (approximately) parallel to the specimen surface, particularly when the divergence angle of the incident beam, and therefore the irradiated surface of the specimen, is small. In situations in which the  $d_{hkl}$  spacings of planes which lie at large angles to the specimen surface need to be measured (e.g. in determining the variation of lattice strains from planes in different orientations), the specimen is rotated as shown in Fig. 10.3(c); the angle of rotation  $\alpha$  is of course (approximately) equal to the angle of the reflecting planes to the specimen surface (Fig. 9.16). In doing so, however, the symmetrical Bragg-Brentano focusing geometry is lost; the focusing circle changes both in diameter and position, as shown in Fig. 10.3(c), and the detector slit is no longer at the approximate line of focus, but in this case beyond it where the beam diverges and broadens. This deviation from the focusing geometry may be serious because the observed 'broadening' at the detector slit could be misinterpreted as arising from a variation in reflection angle as a result of a variation in lattice strain. The problem may be partially overcome in two ways. First, the detector slit may be moved along a sliding-arm arrangement so as to coincide more precisely with the line of focus. However, this may itself introduce errors in the angular measurements because of the difficulty of achieving a precise radial alignment of the slider. Second, the angular divergence of the incident beam may be restricted to very low values—say  $0.25^\circ$ – $0.5^\circ$ —such that the broadening of the beam at the detector slit is very small, and this is now the preferred option.

An example of an X-ray diffractometer chart or 'trace' for quartz ( $\text{SiO}_2$ ) is given in Fig. 10.4. The  $d_{hkl}$ -spacings and relative intensities of the reflections may be used to identify the material, as described in Section 10.3 below.

There are two other 'classical' X-ray powder techniques of interest—the back reflection method in which the whole or part of the diffraction cones are recorded on flat film (an experimental arrangement identical to that for the Laue back reflection method) and the Debye-Scherrer technique in which a thin rod-shaped specimen or a powder in a capillary tube is set at the centre of a cylindrical camera.

The geometry of the back reflection powder method is shown in Fig. 10.5. The effective position of the source S is determined by the design of the collimator tube which passes through a hole in the centre of the film. In practice the divergence angle is very small, of the order  $0.5^\circ$ – $2^\circ$ . Notice that, like the diffractometer, it is a semi-focusing method—all the reflected beams from the (flat) specimen surface focus approximately at the circumference of the

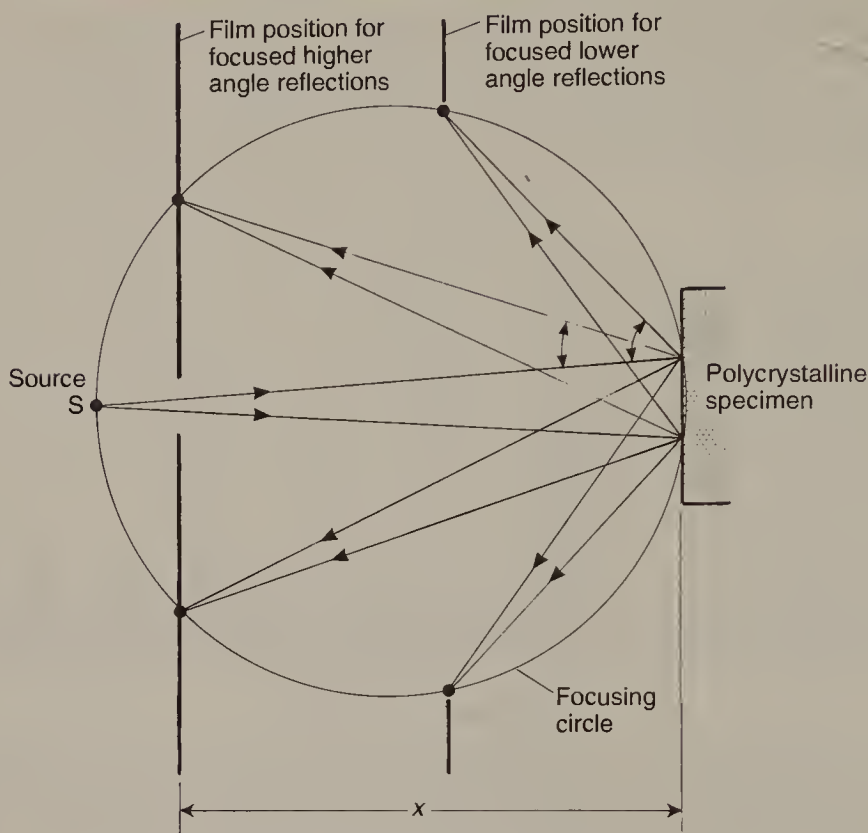


**Fig. 10.4.** An example of an X-ray diffractometer chart of intensity of the reflected beams (ordinate) vs  $2\theta$  angle (abscissa). The intensity scale is non-linear (square root) to emphasize the weaker reflections. The specimen is polycrystalline  $\text{SiO}_2$  (quartz),  $\text{CuK}\alpha_1$  radiation ( $\lambda = 1.541 \text{ \AA}$ ). The  $d$ -spacings ( $\text{\AA}$ ) of the reflections are indicated (compare with Figs. 10.7 and 10.8).

focusing circle. However, the flat film can be placed only at one distance  $x$  from the specimen: if  $x$  is the focal distance of the high  $2\theta$  angle reflections as shown, it will not be at the focal distance of the lower  $2\theta$  angle reflections. In practice a 'compromise' value of  $x$  is chosen such that the diffraction rings of particular interest are most sharply focused.

The great advantage of the Debye-Scherrer method over the diffractometer (and to a lesser extent the Seeman-Bohlin method and its variants) is that only very small amounts of material are required for, say, insertion into a capillary tube.

The geometry and specimen-film arrangement in the Debye-Scherrer camera are shown in Fig. 10.6. The cylindrical specimen (a powder in a capillary tube or a cemented powder in the form of a little rod) is placed at the centre of a cylindrical camera. The strip of film may be fitted round the circumference of the camera in several ways: it may have a single hole punched at its centre and so arranged to coincide with the 'exit' direction of the X-ray beam (the ends of the film being each side of the 'entrance' direction of the X-ray beam) or *vice versa*. However, the usual way is to punch two holes in the film, one to match the 'entrance' and the other to match the 'exit' directions of the X-ray beam, the two ends of the film now being at the 'top' or 'bottom' of the camera as shown. This 'asymmetrical' arrangement or 'setting' has the advantage that a complete



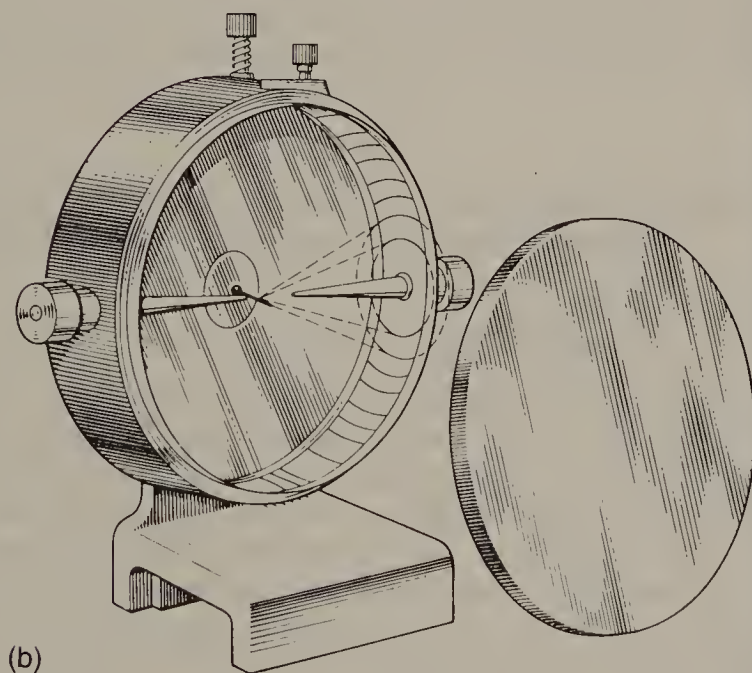
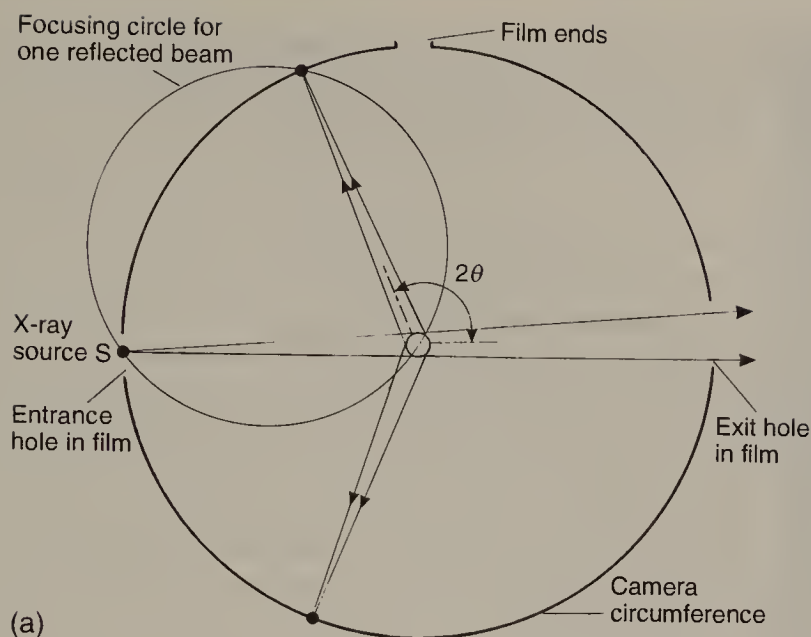
**Fig. 10.5.** The geometry of the back reflection X-ray powder method; the diverging X-ray beam from an (effective) source S passes through a hole at the centre of the film. The reflected beams for two reflections are shown. The film is shown placed at a specimen–film distance  $x$  so as to intercept the higher angle reflections such that they are sharply focused. In order to intercept the lower angle reflections such that they are sharply focused it would need to be moved closer to the specimen as indicated. In practice a ‘compromise’ value for  $x$  is chosen which is acceptable since the divergence angle, and the de-focusing of the incident beam, is small.

range of  $2\theta$  angles—from  $0^\circ$  to  $180^\circ$ —may be recorded on one side of the film without a ‘cut-off’ occasioned by the presence of a film end. In this way accurate  $d_{hkl}$ -spacings may be determined and any effects of film shrinkage accounted for.

The position of the effective source S is determined by the design of the collimator. The focusing circle for a particular reflection is shown; however, this only represents the physical situation very approximately since the reflected beams arise to different extents from the whole volume of the specimen and the position of the source S and the focusing effect is by no means as precise as that drawn in Fig. 10.6.

An example of a Debye–Scherrer film (asymmetrical setting) is shown in Fig. 10.7. The  $2\theta = 0^\circ$  and  $2\theta = 180^\circ$  positions can be worked out exactly by determining the centres of the ‘exit’ and ‘entrance’ rings, the distance between them





**Fig. 10.6.** (a) The geometry of the Debye-Scherrer camera; the reflected beams from a cylindrical specimen *tend* towards a focus on the film around the circumference of the camera and the focusing circle for a particular reflected beam is shown. In practice deviations from this idealized situation occur because the reflected beams originate with varying intensities from the whole volume of the specimen and the effective source S may not coincide with the circumference of the camera. (b) The camera with the light-tight lid removed showing the specimen at the centre, the collimator and receiving tube and the (low angle) X-ray diffraction rings on the film. The screws at the top are for locating and fixing the ends of the film (from *Manual of Mineralogy*, 21st edn, by C. Klein and C. S. Hurlbut Jr., John Wiley & Sons Inc., 1993).



**Fig. 10.7.** An example of a Debye-Scherrer X-ray film ( $\text{CuK}\alpha$  X-radiation) for  $\text{SiO}_2$  (quartz). S is the 'entrance' hole and O the 'exit' hole. The 'spotty' appearance of the rings arises because of the relatively coarse crystallite size in the specimen. At high  $2\theta$  angles (near the entrance hole) the  $\text{K}\alpha_1/\text{K}\alpha_2$  doublets are resolved but at low  $2\theta$  angles (near the exit hole) they are unresolved. The streaks around the exit hole arise from the presence of residual 'white' X-radiation in the incident beam.

on the film corresponding to  $180^\circ$  exactly. Hence the camera diameter does not need to be known, although in practice cameras are made with diameters 57.53 mm or 114.83 mm such that (and accounting for film thickness) the circumference is 180 mm or 360 mm. Hence for quick work the angles can simply read in terms of millimetres on the film.

Finally, a note about X-ray diffraction techniques for materials in which the crystals are in a preferred orientation—fibres or sheets. Fibres may be examined in an oscillation or rotation camera in the same way as for single crystals (Section 9.6), the important measurement being the spacings between the layer lines which correspond to the repeat distance of the crystallographic direction aligned along the fibre axis. The cones of reflected beams of non-uniform intensity for both fibres and sheets may be recorded using flat plate film methods (such as the back reflection method shown in Fig. 10.5), separate exposures being made for different settings of the specimen. Such data however is not easy to quantify because the observed intensities are also affected by extraneous factors such as absorption in the specimen, etc. By far the most useful techniques are those in which the specimen is mounted in a goniometer, the diffracted intensity for particular reflections being measured by a counter, the data processed by a computer and plotted out in the form of pole figures or an orientation distribution function (ODF).

### 10.3 Some applications of X-ray and electron diffraction techniques in polycrystalline materials

#### 10.3.1 Accurate lattice parameter measurements

The accurate measurement of  $d_{hkl}$ -spacings is now largely carried out with the X-ray diffractometer using monochromatized ( $K\alpha_1$ ) radiation, narrow divergence and receiving slit systems, internal calibration systems and peak profile measurement procedures. However, as shown below, it is the high  $2\theta$  angle reflections which are most sensitive to small variations in  $d_{hkl}$ -spacings and for this reason the Debye–Scherrer powder camera and back reflection flat film techniques in which  $2\theta$  angles up to nearly  $180^\circ$  can be recorded, are still used. By contrast, the largest  $2\theta$  angles measurable with a diffractometer are about  $150^\circ$  because the near approach and possible contact between the source and receiving slit assemblies.

Given the crystal system and the  $hkl$  values of the reflections, the lattice parameter(s) can be determined using the appropriate equation (Appendix A4.1). This procedure is clearly simplest for the cubic system in which the  $d_{hkl}$ -values depend only upon the one variable,  $a$ . In other systems several  $d_{hkl}$ -spacings need to be measured and the values inserted into simultaneous equations from which values of the lattice parameters are extracted.

The sensitivity of change of the  $2\theta$  angle for a reflection with a change in  $d_{hkl}$ -spacing is a measure of the resolving power of the diffraction technique.

The resolving power, or rather the limit of resolution,  $\delta d/d$ , can be obtained by differentiating Bragg's law with respect to  $d$  and  $\theta$  ( $\lambda$  fixed), i.e.

$$\lambda = 2d \sin \theta$$

differentiating:

$$0 = 2d \cos \theta \delta \theta + 2 \sin \theta \delta d$$

hence

$$\delta d/d = -\cot \theta \delta \theta.$$

This equation may be 'read' in two ways. For a given value of  $2 \delta \theta$ , which may be expressed in terms of the minimum resolved distance between two reflections on the film, chart, etc., for the smallest limit of resolution we want  $\cot \theta$  values to be as small as possible; or, for a given value of  $\delta d/d$ , we want the angular separation of the reflections  $2 \delta \theta$  to be as large, and hence again  $\cot \theta$  values to be as small as possible.

A glance at cotangent tables shows that  $\cot \theta$  values are high at low  $\theta$  angles and rapidly decrease towards zero as  $\theta$  approaches  $90^\circ$ . Hence  $d_{hkl}$ -spacing measurements are most accurate using high-angle X-ray diffraction methods and least accurate with low-angle electron diffraction methods.

### 10.3.2 Identification of unknown phases

For powder specimens in which the crystals are randomly orientated, the set of  $d$ -spacings and their relative intensities serves as a 'fingerprint' (or 'genetic strand') from which the phase can be identified by comparison with the 'fingerprints' of phases in the *X-ray Powder Diffraction File*—a data bank of over 70 000 inorganic and 20 000 organic phases. The File is administered by the International Centre for Diffraction Data (ICDD)—formerly the Joint Committee for Powder Diffraction Standards (JCPDS)—and new and revised sets of data are published annually in book form (replacing the original 5 inch by 3 inch cards) or as a computer database. In addition, there are published Indexes with the phases arranged alphabetically by chemical name, search manuals and abstracts from the File (including Indexes and Search Manuals) or Frequently Encountered Phases (FEP).

The entry for each phase in the File or computer database (which differ slightly in their layout) includes: file number, chemical formula and name, experimental conditions, physical and optical data (where known), references and the set of  $d$ -spacings (given in Å), their Laue indices and their relative intensities arranged in order of decreasing  $d$ -spacing. Finally, the ICDD editors assign a 'quality mark' to indicate the reliability of the data (e.g. a '\*' indicates that the chemistry, structure and X-ray data of the phase is well characterized); or whether the X-ray data has been derived by calculation, rather than observed (a 'c' mark). Figure 10.8 shows an example of a Powder Diffraction File card, that for quartz, set number 33, card number 1161.

A comparison of an unknown phase with 70 000 others is potentially a daunting task! It is greatly facilitated by a search procedure based on that first



33-1161



SiO <sub>2</sub>					d Å	Int	hkl	d Å	Int	hkl
Silicon Oxide Quartz, syn					4.257	22	100	1.1532	1	311
					3.342	100	101	1.1405	<1	204
					2.457	8	110	1.1143	<1	303
					2.282	8	102	1.0813	2	312
					2.237	4	111	1.0635	<1	400
					2.127	6	200	1.0476	1	105
					1.9792	4	201	1.0338	<1	401
					1.8179	14	112	1.0347	<1	214
					1.8021	<1	003	1.0150	1	223
					1.6719	4	202	0.9898	1	402
					1.6591	2	103	0.9873	1	313
					1.6082	<1	210	0.9783	<1	304
					1.5418	9	211	0.9762	1	320
					1.4536	1	113	0.9636	<1	205
					1.4189	<1	300			
					1.3820	6	212			
					1.3752	7	203			
					1.3718	8	301			
					1.2880	2	104			
					1.2558	2	302			
					1.2285	1	220			
					1.1999	2	213			
					1.1978	1	221			
					1.1843	3	114			
					1.1804	3	310			

**Fig. 10.8.** The Powder Diffraction File Card No. 33-1161, for quartz. The left-hand side gives crystallographic, optical and physical information and the source of the data. The right-hand side lists the  $d$ -spacings, in descending order, with the strongest line assigned an intensity of 100. Formerly (up to set 24) the cards included along the top left edge the  $d$ -spacings of the three strongest lines and the largest  $d$ -spacing recorded in the pattern. (International Centre for Diffraction Data).

devised by J. D. Hanawalt in 1936 and now refined and speeded up using computer search procedures.

The phases are grouped together (into what is known as Hanawalt groups) according to the  $d$ -spacing of their strongest reflection. There are forty Hanawalt groups covering the whole range of  $d$ -spacings. For example, the strongest line of quartz (relative intensity 100) is that at 3.34 Å (Figs 10.4 and 10.7); quartz therefore lies in the Hanawalt group with  $d$ -spacings in the range from 3.39 to 3.32 Å (Figure 10.9—first column). Within each Hanawalt group the patterns are listed in the second column in order of decreasing  $d$ -spacings of the second strongest line which for quartz is that at 4.26 Å; on reading down the list of patterns in the second column of the Hanawalt group a potential 'match' can be made with the second strongest line and then (from the number of possibilities available) final confirmation made with the  $d$ -spacings and intensities of the third, fourth etc. strongest lines in the subsequent columns. Figure 10.9 is from the Hanawalt Inorganic Search Manual showing some entries in the Hanawalt group 3.39–3.32 Å which includes that for quartz, File No. 33-1161.

In practice the procedure is by no means as straightforward as this. First, many minerals and metallic alloys give very nearly the same diffraction pattern because of the existence of solid solution ranges, which result in very small shifts in lattice parameter. Second, the crystals in the powder specimen may not be

3.39 – 3.32 ( + 02)													File No	File
i	3.31 <sub>x</sub>	4.30 <sub>6</sub>	4.53 <sub>4</sub>	2.03 <sub>4</sub>	2.85 <sub>1</sub>	2.00 <sub>4</sub>	7.74 <sub>1</sub>	3.24 <sub>1</sub>	Na <sub>2</sub> CeF <sub>11</sub>				25 – 817	
i	3.30 <sub>x</sub>	4.30 <sub>6</sub>	2.13 <sub>3</sub>	2.79 <sub>3</sub>	2.33 <sub>3</sub>	2.01 <sub>1</sub>	1.79 <sub>3</sub>	1.52	Hg <sub>2</sub> Br <sub>2</sub> Kuzminite, syn				8 – 468	
	3.40 <sub>x</sub>	4.29 <sub>6</sub>	4.09 <sub>6</sub>	6.63 <sub>3</sub>	4.82 <sub>4</sub>	3.31 <sub>4</sub>	2.67 <sub>4</sub>	2.33 <sub>4</sub>	ClF <sub>3</sub> OB <sub>2</sub> F <sub>3</sub>				26 – 235	
	3.39 <sub>x</sub>	4.29 <sub>6</sub>	5.88 <sub>8</sub>	3.12 <sub>8</sub>	2.98 <sub>8</sub>	2.30 <sub>8</sub>	1.96 <sub>8</sub>	1.78 <sub>8</sub>	Li <sub>2</sub> 33Fe <sub>10</sub> Si <sub>5</sub>				36 – 1089	
	3.39 <sub>x</sub>	4.29 <sub>6</sub>	2.47 <sub>1</sub>	2.31 <sub>1</sub>	2.23 <sub>1</sub>	2.14 <sub>1</sub>	1.99 <sub>1</sub>	1.83 <sub>1</sub>	BPO <sub>4</sub>				11 – 237	
o	3.36 <sub>6</sub>	4.29 <sub>x</sub>	2.85 <sub>6</sub>	5.60 <sub>3</sub>	4.02 <sub>3</sub>	2.58 <sub>3</sub>	1.98 <sub>3</sub>	1.90 <sub>3</sub>	V <sub>0.87</sub> Cr <sub>0.13</sub> O <sub>2.7</sub>				35 – 332	
i	3.35 <sub>x</sub>	4.29 <sub>x</sub>	3.43 <sub>6</sub>	2.02 <sub>6</sub>	4.35 <sub>6</sub>	3.39 <sub>6</sub>	2.07 <sub>6</sub>	4.93 <sub>3</sub>	KNaSiF <sub>6</sub>				38 – 686	
i	3.34 <sub>x</sub>	4.29 <sub>x</sub>	10.5 <sub>6</sub>	2.64 <sub>6</sub>	2.71 <sub>6</sub>	5.27 <sub>6</sub>	3.79 <sub>6</sub>	3.79 <sub>6</sub>	Na <sub>2</sub> Ta <sub>2</sub> O <sub>6</sub> F <sub>3</sub>				25 – 871	
	3.32 <sub>x</sub>	4.29 <sub>6</sub>	2.99 <sub>6</sub>	2.87 <sub>6</sub>	2.52 <sub>6</sub>	4.70 <sub>6</sub>	2.38 <sub>6</sub>	2.30 <sub>6</sub>	Cs <sub>2</sub> Al(NO <sub>3</sub> ) <sub>3</sub>				28 – 274	
o	3.31 <sub>x</sub>	4.29 <sub>x</sub>	3.68 <sub>x</sub>	2.91 <sub>x</sub>	2.34 <sub>x</sub>	2.06 <sub>x</sub>	1.99 <sub>x</sub>	1.93 <sub>x</sub>	Pu(OH)CO <sub>3</sub> · xH <sub>2</sub> O				33 – 982	
i	3.37 <sub>x</sub>	4.28 <sub>3</sub>	1.84 <sub>2</sub>	1.55 <sub>1</sub>	2.47 <sub>1</sub>	2.31 <sub>1</sub>	1.39 <sub>1</sub>	2.14 <sub>1</sub>	AlPO <sub>4</sub> Berlinite, syn				10 – 423	
	3.35 <sub>6</sub>	4.28 <sub>x</sub>	3.71 <sub>6</sub>	2.85 <sub>6</sub>	2.17 <sub>6</sub>	4.07 <sub>6</sub>	3.03 <sub>6</sub>	2.73 <sub>6</sub>	K <sub>2</sub> N <sub>2</sub> V <sub>6</sub> O <sub>21</sub>				20 – 1379	
	3.35 <sub>x</sub>	4.28 <sub>6</sub>	2.97 <sub>1</sub>	1.91 <sub>6</sub>	7.61 <sub>3</sub>	2.21 <sub>6</sub>	1.63 <sub>6</sub>	1.38 <sub>6</sub>	(Zn <sub>2</sub> Co <sub>2</sub> Al <sub>2</sub> P <sub>2</sub> H <sub>6</sub> O <sub>12</sub> · 3H <sub>2</sub> O) Kehoite				27 – 94	
i	3.34 <sub>x</sub>	4.28 <sub>3</sub>	4.27 <sub>3</sub>	3.38 <sub>3</sub>	2.77 <sub>3</sub>	2.33 <sub>3</sub>	2.79 <sub>3</sub>	2.32 <sub>3</sub>	CsLiSeO <sub>4</sub>				29 – 411	2.60
i	3.33 <sub>x</sub>	4.28 <sub>x</sub>	3.24 <sub>x</sub>	8.58 <sub>8</sub>	2.91 <sub>8</sub>	2.37 <sub>8</sub>	1.87 <sub>8</sub>	4.95 <sub>3</sub>	Cs <sub>30</sub> 33V <sub>5</sub> O <sub>7</sub>				30 – 385	
i	3.34 <sub>x</sub>	4.27 <sub>1</sub>	3.19 <sub>2</sub>	2.70 <sub>2</sub>	7.28 <sub>3</sub>	4.91 <sub>3</sub>	1.82 <sub>3</sub>	3.13 <sub>3</sub>	CaAl <sub>2</sub> Si <sub>2</sub> O <sub>8</sub> · 4H <sub>2</sub> O Gismondine				20 – 452	
i	3.30 <sub>x</sub>	4.27 <sub>1</sub>	3.71 <sub>1</sub>	3.45 <sub>1</sub>	3.92 <sub>1</sub>	3.34 <sub>1</sub>	3.27 <sub>1</sub>	2.96 <sub>1</sub>	KFeSi <sub>2</sub> O <sub>7</sub>				16 – 153	
	3.38 <sub>x</sub>	4.26 <sub>x</sub>	4.16 <sub>x</sub>	1.68 <sub>6</sub>	6.70 <sub>6</sub>	2.97 <sub>6</sub>	2.86 <sub>6</sub>	2.56 <sub>6</sub>	Cs <sub>2</sub> VCl <sub>4</sub> · 4H <sub>2</sub> O				20 – 301	
i	3.37 <sub>x</sub>	4.26 <sub>6</sub>	4.18 <sub>6</sub>	2.98 <sub>6</sub>	8.56 <sub>6</sub>	6.76 <sub>6</sub>	3.49 <sub>6</sub>	3.09 <sub>6</sub>	Cs <sub>2</sub> VCl <sub>4</sub> · 4H <sub>2</sub> O				34 – 322	
o	3.36 <sub>x</sub>	4.26 <sub>x</sub>	4.21 <sub>x</sub>	2.86 <sub>x</sub>	5.99 <sub>6</sub>	5.55 <sub>6</sub>	3.26 <sub>6</sub>	2.94 <sub>6</sub>	KAlH(P <sub>3</sub> O <sub>10</sub> )				38 – 55	
o	3.36 <sub>6</sub>	4.26 <sub>x</sub>	2.98 <sub>x</sub>	5.95 <sub>6</sub>	5.55 <sub>6</sub>	4.02 <sub>6</sub>	3.26 <sub>6</sub>	2.87 <sub>6</sub>	KCrHP <sub>3</sub> O <sub>10</sub>				41 – 442	
	3.34 <sub>x</sub>	4.26 <sub>6</sub>	3.66 <sub>6</sub>	2.61 <sub>6</sub>	2.48 <sub>6</sub>	1.80 <sub>6</sub>	3.97 <sub>6</sub>	3.05 <sub>6</sub>	3PbCO <sub>3</sub> · 2Pb(OH) <sub>2</sub> · H <sub>2</sub> O				9 – 356	
i	3.34 <sub>x</sub>	4.26 <sub>2</sub>	2.13 <sub>2</sub>	7.40 <sub>3</sub>	3.49 <sub>3</sub>	2.58 <sub>3</sub>	2.24 <sub>3</sub>	2.21 <sub>3</sub>	Ca <sub>2</sub> Gd <sub>2</sub> (SO <sub>4</sub> ) <sub>12</sub> (OH) <sub>6</sub> · 3H <sub>2</sub> O Schaurteite				19 – 225	
	3.34 <sub>x</sub>	4.26 <sub>2</sub>	2.13 <sub>2</sub>	7.40 <sub>3</sub>	2.57 <sub>3</sub>	2.03 <sub>3</sub>	3.49 <sub>3</sub>	2.24 <sub>3</sub>	Ca <sub>2</sub> Mn <sub>2</sub> (SO <sub>4</sub> ) <sub>12</sub> (OH) <sub>6</sub> · 3H <sub>2</sub> O Oespujolsite				20 – 226	
*	3.34 <sub>x</sub>	4.26 <sub>2</sub>	1.82 <sub>1</sub>	1.54 <sub>1</sub>	2.46 <sub>1</sub>	2.28 <sub>1</sub>	1.37 <sub>1</sub>	1.38 <sub>1</sub>	SiO <sub>2</sub> Quartz, syn silica				33 – 1161	3.60
o	3.33 <sub>x</sub>	4.26 <sub>6</sub>	3.27 <sub>6</sub>	4.31 <sub>3</sub>	2.89 <sub>3</sub>	2.75 <sub>3</sub>	3.88 <sub>3</sub>	3.19 <sub>3</sub>	K <sub>2</sub> Ca(VO <sub>3</sub> ) <sub>4</sub>				37 – 180	
	3.30 <sub>x</sub>	4.26 <sub>6</sub>	4.24 <sub>6</sub>	3.66 <sub>6</sub>	2.89 <sub>6</sub>	2.30 <sub>6</sub>	2.63 <sub>6</sub>	2.32 <sub>6</sub>	5m <sub>2</sub> O(CO <sub>3</sub> ) <sub>12</sub> · xH <sub>2</sub> O				28 – 994	
	3.31 <sub>6</sub>	4.25 <sub>x</sub>	4.09 <sub>6</sub>	3.72 <sub>6</sub>	2.98 <sub>6</sub>	2.20 <sub>6</sub>	1.93 <sub>6</sub>	5.47 <sub>6</sub>	ClPiOF <sub>11</sub>				26 – 415	
	3.30 <sub>6</sub>	4.25 <sub>x</sub>	4.09 <sub>6</sub>	3.67 <sub>6</sub>	7.42 <sub>6</sub>	5.47 <sub>6</sub>	2.96 <sub>6</sub>	1.91 <sub>6</sub>	(ClF <sub>2</sub> O)AsF <sub>6</sub>				26 – 117	
	3.40 <sub>x</sub>	4.24 <sub>6</sub>	3.00 <sub>6</sub>	5.72 <sub>1</sub>	2.65 <sub>1</sub>	2.85 <sub>1</sub>	2.37 <sub>1</sub>	0.00 <sub>1</sub>	KAuF <sub>4</sub>				27 – 395	
*	3.37 <sub>x</sub>	4.24 <sub>3</sub>	2.32 <sub>2</sub>	2.12 <sub>2</sub>	2.45 <sub>1</sub>	1.84 <sub>1</sub>	1.83 <sub>1</sub>	1.54 <sub>1</sub>	GePO <sub>4</sub>				8 – 497	
o	3.36 <sub>x</sub>	4.24 <sub>6</sub>	2.86 <sub>x</sub>	5.90 <sub>6</sub>	5.55 <sub>6</sub>	3.26 <sub>6</sub>	2.94 <sub>6</sub>	6.60 <sub>6</sub>	KAlH(P <sub>3</sub> O <sub>10</sub> )				38 – 55	
*	3.33 <sub>x</sub>	4.24 <sub>6</sub>	3.39 <sub>6</sub>	2.64 <sub>6</sub>	3.25 <sub>6</sub>	2.60 <sub>6</sub>	4.38 <sub>6</sub>	3.44 <sub>6</sub>	SrUMa <sub>2</sub> O <sub>16</sub>				38 – 1360	
i	3.41 <sub>6</sub>	4.23 <sub>x</sub>	2.87 <sub>x</sub>	2.49 <sub>6</sub>	2.06 <sub>6</sub>	1.99 <sub>6</sub>	1.95 <sub>6</sub>	1.93 <sub>6</sub>	Li <sub>2</sub> WP <sub>2</sub>				35 – 1467	
	3.39 <sub>6</sub>	4.23 <sub>x</sub>	5.06 <sub>6</sub>	3.45 <sub>6</sub>	3.18 <sub>6</sub>	3.05 <sub>6</sub>	5.25 <sub>6</sub>	3.76 <sub>6</sub>	RbAl <sub>2</sub> (H <sub>2</sub> P <sub>2</sub> O <sub>7</sub> ) <sub>2</sub> (P <sub>4</sub> O <sub>12</sub> )				37 – 261	
o	3.39 <sub>6</sub>	4.23 <sub>x</sub>	2.99 <sub>x</sub>	2.89 <sub>6</sub>	2.77 <sub>6</sub>	5.93 <sub>3</sub>	3.24 <sub>3</sub>	4.75 <sub>3</sub>	RbGaHP <sub>3</sub> O <sub>10</sub>				34 – 1347	
o	3.37 <sub>x</sub>	4.23 <sub>x</sub>	3.46 <sub>x</sub>	3.00 <sub>6</sub>	2.13 <sub>6</sub>	6.00 <sub>6</sub>	2.69 <sub>6</sub>	2.45 <sub>6</sub>	CsSnFBr				30 – 369	
o	3.36 <sub>x</sub>	4.23 <sub>x</sub>	2.37 <sub>x</sub>	2.29 <sub>6</sub>	2.15 <sub>6</sub>	1.90 <sub>6</sub>	9.50 <sub>6</sub>	3.95 <sub>6</sub>	Al <sub>14</sub> La <sub>2</sub> S <sub>13</sub>				41 – 734	
o	3.36 <sub>x</sub>	4.23 <sub>3</sub>	1.64 <sub>3</sub>	2.72 <sub>4</sub>	2.44 <sub>3</sub>	2.22 <sub>4</sub>	1.93 <sub>3</sub>	3.14 <sub>3</sub>	Mo <sub>2</sub> O <sub>3</sub> · xH <sub>2</sub> O Ilseemannite				21 – 574	
	3.35 <sub>6</sub>	4.23 <sub>x</sub>	3.12 <sub>x</sub>	3.43 <sub>6</sub>	3.84 <sub>6</sub>	3.75 <sub>6</sub>	3.39 <sub>6</sub>	3.37 <sub>6</sub>	β-Cs <sub>2</sub> Cu(SO <sub>4</sub> ) <sub>2</sub>				28 – 288	
o	3.40 <sub>x</sub>	4.22 <sub>6</sub>	3.20 <sub>6</sub>	3.14 <sub>6</sub>	5.81 <sub>6</sub>	3.62 <sub>6</sub>	3.03 <sub>6</sub>	2.64 <sub>6</sub>	Na <sub>2</sub> VO <sub>2</sub> (SO <sub>4</sub> ) <sub>2</sub>				41 – 175	
	3.41 <sub>6</sub>	4.21 <sub>x</sub>	3.11 <sub>x</sub>	2.75 <sub>6</sub>	7.58 <sub>6</sub>	5.60 <sub>6</sub>	4.46 <sub>6</sub>	3.31 <sub>6</sub>	Na <sub>2</sub> SbF <sub>3</sub> SO <sub>4</sub>				28 – 1038	
o	3.41 <sub>6</sub>	4.21 <sub>x</sub>	2.99 <sub>x</sub>	3.24 <sub>6</sub>	2.91 <sub>6</sub>	2.77 <sub>6</sub>	5.95 <sub>6</sub>	4.77 <sub>6</sub>	RbCrHP <sub>3</sub> O <sub>10</sub>				41 – 443	
o	3.39 <sub>x</sub>	4.21 <sub>6</sub>	3.92 <sub>6</sub>	2.78 <sub>6</sub>	1.89 <sub>6</sub>	3.78 <sub>6</sub>	2.96 <sub>6</sub>	2.08 <sub>6</sub>	Pb <sub>2</sub> Sb <sub>2</sub> S <sub>3</sub>				36 – 94	
	3.33 <sub>6</sub>	4.21 <sub>x</sub>	3.82 <sub>2</sub>	2.96 <sub>2</sub>	2.47 <sub>2</sub>	2.34 <sub>2</sub>	2.01 <sub>2</sub>	1.89 <sub>2</sub>	CsXeOF <sub>5</sub>				35 – 1267	
o	3.41 <sub>6</sub>	4.20 <sub>x</sub>	3.65 <sub>x</sub>	2.77 <sub>2</sub>	2.71 <sub>2</sub>	2.96 <sub>2</sub>	2.11 <sub>2</sub>	4.00 <sub>4</sub>	Ti <sub>2</sub> Si <sub>2</sub> S <sub>3</sub>				38 – 914	
o	3.33 <sub>x</sub>	4.20 <sub>6</sub>	3.08 <sub>6</sub>	2.73 <sub>6</sub>	1.80 <sub>6</sub>	3.00 <sub>6</sub>	2.48 <sub>6</sub>	1.56 <sub>6</sub>	PbMoP <sub>3</sub> O <sub>9</sub>				36 – 198	
	3.39 <sub>x</sub>	4.19 <sub>6</sub>	3.67 <sub>6</sub>	2.81 <sub>6</sub>	2.53 <sub>6</sub>	2.17 <sub>6</sub>	1.89 <sub>6</sub>	1.94 <sub>6</sub>	Li <sub>2</sub> H <sub>2</sub> Si <sub>2</sub> O <sub>7</sub>				23 – 1185	
i	3.35 <sub>x</sub>	4.18 <sub>6</sub>	2.95 <sub>6</sub>	5.59 <sub>6</sub>	2.61 <sub>6</sub>	2.31 <sub>6</sub>	0.00 <sub>6</sub>	0.00 <sub>6</sub>	KAgF <sub>4</sub>				26 – 1464	
	3.32 <sub>x</sub>	4.18 <sub>6</sub>	3.59 <sub>6</sub>	4.30 <sub>6</sub>	3.70 <sub>6</sub>	2.82 <sub>6</sub>	2.77 <sub>6</sub>	2.08 <sub>6</sub>	CsVO <sub>2</sub> SO <sub>4</sub>				36 – 704	

**Fig. 10.9.** Part of the Hanawalt Search Manual for Inorganic Phases, showing some entries in the Hanawalt Group 3.39–3.32 Å. The intensities of the reflections are indicated by subscripts  $x = 100$ ,  $9 = 90$ ,  $8 = 80$  and so on. Notice that some patterns are entered in this Hanawalt Group according to their *second*-strongest or *third*-strongest lines; e.g.  $K_2N_2V_6O_{21}$  (20-1379) or  $RbGaHP_3O_{10}$  (34-1347) respectively. This is because they have intensities over 75% of that of the strongest line and may experimentally be identified as the strongest lines. (International Centre for Diffraction Data).

randomly orientated—the specimen may be textured or may show preferred orientation, which implies that the relative intensities of the reflections may be altered as compared with those in the File. Third, the unknown specimen may consist of more than one phase—and if they are in roughly equal proportions the strongest lines may be ‘mixed up’.

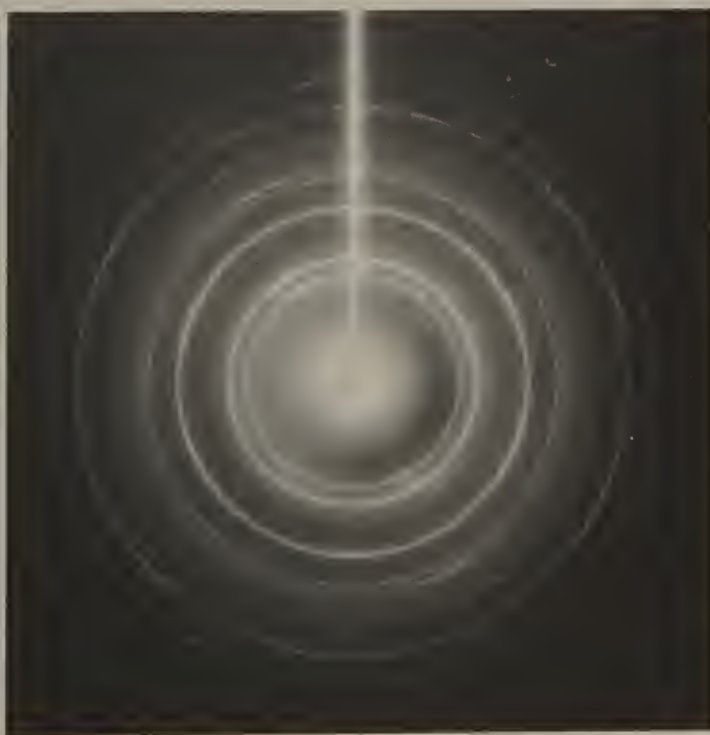
These problems are partly (but not wholly) circumvented by a series of ‘entry rules’, the details of which are given in the Search Manual. First, those patterns in which the  $d$ -spacing of the strongest reflection lies close to one of the boundary values of the Hanawalt group are entered in both groups—the one above and the one below. Second, those patterns in which the intensity of the second strongest reflection is greater than 75% of the intensity of the strongest (and in which there is therefore a strong possibility of the mis-identification of the strongest reflection) are entered twice; the second strongest reflection

determining the Hanawalt group and the position in the group listed (as before) in accordance with the (decreasing)  $d$ -spacing of the second strongest reflection. Similar rules apply to the third and fourth strongest reflections such that a pattern may be listed several times. Examples of such permutations are shown in Fig. 10.9.

The Powder Diffraction File may be used to identify polycrystalline specimens from their electron diffraction patterns. However, its use is much more limited owing to the fact that the  $d$ -spacings of the diffraction rings can be measured to a much lower level of accuracy and only qualitative estimates can be made of their relative intensities. Hence the use of search procedures, as described above, is uncommon. Usually we have a fair idea as to what the specimen might be and make direct comparisons between the experimental data and that of 'possible' patterns in the File. Exercise 9.5 gives an example of this in the case of a single-crystal electron diffraction pattern.

Figure 10.10 gives an example of an electron diffraction 'ring' pattern from a fine-grained polycrystalline thin foil specimen of aluminium. It is, in effect, the superposition of many single-crystal patterns. Notice the variations in intensity and the sequence of spacings of the rings. Aluminium can immediately be recognized as having the fcc structure since the rings occur in the characteristic sequence 'two-together', 'one-on-its-own', 'two-together' etc. (see Note 3, Table A6.2). Hence the rings may simply be indexed 'by inspection', i.e.

111, 200,                      220,                      311, 222,                      400,                      331, 420.



**Fig. 10.10.** An electron diffraction pattern of polycrystalline aluminium, showing varying intensities of the diffraction rings and the sequence of ring spacings characteristic of the fcc structure.



### 10.3.3 Measurement of crystal (grain) size

This is based on the determination of  $\beta$ , the line broadening in the Scherrer equation (Section 9.3) and an estimate of  $K$ , the 'shape' correction factor (which does not differ significantly from unity). However, this is not a straightforward business because the *observed* broadening,  $\beta_{\text{obs}}$ , also includes 'instrumental' factors such as detector slit width, area of specimen irradiated, possible presence of a  $K\alpha_2$  component in the X-ray beam etc. The contributions from these factors have to be 'subtracted' from the observed peak breadth (or, strictly speaking, they have to be deconvoluted from the peak). The usual procedure is to measure the instrumental broadening,  $\beta_{\text{inst}}$ , in a large-grained material in which grain size broadening is assumed to be negligible, and to determine  $\beta$  either by a simple subtraction, due to Scherrer, i.e.  $\beta = \beta_{\text{obs}} - \beta_{\text{inst}}$ , or by a subtraction of squares, due to Warren, i.e.  $\beta^2 = \beta_{\text{obs}}^2 - \beta_{\text{inst}}^2$ . In practice, attempts to measure 'absolute' grain sizes by X-ray diffraction are fraught with difficulty because of the presence of imperfections (particularly sub-grain boundaries), lattice strains etc. which contribute to the broadening of the X-ray peaks.

### 10.3.4 Measurement of internal elastic strains

The elastic strains to be measured can be distinguished into those occurring on a 'macro' scale and those occurring on a 'micro' scale. Macroscale refers to the situation where the whole material is subject to some directional residual tension or compression; the resultant strains, which are manifested in terms of increases (tension) or decreases (compression) in the  $d_{hkl}$ -spacings are therefore also directional and the measured values vary with the orientation of the reflecting planes—those parallel to the stress axis for example suffering no change.

In order to measure such strains (and to determine the stress axis) in the diffractometer, the specimen needs to be rotated from the symmetrical (Bragg–Brentano) geometry as described above. In practice, measurements of peak shift are made for various settings of the specimen and from which the direction and magnitude of the stress can be extrapolated.

Microscale refers to the situation in which the directions (and magnitudes) of the internal strains vary from crystal to crystal. The subsequent elastic strains give rise, not to a shift, but to a broadening of the diffraction peaks from which an estimate of the micro-stress can be made. The relevant equation is that derived for the limit of resolution (Section 10.3.1), in which  $\epsilon$ , the elastic strain, is substituted for  $\delta d/d$ , i.e.

$$\epsilon = -\cot \theta \delta \theta.$$

Hence the broadening,  $\beta$ , expressed as the half-height peak width  $2 \delta \theta$ , is:

$$\beta = -\frac{2\epsilon}{\cot \theta} = -2\epsilon \tan \theta.$$

Notice that this equation is very similar to the Scherrer equation for broadening arising from crystal size; the important difference being that in this case  $\beta$

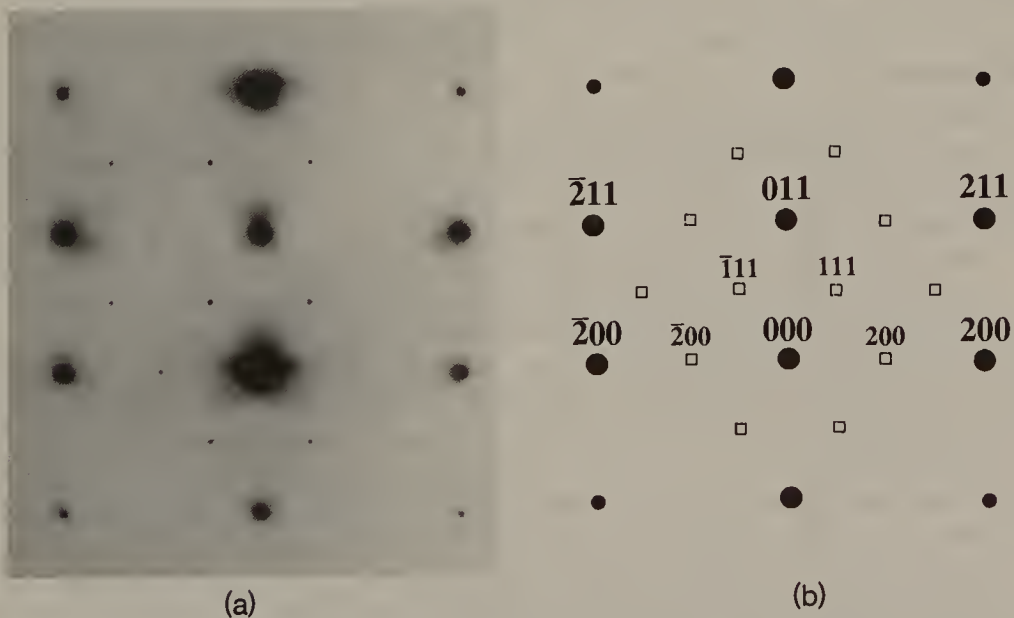


varies as  $1/\cot \theta$  or  $\tan \theta$  and in the Scherrer equation  $\beta$  varies as  $1/\cos \theta$  or  $\sec \theta$ . As in the case of grain size broadening (Section 10.3.3), the instrumental broadening,  $\beta_{\text{inst}}$ , measured for a stress-free material, must be subtracted from  $\beta_{\text{obs}}$ , the observed broadening for the micro-strained material. Finally, having measured the strain  $\epsilon$ , the stress may be determined by substituting the appropriate value of the Young modulus,  $E$ .

### 10.3.5 Determining orientation relationships between crystals from electron diffraction patterns

One of the greatest advantages of electron diffraction is the facility in the electron microscope of being able to select a particular area of the specimen and to vary the diameter of the beam to obtain diffraction patterns simultaneously from those phases of interest. Moreover, the reflections from the phases present may be distinguished by the technique of dark field imaging. Each electron diffraction pattern may be indexed according to the procedures described in Section 9.7. The orientation relationship(s) may then be given in terms of parallelisms between zone axes and planes.

Figure 10.11(a) shows an electron diffraction pattern of  $\alpha$ -iron  $a = 2.866 \text{ \AA}$  (bcc—strong reflections) in which are precipitated (or exsolved) particles of  $\text{Fe}_2\text{TiSi}$ ,  $a = 5.732 \text{ \AA}$  (fcc—weak reflections) in a single crystallographic orientation. It is obvious, simply by inspection or *looking*, that there is a clearly defined



**Fig. 10.11.** (a) An electron diffraction pattern of  $\alpha$ -iron (bcc,  $a = 2.866 \text{ \AA}$ : strong reflections) and  $\text{Fe}_2\text{TiSi}$  (fcc,  $a = 5.732 \text{ \AA}$ : weak reflections) in a single crystallographic orientation. The camera constant  $\lambda L = 31.5 \text{ \AA mm}$ . (b) The patterns indexed according to one (arbitrary) variant of the 'cube-cube' orientation relationship:

$$(200)_{\text{Fe}_2\text{TiSi}} \parallel (200)_{\alpha\text{-Fe}}; [\bar{0}11]_{\text{Fe}_2\text{TiSi}} \parallel [\bar{0}11]_{\alpha\text{-Fe}}$$

orientation relationship between the iron matrix and the precipitate and, because of the coincidence of many of the reflections, that the lattice parameters are related in some rational ratio. The  $d$ -spacings of the reflections may be measured (Section 9.7) and, given the lattice parameters and the conditions for reflection for the cubic  $F$  (fcc) and cubic  $I$  (bcc) lattices (Table A6.2), the reflections may be indexed. Figure 10.11(b) shows the patterns indexed according to one (arbitrary) variant of the orientation relationship. Note that the 200  $\text{Fe}_2\text{TiSi}$  spot is *half* the distance (and therefore *twice* the  $d$ -spacing) of the 200  $\alpha\text{-Fe}$  spot from the centre; these planes are therefore parallel and the lattice parameter of  $\text{Fe}_2\text{TiSi}$  is twice that of  $\alpha\text{-Fe}$ . Similarly, the 022  $\text{Fe}_2\text{TiSi}$  reflection (by vector addition of  $\bar{1}11$  and  $111$ ) is coincident with 011  $\alpha\text{-Ti}$ . The zone axes, obtained by cross-multiplication (Section 9.7), are both  $[0\bar{1}1]$ . The orientation relationship may be specified by quoting the parallelisms:

$$(200)_{\text{Fe}_2\text{TiSi}} \parallel (200)_{\alpha\text{-Fe}}$$

$$[0\bar{1}1]_{\text{Fe}_2\text{TiSi}} \parallel [0\bar{1}1]_{\alpha\text{-Fe}}.$$

This is known as the ‘cube–cube’ orientation relationship because it is equivalent to the statement that the  $x, y, z$  axes of both crystals are mutually parallel.

Other, more complicated, orientation relationships may be determined by the same simple approach, but to go from the parallelisms between the planes and zone axes observed for the particular patterns to the establishment of possible parallelisms between planes not observed in the patterns (i.e. those that are not (nearly) parallel to the electron beam direction), requires a knowledge of the stereographic projection (see footnote on page 149).

## Exercises

- 10.1 Show, by simple geometrical reasoning, that in the X-ray monochromator (Fig. 10.2) the curved reflecting crystal planes should have a radius twice that of the focusing circle.
- 10.2 Show, by simple geometrical reasoning, that in the back-reflection X-ray powder photograph (Fig. 10.5), the reflections are most sharply focused when  $R^2 = xy$  where  $R$  = the radius of the ring,  $x$  = the specimen–film distance and  $y$  = the distance of the (effective) source  $S$  behind the film.
- 10.3 Determine the  $d$ -spacings of the strongest low-angle reflections in the Debye–Scherrer film of quartz (Fig. 10.7) and check that they correspond (within the limits of experimental accuracy) with those indicated in Fig. 10.4 or listed in Fig. 10.8.  
(*Hint:* the precise locations at which  $2\theta = 0$  and  $180^\circ$  are *not* found from the centres of the holes in the film (which might be slightly displaced) but by determining the mid-points of the low-angle and high-angle reflections, respectively. The distance between these mid-points corresponds to an angle of  $180^\circ$  and the linear scale can be related to the angular scale and the  $2\theta$  values. Hence the  $d$ -spacings of the reflections can be found using Bragg’s law. (The film is taken using filtered  $\text{CuK}\alpha$  radiation which includes both the  $\text{K}\alpha_1$  and  $\text{K}\alpha_2$  components. At low angles these are unresolved,  $\lambda \text{CuK}\bar{\alpha} = 1.542 \text{ \AA}$ , but at high angles they are resolved,  $\lambda \text{CuK}\alpha_1 = 1.541 \text{ \AA}$ ,  $\lambda \text{CuK}\alpha_2 = 1.544 \text{ \AA}$ .)

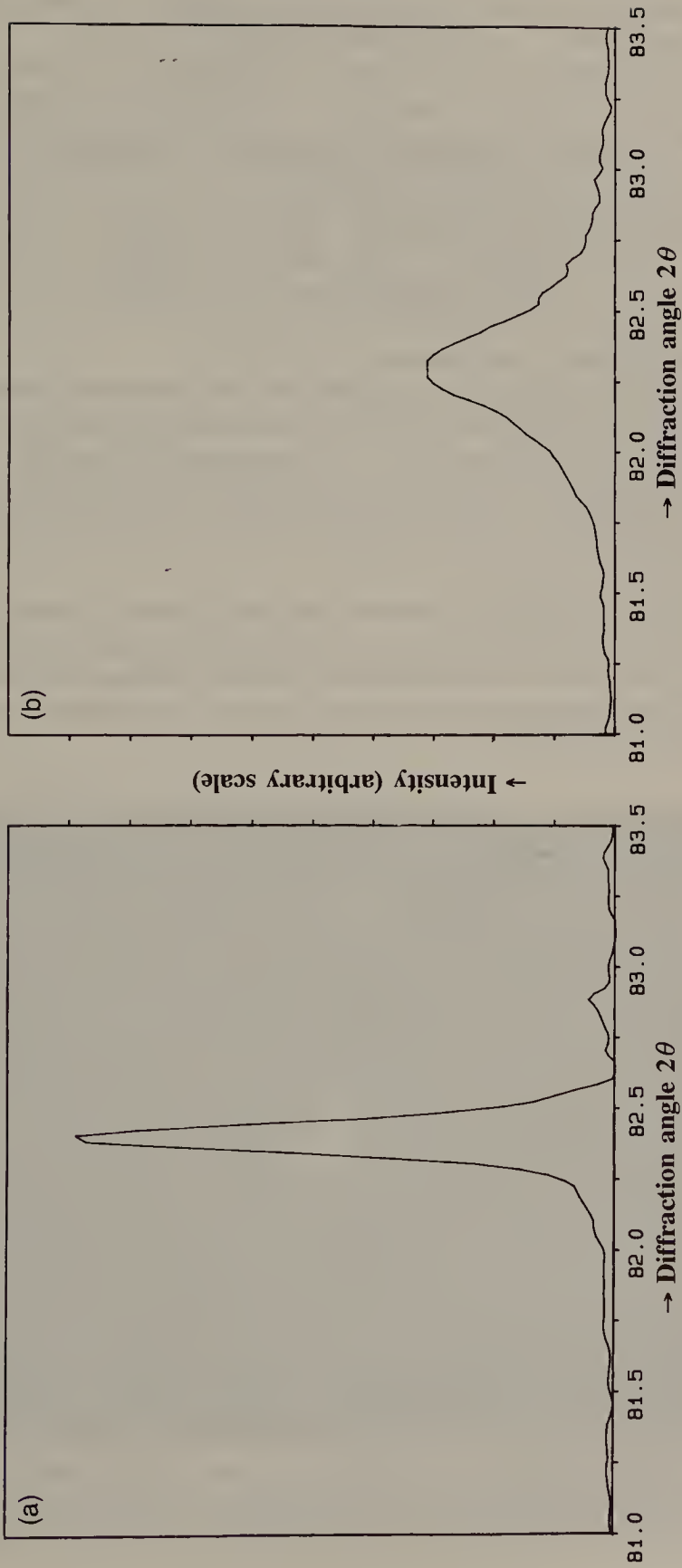


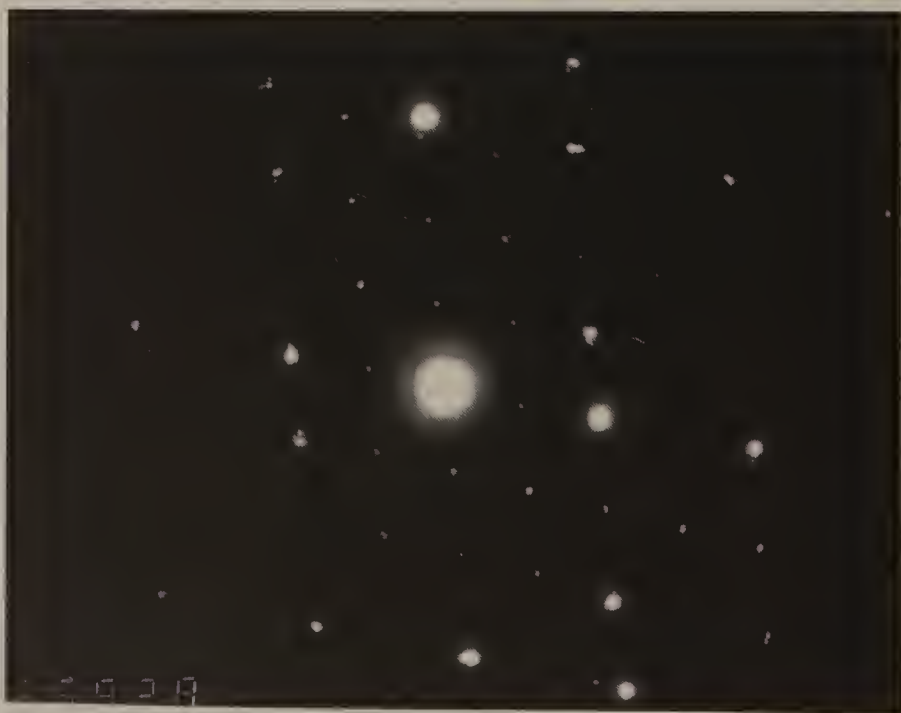
Fig. 10.12. X-ray diffraction peaks from (a) an annealed mild steel specimen and (b) the same specimen in which the surface has been heavily abraded. The X-radiation used was  $\text{CuK}\alpha$  but the  $\text{CuK}\alpha_2$  component of the peak profiles has been eliminated by a peak stripping program; hence the broadening due to the  $\text{K}\alpha_1/\text{K}\alpha_2$  doublet is eliminated.

- 10.4 Given the lattice parameter of aluminium  $a = 4.041 \text{ \AA}$ , find the camera constant  $\lambda L$  of Fig. 10.10.
- 10.5 Figure 10.12 shows X-ray diffraction peaks from (a) an annealed mild steel specimen and (b) the same specimen in which the surface has been heavily abraded. The X-radiation used was  $\text{CuK}\alpha$  but the  $\text{CuK}\alpha_2$  component of the peak profiles has been eliminated by a peak stripping program; hence the broadening due to the  $\text{K}\alpha_1/\text{K}\alpha_2$  doublet is eliminated.

Given that the lattice parameter,  $a$ , of mild steel is that for  $\alpha\text{-Fe}$  ( $2.866 \text{ \AA}$ ) and  $\lambda_{\text{CuK}\alpha_1} = 1.541 \text{ \AA}$ , identify the peaks. From the difference in peak broadening, determine  $\beta$  and on the assumption that it arises wholly from residual elastic strain, estimate the residual stress in the surface of the abraded specimen. (Assume that the Young Modulus,  $E = 200 \text{ GPa}$ .)

- 10.6 Figure 10.13 is a selected area electron diffraction pattern of a thin foil of a steel (Fe, 1.3% Mn, 0.5% Mo, 0.7% Ni, 0.2% Cr, 0.2% C) which has been quenched from  $1300^\circ\text{C}$  and tempered at  $615^\circ\text{C}$ . The microstructure consists of a matrix of tempered martensite ( $\alpha\text{-Fe}$ , bcc) and particles of cementite, iron carbide,  $\text{Fe}_3\text{C}$ . The pattern includes  $\alpha\text{-Fe}$  (strong spots) and  $\text{Fe}_3\text{C}$  (weak spots). Index the patterns and determine the orientation relationship between  $\alpha\text{-Fe}$  and  $\text{Fe}_3\text{C}$ . The camera constant  $\lambda L = 35 \text{ \AA mm}$ .

(Hint: A list of  $d_{hkl}$ -spacings for  $\alpha\text{-Fe}$  should be worked out given  $a_{\alpha\text{-Fe}} = 2.866 \text{ \AA}$  and given the condition for allowed reflections for the Cubic  $I$  lattice (Table A6.2). The  $d_{hkl}$ -spacings for  $\text{Fe}_3\text{C}$  are given in Exercise 9.5. Notice that the  $\alpha\text{-Fe}$  pattern also consists of two twin-related variants (see Fig. 7.14(a) for the analogous case in the diffraction of light).



**Fig. 10.13.** A selected area electron diffraction pattern of a thin foil of a quenched and tempered steel showing reflections from  $\text{Fe}_3\text{C}$  precipitates in a single crystallographic orientation (weak spots) and two twin-related orientations of the ferrite ( $\alpha\text{-Fe}$ ) matrix (strong spots).



# Appendix 1

---

## Useful components for a crystallography model-building kit and suppliers

Crystal models may be made from expanded polystyrene or solid plastic balls. A range of sizes is available and the cost increases roughly in proportion to the cube of the diameter. Unfortunately, it is not possible to select balls with diameter ratios 1:0.732:0.414:0.225:0.291 (i.e. the useful diameter ratios for interstitial sites) and it is simplest to make interstitial atoms out of Plasticine.

**Beevers Miniature Models Unit**, Department of Chemistry, Edinburgh University, West Mains Road, Edinburgh EH 9 3JJ (Tel: 0131 667 1081 Ext. 3405; Fax 0131 662 4045) markets molecular model kits based on 6.9 and 4.9 mm diameter balls, available in different colours and drilled with a range of hole configurations, and which can be linked with wire rods. Complete models of a wide range of crystal structures are also available.

**Cochranes of Oxford Ltd**, Leafield, Witney OX8 5NY (Tel: 01993 878641; Fax: 01993 878416) manufactures the 'Orbit' and 'Minit' molecular model kits based on plastic atom centres joined by short plastic tubes. The centres are moulded in a variety of shapes, and are colour coded according to the element. The kits can be used to build a range of molecules and extended lattices. Complete models of a wide range of crystal structures are also available, as are atom centres and bonds in packets of 100.

**Philip Harris Education**, Lynn Lane, Shenstone, Lichfield, Staffordshire, WS14 0EE (Tel: 01543 480077; Fax: 01543 480068) stock polystyrene spheres of a range of sizes for making into sphere-filling models, 'Molymod' system molecular models consisting of moulded plastic spheres and connectors for open (skeletal) and semi-space-filling models; 'Orbit' system molecular models comprising colour-coded atom centres and tube connectors and also Beevers miniature models.

**Polydron**, 11 Scotia Close, Brackmills Industrial Estate, Northampton NN4 7HR (Tel: 01604 769144; Fax: 01604 701674) manufacture both solid and 'framework' shapes useful for model building. They can be obtained from toy shops or suppliers of primary schools mathematics equipment.

**Tarquin Publications**, Stradbroke, Diss, Norfolk IP21 5JP (Tel: 01379 384218; Fax: 01379 384289) supply many types of paper cut-out books, posters, sets of blocks and books associated with mathematical shapes.

**The Yorkshire Purchasing Organisation**, 41 Industrial Park, Wakefield WF2 0XE (Tel: 01924 824477; Fax: 01924 834805) markets expanded polystyrene spheres in 35 mm and 70 mm diameter sizes.

**Your local grocery shop or supermarket** sells sugar cubes from which cubic crystal models showing different point symmetries may be made. Woodworkers' water-based resin gives a satisfactory bond; saturated sugar solution is slow and rather ineffective.

**Your High Street toy shop** sells all manner of building bricks, multi-coloured shapes (triangles, squares, pentagons etc.) which can be used to make two-dimensional tessellations or linked together to form three-dimensional shapes. These are usually in the '3- to 9-year-old' department, but they are suitable for crystallographers of all ages.

# Appendix 2

---

## Computer programs in crystallography

The British Crystallographic Association (BCA) maintains useful information on crystallographic software on the Internet at URL <http://www.cryst.bbk.ac.uk/BCA/index.html>. Lists of meetings and courses, suppliers of educational materials and programs for microcomputers are continually updated. Some software programs can be collected via the Internet; in other cases you can get a 'Demonstration Version' to try out before purchase. Results of software surveys and reviews of programs are published regularly in 'Crystallography News' which has been accessible on the Internet since March 1995.

Further details from The BCA Webmaster, E-mail: [BCA@ISISE.RL.ac.uk](mailto:BCA@ISISE.RL.ac.uk) (Tel: 01235 834357) or from the BCA Administrative Secretary, 2 Staplow Road, Worcester WR5 2LZ. Tel:/Fax: 01905 358550; E-mail: [s.e.harris@aston.ac.uk](mailto:s.e.harris@aston.ac.uk).

**ATOMIC PACKING AND CRYSTAL STRUCTURE** (K. M. Crennell and L. S. Dent-Glasser)—a self-contained learning program with sophisticated 3D graphics; includes hexagonal and cubic close-packing, cubic closest-packing of spheres, face- and body-centred unit cells and interstitial sites in close-packed structures.

**ELECTRON DIFFRACTION** (P. J. Goodhew)—examines various aspects of electron scattering and diffraction as encountered in electron microscopy.

Both programs run on PCs with MS-DOS and on any Acorn computer running RISC-OS or BBC Micros.

From: The Institute of Materials Marketing Department, 1 Carlton House Terrace, London SW1Y 5DB (Tel: 0171 8344071; Fax: 0171 8392078). Further programs involving crystallography are being produced as part of the TLTP MATTER project for the production of microcomputer software for students of Materials Science and Engineering. A CD-ROM will be published annually (commencing 1996) by Chapman & Hall, 2-6 Boundary Row, London SE1 8HN (Tel: 0171 8650066; Fax: 0171 5229624).

**ATOMS**—a program for three-dimensional representation of all types of atomic structures, including crystals, polymers and molecules.

The standard display model can show ball-and-stick, wire-frame, interpenetrating atoms (space-filling) or coordination polyhedra, or combinations thereof. The new thermal ellipsoid mode makes drawings in the style of ORTEP. The drawing features include: shading, front-to-back fading, stereopairs and perspective. The program supports multiple structure fragments, isolation of molecules,

full use of symmetry, several boundary options, importation of files. Windows and Mac versions have a completely graphical user interface; the DOS version has an interactive keyboard user interface.

Libraries of ATOMS include: 120+ minerals, 13 basic inorganic structures and 25 silicates.

From: Shape Software, 521 Hidden Valley Road, Kingsport TN 37663, USA (Tel: (432) 239 4771; Fax: (423) 239 6360; E-mail: 74457.1703@compuserve.com).

**BALL AND STICK**—molecular graphics software for chemistry presentation and animation. Ball & Stick automatically recognizes a wide range of standard molecular file formats for importing structures and offers an interactive environment in which to view, manipulative, calculate and edit molecular models. New Power Mac version available (v3.7).

From: Cherwell Scientific Publishing Ltd, The Magdalen Centre, Oxford OX4 4GA (Tel: 01865 784800; Fax: 01865 784801; E-mail: csp@cherwell.com).

**CELLX**—an interactive program for the presentation of unit cells and reciprocal space aimed at senior undergraduate or postgraduate levels, the principal function of which is the familiarize the student with the relationship between real space and reciprocal space. A pragmatic, visual approach is adopted to achieve this. The orientation or contents of the unit cell can be easily changed and the corresponding change in reciprocal space viewed immediately. For orthogonal systems only. For PCs with VGA graphics.

From: K. D. Rogers, Cranfield University, Shrivenham, Swindon SN6 8L, (Tel: 01793 785399; Fax: 01793 7855774; E-mail: rogersk@rmcs.cranfield.ac.uk).

**CHEMSOFT**—four programs (Periodic, Crystal, Organic and Alkanes). 'Crystal' shows three-dimensional views of the most important structures of inorganic compounds. Two structures may be displayed simultaneously and rotated, expanded or highlighted in various ways to make clear the features of each. Acorn compatible.

From: AVP, School Hill Centre, Chepstow NP6 5PH (Tel: 01291 625439; Fax: 01291 629671; E-mail: 100441.130@compuserve.com).

**CRYSTALLOGRAPHICA**—an MS-Windows software tool kit for research and teaching in crystallography. Crystallographica includes a specially extended Pascal interpreter, crystal structure drawing and powder pattern simulation. Properties of the crystal can be modified using either user-friendly dialogs or else by writing mini-programs which call upon the extensive crystallographic library. The program can read and write various standard file formats, including Shexl and the standard Crystallographic Information File. A demonstration version is available via the World Wide Web, accessible from the BCA pages.

From: Oxford Cryosystems, 3 Blenheim Office Park, Lower Road, Long Hanborough, Oxford OX8 8LN (Tel: 01993 883488; Fax: 01993 883988; E-mail: sales@cgraph.demon.co.uk).



**CRYSTALLOGRAPHY**—an interactive course module aimed primarily at first-year undergraduates; no prior knowledge is assumed and no use is made of the stereographic projection. The module is divided into eight units (fronted by a main menu) which can be run separately. They are: Introduction, Symmetry I, Symmetry II, Indexing I, Indexing II, Crystal Systems, Rotations. Available in PC (MS-DOS Windows 3.1 or later versions) and Macintosh (4Mb RAM). A demonstration version is available.

From: The UK Earth Science Courseware Consortium, Central Unit, Department of Earth Sciences, University of Manchester M13 9PL (Tel: 0161 275-3820/3838; Fax: 0161 275347; E-mail: [ukescc@man.ac.uk](mailto:ukescc@man.ac.uk)).

**Ca.R.lne CRYSTALLOGRAPHY (Version 3.0)**—an interactive program providing rotation and projections of Bravais lattices, space groups and coordination polyhedra. A multiple window can be opened showing X-ray powder diffraction, reciprocal lattices, electron diffraction patterns and stereographic projections. Available in English and French for Windows 3.1 (or later) and for Macintosh v.3. Demonstration versions for both Mac and Windows are available via the BCA World Wide Web pages or free upon request.

From: Cyrille Boudias and Dr Daniel Monceau, CaRine Crystallography, 17 Rue du Moulin du Roy, 60300 Senlis, France (Tel:/Fax: (33) 44 53 29 48; E-mail: [monceau@cict.fr](mailto:monceau@cict.fr)).

**CRYSTALMAKER**—a user-friendly Macintosh program to generate, display and manipulate all kinds of crystal structures in high-quality colour graphics. A major feature of the program is the intuitive click-and-drag real-time rotation of crystal structures, which can be displayed as ball-and-stick, wireframe, polyhedral and space-filling models.

CrystalMaker is distributed in three versions, optimized for Math-coprocessor (FPU), non-FPU, and PowerPC Macs, together with a library of over 200 crystal structures and a 160-page printed manual. A demonstration version is available.

From: Cambridge University Technical Services Ltd, 20 Trumpington Street, Cambridge CB2 1QA (Tel: 01223 334755; Fax: 01223 332797; E-mail: [sjm21@cus.cam.ac.uk](mailto:sjm21@cus.cam.ac.uk)). For technical support contact the author David Palmer (Fax: 01869 369393; E-mail: [D.C.Palmer@eWorld.com](mailto:D.C.Palmer@eWorld.com)).

**CRYSTAL OFFICE**—a program package includes Space Groups for Windows 4.0, Crystal Builder 96 and Space Group Tables 96. The user-friendly graphic system allows you to create multiple-crystal graphic scenes and photo-realistic graphics; label atoms, bonds and scenes; interactively build crystals with space group tables; visually measure distances and angles; create surfaces and clusters; substitute atoms with molecules; visualize symmetry elements, Wyckoff positions and Miller planes; output X-ray and electron diffraction structure factors; access position, symmetry and reflection tables for all of the 230 space groups and generate non-standard setting space group tables.

System requirements: MS Windows 3.1, Windows 95 and Windows NT. A Macintosh version is under development.

From: Atomic Softek, 70 Longwood Road North, Hamilton, Ontario, Canada L8S 3V4 (Tel: 905 528 4506; Fax: 905 528 9084; E-mail: SpaceGrp@wchat.on.ca).

**CRYSTALS**—together with SIR92 forms a unified X-ray crystallography package, including full graphics with colour PostScript output. It has both menu and command-line input, extensive documentation and two data sets for complete worked examples. Requires an Intel™ 486DX processor, 8MB memory, and 10Mb available hard disk.

From: Dr. D. Watkin, Chemical Crystallography Laboratory, 9 Parks Road, Oxford OX1 3PD (Tel: 01865 275263; Fax: 01865 272690; E-mail: Watkin@vax.ox.ac.uk).

**DESKTOP MICROSCOPIST** (formerly entitled **DIFFRACT**)—a very comprehensive program which includes diffraction patterns, HOLZ patterns, stereographic projections, Kikuchi lines and numerical values (*d*-spacings, angles between planes etc.). For the Macintosh version 1.3.

From: Microdev Software, 3120 NW John Olsen Avenue, D-104, Hillsboro, OR 97124, USA.

**DESKTOP MOLECULAR MODELLER**—for PCs with optional structure libraries; it has utilities and symmetry operators to generate crystals and lattices of inorganic materials. There is also a simpler version appropriate for schools.

From: Oxford Electronic Publishing, Oxford University Press, Walton Street, Oxford OX2 6DP (Tel: 01865 267979; Fax: 01865 267990).

**DIAMOND**—a three-dimensional graphics program with an integrated database for the visualization of crystal structures for molecular and solid-state chemists and materials scientists. It includes special functions for complex inorganic structures—neighbouring and bonded atoms around central atoms—and coordination polyhedra. Molecules are found without explicit bonding information. For an IBM-compatible PC and 386 or higher, at least 4 Mb of RAM and 8 Mb of free disc space. The program runs on Windows 3.1, Windows 95 and Windows NT 3.51. A demonstration disc is available.

From: Prof. Dr G. Bergerhoff Software-Entwicklung, Gerhard-dornagk-Str-1, D-53121 Bonn, Germany (Tel: (+49) 228 73 53 55; Fax: (+49) 228 21 01 55; E-mail: Bergerhoff@uni.bonn.de or from the World Wide Web page at URL <http://www/rhrz.uni-bonn.de/~unc442/diamond.html>).

**ELECTRON DIFFRACTION**—a program which allows the simulation of any type of electron diffraction pattern—‘spot’ and Kikuchi patterns, convergent beam and back scattered patterns. The patterns may be indexed, crystals tilted, interplanar spacings and angles determined etc. For PCs Windows 3.1 and Windows 95. A demonstration version is available limited to the silicon and quartz structures.

From: J. P. Morniroli, Laboratoire de Metallurgie, URA, CNRS 234, Université de Lille 1, 59655 Villeneuve d'Ascq Cedex, France (Tel: (33) 20 43 69 37; Fax: (33) 20 43 40 40; E-mail: morniol@omega.univ.lille1.fr).

**K-SPACE NAVIGATOR**—a program specifically designed for indexing electron diffraction patterns for all crystal systems. It provides K-space (reciprocal space) displays of zone axes, spot patterns and Kikuchi lines and, for microscopes with a motor-driven specimen tilt stage (and suitable RS232 interface), can drive the stage to the required crystal orientation, making specimen orientation determinations fast and easy. Runs on most PCs operating under Microsoft Windows. A demonstration disc is also available.

From: Surface Data, 5 Sandhaves Hill, East Grinstead, West Sussex RH19 3ET (Tel:/Fax: 01342 328845; Email: Sales@surface.demon.co.uk).

**PHYSDEMOS**—includes a description of the common lattices and several display forms of the C60 (buckminster fullerene or 'bucky-ball') molecule which can be interactively rotated.

From: The UK Higher Education National Software Archive (HENSA) (available on the World Wide Web at URL: <http://micros.hensa.ac.uk>).

**POLYHEDRA, TILING GENERATOR, 3-D DIFFRACTION PATTERNS**—a set of PC programs which do not need Windows; Polyhedra displays polyhedra derived from crystallographic point groups, Tiling Generator is for quasi-crystal symmetries, 3-D Diffraction Patterns is displayed to aid an understanding of the concept of reciprocal space.

From: the BCA or available directly from Steffen Weber Software on the World Wide Web at URL <http://www.nirim.go.jp/weber/> or via the BCA pages.

**SHAPE**—a program for drawing the external morphology of crystals and also sections of crystals (Windows and DOS versions). It will draw any single crystal and most twins and epitaxial intergrowths. You enter the crystal axis lengths and angles, the symbol for the crystal class, and one face of each form (symmetry equivalent set). The crystal can be rotated, scaled, twinned, etc. A stereonet can be displayed with the crystal, or stereopairs may be drawn automatically. Screen display and hard copy of even complex interpenetrating intergrowths may be made in final finished form, with no extraneous lines. There is a library of 700+ mineral crystals.

From: Shape Software, 521 Hidden Valley Road, Kingsport TN 37663, USA (Tel: (423) 239 4771; Fax: (423) 239 6360; E-mail: 74457.1703@compuserve.com).

**STEREO**—plots 20 cm diameter stereographic projections of plane normals or zone axes. Available in Macintosh or PC versions.

From: Dr P. E. Champness, Department of Earth Sciences, University of Manchester, Oxford Road, Manchester M13 9PL (Tel: 0161 2753804; Fax: 0161 2753947; E-mail: pchampness@fs2.ge.man.ac.uk).

**SYMMETRY**—a self-paced program with self-assessment on symmetry in point groups and lattices. For PCs with MS-Windows.

From: Crystallography Department, Birkbeck College, University of London, WC1E 7HX (Tel: 0171 6316800; Fax: 0171 6316803; can also be downloaded from <http://www/cryst.ac.uk/symmetry/>). `

**3-D MOLECULE**—enables a structural formula to be constructed for an organic molecule. The molecule is built up in stages by selection from a range of functional groups. It can be viewed as a three-dimensional ball-and-spoke model and can be rotated in all planes. Acorn compatible.

From: AVP; School Hill Centre, Chepstow NP6 5PH (Tel: 01291 625439; Fax: 01291 629671; E-mail: 100441.130@Compuserve.com).



## Appendix 3

---

### Biographical notes on crystallographers and scientists mentioned in the text

#### **Ernst Abbe 1840–1905**

Abbe's father was a mill worker in Eisenach, Germany, and it was his employers who provided the scholarships which enabled Abbe to proceed from High School to study physics at the Universities of Jena and Göttingen. In 1863 Abbe achieved his ambition of becoming a lecturer at Jena, but his career may be said to commence in 1866 when he began his long and fruitful collaboration with Carl Zeiss. As a theoretician he established the relation between the aperture and the limit of resolution of a lens (the equation is engraved on his memorial at Jena); as an optical designer he invented the apochromatic objective lens (made possible with the new glasses developed by the Schott glassworks); and as an industrialist he and Zeiss developed systematic microscope production on a large scale.

In 1876 he was made a partner in the Carl Zeiss firm and became the sole owner following the death of Zeiss in 1888. In 1891 he created the Carl Zeiss Foundation whose charter was used in Prussia as a model for progressive social legislation.

#### **George Biddell Airy 1801–92**

Airy's life was characterized, to a remarkable degree, by a determination to succeed and meticulous organization: he made a record of everything that he wrote, with dates, and discarded not the merest note or receipt. His entry to Cambridge in 1819, which was largely facilitated by a wealthy uncle in Colchester, provided him with the opportunity to break away from a modest parental background and thence his career developed rapidly. He was appointed Lucasian Professor of Mathematics in 1826, Plumian Professor of Astronomy in 1828 and Astronomer Royal in 1835, a post he filled for 46 years and which entirely fitted his temperament. He largely re-equipped the Greenwich Observatory and transformed it into a highly efficient Institution—but at a price: it provided no centre for the training of innovative scientific minds and the discoveries of John Herschel and John Couch Adams were made elsewhere. Airy was, in effect, the prototype of the modern government scientist and played a major role in the development of institutional science in Victorian England.

He designed (with the lawyer, Edmund Beckett Denison) the clock for the new Palace of Westminster—it had to be redesigned in 1852 when it was discovered that the interior walls had been made too small—but its continued functioning almost without interruption for over 140 years is a measure of their achievement.

Airy calculated the magnitude of the image formed by a telescope objective of a star—a point source of light—and thereby laid the foundations for the theory of the resolving power of optical instruments. He was knighted in 1872, having refused that honour three times previously on the grounds that he couldn't afford the fees.

### **William Barlow 1845–1934**

Following an inheritance from his father, Barlow, one of the last great English amateurs in science, took up the study of crystallography in his early thirties and attempted to relate the properties of crystals to the packing arrangements of their constituent atoms. He collaborated with W. J. Pope at Cambridge and guessed (correctly) the structure of the alkali halides. His mathematical ability and developing interest in symmetry enabled him to extend the methods of Bravais and Sohncke to find the 'symmetrical groupings to fit the forms and compositions of a variety of different substances' but he did not publish his derivation of the 230 space groups until 1894, three years after Fedorov and Schoenflies, of whose work he almost certainly had no prior knowledge.

### **William Henry Bragg 1862–1942**

W. H. Bragg read mathematics at Cambridge and was appointed Professor of Mathematics and Physics at Adelaide in 1885. For his first eighteen years there he published very little, but in 1903 became involved in problems of radiation, the ionization of gases and the nature of X-rays, which he considered to be 'material' in nature. His increasing reputation led to his appointment in 1908 as Cavendish Professor of Physics in the University of Leeds. In late 1912 he and his son, William Lawrence, became convinced that the Laue experiment made a wave hypothesis for X-rays unavoidable and together they made remarkably rapid advances in crystal structure analysis, the father's main contribution being the construction of an ionization chamber and crystal spectrometer and the solution of the structure of diamond. The work was interrupted by the First World War and, in 1915, Bragg moved from Leeds to University College, London, and then, in 1923, to the Royal Institution, at which places he laid one of the foundations of molecular biology by establishing research groups directed towards the analysis of organic crystals.

### **William Lawrence Bragg 1890–1971**

W. L. Bragg obtained a degree in mathematics at the University of Adelaide and, on the return of the family to England, entered Trinity College, Cambridge,

to study physics at the Cavendish Laboratory under Sir. J. J. Thomson. In 1911 he obtained a lectureship at Trinity College. At that time he supported his father's view that X-rays had the 'properties of material particles rather than those of electromagnetic waves' but during the summer and autumn of 1912 both he and his father abandoned it in the light of Laue's discovery of X-ray diffraction. It is not known how the Braggs became acquainted with Laue's discovery; this may have been through the 250th anniversary meeting of The Royal Society in July 1912 or, somewhat later, a lecture by J. J. Thomson to the Leeds (or Manchester?) Physics Groups. The theory (of Stokes) that X-rays were very short pulses of electromagnetic radiation also gave rise to the notion in Bragg's mind that the pulses should be reflected 'by the sheets of atoms in the crystal as if these sheets were mirrors'—a profoundly simple notion that not only explained the shapes of the diffraction spots but also provided a simple geometrical basis for the analysis of crystal structures. This work progressed extremely rapidly. Bragg's study of Laue's diffraction patterns of ZnS (zinc blende) led to the (correct) postulate that the structure was based on an fcc lattice and in the winter of 1912–13 he had prepared and analysed his own 'Laue' photographs of NaCl and KCl. In collaboration with his father in the summer of 1913, and with the aid of the X-ray spectrometer, Bragg solved the structures of fluorspar ( $\text{CaF}_2$ ), zinc blende ( $\text{ZnS}$ ), iron pyrites ( $\text{FeS}_2$ ), sodium nitrate ( $\text{NaNO}_3$ ) and calcite ( $\text{CaCO}_3$ ). The remainder (if it can be called that) of Bragg's scientific career saw the inexorable development of the techniques of X-ray (and electron) diffraction and the solution of the structures of crystals—particularly mineral and organic crystals—of greater and greater complexity. It was a development in which Bragg himself, as Langworthy Professor of Physics at the University of Manchester, as Cavendish Professor at Cambridge, and towards the end of his life, as Director of the Royal Institution, played no small part.

### **Auguste Bravais 1811–63**

Bravais was born in Annonay in France, studied mathematics in Paris and became a naval cadet in Toulon, which enabled him to participate in explorations to Algeria and the North Cape. He was appointed Professor of Physics at the École Polytechnique in 1845, and his interest in the relationships between the external forms and internal structures of crystals led to the derivation of the fourteen space lattices in 1848, published in his famous *Memoire sur les systèmes formés par des points distribués régulièrement sur un plan ou dans l'espace* (1850)—work which was partly based on Frankenheim's fifteen 'nodal' lattice types. However, constant application to a wide range of studies which aroused his curiosity led, in 1857, to a breakdown of his health.

### **Martin Julian Buerger 1903–86**

Buerger was born in Detroit, USA, and studied mining engineering at the Massachusetts Institute of Technology, specializing after graduation in research



in mineralogy. It was during this time that he attended, in 1927, a course of lectures on X-ray diffraction given by W. L. Bragg, as a result of which Buerger realized that in order to understand the chemical and physical properties of crystals it was necessary to know their structures. Hence began his life-long work in X-ray crystallography, not only in the solving of crystal structures but in the invention of the equi-inclination Weissenberg camera, the precession camera and the writing of several well-known textbooks, the earliest of which *X-Ray Crystallography* is, like Bragg's *The Crystalline State: Volume 1, A General Survey*, a classic which is still current today.

Buerger was closely associated with the founding of the International Union of Crystallography and was a member of the Commission for the International Tables from its establishment in 1948.

### **Peter Joseph William Debye 1884–1966**

Debye was born in Maastricht in the Netherlands, was educated at Aachen and Munich and held a number of Chairs in Physics before becoming Director of the Kaiser Wilhelm Institute for Theoretical Physics 1935–40. He then emigrated to the USA in 1940, becoming Professor of Chemistry at Cornell University.

Debye was primarily a theoretician concerned with the application of physical methods to molecular structure and is best known for his work of specific heat, electrolysis and the electron diffraction of gases. He was a member of staff in the Institute of Experimental Physics at the University of Munich at the time that Laue carried out his famous X-ray diffraction experiments. His development of a technique and camera (with P. H. Scherrer) for the investigation of X-ray diffraction from powders was made at the University of Göttingen in 1915.

### **Peter Paul Ewald 1890–1985**

Ewald deserves greater recognition for his contribution to the interpretation of X-ray diffraction patterns that he has hitherto been accorded—unlike Laue or the Braggs he was not awarded a Nobel Prize. Yet his doctor's thesis of 1912, which he discussed with Laue, contained within it the basis of the 'reciprocal lattice and reflecting sphere construction' analysis of the geometry of (X-ray) diffraction which is equivalent to Bragg's law. Indeed, it was only after reading Laue, Friedrich and Knipping's published papers that Ewald realized the relevance of his own approach and, in particular, the applicability of the formula in his thesis which he had brought to the attention of Laue but which in fact he (Laue) had not used.

### **Evgraph Stepanovich von Fedorov 1853–1919**

Son of an army engineer, Fedorov attended military school in Kiev and became, in turn, a combat officer and member of the revolutionary underground. His first ideas on the derivation of the 230 space groups were contained in his book



*The Elements of Configurations*, started in 1879, when he was 26 years old but not published until 1885. His complete derivation of the space groups was circulated in 1890 to his friends (including Schoenflies) as a series of preprints but was not published until 1891, shortly before Schoenflies' independent derivation.

### **Jean Baptiste Joseph Fourier 1768–1830**

Fourier, son of poor parents who died when he was nine, attended the military school in his home town of Auxerre, France, where his great mathematical ability was first recognized. As a young man he was caught up in the Revolution; he was imprisoned both by Robespierre (being released only as a result of Robespierre's execution in 1794) and, subsequently, by the counter regime, ironically as a supporter of Robespierre.

Fourier's administrative and political talents were recognized by Napoleon who made Fourier secretary of the newly formed Institut d'Egypte, but after Napoleon's fall he found himself out of favour with Louis XVIII and was not elected a member of the Academie Francaise until 1827.

Fourier's main achievements lie in his development of the mathematical techniques applied to the diffusion of heat and (what are now called) Fourier series and Fourier integrals. He also made substantial contributions to the theory of equations, linear inequalities, and probability.

### **Moritz Ludwig Frankenheim 1801–69**

Frankenheim was born and educated in Brunswick and the University of Berlin, where he was appointed lecturer in 1826. He was subsequently appointed Professor of Physics at Breslau, a post which he held until 1866. It was in a work of 1835 that he showed there could be only fifteen 'nodal', i.e. space lattice types, which much later (1856) he corrected to fourteen configurations, 8 years after Bravais' derivation of the fourteen space lattices.

### **Joseph Fraunhofer 1787–1826**

Fraunhofer was the eleventh child of a poor master glazer in Straubing, Germany, who, after the early death of his parents and an unsatisfactory apprenticeship, joined the optical instrument workshop of a scientific instrument maker in Munich in 1806. Here his versatility as experimental scientist, optical instrument technician and glassmaker laid the foundations of the pre-eminence of the German optical instrument industry which was to be consolidated with such success by Otto Schott, Carl Zeiss and Ernst Abbe later in the century. It was a result of his investigations into the optical properties of glass that Fraunhofer discovered that the solar spectrum was crossed by many fine dark lines (some of which William Wollaston had first noticed in 1802), thereby laying the foundations of spectrometry. Following the work of Thomas Young he made

the first quantitative study of diffraction and found the reciprocal relationship between the separation of the lines in diffraction gratings and the dispersion of light. In 1823, three years before his death from tuberculosis, he was appointed to the post of director of the Physics Museum of the Bavarian Academy of Sciences.

### **Augustin Jean Fresnel 1788–1827**

Fresnel was born in Broglie, France, and grew up in a stern Jansenist home environment. In 1804 he entered the Ecole Polytechnique in Paris, his intended career being in civil engineering; from there he entered the Ecole des Ponts et Chaussées, graduating in 1809. His first big job as a civil engineer was the construction of the Imperial Highway to link France and Italy through the Alpine Pass of Col Montgenevre.

Fresnel's interests in optics and the nature of light appear to have begun in about 1814, but were stimulated in 1815 when he was suspended from his engineering work because of his opposition to Napoleon's return to France from exile in Elba—a period of enforced leisure during which time Fresnel was under police surveillance. However, in 1823 he became a member of the French Academy of Sciences and in 1824 was appointed to the lighthouse commission in France and developed the echelon lens which bears his name.

Like Thomas Young, but working entirely independently, Fresnel advocated and elaborated on the wave theory of light, though it is not known to what extent he was familiar with the ideas of Christiaan Huygens. Like Young, he introduced the principle of interference, drawn from analogy with his work on acoustics, publishing the results of his experiments on the diffraction and interference of light in 1815.

Fresnel collaborated closely with François Arago in studies on the polarization phenomena of light and followed Young in the realization that light waves must be transverse rather than longitudinal. For most of his short life Fresnel suffered severe ill-health; he was awarded the Rumford Medal of the Royal Society shortly before his early death.

### **René-Just Haüy 1743–1822**

The son of a poor weaver, Haüy received a classical and theological education at the College de Navarre in Paris and was ordained in 1770. His *Essai d'une théorie sur la structure des cristaux* of 1784 laid the foundation for the mathematical theory of crystal structure. In 1793 he proposed that there were six 'primary forms'—a parallelepiped, rhombic dodecahedron, hexagonal dipyrmaid, right hexagonal prism, octahedron and tetrahedron. In the *Traité de Minéralogie* of 1801 these were further divided, which led to the notion of 'molécules intégrantes'. Haüy survived the Revolution and was made Honorary Canon of Notre Dame in 1802.

**Carl Heinrich Hermann 1898–1961**

Formal structure theory, following the derivation of the 230 space groups by Fedorov, Schoenflies and Barlow, remained dormant even in the early years of crystal structure analyses by X-rays, largely because of the inconvenient and difficult notation then used. Hermann's great contribution (carried out initially independently of Mauguin) was to simplify the notation for the symmetry elements and space groups, making the theory much more accessible. Hermann was also instrumental in the preparation of the *Struktureberichte (Structure Reports)* from 1925 to 1937. He was a member of the Society of Friends and after the Second World War (during which he was jailed for listening to BBC broadcasts) he was appointed Professor of Crystallography at Marburg, a post he held until his death.

**Johann Friedrich Christian Hessel 1796–1872**

Hessel was born and educated at Nuremberg but spent most of his professional life as Professor of Mineralogy and Mining Technology at Marburg. He was the first to show (in 1830) that only two-, three-, four- and six-fold axes of symmetry can occur in crystals and that considerations of symmetry lead to the thirty-two crystal classes. However, his work was unrecognized by his contemporaries and remained so until long after his death.

**Robert Hooke 1635–1703**

Hooke attracted the attention of Robert Boyle at Oxford and it was through his mechanical skill that he made a success of Boyle's air pump. He became a Fellow of the Royal Society and held the post of 'Curator of Experiments' from 1662 until the end of his life. It was in this capacity that Hooke was solicited by the Council of the Royal Society to prosecute his microscopical observations in order to publish them and was also charged to bring in at every meeting one microscopical observation at least. Hooke more than fulfilled this onerous obligation and, in doing so, caused the great capability of the microscope to be realized in England. The fruit of his work, *Micrographia, or Some Physiological Descriptions of Minute Bodies made by Magnifying Glasses, with Observations and Inquiries Thereupon*, was printed in 1665. In his book the word 'cell', so important in biology, was first applied to describe the porous structure of cork.

**Albert Wallace Hull 1880–1966**

Albert W. Hull was born in Connecticut and studied Classics at Yale University. However, he became increasingly interested in physics and after a period teaching modern languages, returned to Yale and completed, as it were, his educational transition by the award of a doctorate in 1909. After a further period of teaching (this time physics), he joined the General Electric Research



Laboratory at Schenectady where he discovered (independently of Debye and Scherrer) the powder diffraction technique. Hull's later achievements were in the fields of electronics (principally the invention of the Thyratron) and what is now called materials (principally the development of metal-glass vacuum seals). He was elected President of the American Physical Society in 1942.

### **Christiaan Huygens 1629–95**

Huygens was born in The Hague, studied at the University of Leiden and Breda and became one of the founding members of the French Academy of Sciences. He made important contributions to dynamics and showed that a pendulum which describes a cycloid (rather than the arc of a circle) is exactly isochronous and succeeded in inventing and constructing a pendulum clock based on this principle. He also made major contributions to observational astronomy and was the first to describe Saturn's rings correctly.

Huygens' greatest achievement was his development of the wave theory of light described in his *Traite de Lumiere* (1690). The notion of action at a distance was abhorrent to him; in his view space is pervaded by particles (the ether), light being the effect of the disturbance of the particles—that of one particle being transmitted to the next and so on. The net effect is a wave spreading out from the point of origin, each point in the wavefront being the source of secondary wavelets. Huygens was thereby able to explain refraction and reflection and to predict (correctly) that the velocity of light decreased in passing from a rarer to a denser medium—whereas Newton's corpuscular theory required the denser medium to attract the corpuscles of light and therefore increase its velocity. However, because the waves were conceived as being longitudinal, rather than transverse, he could not satisfactorily explain double refraction.

The problem of double refraction constituted one of Newton's objections to the wave theory of Huygens for 'Pressions and Motions', as he says in *Opticks*, 'propagated from a shining body through a uniform medium must on all sides be alike', whereas experiment had shown that the 'Rays of Light have different properties in their different sides'—a clear presentiment of the idea of polarization. The other, even more serious objection, was that without the concept of interference, Huygens' wave theory could not explain the most obvious character of a light beam, namely rectilinear propagation. It was not until the work of Fresnel and Young at the beginning of the nineteenth century that the wave theory of light was finally established.

### **Johannes Kepler 1571–1630**

The turmoil of Kepler's life is in strong contrast to his belief in the existence of a mathematical harmony underlying the Universe, the search for which was the guiding inspiration of his life's work. He was born in Würtemberg in Germany and in 1594 was appointed teacher of mathematics at the seminary at Gratz. Here he encountered the work of Nicolaus Copernicus and published his first



book (*Mysterium Cosmographicum*, 1596), in which he tried to show that the orbits of the planets were determined by the nesting, one within the other, of Plato's five regular solids—cube, tetrahedron, dodecahedron, icosahedron and octahedron. Forced, as a Lutheran, to leave Gratz, he joined Tycho Brahe in Prague under the patronage of the emperor Rudolph II, a fruitful but uneasy collaboration. Here Kepler discovered the first two of the three laws of planetary motion which were to be of such importance to Newton, wrote a major work on optics, discovered the second new star visible to the naked eye since antiquity and prepared his astronomical tables, against a background of the social unrest of the Thirty Years' War and continual lack of financial support from the emperor.

In 1611 civil war broke out in Prague, the emperor was forced to abdicate and Kepler's young son and wife died. He moved to Linz, remarried in 1613, and had to face his mother's trial for witchcraft in Württemberg. At Linz he published *Harmonices Mundi* (1619) which contains his third law.

On completion of the astronomical (Rudolphine) tables, Kepler moved to Sagan in Silesia under the patronage of Imperial General Wallenstein. He died of a fever at Ratisbon in the unsuccessful quest of 12 000 florins owed to him by the emperor.

### **Max von Laue 1879–1960**

Laue was educated at the University of Berlin and became an assistant to (and favourite disciple of) Max Planck. He joined Sommerfeld's Theoretical Physics Group at the University of Munich in 1909. His intuition—that the regular arrangement of atoms in a crystal might give rise to an interference effect if the waves travelling through were of a wavelength of the same order as the atom or 'resonator' spacing—almost certainly stems from a meeting with P. P. Ewald in January 1912. Ewald was completing his doctoral thesis and wished to discuss some of his conclusions with Laue. Laue encountered strong disbelief amongst his colleagues of any significant outcome of such a diffraction experiments on the grounds that the thermal motion of the atoms would obscure any diffraction maxima. However, he persevered and, with the assistance of Walter Friedrich (an assistant of Sommerfeld), and Paul Knipping (who had just finished his thesis under Roentgen), the famous experiment on a copper sulphate crystal which 'happened to be in the laboratory' was carried out. Laue's interpretation of the results was based upon the notion that the crystal behaves as a 'three-dimensional' diffraction grating but was also confused by a misapprehension that the wavelengths of the (diffracted) beams were those of characteristic or fluorescence X-rays in a crystal—a property of the atoms rather than the lattice.

### **Charles Mauguin 1878–1958**

Mauguin's early career expectation was that of a teacher in a teacher's training college, but he quickly developed an interest in mathematics and natural

philosophy and commenced his scientific work in the field of organic chemistry. His interest in crystallography probably stems from a course of lectures given by Pierre Curie which he attended in 1905. Mauguin was one of a small group of crystallographers who, in 1933, undertook the publication of the International Tables, and it is his symbolism of the 230 space groups (worked out in collaboration with C. H. Hermann) which is now in almost universal use.

### William Hallowes Miller 1801–80

Miller was educated in St. John's College, Cambridge, where, in 1829, he became a Fellow. In 1839 he published *A Treatise on Crystallography*, in which he made the fundamental assertion that crystallographic reference axes should be parallel to possible crystal edges. His system of indexing was based on a 'parametral' plane making intercepts  $a$ ,  $b$  and  $c$  on such axes [i.e. (111)]; a plane making intercepts  $a/h$ ,  $b/k$  and  $c/l$  was assigned the (integral) indices ( $hkl$ ). Although the algebraic advantages of this system were immediately apparent to his contemporaries (and were quickly adopted), their full significance was not fully appreciated until Bragg's and Ewald's interpretation of X-ray diffraction.

### Isaac Newton 1642–1727

'Nature was to him an open book, whose letters he could read without effort.'

*A. Einstein. Foreword to Newton's Opticks*

Isaac Newton was born, a premature and posthumous child, at Woolsthorpe Manor in Lincolnshire. He was educated at the King's School, Grantham, and was admitted to Trinity College, Cambridge, in 1661. It is while he was an undergraduate that he seems to have made his first acquaintance with optics; he read the works of Kepler and Descartes and from about 1663 was involved in the construction and performance of telescopes and the observation of lunar crowns and haloes. In the summer of 1665 he went home to Woolsthorpe Manor to escape the plague and remained there until April 1667, except for a three-month visit to Cambridge from March 1666. It was during this time that Newton says of himself 'I was in the prime of my age for invention and minded Mathematicks and Philosophy more than at any time since.' Those two years of intellectual achievement—the formulation of the binomial theorem and the differential and integral calculus, the theory of colours and of universal gravitational attraction—together with the two years (1685–86) during which he composed the *Principia*, have never been surpassed.

Newton's first paper to the Royal Society (published in 1672), in which he showed that ordinary white light is a mixture of rays of every variety of colour, received such a hostile reception from Robert Hooke that it made Newton cautious of publishing his work; the *Principia* or the *Mathematical Principles of Natural Philosophy* itself was not published until 1687 and then largely due to the encouragement of Edmund Halley. It immediately brought to Newton

enormous prestige, a place in society and public affairs but thereafter little more science.

The *Opticks* was not published until 1704, a year after the death of Robert Hooke, Newton's most pertinacious antagonist. Further editions came out in 1717, 1721 and 1730, the last being 'corrected by the Author's own hand'. In this great work Newton states that his 'design in this book is not to explain the Properties of Light by Hypothesis but to propose and prove them by Reason and Experiments'. However, there are many comments suggestive of a deeper penetration into the nature of light than exact knowledge could then achieve, including the notion of interference, for in attempting to explain the colours of thin films Newton describes the passage of light as being made up of 'alternate fits of easy Reflection and easy Transmission'.

The greatest interest in the *Opticks* lies in the *Queries*, in which Newton speculates on the nature of light. The question form may have been used to allay criticism that he was departing from his dictum 'hypothesis non fingo' (I frame no hypotheses), but all are couched in the negative 'Do not Bodies act upon Light at a distance?' A negatively phrased question suggests or implies a positive answer; 'do *not* bodies act upon light at a distance?' Is not Newton implying that the answer must be in the affirmative?

### Louis Pasteur 1822–95

Pasteur is perhaps best remembered for his work in microbiology and immunology and, in particular, the practical applications—the discovery of vaccines, the treatments for rabies and anthrax, silkworm disease, etc. His work in crystallography was confined to the early years of his scientific career. Beginning in about 1847 (shortly after completing his dissertation in physics), he began a series of investigations into the relations between optical activity, crystalline structure and chemical composition in organic compounds. His guiding principle was that optical activity was somehow associated with life; that whereas enantiomorphic crystals or molecules produced in the laboratory, or of mineral origin, occurred in equal quantities of left- and right-handed forms, those of organic origin—from plants or animals—were always of one form. The origin of life it seemed was bound up with an original asymmetric chemical synthesis. Hence Pasteur believed that molecular asymmetry was an essential characteristic of the chemistry (and biology) of life.

Pasteur's demonstration that the optically inactive (or racemic) paratartaric acid was composed of equal amounts of two optically active forms of opposite senses was made on crystals of sodium-ammonium paratartrate. In using these, and in separating out the two forms, he was perhaps fortunate, as in no other compounds is the relationship between crystal structure and molecular asymmetry so straightforward; also, the distinctive 'hemihedral' crystalline forms of these compounds occur only under certain conditions of crystallization. From this he was led to study asparagine and its derivatives (aspartic acid and the aspartates, malic acid and the malates).



### **William Jackson Pope 1870–1939**

Pope's major scientific work was in the field of organic chemistry. He was educated at Finsbury Technical College and the City and Guilds of London Institute in Kensington; in 1908 he was appointed Professor of Chemistry at Cambridge at the early age of 38. His crystallographic work extends over the period 1906–10 when, in collaboration with W. Barlow, he developed models of crystal structures based on the close-packing of ions or atoms of different sizes—models which were to prove so valuable to the Braggs in their analyses of crystal structures.

### **John William Strutt, third Baron Rayleigh 1842–1919**

Like his near contemporary the geologist and microscopist Henry Clifton Sorby, Lord Rayleigh (as he became when he succeeded to his father's title in 1873) had the leisure and financial resources to devote his life to science. His early life was dogged by ill health; in 1865 he graduated in mathematics at Cambridge and remained there until 1872 when he went to Egypt for a period of convalescence. It was not, however, a period of idleness; he wrote his classic book *The Theory of Sound* on a houseboat on the Nile.

On his return to England he built his own private laboratory and carried out most of his work there except for a short period (1879–1884) when he was Cavendish Professor of Experimental Physics at Cambridge.

Rayleigh's main contributions to science were in optics and acoustics; his work on the scattering of light by small particles led to the explanation of the blue colour of the sky and his work on the density of gases led to the discovery of argon.

### **Paul Hermann Scherrer 1890–1969**

Scherrer was born at St. Gall, Switzerland. During his education his interests moved away from commercial topics towards natural history, first to botany and then to mathematics and physics. In 1913 he entered the University of Göttingen and became a member of Debye's research group. The stimulus for the investigation of polycrystalline specimens appears to have come from Debye although the construction of the cylindrical camera was due to Scherrer. With it, Debye and Scherrer took the first X-ray powder photographs (of lithium fluoride) in 1915. A very similar method was devised in 1917 by Albert W. Hull at the General Electric Laboratories, USA.

In later years Scherrer was active in the foundation of the European Centre for Nuclear Research (CERN). He was also prolific teacher and brought to his lectures a considerable element of showmanship.

### **Arthur Schoenflies 1853–1928**

Schoenflies was born in Landsberg an der Warthe, now in Poland. He studied mathematics at Berlin and became successively high school teacher, Associate



Professor of Mathematics (at Göttingen), Professor (at Königsberg) and Rector at the University at Frankfurt. He extended the work of Sohncke on periodic discrete groups by taking into consideration rotation–reflection and inversion axes of symmetry, adding another 165 to Sohncke’s sixty-five groups. The work was completed in his book *Kristallsysteme und Kristallstruktur*, published in Leipzig in 1891, a few months after Fedorov’s paper.

### **William Bradford Shockley 1910–89**

William Shockley was born in London to American parents and moved to California (with them) in 1913. He was educated at the California Institute of Technology and Massachusetts Institute of Technology and, after war service with the U.S. Navy’s Submarine Warfare Operations Research Group, became a supervisor in the semiconductor research group at Bell Telephone Laboratories in New York. There, in 1947, together with John Bardeen and Walter Brattain, he discovered the principle of the point contact transistor and then went on to develop the junction transistor. This may be said to be the starting point of the electronic transformation of the latter part of the twentieth century, which was recognized by the award of the Nobel prize for Physics, jointly with Bardeen and Brattain, in 1956.

Shockley then left ‘Bell Labs’ to set up the Shockley Semiconductor Corporation in California and from 1963 became Professor of Engineering at Stanford University.

The latter part of his life was clouded by controversy because of his uncompromisingly held views on dysgenics, i.e. retrogressive evolution through the excessive reproduction of the genetically disadvantaged, and for which, as one example of his increasing isolation, the University of Leeds refused to confirm his nomination for an Honorary Doctorate.

### **Leonhard Sohncke 1842–97**

Sohncke was born in Halle, Germany, where his father was Professor of Mathematics at the University. Like his father he followed an academic career, being appointed to a succession of professorships in physics, firstly at Halle and at the end of his career at the Technische Hochschule in Munich. Sohncke considered the possible arrays of points which have identical environments but not necessarily in the same orientation (as in the definition of Bravais lattices), and arrived at sixty-five of the possible 230 space groups. He published his findings in 1897, while he was professor of Physics at the Technische Hochschule in Karlsruhe, and used cigar-box models by way of illustrations!

### **Gustav Heinrich Johann Apollon Tammann 1861–1938**

Tammann can be regarded as a pioneer physical metallurgist in the light of his work in metallography and the study of solid-state chemical reactions. He was

born in Yamburg (now Kingisepp) in Russia and, after a career as a lecturer at Charlottenburg and Leipzig, was chosen to head the newly formed Institute at Göttingen in 1903. It was here that he began his studies on metallic compounds, the crystal structures and mechanical properties of metals and alloys, and the general problems of the mechanisms of plastic deformation and work hardening in terms of crystallographic slip and crystalline rearrangements. He continued to work on these problems until shortly before his death, applying his ideas at the same time to the flow of ice.

### **Wilhelm Eduard Weber 1804–91**

Weber was Professor of Physics at Göttingen from 1831 for most of his professional life and worked in collaboration with Gauss on magnetic phenomena. His main achievements were the introduction of a logical system of units for electricity, related to the fundamental units of mass, length and time and also the connection between electromagnetic phenomena and the velocity of light—a connection which was later thoroughly worked out by Maxwell. Weber was also one of the ‘Göttingen Seven’ who, in 1837, lost their university posts because of their opposition to the autocracy of King Ernst August of Hanover.

### **Christian Samuel Weiss 1780–1856**

After studying medicine at Leipzig, Weiss switched to chemistry and physics, becoming Professor of Physics there in 1808. In 1810 he was appointed Professor of Physics at the newly established and prestigious University of Berlin, a post which he held until his death. Weiss developed the idea of crystal axes, from which he was able to distinguish crystal systems by the ways in which crystal faces were related to such axes. He also formulated the concept of a zone: originally conceived as a direction of prominent crystal growth, the term was defined as a collection of crystal faces parallel to a line—the zone axis; from this concept the zone law was derived.

### **Thomas Young 1773–1829**

Young was an infant prodigy who could read at the age of 2 and at the age of 14 knew Latin, Greek, French and Italian, and had begun to study several ancient languages—Hebrew, Chaldean, Syriac and the like—linguistic knowledge that he put to use in his contribution to the translation of the text of the Rosetta stone. Young intended to take up a medical career and commenced his education in 1793 at St. Bartholemew’s Hospital, moving from there to Edinburgh, Göttingen and Cambridge. He was elected a Fellow of the Royal Society as early as 1794 for his explanation on how the ciliary muscles of the eye change the shape (and focal length) of the lens.

Young's great contribution to science was his revival in 1800–04 of Huygens' wave theory of light, to which he added the concept of interference to explain rectilinear propagation and the diffraction phenomena at single or double slits or pinholes and in which he was closely shadowed by the work of Fresnel in France. In England Young was strongly attacked because he questioned the hegemony of Newton, but his work quickly won acceptance in the USA and Europe. Young was also first to suggest (in a letter to François Arago in 1816) that light might be propagated as a transverse wave, thus accounting for polarization and meeting the main objection of Newton. Regrettably, Young did not live to witness Foucault's demonstration, in 1850, that the speed of light was less in water than in air—the crucial experiment which distinguished the corpuscular and wave theories.

Young was also active in many other fields. His name comes down to us through his work on the elastic behaviour of solids as the constant of proportionality ( $E$ ) in Hooke's law, called Young's (or latterly Young) modulus.

# Appendix 4

---

## Some useful crystallographic relationships

In Sections A4.1–A4.3 the rather lengthy expressions for the triclinic system are omitted.

### A4.1 Interplanar spacings, $d_{hkl}$ (see Section 6.5.4)

Orthorhombic

$$\frac{1}{d_{hkl}^2} = \frac{h^2}{a^2} + \frac{k^2}{b^2} + \frac{l^2}{c^2}.$$

(Tetragonal:  $a = b$ ; cubic:  $a = b = c$ .)

Hexagonal:

$$\frac{1}{d_{hkl}^2} = \frac{4}{3} \left( \frac{h^2 + hk + k^2}{a^2} \right) + \frac{l^2}{c^2}.$$

Rhombohedral:

$$\frac{1}{d_{hkl}^2} = \frac{(h^2 + k^2 + l^2)\sin^2 \alpha + 2(hk + kl + hl)(\cos^2 \alpha - \cos \alpha)}{a^2(1 - 3\cos^2 \alpha + 2\cos^3 \alpha)}.$$

Monoclinic:

$$\frac{1}{d_{hkl}^2} = \frac{1}{\sin^2 \beta} \left( \frac{h^2}{a^2} + \frac{k^2 \sin^2 \beta}{b^2} + \frac{l^2}{c^2} - \frac{2hl \cos \beta}{ac} \right).$$

### A4.2 Interplanar angles, $\rho$ , between planes $(h_1 k_1 l_1)$ and $(h_2 k_2 l_2)$ (see Section 6.5.5)

Orthorhombic:

$$\cos \rho = \frac{(h_1 h_2 / a^2) + (k_1 k_2 / b^2) + (l_1 l_2 / c^2)}{\sqrt{\{[(h_1^2 / a^2) + (k_1^2 / b^2) + (l_1^2 / c^2)][(h_2^2 / a^2) + (k_2^2 / b^2) + (l_2^2 / c^2)]\}}}.$$

(tetragonal:  $a = b$ ; cubic:  $a = b = c$ .)

Hexagonal:

$$\cos \rho = \frac{h_1 h_2 + k_1 k_2 + \frac{1}{2}(h_1 k_2 + h_2 k_1) + (3a^2 / 4c^2)l_1 l_2}{\sqrt{\{[h_1^2 + k_1^2 + h_1 k_1 + (3a^2 / 4c^2)l_1^2][h_2^2 + k_2^2 + h_2 k_2 + (3a^2 / 4c^2)l_2^2]\}}}.$$



Rhombohedral:

$$\cos \rho = (a^4 d_1 d_2 / V^2) [\sin^2 \alpha (h_1 h_2 + k_1 k_2 + l_1 l_2) + (\cos^2 \alpha - \cos \alpha) (k_1 l_2 + k_2 l_1 + l_1 h_2 + l_2 h_1 + h_1 k_2 + h_2 k_1)].$$

Monoclinic

$$\cos \rho = \frac{d_1 d_2}{\sin^2 \beta} \left[ \frac{h_1 h_2}{a^2} + \frac{k_1 k_2 \sin^2 \beta}{b^2} + \frac{l_1 l_2}{c^2} - \frac{(l_1 h_2 + l_2 h_1) \cos \beta}{ac} \right].$$

### A4.3 Volumes of unit cells (see Section 6.5.6)

Orthorhombic

$$V = abc.$$

(Tetragonal:  $a = b$ ; cubic:  $a = b = c$ .)

Hexagonal:

$$V = (\sqrt{3}/2) a^2 c = 0.866 a^2 c.$$

Rhombohedral:

$$V = a^3 \sqrt{(1 - 3 \cos^2 \alpha + 2 \cos^3 \alpha)}.$$

Monoclinic:

$$V = abc \sin \beta.$$

### A4.4 Angles between planes in cubic crystals (variants between 100 and 221) (see Section 6.5.5)

100	100	0.00	90.00				
	110	45.00	90.00				
	111	54.74					
	210	26.56	63.43	90.00			
	211	35.26	65.90				
	221	48.19	70.53				
110	110	0.00	60.00	90.00			
	111	35.26	90.00				
	210	18.43	50.77	71.56			
	211	30.00	54.74	73.22	90.00		
	221	19.47	45.00	76.37	90.00		
111	111	0.00	70.53				
	210	39.23	75.04				
	211	19.47	61.87	90.00			
	221	15.79	54.74	78.90			
210	210	0.00	36.87	53.13	66.42	78.46	90.00
	211	24.09	43.09	56.79	79.48	90.00	
	221	26.56	41.81	53.40	63.43	72.65	90.00
211	211	0.00	33.56	48.19	60.00	70.53	80.40
	221	17.72	35.26	47.12	65.90	74.21	82.18

### A4.5 Relationships between zones and planes (see Section 6.5.3)

For a plane  $(hkl)$  which lies in a zone  $[uvw]$ :

$$hu + kv + lw = 0.$$

For a plane  $(hkl)$  which lies in a zone  $[UVTW]$ :

$$hU + kV + iT + lW = 0.$$

For a lattice point with coordinates  $[uvw]$  which lies in the  $n$ th  $(hkl)$  plane from the origin:

$$hu + kv + lw = n.$$

For a plane  $(hkl)$  which lies in the zones  $[u_1v_1w_1]$  and  $[u_2v_2w_2]$ :

$$h = (v_1w_2 - v_2w_1); \quad k = (w_1u_2 - w_2u_1); \quad l = (u_1v_2 - u_2v_1).$$

For a zone  $[uvw]$  which contains the planes  $(h_1k_1l_1)$  and  $(h_2k_2l_2)$ :

$$u = (k_1l_2 - k_2l_1); \quad v = (l_1h_2 - l_2h_1); \quad w = (h_1k_2 - h_2k_1).$$

# Appendix 5

---

## A simple introduction to vectors and complex numbers and their use in crystallography

### A5.1 Scalars, vectors, tensors

In science—and, of course, everyday life—we are concerned with different types of quantities as well as quantities of the same type but of different size or magnitude. In many cases the quantities are independent of direction—mass for example, or volume or temperature. Such quantities, which can be represented by points on scales, are known as **scalars** and are denoted algebraically in familiar italic type— $m$  for mass,  $t$  for time,  $x$  and  $y$  for unknown (scalar) quantities and so on. In many other cases, quantities are direction dependent, or, in other words, in order to specify the quantity completely the direction as well as the magnitude of the quantity needs to be described. Such quantities are called **vectors** and are denoted algebraically by printing in bold type— $\mathbf{a}$ ,  $\mathbf{b}$ ,  $\mathbf{x}$ ,  $\mathbf{y}$ , etc. In handwriting wavy underlining is substituted for bold type, i.e.  $\underline{a}$ ,  $\underline{b}$ ,  $\underline{x}$ ,  $\underline{y}$ , etc.

Velocity is an everyday example of a vector quantity—we need to specify not only the speed of an object but the direction in which it is travelling. A motor car travelling  $50 \text{ km h}^{-1}$  due north has the same speed as a motor car travelling  $50 \text{ km h}^{-1}$  due east, but their velocities are different—one has a velocity of  $50 \text{ km h}^{-1}$  *north* and the other has a velocity of  $50 \text{ km h}^{-1}$  *east*. The velocities may be represented as vectors by arrows—one pointing north and one pointing east. The lengths of the arrows or vectors gives the speed—the greater the speed the longer the arrows. In the above case ( $50 \text{ km h}^{-1}$ ), the arrows are of equal length.

Heat and electrical current flow, electrical and magnetic fields are examples of vector quantities of interest in crystal physics, but in geometrical crystallography we are invariably concerned with vectors which denote displacements: for example the displacement from one corner of a unit cell to the next, or the displacement from one atom to another. Crystal axes or directions are examples of such displacement vector quantities. In Fig. 5.1 (p. 77) the directions and lengths of the edges of the unit cell are all denoted by the vectors  $\mathbf{a}$ ,  $\mathbf{b}$ , and  $\mathbf{c}$ . In the special case of cubic crystals (Fig. 3.1, p. 53) these vectors are all at  $90^\circ$  (orthogonal) and are also the same length, but they are *not* identical vectors because they ‘point’ in different directions.

The ‘length’ of a vector is called its **modulus**. In the case of the motor car the modulus of the velocity is the speed. The modulus of a vector is written in two

ways, either in italic type,  $a$  (denoting that it is a scalar quantity), or with the heavy type vector symbol bracketed between straight vertical lines thus:  $|a|$ . Hence  $|a| = a$ .

In Fig. 3.1 the moduli  $a$ ,  $b$ , and  $c$  of the unit cell vectors for the fourteen Bravais lattices are indicated. In the case of cubic (or rhombohedral) crystals, the unit cell edge lengths, or moduli, are all identical and are represented (for all three axes) by  $a$ . Hence  $|a| = |b| = |c| = a$  (as in Fig. 3.1).

Scalars and vectors are particular types of quantities which are known in general as **tensors**. There are other, more complicated types of tensors which are of importance in crystal physics because they are able to describe properties such as conductivity or stress which vary not only with the direction of the applied field or force but also with the orientation of the crystal. 'Everyday' examples of tensors (other than scalars or vectors) are not easy to provide, but the following, perhaps rather contrived example, may illustrate the ideas involved.

Consider rainwater flowing down a corrugated roof. The flow of water (a vector) is obviously down the roof, parallel to the corrugations and parallel also to a vector representing the inclined component of the gravitational field. The effective 'conductivity' may simply be regarded as the quantity that relates these two parallel vectors. Now consider a (badly made) roof in which the corrugations are set at an angle. The water will partly run sideways, along the 'preferred direction' of the corrugations and will partly flow downwards over from one corrugation to the next. The overall water flow will lie in a direction somewhere between the lines of the corrugations and downwards. In this case the effective gravitational field vector and the water flow vector are not parallel, and in estimating the effective conductivity of the roof, both the 'downwards' and 'sideways' components of the water flow need to be taken into account.

In crystals the 'corrugations' may be loosely regarded as preferred or easy directions of, say, heat or electrical flow. The conductivity of the crystal is the quantity which relates one vector (heat or electrical flow) to another vector (temperature or electrical field gradient). As indicated in the example above these vectors may not, except in special cases, be parallel and in general a total of 9 terms or components\* are required in order to specify the conductivity completely.

Conductivity is called a second-rank tensor property. There are, in addition, third-rank tensor properties (e.g. piezoelectricity) which are specified by 27 components and fourth-rank tensor properties (e.g. elasticity) which are specified by 81 components. Scalars, which are specified by one term or component are, in this classification, called zero-rank tensors and vectors which are, as shown below, specified by three components are called first-rank tensors.

\*These components are not all independent; their number is greatly reduced by symmetry considerations. For further information on tensors, see J. F. Nye, *Physical Properties of Crystals*, Clarendon Press, Oxford, Second Edition 1985, and F. G. Fumi *Il Nuovo Cimento* (1952) Volume 9, pp. 739–56.



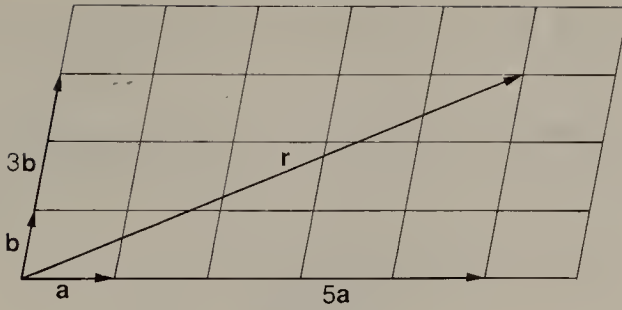


Fig. A5.1

### A5.2 Resolving vectors into components and vector addition

Consider the (displacement) vector  $\mathbf{r}$  drawn in Fig. A5.1 which is outlined in a (two-dimensional) lattice with the unit cell vectors  $\mathbf{a}$  and  $\mathbf{b}$ . Note that all these vectors have a common origin.

The vector  $\mathbf{r}$  may be resolved into its components in the directions of the unit cell vectors  $\mathbf{a}$  and  $\mathbf{b}$ . These components,  $5\mathbf{a}$  and  $3\mathbf{b}$ , are drawn in Fig. A5.1. Added together they give  $\mathbf{r}$ , i.e.  $\mathbf{r} = 5\mathbf{a} + 3\mathbf{b}$ .

In vector analysis in general, cubic or Cartesian axes are chosen, and the unit cell vectors are labelled  $\mathbf{i}$ ,  $\mathbf{j}$ ,  $\mathbf{k}$  rather than  $\mathbf{a}$ ,  $\mathbf{b}$ ,  $\mathbf{c}$ . Also, the moduli of  $\mathbf{i}$ ,  $\mathbf{j}$ ,  $\mathbf{k}$  are unity and they are known as **unit vectors**. The general symbol for a unit vector is  $\mathbf{n}$ , i.e.  $|\mathbf{n}| = 1$ .

### A5.3 Multiplying vectors—scalar products and vector products

There are two ways in which vectors can be multiplied, namely, the scalar product and the vector product, the general significance of which go beyond the scope of this book. We will consider only the multiplication of displacement vectors.

The scalar (or 'dot') product  $\mathbf{a} \cdot \mathbf{b}$  may be thought of as 'representing' the product of the moduli of the vectors resolved in the direction of one or other of the vectors. For example (Fig. A5.2), if the angle between the vectors, drawn from a common origin, is  $\theta$ , the resolved component of the modulus of  $\mathbf{b}$  along

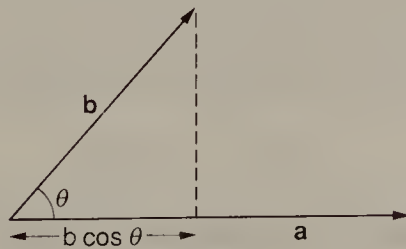


Fig. A5.2

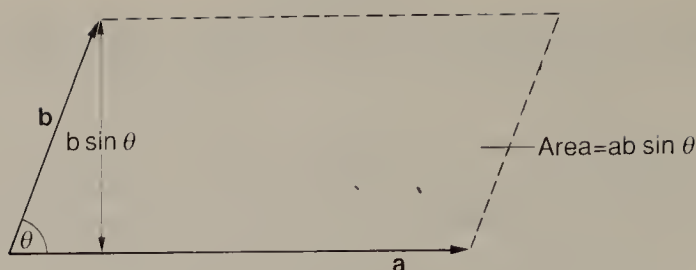


Fig. A5.3

the  $\mathbf{a}$  direction is  $b \cos \theta$ . Hence  $\mathbf{a} \cdot \mathbf{b} = ab \cos \theta$ . The same result applies if  $\mathbf{a}$  is resolved along the direction of  $\mathbf{b}$ .

If one of the vectors is a unit vector:—say in Fig. A5.2  $\mathbf{a} = \mathbf{n}$ , then the scalar product  $\mathbf{n} \cdot \mathbf{b} = b \cos \theta$  (since  $|\mathbf{n}| = 1$ ): it is simply the modulus of  $\mathbf{b}$  resolved along the direction of the unit vector  $\mathbf{n}$ . The scalar product may therefore be thought of as a ‘shorthand’ means of resolving the vectors along different directions.

Clearly, the maximum value of the scalar product occurs when the vectors are parallel ( $\theta = 0^\circ$ ) and the minimum value, zero, occurs when they are at right angles ( $\theta = 90^\circ$ ). The scalar product of a vector multiplied by itself is simply the modulus squared, i.e.  $\mathbf{a} \cdot \mathbf{a} = |\mathbf{a}| |\mathbf{a}| = a^2$ .

The vector (or ‘cross’) product  $\mathbf{a} \times \mathbf{b}$  may be thought of as ‘representing’ the area outlined by two vectors. In Fig. A5.3 the area outlined by the vectors  $\mathbf{a}$  and  $\mathbf{b}$  is  $ab \sin \theta$ . But there is more: the area may represent a crystal plane or surface, the **orientation** of which also needs to be specified. The orientation of the surface may be specified by the direction normal to it, i.e. perpendicular to the page. Let the unit vector along this direction be  $\mathbf{n}$ ; then  $\mathbf{a} \times \mathbf{b} = (ab \sin \theta) \mathbf{n}$ .

In general, the vector product is expressed as  $\mathbf{a} \times \mathbf{b} = \mathbf{c}$ , where  $\mathbf{c}$  is perpendicular to  $\mathbf{a}$  and  $\mathbf{b}$  and  $|\mathbf{c}| = ab \sin \theta$ . The largest value of  $\mathbf{c}$  occurs when  $\mathbf{a}$  and  $\mathbf{b}$  are at right angles and the smallest value, zero, occurs when they are parallel. Finally, the vector product involves the use of a sign convention: the vector  $\mathbf{c}$  and  $\mathbf{n}$  is perpendicular to the plane defined by  $\mathbf{a}$  and  $\mathbf{b}$  but can have one of two directions, i.e. with reference to Fig. A5.3, it can be ‘up’ from the page or ‘down’. One vector must have a  $+$  sign and the opposite must have a  $-$  sign. The sign convention is as follows. Consider in Fig. A5.3 an (ordinary) right-handed screw coming out of the page (i.e. parallel to  $\mathbf{c}$  or  $\mathbf{n}$ ) through the common origin of  $\mathbf{a}$  and  $\mathbf{b}$ . If we ‘screw’ from  $\mathbf{a}$  to  $\mathbf{b}$  the screw will move ‘upwards’ and this upwards direction is the direction or sense of  $\mathbf{c}$ . If we screw in the opposite direction, from  $\mathbf{b}$  to  $\mathbf{a}$ , the screw will move downwards. Hence, the order of the multiplication of vectors is important and leads to the **anticommunicative law** for the vector product:

$$\mathbf{a} \times \mathbf{b} = -(\mathbf{b} \times \mathbf{a}).$$

#### A5.4 Multiplication of vectors in terms of components

Calculations are generally made easier if vectors are expressed in terms of their components on a Cartesian axis system with unit vectors,  $\mathbf{i}$ ,  $\mathbf{j}$ ,  $\mathbf{k}$  at right angles.

In this case  $\mathbf{i} \cdot \mathbf{i} = 1$ ,  $\mathbf{i} \cdot \mathbf{j} = 0$ ,  $\mathbf{i} \times \mathbf{i} = 0$ ,  $\mathbf{i} \times \mathbf{j} = \mathbf{k}$ , and similarly for the other combinations of  $\mathbf{i}$ ,  $\mathbf{j}$  and  $\mathbf{k}$ .

Writing

$$\mathbf{a} = (a_1\mathbf{i} + a_2\mathbf{j} + a_3\mathbf{k}) \quad \text{and} \quad \mathbf{b} = (b_1\mathbf{i} + b_2\mathbf{j} + b_3\mathbf{k}).$$

The scalar product

$$\begin{aligned} \mathbf{a} \cdot \mathbf{b} &= (a_1\mathbf{i} + a_2\mathbf{j} + a_3\mathbf{k}) \cdot (b_1\mathbf{i} + b_2\mathbf{j} + b_3\mathbf{k}) \\ &= a_1b_1\mathbf{i} \cdot \mathbf{i} + a_1b_2\mathbf{i} \cdot \mathbf{j} + \dots \\ &= (a_1b_1 + a_2b_2 + a_3b_3) \end{aligned}$$

(all the other terms cancel because  $\mathbf{i} \cdot \mathbf{i} = 1$  and  $\mathbf{i} \cdot \mathbf{j} = 0$ , etc.)

The vector product

$$\begin{aligned} \mathbf{a} \times \mathbf{b} &= (a_1\mathbf{i} + a_2\mathbf{j} + a_3\mathbf{k}) \times (b_1\mathbf{i} + b_2\mathbf{j} + b_3\mathbf{k}) \\ &= a_1b_1(\mathbf{i} \times \mathbf{i}) + a_1b_2(\mathbf{i} \times \mathbf{j}) + \dots \\ &= (a_2b_3 - b_2a_3)\mathbf{i} + (a_3b_1 - b_3a_1)\mathbf{j} + (a_1b_2 - b_1a_2)\mathbf{k} \end{aligned}$$

(all the other terms cancel because  $\mathbf{i} \times \mathbf{i} = 0$  and  $\mathbf{i} \times \mathbf{j} = \mathbf{k}$ , etc.).

The vector product may be expressed in matrix form as a determinant:

$$\mathbf{a} \times \mathbf{b} = \begin{vmatrix} \mathbf{i} & \mathbf{j} & \mathbf{k} \\ a_1 & a_2 & a_3 \\ b_1 & b_2 & b_3 \end{vmatrix}.$$

### A5.5 Volumes of unit cells in vector notation

The volume of a unit cell defined by vectors  $\mathbf{a}$ ,  $\mathbf{b}$ , and  $\mathbf{c}$  is 'the area of the base times the height'.

The 'area of the base' is  $(\mathbf{a} \times \mathbf{b}) = (ab \sin \theta)\mathbf{n}$ . The 'height' is the component of  $\mathbf{c}$  resolved in the direction of the normal  $\mathbf{n}$  (Fig. A5.4), i.e. the height  $= \mathbf{n} \cdot \mathbf{c} = c \cos \phi$ . Hence the volume  $V = (\mathbf{a} \times \mathbf{b}) \cdot \mathbf{c}$ . It is a scalar quantity. The vectors  $\mathbf{a}$ ,  $\mathbf{b}$ ,  $\mathbf{c}$  in this equation may be 'cycled' but the sequence must be maintained, i.e.

$$V = (\mathbf{a} \times \mathbf{b}) \cdot \mathbf{c} = \mathbf{a} \cdot (\mathbf{b} \times \mathbf{c}) = (\mathbf{c} \times \mathbf{a}) \cdot \mathbf{b}, \text{ etc.}$$

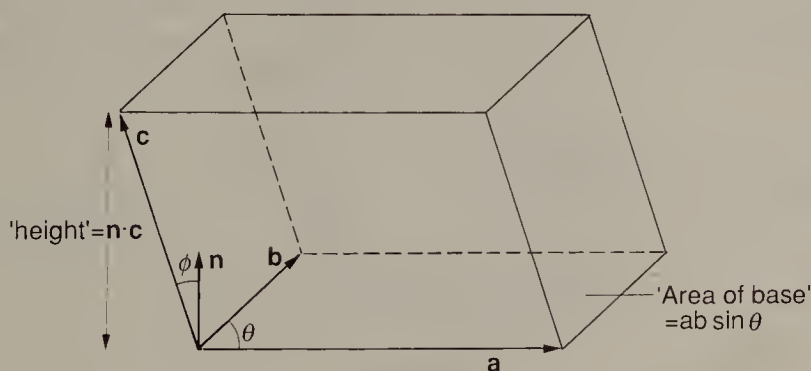


Fig. A5.4

If the sequence is reversed, i.e.  $(\mathbf{b} \times \mathbf{a}) \cdot \mathbf{c}$ , then a negative volume results. In practice this can occur if a left-handed set of axes are substituted, inadvertently or otherwise, for a right-handed set.

The reciprocal unit cell  $\mathbf{a}^*$ ,  $\mathbf{b}^*$ ,  $\mathbf{c}^*$  can be derived from the 'direct' unit cell  $\mathbf{a}$ ,  $\mathbf{b}$ ,  $\mathbf{c}$  in a similar way as outlined in Section 6.5.6. Note that the relationships

$$\mathbf{a}^* = \frac{\mathbf{b} \times \mathbf{c}}{V} \text{ etc.}$$

are valid for the primitive unit cells for any axis system.

### A5.6 Representing vectors by complex numbers: the Argand diagram

The sum of a number of vectors  $\mathbf{a} + \mathbf{b} + \mathbf{c} + \dots$  may be simply obtained graphically by adding them 'top to tail' as shown in Fig. A5.5. In the case where the vectors represent the atomic scattering factors,  $f$ , for the atoms in the motif, the sum is the structure factor  $F_{hkl}$ .

However, although graphical procedures are very instructive in that they clearly show the physical principles involved, they are also very clumsy and do not readily lend themselves to analytical procedures. We need therefore an alternative method of representing vectors and the method we adopt is that of representing vectors as complex numbers.

A complex number,  $z$ , is a number which has two parts of the form

$$z = x + iy$$

where  $x$  and  $y$  are real numbers and  $i = \sqrt{-1}$ . The first part,  $x$ , is called the real part of the complex number and the second part,  $iy$ , is called the imaginary part. These two parts can be represented graphically on what is known as an Argand diagram—a graph in which the horizontal axis (abscissa) represents  $x$ , the real part and the vertical axis (ordinate) represents  $iy$ , the imaginary part (Fig. A5.6).

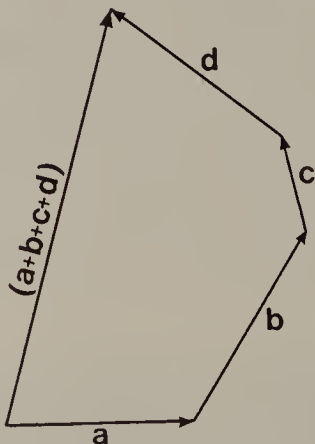


Fig. A5.5



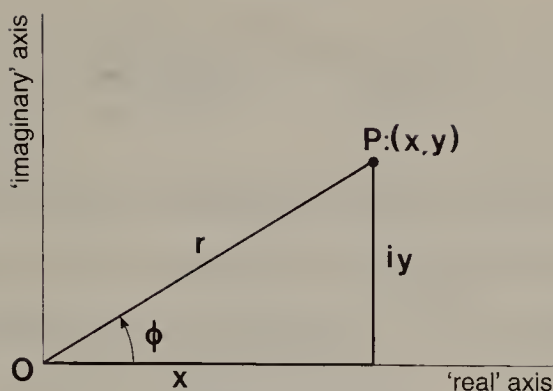


Fig. A5.6

The complex number  $z$  is represented on the Argand diagram by the point  $P:(x, y)$  and the length  $OP = r = \sqrt{x^2 + y^2}$  is called the **modulus** of the complex number  $z$  (or simply 'mod  $z$ ' or  $|z|$ ). Hence (from Fig. A5.6) the complex number  $z$  can be written in the form:

$$z = r \cos \phi + i r \sin \phi$$

where  $r$  (the modulus) and  $\phi$  (the angle) are known as polar coordinates. This expression can further be written in exponential form (Euler's formula);  $\cos \phi + i \sin \phi = \exp i \phi$  and  $\cos \phi - i \sin \phi = \exp -i \phi$ , i.e.  $z = r \exp i \theta$ .

This representation of complex numbers in exponential form by means of the polar coordinates  $r$  and  $\phi$  allows us to add, subtract and carry out other mathematical operations upon them without having to resort to rulers and graph paper.

For example, the addition of complex numbers,  $z_1 + z_2 + \dots$  is simply given by:

$$z_1 + z_2 + \dots = r_1 \exp i \phi_1 + r_2 \exp i \phi_2,$$

or:

$$z_1 + z_2 + \dots = r_1 \cos \phi_1 + r_2 \cos \phi_2 + \dots + i(r_1 \sin \phi_1 + r_2 \sin \phi_2 + \dots)$$

(sum of 'horizontal' components) +  $i$ (sum of 'vertical' components).

This is the procedure used to find the structure factor  $F_{hkl}$ , the sum of all the atomic scattering factors,  $f$ , for the atoms in the motif.

The complex conjugate of a complex number, symbol  $z^*$ , is one which has the same modulus  $r$ , but a negative angle  $\phi$ , i.e.

$$z^* = r \cos \phi - i r \sin \phi = r \exp -i \phi.$$

The complex conjugate can be used, for example to determine the modulus  $r$  of a complex number, i.e.

$$z \cdot z^* = r \exp i \phi \cdot r \exp -i \phi = r^2.$$

# Appendix 6

---

## Systematic absences (extinctions) in X-ray diffraction and double diffraction in electron diffraction patterns

### A6.1 Systematic absences

In X-ray diffraction (and also, except for the complication of double diffraction, in electron diffraction) the intensities of reflections from certain planes with Laue indices  $hkl$  are zero. Such reflections are said to be *forbidden* or *extinguished* or, better, *systematically absent* since they arise from the centring of the unit cell and/or the presence of translational symmetry elements—glide planes and screw axes. The identification of systematic absences is very useful since it provides the ‘first step’ in crystal structure determination.

The subject may be best introduced by considering the diffraction of light from a wide slit diffraction grating (Section 7.4). In the diffraction of light extinctions or ‘missing orders’ occur for certain ratios of the slit spacing  $a$  and the slit width  $d$ . For example, referring to Fig. 7.7, if the slit width  $d$  is set equal to one-third of the slit spacing  $a$ , then the zero order minimum of the central peak from a single slit (Fig. 7.7(b)) coincides with the angle of the third order diffracted peaks  $n = \pm 3$  (Fig. 7.7(a)). These peaks (and subsequently the sixth, ninth etc. order peaks) are therefore of zero intensity (i.e. extinguished). Other sets of systematic absences may be derived for other combinations of  $a$  and  $d$ —the most important being that when  $d = \frac{1}{2}a$  (see Exercise 7.2).

Systematic absences in crystals may be derived in two ways: either by a consideration of the geometrical consequences arising from the use of centred, rather than primitive, unit cells and the presence of glide planes and screw axes, or by application of the structure factor equation. The former approach is the proper one, since systematic absences arise solely as a consequence of the architecture of crystals—but the latter approach is a useful means of gaining practice and familiarity with the structure factor equation. We will start with both approaches for an fcc crystal.

Consider Fig. A6.1 which shows the unit cell vectors **a**, **b**, **c** for the conventional fcc unit cell and the unit cell vectors **A**, **B**, **C** for (one variant) of the primitive rhombohedral unit cell. The origin is drawn at the front left-hand corner to help make clear the shape of the rhombohedral cell.

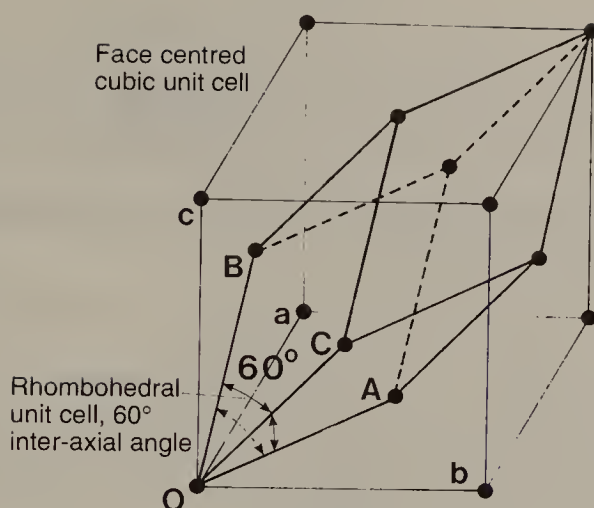


Fig. A6.1

Writing down the transformation equations for unit cell vectors or axes (see Section 5.8):

$$\mathbf{A} = \frac{1}{2}\mathbf{a} + \frac{1}{2}\mathbf{b} + 0\mathbf{c}$$

$$\mathbf{B} = \frac{1}{2}\mathbf{a} + 0\mathbf{b} + \frac{1}{2}\mathbf{c}$$

$$\mathbf{C} = 0\mathbf{a} + \frac{1}{2}\mathbf{b} + \frac{1}{2}\mathbf{c}.$$

Now, as shown in Section 5.8, Miller indices transform in the same way as unit cell vectors. Hence if  $(HKL)$  and  $(hkl)$  are the Miller indices of a plane referred to the primitive and fcc unit cells, respectively:

$$H = \frac{1}{2}h + \frac{1}{2}k + 0l \quad 2H = h + k$$

$$K = \frac{1}{2}h + 0k + \frac{1}{2}l \quad \text{or} \quad 2K = h + l$$

$$L = 0h + \frac{1}{2}k + \frac{1}{2}l \quad 2L = k + l.$$

Now  $H$ ,  $K$ ,  $L$  are all integers, odd or even; hence  $2H$ ,  $2K$ ,  $2L$  are all even integers, from which it follows that  $(h + k)$ ,  $(h + l)$ ,  $(k + l)$  are also all even integers.

An even integer is either the sum of two even integers, or two odd integers, but not mixed. Hence, for each identity,  $h$ ,  $k$ ,  $l$  are either all odd or all even integers. In other words the lattice planes from which reflections occur are those for which  $h$ ,  $k$ ,  $l$  are all even or all odd integers. When  $h$ ,  $k$ ,  $l$  are mixed (some odd, some even) the Miller index  $(hkl)$  describes a set of planes which are not lattice planes since they do not all pass through lattice points.

Now let us derive the same result using the structure factor equation applied to an fcc crystal with an identical atom (atomic scattering factor  $f$ ) at each of the four lattice points in the cell. The  $(u_n v_n w_n)$  fractional coordinate values of these atoms are:

$$(000), \left(\frac{1}{2} \frac{1}{2} 0\right), \left(\frac{1}{2} 0 \frac{1}{2}\right), \left(0 \frac{1}{2} \frac{1}{2}\right).$$

Hence,

$$F_{hkl} = f \exp 2\pi i(h0 + k0 + l0) + f \exp 2\pi i(h\frac{1}{2} + k\frac{1}{2} + l0) \\ + f \exp 2\pi i(h\frac{1}{2} + k0 + l\frac{1}{2}) + f \exp 2\pi i(h0 + k\frac{1}{2} + l\frac{1}{2}).$$

Simplifying, and remembering that since the cell is centrosymmetric the sine components in the exponents vanish:

$$F_{hkl} = f(1 + \cos 2\pi(h + k) + \cos 2\pi(h + l) + \cos 2\pi(k + l)).$$

Now,  $\cos 2\pi$  (even integer) = +1 and  $\cos 2\pi$  (odd integer) = -1. The value of  $F_{hkl}$  will depend on whether  $h, k, l$  are all even, all odd or mixed. It is easily seen that if they are all even or all odd  $F_{hkl} = 4f$  and if they are mixed  $F_{hkl} = 0$ .

The conditions for systematic absences from body- and base-centred lattices can be derived in the same ways: either by referring the lattice to a primitive unit cell or by applying the structure factor equation. For example, for a body-centred cubic crystal with identical atoms at (000) and  $(\frac{1}{2}\frac{1}{2}\frac{1}{2})$

$$F_{hkl} = f \exp 2\pi i(h0 + k0 + l0) + f \exp 2\pi i(h\frac{1}{2} + k\frac{1}{2} + l\frac{1}{2}) \\ = f(1 + \cos \pi(h + k + l)).$$

Hence when  $(h + k + l) = \text{even integer}$   $F_{hkl} = 2f$  and when  $(h + k + l) = \text{odd integer}$   $F_{hkl} = 0$ .

Systematic absences for glide planes and screw axes may be derived in the same way; an example of each will suffice to show the principles involved.

Figure A6.2 shows a (monoclinic) crystal with a  $c$ -glide plane in the  $xz$  plane (the plane of the paper). The action of the  $c$ -glide is to translate any atom, atomic scattering factor  $f$ , with fractional coordinates  $(uvw)$  to  $(u\bar{v}\frac{1}{2} + w)$ . Substituting these two values in the structure factor equation:

$$F_{hkl} = f \exp 2\pi i(hu + kv + lw) + f \exp 2\pi i(hu + k\bar{v} + l(\frac{1}{2} + w)).$$

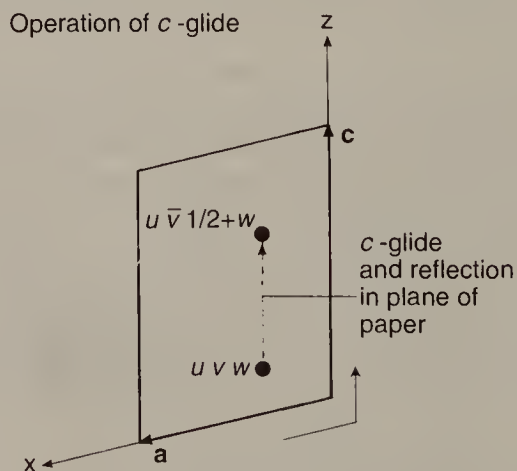


Fig. A6.2



Operation of screw diad

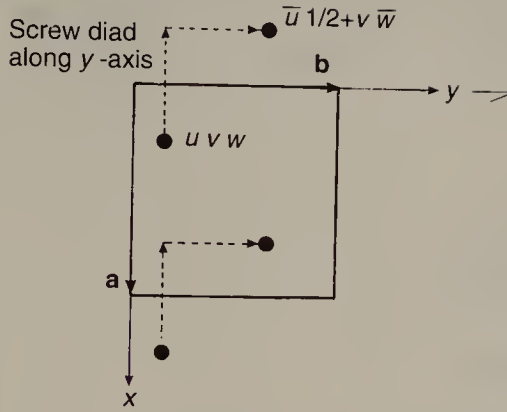


Fig. A6.3

Consider the  $h0l$  reflections ( $k = 0$ ):

$$\begin{aligned} F_{h0l} &= f \exp 2\pi i(hu + lw) + f \exp 2\pi i(hu + lw) \exp 2\pi i \frac{1}{2}l \\ &= f \exp 2\pi i(hu + lw)[1 + \exp \pi il]. \end{aligned}$$

When  $l = \text{odd integer}$ ,  $\exp \pi il = -1$  and  $F_{h0l} = 0$ . This then gives the condition for systematic absences for the  $h0l$  planes; systematic absences occur when  $l$  equals an odd integer and, correspondingly, reflections occur when  $l$  equals an even integer.

Figure A6.3 shows a (monoclinic) crystal with a screw diad axis,  $2_1$  along the  $y$ -axis, the action of which is to translate an atom with fractional coordinates  $(uvw)$  to  $(\bar{u}(\frac{1}{2} + v)\bar{w})$ . Proceeding as before:

$$F_{hkl} = f \exp 2\pi i(hu + kv + lw) + f \exp 2\pi i(h\bar{u} + k(\frac{1}{2} + v) + l\bar{w})$$

consider the  $0k0$  reflections ( $h = l = 0$ )

$$\begin{aligned} F_{0k0} &= f \exp 2\pi i(kv) + f \exp 2\pi i(k\frac{1}{2} + kv) \\ &= f \exp 2\pi i(kv)[1 + \exp \pi ik]. \end{aligned}$$

When  $k = \text{odd integer}$ ,  $\exp \pi ik = -1$  and  $F_{0k0} = 0$  and reflections only occur from  $0k0$  planes when  $k$  equals an even integer. This result can also be seen intuitively: the action of the screw diad axis repeats the atomic layers at spacings equal to half the  $b$  lattice repeat distance.

Table A6.1 summarizes the extinction criteria for lattices and translational symmetry elements.

Table A6.2 lists the reflecting planes in cubic  $P$ ,  $I$ ,  $F$  and diamond-cubic crystals in order of decreasing  $d_{hkl}$ -spacing. For cubic crystals  $d_{hkl} = a/\sqrt{N}$  where  $a$  = the lattice parameter and  $N = (h^2 + k^2 + l^2)$ . The conditions for reflection for a diamond-cubic crystal are  $h, k, l$  are all odd or all even integers (since a diamond-cubic crystal has an fcc lattice) with the additional condition that  $(h + k + l)$  is an odd integer or an integer which is an even multiple of 2.

**Table A6.1** Extinction criteria for lattices and symmetry elements

Lattice or symmetry element type	Symbol	Class of reflections	Condition for presence
Lattice type:		$hkl$	
primitive	$P$		none
body-centred	$I$		$h + k + l = 2n$
centred on the $C$ face	$C$		$h + k = 2n$
centred on the $A$ face	$A$		$k + l = 2n$
centred on the $B$ face	$B$		$h + l = 2n$
			$h, k, l$
centred on all faces	$F$		all = $n$ (odd) or all = $2n$ (even)
rhombohedral, obverse	$R$		$-h + k + l = 3n$
rhombohedral, reverse	$R$		$h - k + l = 3n$
Glide plane $\parallel (001)$	$a$ $b$ $n$ $d$	$hk0$	$h = 2n$ $k = 2n$ $h + k = 2n$ $h + k = 4n$
Glide plane $\parallel (100)$	$b$ $c$ $n$ $d$	$0kl$	$k = 2n$ $l = 2n$ $k + l = 2n$ $k + l = 4n$
Glide plane $\parallel (010)$	$a$ $c$ $d$ $n$	$h0l$	$h = 2n$ $l = 2n$ $h + l = 2n$ $h + l = 4n$
Glide plane $\parallel (110)$	$c$ $b$ $n$ $d$	$hkl$	$l = 2n$ $h = 2n$ $h + k = 2n$ $2h + l = 4n$
Screw axis $\parallel c$	$2_1, 4_2, 6_3$ $3_1, 3_2, 6_2, 6_4$ $4_1, 4_2$ $6_1, 6_5$	$00l$	$l = 2n$ $l = 3n$ $l = 4n$ $l = 6n$
Screw axis $\parallel a$	$2_1, 4_2$ $4_1, 4_3$	$h00$	$l = 2n$ $l = 4n$
Screw axis $\parallel b$	$2_1, 4_2$ $4_1, 4_3$	$0k0$	$k = 2n$ $k = 4n$
Screw axis $\parallel [110]$	$2_1$	$hh0$	$h = 2n$

( $n$  = odd integer,  $2n$  = even integer etc.)

Table A6.2

<i>N</i>	<i>hkl</i>	cubic <i>P</i>	cubic <i>I</i>	cubic <i>F</i>	Diamond cubic
1	100	✓			
2	110	✓	✓		
3	111	✓		✓	✓
4	200	✓	✓	✓	
5	210	✓			
6	211	✓	✓		
7	—				
8	220	✓	✓	✓	✓
9	300/221	✓			
10	310	✓	✓		
11	311	✓		✓	✓
12	222	✓	✓	✓	
13	320	✓			
14	321	✓	✓		
15	—				
16	400	✓	✓	✓	✓
17	410	✓			
18	330/411	✓	✓		
19	331	✓		✓	✓
20	420	✓	✓	✓	

*Note 1* There are no squares of three numbers which add up to 7, 15 etc. This means that there are 'gaps' in the sequence of reflections for cubic *P* crystals, i.e. 'line 7', 'line 15' etc. are missing.

*Note 2* Cubic *I* crystals show a uniform sequence of reflections (with no 'gaps' as in cubic *P* crystals).

*Note 3* Cubic *F* crystals show a characteristic sequence of lines: 'two-together', 'one-on-its-own', 'two-together' etc.

## A6.2 Double diffraction

In electron diffraction the presence of face- or body-centring lattice points also gives rise to systematically absent reflections just as in the case of X-ray diffraction (the first group in Table A6.1). However, reflections which are systematically absent in X-ray diffraction as a result of the presence of translational symmetry elements (glide planes and screw axes, Table A6.1) may, and usually do, occur in electron diffraction patterns. This is known as double diffraction and occurs because the intensities of the diffracted beams may be comparable with that of the direct or undiffracted beam—a consequence of the dynamical interactions between the direct and diffracted beams. The effect, in terms of the geometry of the electron diffraction pattern, is that a strong diffracted beam can behave, as it were, as the direct beam and the whole pattern is in effect shifted so as to be centred about the diffracted beam. In the case of electron diffraction patterns from centred lattices all the spots are coincident and no new ones arise; but in most other cases new ones arise in positions in

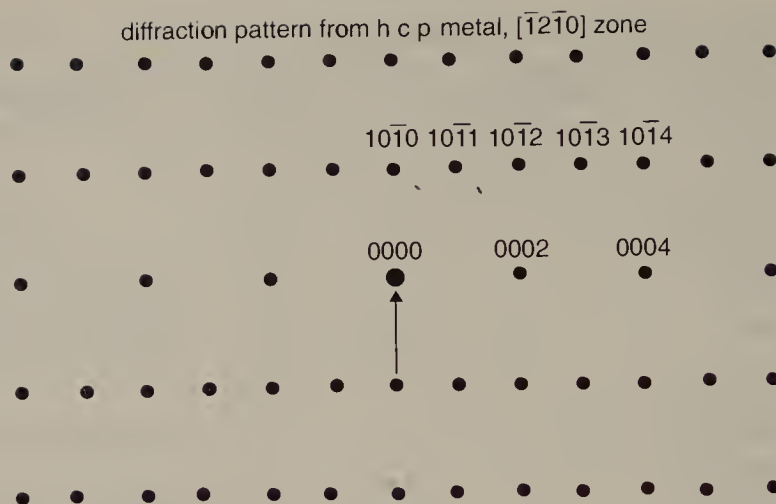


Fig. A6.4

which the diffraction spots should be systematically absent. A simple example—that of electron diffraction from the hcp structure—will make this clear.

In the hcp structure the relevant translational symmetry element is the screw hexad (Fig. 4.9) which describes the symmetry of the sequence of A and B layer atoms (Fig. 1.5(b)). Consider the conditions for constructive interference for Bragg reflections from the A layers of atoms, i.e. the (0001) planes with interplanar spacing  $d_{0001} = c$ . When the path difference (P.D.) is  $1\lambda$  (constructive interference), the path difference between the interleaving A and B layers of atoms, interplanar spacing  $d_{0002} = c/2$  is  $\frac{1}{2}\lambda$ , which is the condition for *destructive* interference; hence the 0001 reflection is (systematically) absent. Second-order reflection from the (0001) planes (P.D. =  $2\lambda$ ) corresponds to the first-order reflection from the (0002) planes (P.D. =  $1\lambda$ ). Continuing in this way it turns out that  $000l$  reflections where  $l$  is odd are systematically absent, as shown in Table A6.1. The same result may be found by applying the structure factor equation to the (0001), (0002), (0003) etc. planes, as in Example 9.2: when  $l$  is odd the atomic scattering factors for the A and B layer atoms are equal and opposite.

Now let us draw a commonly-observed hcp electron diffraction pattern from the  $[\bar{1}2\bar{1}0]$  zone (Fig. A6.4), showing the systematically absent reflections  $0001$ ,  $000\bar{1}$ ,  $0003$ ,  $000\bar{3}$  etc. in the row through the origin\*. Now suppose that the (strong)  $10\bar{1}0$  reflected beam acts as it were as the direct beam: the whole pattern will, in effect, be shifted from the origin  $0000$  to  $10\bar{1}0$  as shown by the arrow and spots will now appear in the systematically absent positions. The same result will be obtained for other choices of strong diffracted beams—as can

\* Systematic absences also occur in every *third* row (not shown in Fig. A6.4). These arise because the A-layer and B-layer atoms are in special equivalent positions in the hexagonal unit cell (see Section 4.6). This leads to the conditions for  $hkl$ : if  $h - k = 3n$ ,  $l = 2n$ , i.e. in the third row the  $30\bar{3}1$ ,  $30\bar{3}3$  etc. reflections are systematically absent.



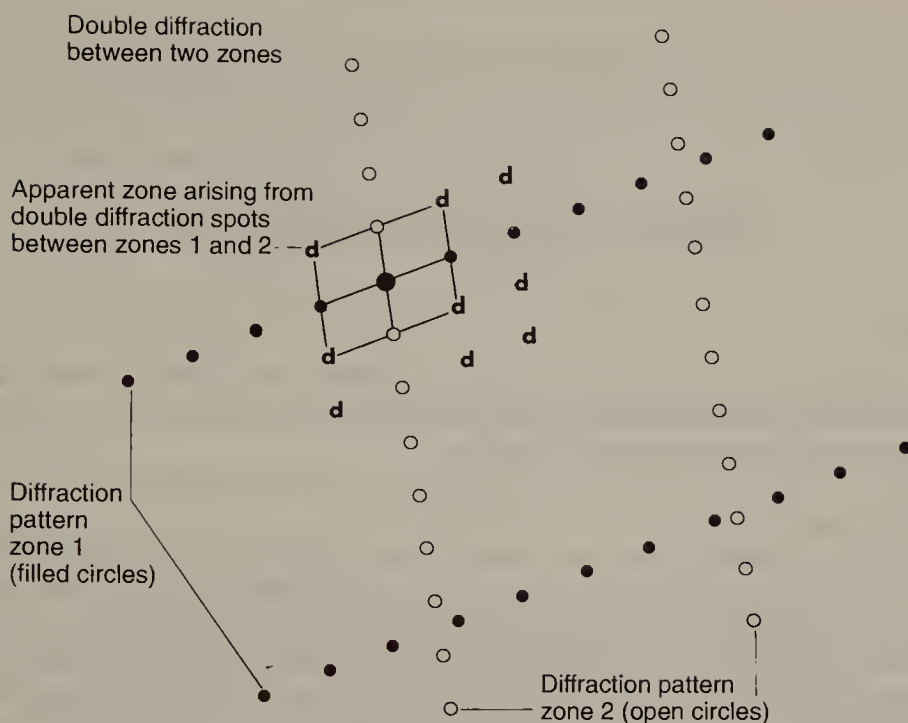


Fig. A6.5

easily be seen by making a tracing paper overlay in Fig. A6.4 and shifting the origin to the positions of different diffracted spots.

Double diffraction can also occur in situations in which the electron diffraction spots of two (or more) crystals are present in the pattern. In such cases the double-diffracted spots which appear may correspond to no  $d$ -spacing in either crystal—and are probably the biggest cause of the frustrated electron microscopists' 'unindexable' patterns. Figure A6.5 indicates the geometry involved. Here, two (high order) patterns are shown consisting of widely separated rows (indicated by filled and open circles). The strong spots in the rows through the origin may act in effect as the direct beam, generating additional double diffraction spots in the positions marked by the letter  $d$ . The pattern *appears* to be from a relatively simple low-order zone—but of course it is not, and is either unindexable or (worse) may be indexed incorrectly. An example of the latter case is that of the electron diffraction patterns from twin-related plates or laths of ferrite (bcc) which occur in the microstructures of some structural steels. In certain twin orientations the double-diffracted spots correspond very closely with those expected of the high temperature austenite (fcc) phase—leading to the erroneous conclusion that this phase is retained between the ferrite plates in the microstructure.

# Answers to exercises

## Chapter 1

- 1.3 (a) In the ccp structure there are four sets of close-packed planes and six close-packed directions and in the hcp structure only one set of close-packed planes and three close-packed directions.  
 (b) In the bcc structure there are six sets of closest-packed planes and four close-packed directions.
- 1.4 In the ccp structure each close-packed plane contains three close-packed directions, i.e. three slip systems share a common close-packed plane. As there are four sets of close-packed planes in the ccp structure there are therefore twelve slip systems. In the bcc structure each closest-packed plane contains two close-packed directions, i.e. two slip systems share a common closest-packed plane. As there are six sets of closest-packed planes in the bcc structure there are therefore also twelve slip systems.
- 1.5 The height of the tetrahedron (i.e. the distance from its vertex to its base) is simply  $\sqrt{(2/3)}$  of the length of its edge which is the unit cell edge length  $a$ . Hence
- $$c/a = 2\sqrt{(2/3)} = 1.633.$$
- 1.6 The atomic coordinates are (000) (for all the 'A layer' atoms situated at the corners of the unit cell), and *either*  $(\frac{1}{3}\frac{2}{3}\frac{1}{2})$  *or*  $(\frac{2}{3}\frac{1}{3}\frac{1}{2})$  for the 'B layer' or the 'C layer' atom within the cell, depending upon the arbitrary choice made between these two possible (B or C) sites.
- 1.7 Faulting one close-packed layer of atoms gives rise to an intrinsic stacking fault, faulting the next layer above (or below) gives an extrinsic stacking fault. (a) A twin is produced by faulting every close-packed layer and (b) the hcp sequence is produced by faulting every alternative layer.
- 1.8 For B6 (carborundum II) the stacking sequence is ABCACBA... giving a six-layer unit cell repeat distance. In the Shockley notation this is  $\triangle \triangle \triangle \nabla \nabla \nabla \dots$ , i.e. an inversion every three layers (rather than an inversion every layer in B4 and an inversion every two layers in B5).

For B7 (carborundum I) the stacking sequence is ABACBCACBABCACBACA... giving a fifteen-layer unit cell repeat distance. In the Shockley notation this is  $\triangle \nabla \nabla \nabla \triangle \triangle \nabla \nabla \nabla \triangle \triangle \nabla \nabla \nabla \triangle \dots$ , i.e. inversions every two and three layers alternately.

## Chapter 2

- 2.1 There are twice as many mirror lines in  $p3m1$  and the triads lie at the intersections of all of them; in  $p31m$  half the triads are not intersected by mirror lines.
- 2.2 The lattice type is  $p3m1$  (refer to your drawings or Question 2.1).
- 2.3 The lattice type is  $p2$ —i.e. the pattern has identical symmetry to Fig. 2.7; it is based on the oblique plane lattice, *not* a rectangular plane lattice (primitive or centred) because there are no mirror lines of symmetry present.

- 2.4 The lattice type is  $pg$ . The glide lines run vertically through the back heels of the black men and the raised hands of the white men.
- 2.5 A  $4'$  axis with vertical and horizontal  $m'$  lines and diagonal  $m$  lines (see Fig. 2.11).
- 2.6 The one-dimensional lattice types (Fig. 2.15) are:
- (a)  $p112$       (b)  $p112$       (c)  $p112$   
 (d)  $p112$       (e)  $pmm2$       (d)  $pmm2$   
 (g)  $p1a1$       (h)  $p111$       (i)  $p112$ .
- 2.7 The plane point group symmetries (Fig. 2.16) are:
- $1$        $m$        $mm$        $3$        $3m$   
 $2$        $4$        $4m$        $6$        $6m$ .
- 2.8 The asymmetric plane point group and the plane point group with triad symmetry only.

## Chapter 3

- 3.1 (a) is orthorhombic  $C$ ; (b) is not a Bravais lattice because the points *do not* all have an identical environment [see the two-dimensional examples, Figs 2.2(b) and (c)]; (c) is orthorhombic  $P$  (two primitive cells are drawn together).
- 3.2 (a) is orthorhombic  $P$  (relocate the origin at  $x'y'z'$ ); (b) is orthorhombic  $I$  (relocate the origin at  $0\frac{1}{2}0$ ); (c) is orthorhombic  $C$  (relocate the origin at  $00z'$ ; the motif is two atoms, one of each type).

## Chapter 4

4.2	Structure	Bravais lattice	Motif
	NaCl	Cubic $F$	(Na and Cl)
	CsCl	Cubic $P$	(Cs and Cl)
	Diamond	Cubic $F$	(C and C)
	ZnS (sphalerite)	Cubic $F$	(Zn and S)
	ZnS (wurtzite)	Hexagonal $P$	(2Zn and 2S)
	$\text{Li}_2\text{O}$ (or $\text{CaF}_2$ )	Cubic $F$	(2Li and 1O)
	$\text{CaTiO}_3$	Cubic $P$	(1Ca, 1Ti, and 3O).

NB: in ferroelectric crystals the distortions which occur at the Curie temperature and below change the Bravais lattice from Cubic  $P$  to Tetragonal  $P$  to Orthorhombic  $P$  and to Rhombohedral with decreasing temperature.

## Chapter 5

- 5.1 In fcc crystals the slip planes are  $\{111\}$ , slip directions are  $\langle 110 \rangle$ .  
 In bcc crystals the slip planes are  $\{110\}$ , slip directions are  $\langle 111 \rangle$ .
- 5.2  $[23\bar{1}]$ , i.e.  $2.1 + 3.1 + \bar{1}.5 = 0$ .  
 $(321)$ , i.e.  $3.1 + 2.\bar{1} + 1.\bar{1} = 0$ .
- 5.3 Triclinic, none; monoclinic,  $(010)$  and  $[010]$ ; tetragonal,  $(001)$  and  $[001]$ ;  $(hk0)$  and  $[hk0]$ .
- 5.4  $(4\bar{1}\bar{1})$ ;  $(\bar{2}\bar{3}1)$ ;  $(\bar{1}\bar{2}11\bar{4})$ ;  $[3\bar{3}1]$  (or, their opposites, e.g.  $(\bar{4}11)$ , etc.).
- 5.5 (a)  $d_{101} = 375$  pm;  $d_{100} = 452$  pm;  $d_{111} = 302$  pm;  $d_{202} = 188$  pm.  
 (b)  $\alpha = 48.1^\circ$ ;  $\beta = 53.5^\circ$ ;  $\gamma = 63.4^\circ$ .  
 (c)  $p = 61.8^\circ$ ;  $q = 58.0^\circ$ ;  $r = 45.3^\circ$ .

$\alpha$ ,  $\beta$ ,  $\gamma$  are not identical to  $p$ ,  $q$ ,  $r$  because the (111) plane normal is not parallel to the [111] direction in orthorhombic crystals. These directions are only parallel in the case of cubic crystals.

5.6  $[001] = [0001]$ ;  $[010] = [\bar{1}2\bar{1}0]$ ;  $[210] = [30\bar{3}0] = [10\bar{1}0]$ ;  $[110] = [11\bar{2}0]$ .

5.7 Writing planes as row matrices (Section 5.8);

$$\text{Cubic } I: \quad (HKL) \Leftrightarrow (hkl) \begin{pmatrix} \frac{1}{2} & \frac{1}{2} & \frac{1}{2} \\ \frac{1}{2} & \frac{1}{2} & \frac{1}{2} \\ \frac{1}{2} & \frac{1}{2} & \frac{1}{2} \end{pmatrix}$$

$$\text{Cubic } F: \quad (HKL) \Leftrightarrow (hkl) \begin{pmatrix} \frac{1}{2} & 0 & \frac{1}{2} \\ \frac{1}{2} & \frac{1}{2} & 0 \\ 0 & \frac{1}{2} & \frac{1}{2} \end{pmatrix}.$$

The answers you obtain will depend upon your particular choices of **A**, **B**, **C** and **a**, **b**, **c**—but they will be the same form as those given above. The reverse transformations for planes are given by the inverse of the matrix in each case. Note that each matrix and its inverse also gives the transformation for direction symbols  $[UVW] \Leftrightarrow [uvw]$  when these are written as column matrices (see for example, Section 5.9). Finally, check that your determinants are positive ( $\frac{1}{2}$  for Cubic *I*,  $\frac{1}{4}$  for Cubic *F* in the examples above). A *negative* value means that you have inadvertently chosen a left-handed axial system to describe one or other of the unit cells.

## Chapter 6

- 6.1 These reciprocal lattice sections all consist of hexagonal arrays of reciprocal lattice points, those closest to the origin representing the {1010} planes (hexagonal lattice), {110} planes (cubic *I* lattice) and {220} planes (cubic *F* lattice).
- 6.2 Check your answers with the equations given in Appendix 4.
- 6.3 Yes.

## Chapter 7

- 7.1 The unit cells of the net are 'skew', like that for the monoclinic crystal (Fig. 6.2(a)) or the net (Fig. 7.1(d)). The (reciprocal lattice) unit cells of each twin orientation indicated by circles and squares are shown in Fig. E7.1. The vertical row of spots through the origin and perpendicular to the twin plane is common to both twin orientations and the spots are unstreaked. Similarly, in every third row spots are common to both twin orientations and are also unstreaked. This arises because one-in-three of the points in the net have the same position, or are *coincident* in both twin orientations. Streaking, or the extension of the reciprocal lattice points normal to the twin plane, increases as the twin thickness decreases, *except* for those reciprocal lattice points common to both orientations.
- 7.2 The angles at which the second, fourth etc. maxima occur, i.e.  $2(\lambda/a)$ ,  $4(\lambda/a)$ , etc., coincide with the angles at which the zero order, first order etc. minima occur, i.e.  $(1\lambda/d)$ ,  $2(\lambda/d)$ . Hence alternate peaks or maxima in the diffraction pattern are missing.



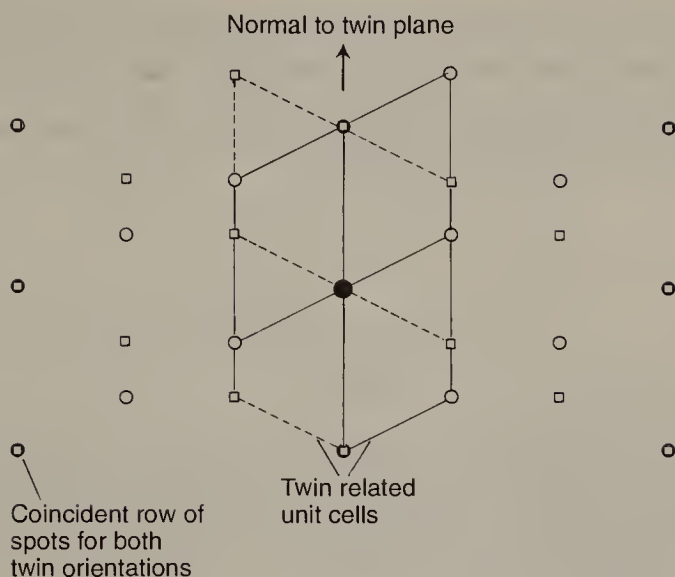


Fig. E7.1

- 7.3 The equation to be derived follows from the footnote on page 109. Since  $eV = \frac{1}{2}mv^2$ , then  $\sqrt{2meV} = mv$ . Substituting in de Broglie's equation gives  $\lambda = h / \sqrt{2meV}$ . The numerical values obtained by substituting the  $m$ ,  $e$  and  $V$  values are 10 kV: 12.2 pm (12.2 pm); 100 kV: 3.88 pm (3.70 pm); 1 MV: 1.22 pm (0.87 pm). The relativistically corrected values are in brackets, from which it is seen that the differences between the values are insignificant at 10 kV, significant at 100 kV and very significant at 1MV.

## Chapter 8

- 8.1  $\alpha_n$ , the angle between the direct and diffracted beams, is equal to  $2\theta$  (see Fig. E8.1); the planes are inclined to the diffraction grating such that they make equal angles with the incident and reflected beams. Hence  $d_{hkl} = a \cos \theta$ . Substituting for  $\theta$  and  $d_{hkl}$  in the equation  $n\lambda = a \sin \alpha_n$  gives  $n\lambda = (d_{hkl} / \cos \theta) \sin 2\theta = (d_{hkl} / \cos \theta) 2 \cos \theta \sin \theta = 2d_{hkl} \sin \theta$ —i.e. Bragg's law.
- 8.2  $d_{110} = 0.2027$  nm;  $d_{200} = 0.1433$  nm; and  $d_{211} = 0.1170$  nm. Planes whose  $d$ -spacings are smaller than  $\lambda/2$  ( $= 0.1146$  nm) do not satisfy Bragg's law since the maximum possible value of  $\theta$  is  $90^\circ$ .

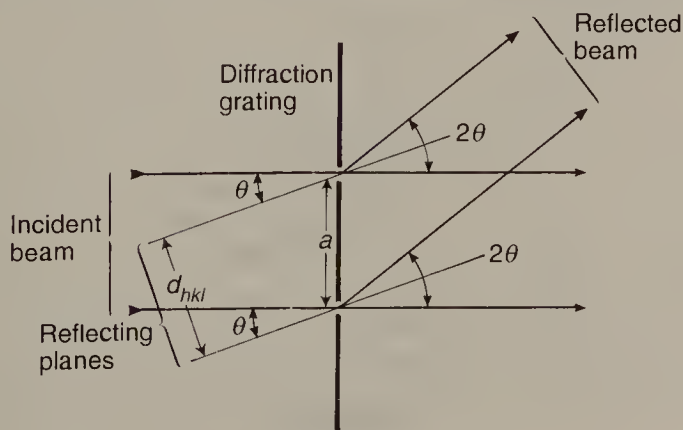


Fig. E8.1

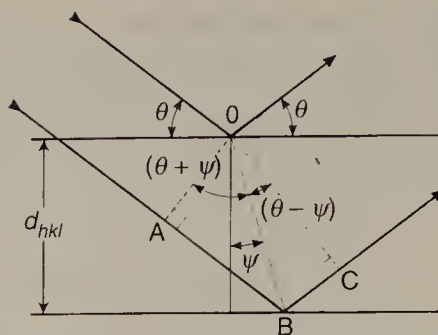


Fig. E8.3

- 8.3 Let the angle  $\Psi$  and distance  $OB$  be as shown in Fig. E8.3. Then  $AB = OB \sin(\theta + \Psi)$  and  $BC = OB \sin(\theta - \Psi)$ . Summing and expanding the sine terms:

$$(AB + BC) = OB \sin \theta \cos \Psi + OB \cos \theta \sin \Psi + OB \sin \theta \cos \Psi - OB \cos \theta \sin \Psi.$$

Hence, cancelling and substituting  $OB \cos \Psi = d_{hkl}$ :

$$(AB + BC) = 2OB \sin \theta \cos \Psi = 2d_{hkl} \sin \theta;$$

i.e. the path difference is independent of the value of  $\Psi$ .

## Chapter 9

- 9.1 Bragg's law is satisfied for the planes  $(2\bar{2}0)$ ,  $(3\bar{1}0)$ ,  $(400)$ ,  $(310)$ ,  $(220)$  (in the  $hk0$  section);  $(4\bar{1}1)$ ,  $(4\bar{1}\bar{1})$ ,  $(301)$ ,  $(411)$ ,  $(41\bar{1})$  (in the  $hk1$  and  $hk\bar{1}$  sections) and  $(3\bar{1}\bar{2})$ ,  $(3\bar{1}\bar{2})$ ,  $(202)$ ,  $(20\bar{2})$ ,  $(312)$ ,  $(31\bar{2})$  (in the  $hk2$  and  $hk\bar{2}$  sections). The (larger) reflecting sphere does not extend beyond the  $hk2$  and  $hk\bar{2}$  sections.
- 9.2 Bragg's law is satisfied for the planes  $(420)$ ,  $(4\bar{2}0)$ ,  $(220)$  and  $(2\bar{2}0)$ .
- 9.3 The zone axis of the pattern is  $\langle 112 \rangle$ . The particular variant obtained depends upon the variants of the indices chosen to index the pattern consistently.
- 9.4 This problem is essentially the same as that for the simple cubic crystal as shown in Figs 9.18 and 9.19, except that the cubic  $P$  reciprocal lattice is replaced by the cubic  $F$  reciprocal lattice (for a cubic  $I$  crystal—see Section 6.4). In the ZOLZ  $0kl$  and FOLZ  $1kl$  the reflecting planes are those for which  $(h + k + l) = \text{an even number}$  (see Fig. 6.5).



Fig. E9.5

- 9.5 The diffraction pattern is from  $\text{Fe}_3\text{C}$  (cementite) and is indexed in Fig. E9.5 above. Notice that the pattern is *not* rectangular, but slightly skew. Since the structure is orthorhombic the order of the indices  $hkl$  may not be changed; only their signs may be changed, e.g. the allowed permutations of 103 are: 103,  $\bar{1}03$ ,  $10\bar{3}$ ,  $\bar{1}0\bar{3}$ .

## Chapter 10

- 10.4 In Fig. 10.10 the camera constant  $\lambda L = 27.2 \text{ \AA mm}$ .
- 10.5 The  $d$ -spacing of the peaks ( $\sim 1.17 \text{ \AA}$ ) is determined using Bragg's law. Substituting this value and the lattice parameter  $a$  into the equation  $d_{hkl} = a/\sqrt{N}$  (Appendix 6) gives  $N = 6$ , hence the Laue indices  $hkl = 211$ . This result is in accordance with the conditions for reflection from a cubic  $I$  lattice (Table A6.2).  
Since the broadening due to the  $\text{CuK}\alpha_2$  component is eliminated,  $\beta_{\text{INST}}$  and  $\beta_{\text{OBS}}$  may simply be estimated from the half height peak widths; these should be measured in mm and converted to angular values in radians. This gives  $\beta = \beta_{\text{INST}} - \beta_{\text{OBS}} \sim 4.4 \times 10^{-3}$  rads. Hence  $\epsilon = \frac{1}{2}\beta \cot \theta \sim 2.5 \times 10^{-3}$  and the residual stress  $\sigma = E\epsilon \sim 500 \text{ MPa}$ —a value close to that of the yield stress in mild steel. (However, it should be borne in mind that some part of  $\beta$  will have arisen from a reduced sub-grain size.)
- 10.6 The diffraction patterns may be indexed as shown in Fig. E10.6. The 'matrix'  $\alpha$ -Fe orientation is outlined by solid lines and the twin orientation by dashed lines. The trace of the twin plane and the twin plane normal are indicated (compare with the

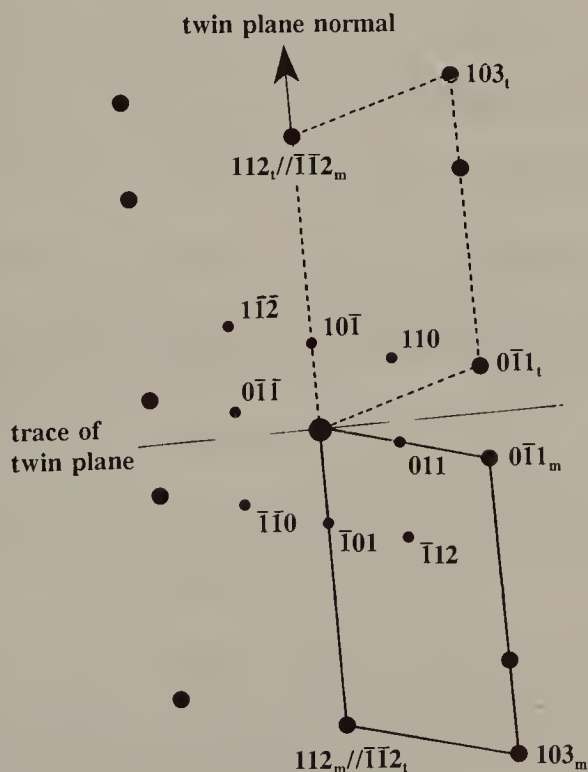


Fig. E10.6

twin-related unit cells in the optical diffraction pattern as shown in the answer to Exercise 7.1). The reflections for matrix (m) and twin (t) orientations are indexed such that (e.g.)  $0\bar{1}1_t$  is related to  $0\bar{1}1_m$  by reflection in the twin plane. The  $\text{Fe}_3\text{C}$  reflections may be indexed as shown, giving the orientation relationship between the  $\alpha\text{-Fe}$  (matrix) and  $\text{Fe}_3\text{C}$  as:

$$(011)_{\text{Fe}_3\text{C}} \parallel (0\bar{1}1)_{\alpha\text{-Fe}} \quad \text{and} \quad (\bar{1}01)_{\text{Fe}_3\text{C}} \parallel (112)_{\alpha\text{-Fe}}.$$

For the zone axes, obtained by cross multiplication (see Section 5.6.2):

$$[\bar{1}1\bar{1}]_{\text{Fe}_3\text{C}} \parallel [3\bar{1}\bar{1}]_{\alpha\text{-Fe}}.$$



# Further reading

## **Introductory books on crystallography**

- Bhadeshia, H. (1987). *Worked Examples in the Geometry of Crystals*. The Institute of Materials, London.
- Glazer, A. M. (1987). *The Structures of Crystals*. Adam Hilger, Bristol.
- Holden, A. and Morrison, P. (1982). *Crystals and Crystal Growing*. MIT Press.
- Kennon, N. F. (1978). *Patterns in Crystals*. John Wiley, New York.
- Steadman, R. (1982). *Crystallography*. Van Nostrand Reinhold, Wokingham.
- Windle, A. (1977). *A First Course in Crystallography*. G. Bell and Sons Ltd, London.

## **Books mainly concerned with crystal structure and symmetry**

- Buerger, M. J. (1970). *Contemporary Crystallography*. McGraw-Hill, New York.
- Buerger, M. J. (1971). *Introduction to Crystal Geometry*. McGraw-Hill, New York.
- Evans, R. C. (1964). *An Introduction to Crystal Chemistry* (2nd edn). Cambridge University Press, Cambridge.
- Hann, M. A. and Thomson, G. M. (1992). *The Geometry of Regular Repeating Patterns*. The Textile Institute, Manchester.
- McKie, D. and McKie, C. (1986). *Essentials of Crystallography*. Blackwell Scientific Publications, Oxford.
- Phillips, F. C. (1977). *Introduction to Crystallography* (3rd edn). Longmans, London.

## **Books which cover, generally in more detail, structural crystallography, symmetry, X-ray and electron diffraction techniques from the standpoint of the chemist, geologist, materials scientist or physicist**

- Barrett, C. S. and Massalski, T. B. (1980). *The Structure of Metals* (3rd edn). Pergamon, Oxford.
- Brown, P. J. and Forsyth, J. B. (1973). *The Crystal Structure of Solids*. Arnold, London.
- Bunn, C. W. (1967). *Chemical Crystallography* (2nd edn). Oxford University Press, Oxford.
- Dent-Glasser, L. S. (1977). *Crystallography and its Applications*. Van Nostrand Reinhold, New York.
- Giacovazzo, C., Monaco, H. L., Viterbo, D., Scordari, F., Gilli, G., Zanotti, G. and Catti, M. (1992). *Fundamentals of Crystallography*. IUCr Texts on Crystallography 2, Ed. C. Giacovazzo. International Union of Crystallography/Oxford Science Publications. Oxford University Press, Oxford.
- Glusker, J. P., Lewis, M. and Rossi, M. (1994). *Crystal Structure Analysis for Chemists and Biologists*. VCH Publishers, New York.

- Kelly, A. and Groves, G. W. (1970). *Crystallography and Crystal Defects*. Longman, London.
- McKie, D. and McKie, C. (1986). *Essentials of Crystallography*. Blackwell Scientific Publications, Oxford.
- Nye, J. F. (1985). *Physical Properties of Crystals: Their Representation by Tensors and Matrices*. Oxford University Press, Oxford.
- Smith, J. V. (1982). *Geometrical and Structural Crystallography*. John Wiley, New York.
- Verma, A. R. and Srivastava, O. N. (1982). *Crystallography for Solid State Physics*. Wiley Eastern, New Delhi.
- Whittaker, E. J. W. (1981). *Crystallography for Earth Science (and other solid state) Students*. Pergamon, Oxford.

### Books on optics and the diffraction of light

- Harburn, G., Taylor, C. A., and Welberry, T. R. (1983). *Atlas of Optical Transforms*. Bell & Hyman Ltd. London (first published in 1975 by G. Bell & Sons Ltd).
- Hecht, E. and Zajak, A. (1987). *Optics* (2nd edn). Addison-Wesley, London.
- Jenkins, F. A. and White, H. E. (1976). *Fundamentals of Optics* (4th edn). McGraw-Hill, New York.
- Robinson, P. C. and Bradbury, S. (1992). *Qualitative Polarized Light Microscopy*. Royal Microscopical Society Handbook No. 09. Oxford University Press/Royal Microscopical Society.
- Taylor, C. A. (1978). *Images: a Unified View of Diffraction and Image Formation with all Kinds of Radiation*. Wykeham Publications, London and Basingstoke.
- Wood, E. A. (1977). *Crystals and Light* (2nd edn). Dover Publications, New York.

### Books on X-ray diffraction and X-ray crystallography

- Azaroff, L. V. (1968). *Elements of X-ray Crystallography*. McGraw-Hill, New York.
- Bragg, W. H. and Bragg, W. L. (1966). *The Crystalline State*, Vol. 1. *A General Survey* by W. L. Bragg. G. Bell and Sons Ltd, London.
- Buerger, M. J. (1942). *X-ray Crystallography*. John Wiley, New York.
- Cullity, B. D. (1978). *Elements of X-ray Diffraction* (2nd edn). Addison-Wesley, Reading, MA.
- Henry, N. F. M., Lipson, H. and Wooster, W. A. (1961). *The Interpretation of X-ray Diffraction Photographs* (2nd edn). Macmillan, New York.
- Ladd, M. F. C. and Palmer, R. A. (1977). *Structure Determination by X-ray Crystallography*. Plenum Press, New York.
- Rhodes, G. (1993). *Crystallography Made Crystal Clear*. Academic Press, New York.
- Woolfson, M. M. (1978). *An Introduction to X-ray Crystallography*. Cambridge University Press, Cambridge.

### Books on electron diffraction techniques

- Dyson, D. J., Andrews, K. W. and Keown, S. R. (1971). *Interpretation of Electron Diffraction Patterns* (2nd edn). Hilger & Watts, London.
- Edington, J. W. (1975). *Electron Diffraction in the Electron Microscope. Monograph 2. Practical Electron Microscopy in Materials Science*. Philips Technical Library, Macmillan, London.

- Loretto, M. H. (1994). *Electron Beam Analysis of Materials* (2nd edn). Chapman & Hall, London.
- Thomas, G. and Goringe, M. J. (1979). *Transmission Electron Microscopy of Materials*. Wiley, Chichester.

## Books of Reference

The *International Tables for Crystallography* is the re-publication of the *International Tables for X-Ray Crystallography*. The volumes, and their first dates of publication, are listed below.

### *International Tables for X-ray Crystallography*

Volume I: *Symmetry Groups* (1952)

Volume II: *Mathematical Tables* (1959)

Volume III: *Physical and Chemical Tables* (1962)

Volume IV: *Revised and Supplementary Tables to Vols. II and III* (1974).

Published for the International Union of Crystallography by the Kynoch Press, Birmingham, England.

### *International Tables for Crystallography*

Volume A: *Space-Group Symmetry* (1983); Brief Teaching Edition (1995).

Volume B: *Reciprocal Space* (1993)

Volume C: *Mathematical, Physical and Chemical Tables* (1992).

Published for the International Union of Crystallography by Kluwer Academic Publishers, Dordrecht.

The *X-Ray Powder Diffraction File* is published by the International Centre for Diffraction Data (ICDD) (the Joint Committee for Powder Diffraction Standards, JCPDS), 12 Campus Boulevard, Newtown Square, PA 19073-3273, USA. It is updated as sets are added at approximately yearly intervals, together with the following manuals.

*Alphabetical Indexes: Inorganic Phases*

*Hanawalt Search Manual: Inorganic Phases*

*Organic and Organometallic Phases Search Manual*

*Indexes and Search Manual: Frequently Encountered Phases.*

## Books of general or historical interest

Bragg, W. H. and Bragg, W. L. (1966). *The Crystalline State*, Vol. 1. *A General Survey* by W. L. Bragg. G. Bell and Sons Ltd, London.

A book which shows the clarity and incisiveness of Bragg's scientific method. It is so well written that it remained in print, substantially unrevised from its first publication in 1933, for nearly forty years. Even today very little is 'out of date' and it contains much material which is not adequately covered at the same level elsewhere.

Bunn, C. (1964). *Crystals, their Role in Nature and in Science*. Academic Press, New York and London.

A book very much in the same category as A. F. Wells (1968) (see below) but with an even wider range of subject matter (including speculations on crystals and the origin of life) to appeal to the general scientific reader.



Ewald, P. P. and numerous crystallographers (1962). *Fifty Years of X-ray Diffraction*. Published for the International Union of Crystallography by N. V. A. Oosthoek's Uitgeversmaatschappij, Utrecht.

An invaluable source-book which describes the beginnings of X-ray diffraction, the growing field and development of schools of crystallography throughout the world, and the personal reminiscences and memoirs of those who participated. One of the strongest impressions is that of an international community of scientists which transcended the barriers of nationality, politics and war.

Lima de Faria, J. (Editor) (1990). *An Historical Atlas of Crystallography*. Kluwer Academic Publishers, Dordrecht.

A very comprehensive historical survey of the development of geometrical, physical and chemical crystallography and crystal structure determination—topics which are covered in most histories of science in a fragmentary manner. Special features of the book are the beautifully presented 'time maps' of crystallography, the title pages of important works and a bibliography on the history of crystallography.

Lipson, H. (1970). *Crystals and X-rays*. Wykeham Publications (London) Ltd.

An excellent introduction to X-ray diffraction, largely treated historically and with reference to the diffraction of light and microscopy. Crystal structure analysis is also described in a very clear and simple manner.

MacGillavry, C. H. (1976). *Symmetry Aspects of M. C. Escher's Periodic Drawings* (2nd edn). Published for the International Union of Crystallography by Bohn, Scheltema & Holkema, Utrecht.

Superb illustrations with clear descriptive analyses of the development of symmetry in Escher's work. The notion of colour symmetry is also included.

Newton, I. (1979). *Opticks or A Treatise of the Reflections, Refractions, Inflections and Colours of Light*. Dover Publications, New York, based on the Fourth Edition, London, 1730. Published by G. Bell & Sons Ltd. in 1931.

First published in 1704, Newton's *Opticks* is one of the most readable of all the great classics of physical science; in simple language Newton describes his famous experiments with colours, lenses, reflection and diffraction of light, the colours of rainbows and soap bubbles. This (Dover) edition has a foreword by Albert Einstein, a preface by I. Bernard Cohen and an introduction by Sir Edmund Whittaker.

Watson, J. D. (1968). *The Double Helix: A Personal Account of the Discovery of the Structure of DNA*. With a Foreword by Sir Lawrence Bragg. Weidenfield & Nicholson, London, and Penguin Books, Harmondsworth (1970).

A book which has become notorious for its lop-sided treatment of the other scientists in the UK and USA whose work also contributed to the discovery of the structure of deoxyribonucleic acid (DNA)—but which should not detract from Watson and Crick's great achievement in recognizing that the helices ran in opposite directions and the crucial idea of base-pairing.

Wells, A. F. (1968). *The Third Dimension in Chemistry*. Clarendon Press, Oxford.

A very scholarly work, with a much wider range of subject matter than its title suggests: includes elegant descriptions of polygons and plane nets, polyhedra and the symmetry of crystals from a broad scientific and historical framework.



# Index

Note: Illustrations are indicated by *italic* page numbers, footnotes are indicated by the letter *n*.

- Abbe criterion (for limit of resolution of microscopes) 121–3, 214
- Abbe, E. 121, 199
- addition rule 85, 85, 167
- Airy disc 116, 118, 119, 120
- Airy, G.B. 116, 199
- aluminium boride ( $\text{AlB}_2$ ), structure of 16
- ammonium magnesium phosphate ( $\text{NH}_4\text{MgPO}_4 \cdot 6\text{H}_2\text{O}$ ) crystal 61
- angles (between planes) 99, 214
- angstrom units, use of in X-ray and electron diffraction 166
- anisotropy of crystal properties 66–8
- answers (to exercises) 232–8
- antifluorite structure 17, 18
- applications of X-ray and electron diffraction techniques
  - determination of orientation relationships 187–8
  - identification of unknown phases 182–5
  - measurement of crystal (grain) size 186
  - measurement of internal elastic strains 186–7
  - measurement of lattice parameters 181–2
- approaches (to the study of crystal structures) 1–4
- Argand diagram 141, 142, 143, 222–3
- atomic radii, variation of 14–15
- atomic scattering factor  $f$  135, 136, 138–41
- back reflection X-ray flat-film techniques 176, 178
  - Laue method, photograph of aluminium single crystal 148–9, 150
  - powder method 176, 178
- Barlow, W. 72, 200
- base-centred monoclinic lattice 53
- base-centred orthorhombic lattice 53
- biographical notes 199–213
- body-centred cubic (bcc) structure 10, 10
  - crystal plan of 18, 18, 96
  - interstitial sites in 13, 14
  - unit cell of 13
- body-centred cubic lattice 53, 54
  - reciprocal unit cell of 96, 97
- body-centred orthorhombic lattice 53
- body-centred tetragonal lattice 53, 55, 55
- border (or frieze) patterns 42, 44, 49
- Bragg–Brentano focusing geometry 174, 176
- Bragg's Law 83, 125, 128–30, 129, 235, 236
  - for electron diffraction 165, 166
  - order of reflection  $n$  83, 129
  - vector notation for 130, 130
- Bragg, W.H. 125, 126, 200
- Bragg, W.L. 125, 126, 200
- Bravais, A. 51, 92, 201
- Bravais lattices 51–7
  - development from plane lattices 52
  - motifs and crystal structures 74–5
  - symmetry of 55
  - table of 57
  - unit cells of 52, 53, 54, 54–5, 55
- broadening of X-ray reflected beams 145–7, 147
- caesium chloride ( $\text{CsCl}$ )
  - Bravais lattice for 75
  - structure of 11, 13
- calcite 3, 3, 81
- calcium fluoride ( $\text{CaF}_2$ -fluorite) structure
  - Bravais lattice for 74
  - structure of 15, 17, 18
- camera constant 166
- camera length 165–6, 166
- carborundum ( $\text{SiC}$ ) structures 24, 25
- centre of symmetry 61, 62
- close-packed hexagonal arrays 4, 4
- cobalt-copper multilayer specimen, low angle
  - X-ray diffraction trace of 158, 160, 161
- cobalt-gold multilayer specimen, high angle
  - X-ray diffraction trace of 157, 160, 161
- coherence, conditions for 109–10
- complex number representation of vectors 222–3
- computer programs in crystallography 193–8
- conductivity 66, 218
- counter-change (colour) symmetry elements 45, 46
- covalent structures 16–17
- crystal classes 60
  - distribution in the seven crystal systems 64
  - holosymmetric classes 65
  - nomenclature for 64–5

- table of 57
- crystal faces, Miller indices applied to 80
- crystal habit 1
  - symmetry related to 59–60
- crystalline state, nature of 1–4
- crystal planes or projections 17–19
  - axis convention 17
  - equivalent positions in 18
  - fluorite and antiferite structures 18
- crystal structure determination 136–7, 144
- crystal symmetry, properties related to
  - ferroelectricity 66
  - optical properties 67–8
  - piezoelectricity 67
  - pyroelectricity 66
- crystal systems 55–8
  - Bravais lattices for 56
  - table of 57
- cubic close-packed (ccp) structure 5–6
  - crystal plan of 18, 18
  - interstitial sites in 11–13, 12
  - symmetry of 8
  - unit cells of 6–9, 7, 8
- cubic crystals
  - angles between planes in 215
  - crystal habits of 59–60
  - Miller indices and zone axis symbols for 81–2
  - reciprocal lattice unit cells for 96, 97
- cubic crystal system
  - point group symbols for 57, 64
- cubic *F* lattice 53
  - reciprocal unit cell for 96, 97
- cubic interstitial sites 11, 12, 13
- cubic lattices 52, 53
  - geometrical relationships between 52, 54
- cubic *P* lattice 53
  - reciprocal unit cell for 96
- cubic space groups 74
- cubic unit cell
  - point group symmetry of 55, 56
- cultures (relationship to symmetry and patterns) 44–6
- Curie temperature 66
- de Broglie's equation 109, 109n
- Debye, P.J.W. 171, 202
- Debye–Scherrer X-ray powder method 176, 177–81, 179, 180
- diad (two-fold) axis of symmetry 33, 35–6, 55
- diffraction angles
  - for electrons 101, 163–5
  - for light 101, 103–8
  - for X-rays 102, 128–130, 157–8
- diffraction-grating
  - with limited number of slits 117–18, 117
  - with narrow slits 112–14, 113, 114
  - with wide slits 114, 115–17
- diffraction and interference 111
- diffractometer X-ray powder method, *see* X-ray diffractometer
- direction symbols 77–8
- displacement vectors 217, 219
- dog-tooth spar 3, 3, 81
- double diffraction
  - origin of 229–30
  - in hcp structure 229–30, 230
  - between two crystals 230, 231
  - and 'unindexable' patterns 231
- $d_{hkl}$ -spacings, *see* lattice plane spacings
- electron diffraction 160–7
  - comparison with light and X-ray diffraction 102
- electron diffraction patterns 164–7, 164, 165, 168, 169, 187, 190
- electron diffraction techniques
  - identification of polycrystalline specimens 185
  - indexing procedures 166–7
  - orientation relationships between crystals 187–8, 187
  - polycrystalline (ring) pattern of aluminium 185, 185
- Elements of Euclid* 172
- enantiomorphic crystals 68, 68, 71
- Escher, M.C. 46
- Euler's formula 223
- Ewald, P.P. 92, 125–6, 202
- Ewald reflecting sphere construction
  - and broadening of reflected beams 146–7, 147
  - and electron diffraction 160–4, 162, 164
  - and Laue technique 133–4, 134
  - for monoclinic crystal 131–3, 132
  - and oscillation method 151–2, 152, 153
  - and precession method 153–5, 156, 157, 158
  - and rotation method 152–3, 154
  - for a single set of planes 130–1, 131
  - and X-ray diffractometer 159–60, 159
- Ewald's synthesis 130–4
- exercises 27–31, 58, 91, 100, 123–4, 134, 167, 188–90
- extrinsic stacking faults 20
- face-centred cubic lattice 53
  - reciprocal lattice unit cell of 96, 97
- face-centred cubic (fcc) structure 16
  - crystal plan of 18, 18
  - distinction between ccp structure 16
  - interstitial sites in 11–12, 12
  - unit cells of 6–8, 7, 8
- face-centred orthorhombic lattice 53
- Fedorov, E.S. 32, 72, 202
- ferroelectricity 66
- first-order Laue zone 162, 164, 164

- five-fold (pentad) rotation axis 36
- fluorite structure 15, 17, 18
- f*-number (for camera lens) 120, 120
- focusing circle 173–5, 173, 174, 175, 178
- focusing X-ray diffraction geometry 172–3, 173
- focusing X-ray diffraction methods 173–4
- four-fold (tetrad) rotation axis 36
- Frankenheim, M.L. 51, 203
- Fraunhofer diffraction 112, 112, 113
- Fraunhofer, J. 112, 203
- Fresnel, A.J. 109, 204
- Fresnel diffraction 112
- Friedel's Law 143, 143n
- further reading 239–42
- geometrical relationships
  - addition rule 85, 98
  - angle between planes 99
  - $d_{hkl}$ -spacings of lattice planes 99
  - plane parallel to two directions 85, 100
  - reciprocal and (direct) lattice unit cell vectors 97, 100
  - Weiss zone law 84, 87, 98–9, 140
  - zone axis for two planes 84, 100
- glide line of symmetry 39
- glide plane of symmetry 68–9
  - and systematic absences 226–7, 226
- The Grammar of Ornament* 46, 46n
- Hanawalt groups 183–5, 184
- Hanawalt, J.D. 183
- Hanawalt search procedure 182–5
- hard sphere model (for crystal structures) 4
- Haüy, R.-J. 1, 55, 81, 204
- Hermann, C.H. 72, 205
- Hermann-Mauguin space group symbols 72–4
- Hessel, J.F.C. 61, 205
- hexad (six-fold) axis of symmetry 36, 55
- hexagonal arrays 4, 4
  - constructing ccp and hcp structures from 5, 6, 7, 8
- hexagonal close packed (hcp) structure 5–6
  - interstitial sites in 13
  - unit cells of 6, 7
- hexagonal crystal system
  - indexing in 85–7
  - point group symbols for 65
- hexagonal (Bravais) lattice 52–4, 53, 54
- hexagonal (plane) lattice 37, 38
- high-order Laue zone 164
- holosymmetric crystal classes 55
- honeycomb arrangement 4
- Hooke, R. 1, 2, 4, 8, 205
- Hull, A.W. 171, 205
- Huygens, C. 109, 206
- Huygens' construction 110
- Huygens' wavelets 110, 112, 113–15, 137
- image formation (in light microscope) 120–3
- indexing
  - in hexagonal/trigonal systems 85–7
  - for lattice directions (zone axes) 77–8, 77
  - for lattice planes 78–81, 78, 79
- intensities of X-ray diffracted beams 138, 142–4
- interference and diffraction 111
- International Tables for Crystallography* 64, 92, 241
- interplanar angles, geometrical relationships for 99, 214
- interplanar spacings, geometrical relationships for 82–3, 214
- interstices
  - in body-centred cubic (bcc) structure 13, 14
  - in cubic close packed (ccp) structure 11–12, 12
  - in hexagonal arrays 4, 4
  - in simple cubic structure 11–12, 13
  - in square arrays 4, 4
- interstitial structures 11, 15, 16
- intrinsic stacking faults 20
- inversion axes of symmetry 62–4
- inversion diad 64
- inversion hexad 63, 64
- inversion tetrad 63, 63
- inversion triad 64
- ionic structures 16
- iron, fracture appearance of 3
- Jones, O. 46, 46n, 49
- Keissig fringes (in X-ray diffraction) 158–9, 161
- Kepler, Johannes 1, 206
- lattice
  - definition of 34
  - three-dimensional (Bravais) types of 51–3, 57
  - two-dimensional (plane) types of 34, 36
- lattice plane spacings,  $d_{hkl}$  82–3, 93–4, 99
  - in relation to Bragg's Law 129, 140, 165
- lattice points 33, 34
- lattice unit cell vectors 76, 94–5
- lattice vectors 52

- Laue cones 127–8, 128  
 Laue equations 126–8, 127  
 Laue–Friedrich–Knipping experiments 126  
 Laue indices 83–4, 148, 166  
 Laue, M. von 125, 126, 207  
 Laue point groups 144  
 Laue X-ray diffraction technique 133–4, 134, 148–9, 150  
 Laue zones 163–4, 169  
 Law of rational indices 80  
 layer lines (in X-ray diffraction) 151, 152, 153, 154  
 lead sulphate ( $\text{PbSO}_4$ ) crystal 61  
 light  
   coherence, scattering and interference 108–111  
   diffraction of 111–18  
   interference of 110–11, 113  
   nature of 108–10  
 light diffraction  
   from a circular aperture 106, 107, 116, 119  
   corollary with X-ray and electron diffraction 102, 137, 158–9  
   geometry of 111  
   and limit of resolution of optical instruments 102, 118–123  
   observations using a laser 106–8, 107  
   observations using nets 103–6, 104, 105, 124  
   from a single slit 115, 115  
 limit of resolution, *see* resolving power  
 line broadening in X-ray diffraction  
   grain size and shape factors 145–7, 146, 147, 186  
   instrumental factors 186  
   internal elastic strain factors 186–7, 189  
 lithium oxide ( $\text{Li}_2\text{O}$ -antifluorite) structure  
   Bravais lattice for 17, 18  
   structure of 74  
 low-angle Bragg reflections 158, 161  
   for cobalt–copper multilayer specimen 158, 160, 161  
  
 magnesium sulphate ( $\text{MgSO}_4 \cdot 7\text{H}_2\text{O}$ ) crystal 61  
 ‘map scales’ for (direct) and reciprocal lattices 93  
 Mauguin, C. 72, 207  
 maxima (in light diffraction)  
   principal 117, 117  
   subsidiary 117, 117  
 ‘memograms’ (for geometrical relationships) 84–5  
*Micrographia* 1, 2  
 microscope, limit of resolution of 120–3, 121, 123  
 Miller–Bravais indices 85–7  
 Miller indices 78–81, 148  
   for cubic crystals 81–2  
   row matrix form 88–90  
   transformation of 80–9  
 Miller, W.H. 79, 208  
 mirror line of symmetry 33, 35, 35, 39  
 mirror plane of symmetry 55, 62  
 model building 4, 5, 8  
 model building kit suppliers 191–2  
 monoclinic crystal  
   reciprocal lattice unit cell for 94–5, 94, 95  
 monoclinic crystal system  
   point group symbols for 57, 65  
 monoclinic lattices 53  
 motifs  
   in cubic structures 74–5  
   in hexagonal structures 75  
   meaning of term 33  
   symmetries of 35, 35, 37–9  
 multilayer specimens, X-ray diffraction of  
   cobalt–copper 158, 160, 161  
   cobalt–gold 157, 160, 161  
  
 nature of crystalline state 1–4  
 Newton, I. 109, 130, 208  
 Newton’s Laws 130  
 non-centrosymmetric point groups 67  
   table of 57  
 numerical aperture (of a microscope) 122  
  
 oblique lattice 34, 34, 37, 38  
 octahedral interstitial sites 11  
   in bcc structure 13, 14  
   in ccp structure 12, 12  
 one-dimensional patterns or groups 42, 44, 49  
   systematic identification of 44, 45  
 one-dimensional symmetry 42  
 optical activity 67  
   in enantiomorphous crystals 68  
   in liquids 71–2  
 optic axis  
   in biaxial crystals 67  
   in uniaxial crystals 67, 71  
*Opticks* 109, 206, 209  
 orthorhombic crystals—examples of crystal classes in 60, 61  
 orthorhombic crystal system 56–8, 57  
   point group symbols for 64  
 orthorhombic lattices 53  
 orthorhombic unit cell  
   point group symmetry of 56, 56  
 oscillation (X-ray diffraction) method 151–2, 152, 153  
   Ewald reflecting sphere construction for 151–2  
  
 particle-like character of light 108–9  
 Pasteur, L. 68, 209



- path difference 112, 113, 115, 115, 116, 126, 127, 127, 129, 129, 139, 140
- patterns  
   in one dimension 42–4, 44, 49  
   in two dimensions 4, 32–5, 40, 41, 44–6, 47, 48  
   in three dimensions 5–6, 32–3, 72–5, 73
- pentad (five-fold) axis of symmetry 36
- perovskite ( $\text{ABO}_3$ ) structure 19, 19, 66
- phase angle (difference) 140, 141, 141, 142, 143, 223
- piezoelectricity 67, 218
- plane indices, *see* Miller indices
- plane lattices 36–7, 38, 39
- plane parallel to two directions 85, 100, 216
- plane patterns (groups) 33, 37, 40, 41, 41, 47, 48  
   symbols for 41  
   systematic identification of 42, 43
- plane point groups 36, 36n, 49
- planes, relationship to zones 98, 216
- point group symbols 64–5  
   for plane point groups 36, 36n
- point group symmetry 56, 59  
   of cubic crystals 55–6, 56, 59–60  
   of orthorhombic crystals 55–6, 56  
   table of 57
- polar point groups 66
- Pope, W.J. 32, 210
- powder (X-ray diffraction) methods  
   Debye–Scherrer 176, 177–81, 179, 180  
   diffractometer, *see* X-ray diffractometer  
   flat film 176, 178
- precession (X-ray diffraction) method 153–5, 156, 157, 158  
   Ewald reflecting sphere construction for 154–5, 156  
   zero level photograph (of tremolite  $\text{Ca}_2\text{Mg}_5\text{Si}_8\text{O}_{22}(\text{OH})_2$ ) 158
- principal maxima 117, 117
- pyroelectricity 66, 218
- quartz 70, 71, 72  
   *Hanawalt Search Manual* listing for 184  
   Powder Diffraction File Card for 183  
   X-ray diffraction from 176, 177, 180
- radius ratios of interstitial sites 11–13  
   in bcc structure 13, 14  
   in ccp structure 12, 12  
   in simple cubic structure 12, 13
- Rayleigh, Baron (J.W. Strutt) 119, 210
- Rayleigh criterion 119, 119
- reading list (further reading) 239–42
- reciprocal lattice  
   construction of 92–3  
   reciprocal lattice nodes 145, 147–8, 147  
   reciprocal lattice points 93  
   reciprocal lattice unit cells  
     for cubic crystals 96–7, 97  
     for a monoclinic crystal 94–5, 94, 95  
     referred to rhombohedral axes (primitive cells) 96  
   reciprocal lattice unit cell vectors 95  
   relationships with (direct) lattice unit cell vectors 97  
   reciprocal lattice vectors 92–3  
     expressed as components of reciprocal lattice unit cell vectors 95  
   rectangular *c* (diamond) lattice 37, 38  
   rectangular *p* lattice 34, 34, 37, 38  
   reflecting sphere construction, *see* Ewald reflecting sphere construction  
   reflection-glide symmetry, *see* glide line of symmetry; glide plane of symmetry  
   reflection indices, *see* Laue indices  
   reflection symmetry, *see* mirror line of symmetry; mirror plane of symmetry  
   resolving power of optical instruments  
     Abbe criterion for 121–2  
     of a camera 120, 120  
     limited by diffraction 116, 121–3  
     of a microscope 120–3, 121, 123  
     of a telescope 118–20, 119, 120  
   resolving power of X-ray diffraction techniques 181–2  
   rhombohedral lattices 52–5, 53  
     transformation matrices for 85–7  
   rhombohedral unit cells 53–5, 53, 54  
     for cubic *F* Bravais lattice 54, 54, 55  
     for cubic *I* Bravais lattice 54, 54, 55  
   rotation axes of symmetry 33, 35, 36, 55  
   rotation (X-ray diffraction) method 152–3  
     photograph of topaz  $\text{Al}_2(\text{SiO}_4)(\text{OH},\text{F})_2$  154
- satellite reflections 157, 161
- scalar product 219, 219
- scalars 217
- scattering processes 111
- Scherrer equation 146, 148, 157, 186
- Scherrer, P.H. 171, 210
- Schoenflies, A. 32, 72, 210
- screw axes of symmetry 68–9, 69, 70, 71
- screw diad axis of symmetry, extinction conditions for 227, 227
- self consistency in indexing electron diffraction patterns 167
- semi-focusing X-ray diffraction methods 175–8
- Shockley notation  
   for close-packed structures 20  
   for faulted structures 20  
   for tetrahedral structures 24, 25

- for twinned structures 20, 21
- Shockley, W.B. 20, 211
- silicate structures 25–30, 28, 29, 30
- simple cubic lattice 53
- simple cubic structure 9–11, 9
  - interstitial sites in 11, 13
  - unit cell of 9
- simple hexagonal structure 5, 6, 16, 16
  - interstitial sites in 16, 16
  - unit cell of 7
- simple monoclinic lattice 53
- simple orthorhombic lattice 53
- simple tetragonal lattice 53
- six-fold (hexad) rotation axis 36
- slip systems 27
- snowflake 1
- sodium chloride (NaCl)
  - Bravais lattice for 74–5
  - structure of 15, 17
- software suppliers (computer programs in crystallography) 193–8
- Sohncke groups 72
- Sohncke, L. 72, 211
- Sorby, H.C. 210
- space group Pba2 73–4
- space groups 72
  - general equivalent positions in 73
  - Hermann–Mauguin notation for 72–4
  - special positions in 74
- space lattices, *see* Bravais lattices
- square arrays 4, 4
  - constructing ccp and simple cubic structures from 9, 9
- square lattice 37, 38
- stacking fault energy 21–3
- stacking faults 6
  - in  $\alpha$ -brass 21, 23
  - in ccp structure 19
  - in cobalt 21
  - occurrence of 19, 22
- stacking sequence
  - in bcc structure 10, 10
  - in carborundum (SiC) structures 24, 25
  - in ccp structure 5, 6, 7
  - in faulted structures 20
  - in simple hexagonal structure 5, 7
  - Shockley notation for 20
  - in twinned ccp structures 24, 25
- stereographic projection 62, 149n
- structure factor  $F_{hkl}$  136, 138–41
- structure factor equation, derivation of 140–1
- structure factor equation
  - application to CsCl structure 141, 142
  - application to crystal with a centre of symmetry 143, 143
  - application to crystal without a centre of symmetry 143
  - application to hcp metal structure 141–2, 142
  - and crystal structure determination 144
- subsidiary maxima 117, 117
- suppliers
  - of computer programs 193–8
  - of model-building kits 191–2
- symmetry 8, 34, 59
- Symmetry Aspects of M.C. Escher's Periodic Drawings* 47, 48, 242
- symmetry elements, self-consistency of 56
- symmetry, patterns and cultures 44–6
- systematic absences (extinction) in X-ray diffraction
  - for a bcc crystal 226
  - for a crystal with a glide plane of symmetry 226–7, 226
  - for a crystal with a screw diad axis of symmetry 227, 227
  - for an fcc crystal 224–6
  - table (of allowed reflections) for cubic structures 229
  - table (of extinction criteria) for lattices and symmetry elements 228
- Tammann, G.H.J.A. 32, 211
- tartaric acid, enantiomorphic forms of 68, 68, 71–2
- telescope, limit of resolution of 118–20, 119, 120
- tennis ball, symmetry of 63, 63
- tensor rank 218
- tensors 218, 218n
- tetrad (four-fold) axis of symmetry 36, 55
- tetragonal crystal, example of (urea,  $\text{CO}(\text{NH}_2)_2$ ) 63, 63
- tetragonal crystal system 57
  - point group symbols for 65
- tetragonal lattices 52, 53
  - unit cells for 55, 55
- tetrahedral interstitial sites 11
  - in bcc structure 13, 14
  - in ccp structure 12, 12
- texture (preferred orientation) 172
- three-fold (triad) rotation axis 36, 55
- titanium hydride (TiH)
  - Bravais lattice for 74
  - structure of 15–17, 15
- titanium hydride ( $\text{TiH}_2$ )
  - Bravais lattice for 74
  - structure of 15–17, 15
- titanium nitride (TiN)
  - Bravais lattice for 74
  - structure of 15–17, 15
- transformation matrices
  - for lattice (unit-cell) vectors 87–8
  - for Miller indices 88–9, 90
  - for trigonal crystals with rhombohedral lattices 90–1
  - for zone-axis symbols 89–90
- transformations in crystal structures 10
- translational symmetry elements 68–70

- triad (three-fold) axis of symmetry 36, 55
- triclinic crystal system 57–8
- triclinic lattice 52, 53
- trigonal crystals, transformation matrices for 90–1
- trigonal crystal system 57–8
  - indexing in 85–7
  - point-group symbols for 65
- tungsten carbide (WC) structure 16, 16
- twinned crystals 20, 21, 22, 23
  - diffraction patterns from 123–4, 124, 234, 235, 237, 237
- twins 19, 21–4
- two-colour (one-dimensional) patterns 45–6
- two-colour (plane) patterns or groups 45–6
- two-dimensional (plane) patterns or groups 33–5, 41–2
  - systematic identification of 43
  - table of 40
- two-dimensional symmetry elements 35–6, 35
- two-fold (diad) rotation axis 35–6, 55
- unit cells
  - for the 14 Bravais lattices 53, 53
  - for the ccp structure 6–9, 7, 8
  - for the hcp structure 6, 7
  - for the simple hexagonal structure 6, 7
- unit cell, choices of
  - for the ccp structure 6–9, 7, 8
  - for hexagonal and rhombohedral lattices 86–7, 86
  - for plane lattices 37
- units (Système International) 166
- urea crystal, symmetry of 63, 63
- useful crystallographic relationships
  - angles between planes in cubic crystals 215
  - interplanar angles 214
  - interplanar ( $d_{hkl}$ ) spacings 214
  - relationships between planes and zones 216
  - volumes of unit cells 215
- vector components 219–21
- vector modulus 217–18
- vector notation for unit cell volume 100, 221–2, 221
- vector–phase diagrams 140, 141
- vector product 220, 220
- vectors 78, 87–9, 217–22
  - addition of 219
  - multiplication of 219–21, 219, 220
  - resolution into components 219–21
- wave-like character of light 108–9
- wavetrain 109–11
- Weber, W.E. 212
- Weber (zone axis) symbols 85–7
- Weiss, C.S. 84, 212
- Weiss zone law 84, 87, 98–9, 140
- white X-radiation 173
- wurtzite (ZnS) structure 17, 24
- X-ray diffraction
  - Bragg's interpretation of 128–30
  - Ewald's interpretation of 130–14
  - Laue's interpretation of 126–8
- X-ray diffraction—corollary with light and electron diffraction 102, 137, 158–9
- X-ray diffraction techniques
  - for polycrystalline (powder) specimens 173–81
  - for single crystal specimens 148–55
  - for thin films and multilayers 155–8
- X-ray diffractometer 155, 174–6, 175, 177, 189
  - and reciprocal space 159, 160
  - asymmetrical setting 159, 159, 175, 176
  - symmetrical (Bragg–Brentano) setting 155, 159, 174, 175
- X-ray line broadening factors
  - grain size and shape 145–7, 146, 147, 186
  - instrumental 186
  - internal elastic strains 186–7, 189
- X-ray monochromator 173–4, 174
- X-ray Powder Diffraction File* 182, 241
  - file cards 182, 183
  - Hanawalt groups 183–5, 184
  - Hanawalt search procedure 182–5
- Young, T. 109, 212
- zero-order Laue zone 162–4, 162, 164
- zinc blende (ZnS—sphalerite)
  - Bravais lattice for 74–5
  - structure of 15, 17, 24
- zone axis 77
  - at intersection of two planes 84, 100
- zone axis (direction) symbols 77–8
  - column matrix form 89, 90
  - for cubic crystals 81–2
  - transformation of 89
- zone, definition of 76–7
- zone law 84, 87, 98–9, 140
- zones, relationship to planes 84, 100











A knowledge of crystallography opens the door to a better and clearer understanding of many topics in physical sciences and pattern design. In this new text, the basic ideas in crystallography and diffraction are explained simply and comprehensively.

The subject of diffraction flows naturally from that of crystallography since by its means the structures of materials may be revealed. The topic is developed by simple analogies and demonstrations—from familiar examples of the diffraction of light from nets and gratings through to X-ray and electron diffraction from crystals. The physical concepts and geometrical features common to all these diffraction modes are emphasized and described in very simple mathematical terms. Similarly, the relationship between diffraction and image formation in telescopes, cameras, and light and electron microscopes is developed and explained, and simple expressions are derived for the limits of resolution of optical instruments.

The applications of X-ray and electron diffraction techniques in the identification of the structures of materials and the measurement of crystal size, orientation relationships, and internal stress are also described and exercises (with 'helpful hints') given.

*The Basics of Crystallography and Diffraction* gives a good foundation to many other topics in physics, chemistry, earth, materials, and textile sciences, microscopy and pattern design, and it is hoped that all readers will find the topics treated in ways which are 'crystal clear' throughout.

**Christopher Hammond** is Senior Lecturer in the School of Materials at the University of Leeds. He is the author of the successful *Introduction to Crystallography* (1990, 1992), from which the present text has developed.

ALSO PUBLISHED BY OXFORD UNIVERSITY PRESS AND THE  
INTERNATIONAL UNION OF CRYSTALLOGRAPHY

*The solid state: from superconductors to superalloys*

A. Guinier and R. Jullien, translated by W. J. Duffin

*Fundamentals of crystallography*

C. Giacovazzo

*X-ray charge densities and chemical bonding*

P. Coppens

ISBN 0-19-855945-3



9 780198 559450 >

OXFORD UNIVERSITY PRESS